

NACA RM L56I18



# RESEARCH MEMORANDUM

MEASUREMENT OF STATIC FORCES ON INTERNALLY CARRIED BOMBS  
OF THREE FINENESS RATIOS IN FLOW FIELD OF A SWEEP-WING  
FIGHTER-BOMBER CONFIGURATION AT A MACH  
NUMBER OF 1.61 WITH ILLUSTRATIVE  
DROP-PATH CALCULATIONS

By Norman F. Smith and Harry W. Carlson

Langley Aeronautical Laboratory  
Langley Field, Va.

**LIBRARY COPY**

JAN 23 1957

LANGLEY AERONAUTICAL LABORATORY  
LIBRARY, NACA  
LANGLEY FIELD, VIRGINIA

CLASSIFIED DOCUMENT

This material contains information affecting the National Defense of the United States within the meaning of the espionage laws, Title 18, U.S.C., Secs. 793 and 794, the transmission or revelation of which in any manner to an unauthorized person is prohibited by law.

## NATIONAL ADVISORY COMMITTEE FOR AERONAUTICS

WASHINGTON

January 10, 1957

By N.F. Smith and H.W. Carlson  
NACA SCN 187

Langley 1-14-78

On file  
1-7-58  
11-30-59



FIELD

NATIONAL ADVISORY COMMITTEE FOR AERONAUTICS

RESEARCH MEMORANDUM

MEASUREMENT OF STATIC FORCES ON INTERNALLY CARRIED BOMBS  
 OF THREE FINENESS RATIOS IN FLOW FIELD OF A SWEEP-WING  
 FIGHTER-BOMBER CONFIGURATION AT A MACH  
 NUMBER OF 1.61 WITH ILLUSTRATIVE  
 DROP-PATH CALCULATIONS

By Norman F. Smith and Harry W. Carlson

SUMMARY

A wind-tunnel investigation of bomb-release problems can be made by the technique of measuring static forces for computation of bomb drop paths. As part of an extensive program, forces and moments were measured at a Mach number of 1.61 in the Langley 4- by 4-foot supersonic pressure tunnel on bombs of three fineness ratios and on a swept-wing fighter-bomber airplane configuration for a great number of positions of the bomb under an open bomb bay. The results show that the interference forces and moments imposed upon the bombs by the airplane are large and change rapidly as the bomb is moved through the flow field. The wing is shown to have a very large effect on the bomb forces after the bomb has emerged from the bomb bay. Calculations of bomb drop path were performed for one bomb (by using the force data) to show graphically the effects of release altitude, bomb attitude, ejection velocity, weight, and moment of inertia. These results showed that obtaining satisfactory bomb release at low altitude is made very difficult by the rapid rearward motion of the bomb resulting from the large dynamic pressures. Releasing the bomb from a position just below the bomb bay did not improve the release without the addition of an adequate ejection velocity.

INTRODUCTION

With the development of supersonic bombing airplanes, the problems of bomb release have become increasingly important. In addition to the higher dynamic pressures, the extremely turbulent circulatory flow in the bomb bay, as well as the nonuniform flow field surrounding the airplane, can cause bomb-release motions that endanger both the bomb and the airplane.

UNCLASSIFIED

CLASSIFICATION CHANGED

UNCLASSIFIED

By authority of  
 NASA CIVIL DIVISION

1-14-78  
 [Signature]

187  
 11-30-64

1-7-78

In general, there are four methods of investigating release problems. These are:

- (1) Full-scale drop tests
- (2) Model drop tests in wind tunnels
- (3) Theoretical calculations of flow fields, bomb forces, and drop paths
- (4) Static-force measurements in wind tunnels followed by drop-path calculations

Full-scale drop tests are obviously hazardous and do not readily permit investigation of the effects of the large number of parameters involved. Furthermore, with existing airplanes and bombs the equipment and speed ranges of the future cannot be investigated. For these reasons, other methods must be used, at least in the initial stages of investigation.

Model drop tests in wind tunnels have been performed (refs. 1, 2, and 3, for example) and several techniques were well established. Within the limits of rather stringent similarity requirements, such drop tests can provide useful information for a particular airplane under a particular set of release conditions. In general, however, only limited variations of some of the important parameters can be simulated in drop tests in available wind tunnels. Hence, detailed investigation of many factors affecting bomb release is not readily accomplished by this method.

The development of theoretical methods for calculation of flow fields, bomb forces, and bomb drop paths is, of course, desirable and would reduce the need for specific testing. Some work has been done along these lines at subsonic speeds for externally carried bombs (refs. 4 and 5), but the problems are difficult and the solutions tedious. Little, if any, analysis has been attempted for internally carried bombs. Development of theoretical methods will depend on a careful check with experiments not only for flow-field calculations but also for calculation of bomb forces and the resultant drop paths.

The measurement of static forces on the bomb through the drop region, with calculation of bomb motion and drop path from these measurements (the method utilized in this report) represents a relatively versatile technique. Although one set of measurements obtained by this method applies only to one configuration at one Mach number, a rather complete investigation of the various factors affecting bomb motion can be performed by simply varying the appropriate parameter throughout a series of drop calculations. Such calculations are readily performed in automatic computing machines. In addition to use in the drop calculations, the force

data may also be valuable as a check in the development of theoretical methods of computing bomb forces and trajectories.

This report utilizes the fourth method outlined. Forces and moments on bombs of three fineness ratios and on a fighter-bomber airplane are presented for a large number of positions of the bomb under an open bomb bay. A number of bomb drops have been calculated and are shown in order to illustrate the procedure and demonstrate the type of analyses that can be made.

#### SYMBOLS

$C_D$	drag coefficient of wing-fuselage combination, $\frac{\text{Drag}}{qS}$
$C_L$	lift coefficient of wing-fuselage combination, $\frac{\text{Lift}}{qS}$
$C_m$	pitching-moment coefficient of wing-fuselage combination, referred to $\frac{\bar{c}}{4}$ , $\frac{\text{Pitching moment}}{qS\bar{c}}$
$C_{D_b}$	drag coefficient of bomb, $\frac{\text{Drag}}{qS_b}$
$C_{L_b}$	lift coefficient of bomb, $\frac{\text{Lift}}{qS_b}$
$C_{m_b}$	pitching-moment coefficient of bomb, $\frac{\text{Pitching moment}}{qS_b}$ (center of moments is nose of bomb)
$\bar{c}$	mean aerodynamic chord of wing, in.
$S$	total area of wing, sq ft
$S_b$	maximum frontal area of bomb, sq ft
$l'$	assumed bomb center-of-gravity position measured from bomb nose, in.
$l$	bomb length, in.

$q$	dynamic pressure, lb/sq ft
$P_{Bb}$	pressure coefficient on bomb base
$x$	longitudinal distance between bomb midpoint and bomb-bay midpoint (see fig. 1(b)), in.
$z$	vertical distance between bomb midpoint and a horizontal line drawn through the fuselage center line at bomb-bay center line (station 20, see fig. 1(b)), in.
$\theta$	attitude angle of bomb center line referenced to the horizontal, deg
$\alpha_b$	angle of attack of bomb, $\theta + \tan^{-1} \frac{u_z}{u_x}$ (for static tests $\alpha_b = \theta$ )
$\alpha_{WF}$	angle of attack of wing-fuselage center line, referenced to free-stream direction, deg
$u$	velocity of bomb in direction indicated by subscripts, in./sec
$U$	free-stream velocity, in./sec
$d/d'$	ratio of bomb sting diameter to bomb base diameter
$f$	fineness ratio of bomb
Subscripts:	
$x$	horizontal (streamwise) direction
$z$	vertical (gravity) direction

#### APPARATUS AND TESTS

##### Models

The general arrangement of the test setup is shown in figure 1. Dimensions of the wing-fuselage combination are also given in this figure. The wing-fuselage combination was designed to simulate a swept-wing fighter-bomber airplane and was geometrically similar to the configuration used in reference 6. If a model scale of 1/20 is assumed, bombs 2 and 3 (figs. 1 and 2) correspond to a full-scale diameter of 26 inches.

The wing and fuselage were constructed of metal and were sting-mounted on the regular support sting of the Langley 4- by 4-foot supersonic pressure tunnel. Both pitch and translation were provided in the angle-of-attack plane by this support system. A six-component strain-gage internal balance was housed within the fuselage to measure airplane forces. The fuselage bomb bay was open for all tests and was rectangular and square-cornered. At the rear of the bomb bay a slot was provided into which the bomb-support strut could move for the more rearward bomb positions (fig. 1).

The bombs were constructed of metal and were mounted on a six-component electrical strain-gage balance, which was supported on a separate mechanism as shown in figure 1. Attitude angles of the bomb were provided by this support system from  $-15^{\circ}$  to  $15^{\circ}$ , the center of rotation lying on the axis of the bomb.

A series of bombs of various shapes and fineness ratios was investigated. This report presents the results of tests of three, having fineness ratios of 2.36, 4, and 7 (fig. 2). In order to design a fineness-ratio series which would represent a geometric family and at the same time be practical, particularly from the volume standpoint, a combination of ogive nose, cylindrical center section, and ogive-cone tail section was used. The derivation of the proportions for the geometric family is shown in the sketch on the right-hand side of figure 2.

The bomb fins employed a slab-sided double-wedge section. All three bombs were investigated with and without fins, whereas bomb 2 (fig. 2) was tested in one chordwise position with a set of fins approximately two-thirds the area of the original set.

#### TESTS AND METHODS

The angle of attack of both the airplane and bomb and the position of the airplane with respect to the bomb could be remotely varied in the plane of symmetry during tunnel operation. (No lateral movement or yaw angles were obtained.) Hence, for each run the bomb was located at one chordwise (x) position. During each run the fuselage and bomb angles of attack were set at nominal values and the wing-fuselage model was then moved through a series of vertical positions. The angle of attack of the airplane or the bomb was then changed and the position of the airplane

with respect to the bomb again varied. The nominal ranges of angles and positions are shown in the following table:

Bomb	Angle of attack of airplane, deg	Angle of attack of bomb, deg	x-values, in.	Nominal z-range, in.
1	4	0, $\pm 5$ , $\pm 10$ , $\pm 15$	-2.55, 2.95	0 to 6
	0	0, $\pm 10$	-2.8, 2.7	0 to 6
	8	0, $\pm 10$	-2.67, 2.83	0 to 6
2	4	0, $\pm 5$ , $\pm 10$ , $\pm 15$	-2.55, -1.05, 0.7, 2.95, 5.95	0 to 6
	0	0, $\pm 10$	-2.8, -1.3, 0.7, 2.7, 5.7	0 to 6
	8	0, $\pm 10$	-2.67, -1.17, 0.83, 2.83, 5.83	0 to 6
3	4	0, $\pm 5$ , $\pm 10$ , $\pm 15$	-0.05, 1.85, 3.85	0 to 10
	0	0, $\pm 10$	-0.4, 1.6, 3.6	0 to 10
	8	0, $\pm 10$	-0.17, 1.73, 3.73	0 to 10

The forces on the models in each position were recorded. Both the bomb and the airplane configurations were also pitched in an interference-free position to obtain the force characteristics of the isolated configurations.

For all tests a 1/4-inch-wide strip of no. 60 carborundum grains and shellac was located on both surfaces of the wing at the 10-percent-chord point and on the fuselage and bomb nose 1/2 inch from the tip in order to insure a turbulent boundary layer.

Inasmuch as the bomb-support system was relatively flexible in the lift direction, calibration of change in bomb position  $z$  and bomb angle of attack  $\alpha$  with bomb lift and pitch were made during balance calibrations. The bomb-position corrections were calculated based on loads measured in isolated bomb tests for the nominal bomb angle and were

included in the precalculated values of  $z$  by which the bomb-airplane positions were set. These corrections were small, 0.060 inch at the maximum.

The corrections to bomb angle of attack were not applied in advance to the angles used. Instead, the corrections were introduced into the computing equations. The actual value of  $\alpha$  for each point was computed for the loads incurred and was then used in the resolution of forces. Plots of actual  $\alpha$  (computed) are shown in figure 3 for the three bombs. The nominal values which were chosen to be used in subsequent figures and in the drop-path calculations are shown on each plot. Since it appeared possible that the bomb support strut and the slot at the rear of the bay (fig. 1) could affect the flow and cause erroneous results, for one check run a filler block which supported the bomb sting and bomb in the bay without the strut was provided for this slot. An indication of the interferences produced by the bomb-support system can be obtained from figure 4. The single data point with the bomb sting supported from the rear of the bay agrees well with the curves from data taken in the usual manner. This result indicates that inaccuracies due to this source are small, at least for the zero angle-of-attack condition shown in the figure.

In order to determine the effect on base pressure of the large diameter of the bomb sting or balance shield, a smaller diameter sting (with balance removed) was provided for one run. The base pressures thus obtained are compared with base pressures obtained in the standard manner in figure 5. Although base pressure is shown to be affected by  $d/d'$ , the shapes of the curves for the two cases are similar. The maximum difference shown in this figure corresponds to 0.03 in bomb drag coefficient.

#### Precision of Test Data

The repeatability or relative accuracies are estimated from an inspection of repeat test points, zero shifts and static deflection calibrations to be as follows:

x, in. . . . .	±0.05
y, in. . . . .	±0.10
z, in. . . . .	±0.10
Bomb:	
$C_{D_b}$ . . . . .	±0.01
$C_{L_b}$ . . . . .	±0.03
$C_{m_b}$ . . . . .	±0.03
$\alpha_b$ , deg . . . . .	±0.10

## Wing-fuselage:

$C_D$ . . . . .	$\pm 0.001$
$C_L$ . . . . .	$\pm 0.002$
$C_m$ . . . . .	$\pm 0.001$
$\alpha_{wf}$ , deg . . . . .	$\pm 0.10$

## RESULTS AND DISCUSSION

## Basic Data

Isolated bomb and wing-fuselage data.- Lift, drag, and pitching-moment data for the three bombs are presented in figure 6 for angles of attack up to  $15^\circ$ . Data are included for bombs 1 and 3 with and without fins and for bomb 2 without fins and with fins of two different sizes. It should be noted that the bomb pitching moments are in all cases computed about the bomb nose.

Plots of bomb force coefficients.- Lift, drag, and pitching-moment coefficients for bombs 1, 2, and 3 in the presence of the airplane configuration are presented in figures 7 to 14. A convenient index to configurations and figure numbers is presented in table I.

The basic data are presented in the form of plots of coefficients against the vertical distance between the bomb midpoint and the midpoint of the bomb bay (on the fuselage center line). The data for seven bomb angles of attack at an angle of attack of the airplane of  $4^\circ$  is shown in the left-hand part of each figure. From this comprehensive data, contour maps of bomb forces and calculations of bomb drop paths can be made. The data for three bomb angles of attack at airplane angles of attack of  $0^\circ$  and  $8^\circ$  is shown in the right-hand part of each figure. These data provide less complete information at these airplane angles of attack and serve to illustrate the effects of changing this angle of attack.

The effects of bomb position, bomb angle of attack, and airplane angle of attack on bomb forces are clearly shown in these figures. In order to illustrate the effect of bomb fins and the effect of the wing on bomb forces, figures 15 and 16 have been prepared from data of the previous figures. A comparison of the force data on bomb 2 with small fins, large fins, and no fins in the presence of the wing-fuselage combination is shown in figure 15. Also shown in figure 15 are the force coefficients for each isolated bomb configuration at each angle of attack. The difference between the curves for the various fin configurations is shown to be equal roughly to the difference between the interference-free values of the corresponding coefficient for values of  $z$  greater than about 2 inches. The character of the curves is generally similar for the

three fin configurations. Similar results have been found for the other bombs (1 and 3, see basic data figures) which were tested with and without fins.

A comparison of the forces on bomb 3 with the airplane wing on and off is presented in figure 16. The wing is shown in this figure to have an important effect upon the bomb forces although the basic shape of the curves remains similar. At  $x = -0.4$ , the effect (shown by the difference between the curves for wing on and wing off) is significant even when the bomb is within the bomb bay ( $z$  of 0 to  $2\frac{1}{2}$  inches approximately), becomes a maximum after the bomb has completely emerged ( $z$  of 4 to 5 inches), and decreases slowly as the bomb is moved still further from the airplane. For the further rearward position of the bomb,  $x = 1.6$ , these effects have shifted to larger values of  $z$ . The direction of the drag, lift, and pitch increments incurred by the bomb at the higher  $z$ -values is explained by the downwash produced by the wing at this airplane angle of attack ( $4^\circ$ ).

A quantitative evaluation of the effect of the wing on a bomb drop path has not been made. It seems likely, however, that the effects indicated are large enough to require that the wing be properly simulated in model tests such as those reported herein or in model drop tests.

Plots of wing-fuselage force coefficients.- The lift, drag, and pitching-moment coefficients measured on the wing-fuselage combination and plotted against bomb position  $z$  for the three bombs investigated are presented in figures 17, 18, and 19. It will be noted from examination of figure 1 that some interference would be produced by the bomb support strut on the wing-fuselage combination. This interference has not been isolated and is included in the data shown in figures 17 to 19.

Although no evaluation of the effect of the interferences as measured on the airplane flight path has been made, it is believed that such effects would be small. It should be noted that the results presented in figures 17 to 19 are for a wing-fuselage combination without a tail. It is expected that the effect of a bomb on a horizontal-tail surface would add significantly to the interference forces measured herein.

#### Contour Plots

Figures 20 to 25 present contour maps of each coefficient for bomb 2 and bomb 3. (From figs. 9 and 12, see preceding table.) The bomb mid-point is the reference point (the point at which the force coefficient is plotted) for all contour plots. The bomb and bomb bay are shown to scale on each plot.

These contour maps, in general, show rapid changes in bomb forces and moments with  $z$  and  $x$ . The data in this form illustrate well the complexity of the flow field in which the bomb is located. An evaluation of the effect of these measured forces and moments on the bomb drop path can be obtained only by utilizing these data in the calculation of bomb drop path.

### Drop-Path Calculations

Measured bomb forces and moments, as presented in this report, have their principal use in the calculation of drop paths. In order to illustrate the manner in which these data can be used, a series of calculations has been performed for bomb 3. The effect of some of the primary variables, such as altitude, bomb attitude, ejection velocity, and weight have been treated. The cases calculated represent a brief illustrative analysis rather than an exhaustive one.

The calculations were performed in a magnetic-drum electronic data-processing machine by using the equations presented in the appendix and the data presented in figures 12 or 23 to 25. Full-scale conditions are assumed, the model data being considered as 1/20 scale.

The variable parameters are as follows:

Figure	$\theta_0$ , deg	Release altitude, ft	$z_0$ , in.	Bomb weight, lb	Bomb moment of inertia, lb-sec <sup>2</sup> -in.	Ejection velocity, ft/sec
26	4	0, 10,000, 20,000, 30,000, 40,000, 50,000	15	1,750	5,176	0
27	-4, 0, 4, 8	10,000	15	1,750	5,176	0
28	4	0	45	1,750	5,176	0, 10, 20, 30
29	4	10,000	45	1,750	5,176	0, 10, 20, 30
30	4	10,000	15	875, 1,750, 2,625, 3,500	5,176	0
31	4	10,000	15	1,750	2,558, 5,176, 7,764, 10,352	0

The figures listed in the preceding table also show bomb positions  $x$  and  $z$ , and bomb attitude angle  $\theta$  plotted against elapsed time after release. The sketch within the figure shows the bomb release path with bomb position and attitude drawn to scale for each 0.1-second interval of time. (The time interval for the calculations was generally 0.01 second; in some cases, 0.005 second.) The bomb-bay outlines are also shown.

Effect of release altitude.- Figure 26 presents drop-path data for six altitudes from sea level to 50,000 feet. The low-altitude drops are characterized by rapid rearward movement because of the high drag at the high dynamic pressures. At sea level and 10,000 feet, collision of bomb fins with the rear of the bomb bay occurs, whereas at an altitude of 20,000 feet the release appears to be marginal. At 30,000 feet and above, the rearward motion of the bomb is reduced to the point where the drop appears to be safe. Although the overall changes in bomb attitude angle which occur are of similar magnitude for all altitude cases, the variations are of higher frequency and reach higher positive values at low altitudes. The tendency of the bomb to remain at higher positive attitude angles at low release altitudes (in the particular cases calculated) tends to make the problem of low-altitude release worse by decreasing the vertical velocity of the bomb. Bomb-release attitude is therefore one of the variables to be considered.

Effect of release attitude.- Figure 27 presents drop-path data for four initial bomb angles of attack ( $-4^\circ$ ,  $0^\circ$ ,  $4^\circ$ , and  $8^\circ$ ) for an altitude of 10,000 feet. This figure shows that the release is not improved by giving the bomb either positive or negative incidence with respect to the airplane. The release is in most cases made less desirable as a result of the large angular oscillation induced by either positive or negative incidence.

Effect of ejection.- Drop-path data calculated for four ejection velocities (0, 10, 20, and 30 feet per second) at two altitudes (0 and 10,000 feet) are presented in figures 28 and 29. In these cases, the ejection mechanism was assumed to release the bomb at  $z = 45$  inches (corresponding to a 30-inch ejection stroke) with the specified downward velocity (in the  $z$ -direction). The angle of attack of both bomb and airplane was  $4^\circ$ .

For the case for an ejection velocity of zero, the bomb at either altitude moves almost straight rearward and collides with the bomb bay. For all cases in which an ejection velocity of 10 feet per second was assumed, the bomb clears the bomb bay. This result indicates that the release of a bomb from a point below the airplane may not produce a satisfactory release at low altitudes. Imparting a downward velocity to the bomb also appears to be necessary.

It will be noted that, although in the case for an ejection velocity of 10 feet per second the bomb clears the bomb bay, the rapid rearward motion of the bomb makes this drop appear somewhat marginal, particularly for the lower altitude. For the cases calculated, an ejection velocity of 20 feet per second or greater appears desirable. The drop paths for the bombs ejected at the higher velocities at low altitude compare favorably with the drop paths obtained without ejection at high altitudes. In this investigation, no attempt was made to simulate the ejection

apparatus, which as indicated in reference 4, can have a large effect on the bomb forces and the resulting motion.

Effect of bomb weight.- Figure 30 shows the drop paths for four values of bomb weight ( $1/2$ , 1,  $1\frac{1}{2}$ , and 2 times the original weight of 1,750 pounds) for an altitude of 10,000 feet. As might be expected, increasing the bomb weight improves the drop characteristics by increasing the downward motion in relation to the rearward motion. For the cases calculated, a bomb weight of 3,500 pounds or twice the original weight was required to alter the drop path from unsatisfactory or marginal to satisfactory.

The plots of  $\theta$  show that the angular motion increases in magnitude as the weight is increased; however, because the angular moment of inertia was not changed for these different weights, this result must be due to the fact that the bomb incurred a different schedule of pitching moment on the different drop paths. (See fig. 25.)

Effect of moment of inertia.- The results of drop-path calculations for four values of bomb rotary moments of inertia ( $1/2$ , 1,  $1\frac{1}{2}$ , and 2 times the original value of 5,176 lb-sec<sup>2</sup>-in.) are presented in figure 31 for a bomb weight of 1,750 pounds. Bomb moment of inertia is shown in these figures to have insignificant effect upon the bomb flight path. Bomb angular motion, however, is progressively decreased both in magnitude and frequency as the moment of inertia is increased.

#### CONCLUDING REMARKS

Forces and moments have been measured at a Mach number of 1.6 on bombs of three fineness ratios and on a swept-wing fighter-bomber airplane configuration for a great number of positions of the bomb under an open bomb bay. The results show that the interference forces and moments imposed upon the bombs by the airplane are large and change rapidly as the bomb is moved through the flow field. The wing is shown to have a significant effect on the bomb forces both before and after the bomb has emerged from the bomb bay.

Calculations of bomb drop path were performed for one bomb (using the force data) to show graphically the effects of release altitude, bomb attitude, ejection velocity, weight, and moment of inertia. The results showed that obtaining satisfactory bomb release at low altitude is made very difficult by the rapid rearward motion of the bomb resulting

from the large dynamic pressures. Releasing the bomb from a position just below the bomb bay did not improve the release without the addition of an adequate ejection velocity.

Langley Aeronautical Laboratory,  
National Advisory Committee for Aeronautics,  
Langley Field, Va., August 23, 1956.

## APPENDIX

## EQUATIONS USED IN THE CALCULATIONS OF BOMB DROP PATHS

With a knowledge of the static forces and moments acting on the bomb due to its position and attitude in the airplane flow field and the forces and moments arising from the translational and rotary motion of the bombs, the release path can be determined by a step-by-step solution of the equations of motion. In order to approximate a true integration, it is necessary that a small time interval be used. Since the rotary motion is the most critical, it has been found (ref. 3) that a practical criterion for the time interval is that it produce corresponding angular changes not exceeding three-quarters of one degree (time interval 0.01 second or less for the cases studied).

The forces which produce accelerations of the bomb in the x- and z-directions and the moments which produce angular accelerations are:

$$F_x = C_{D_b} q F$$

$$F_z = W - \left( C_{L_b} + C_{L_{\alpha_b}} \tan^{-1} \frac{u_z}{U} \right) q F$$

$$M_{CG} = \left[ C_{m_b} + C_{m_{\alpha_b}} \tan^{-1} \frac{u_z}{U} + \left( C_{L_b} + C_{L_{\alpha_b}} \tan^{-1} \frac{u_z}{U} \right) \frac{l'}{l} + C_{m_q} \frac{\dot{\theta} l}{2V} \right] q F l$$

where  $C_{L_b}$  and  $C_{m_b}$  are from contour plots and  $C_{L_{\alpha_b}}$  and  $C_{m_{\alpha_b}}$  are from isolated bomb data. The value of the damping coefficient  $C_{m_q}$  was obtained by the method of reference 7.

The velocities produced by these forces and moments are:

$$u_x = u_{x,n-1} + \frac{F_{x,n-1} \Delta t}{m}$$

$$u_z = u_{z,n-1} + \frac{F_{z,n-1} \Delta t}{m}$$

$$\dot{\theta} = \dot{\theta}_{n-1} + \frac{57.3 M_{n-1} \Delta t}{I}$$

The corresponding motions or displacements are given by:

$$x = x_{n-1} + \frac{1}{2} \frac{F_{x,n-1} \Delta t^2}{m} + u_{x,n-1} \Delta t$$

$$z = z_{n-1} + \frac{1}{2} \frac{F_{z,n-1} \Delta t^2}{m} + u_{z,n-1} \Delta t$$

$$\theta = \theta_{n-1} + \frac{57.3}{2} \frac{M_{n-1} \Delta t^2}{I} + \dot{\theta}_{n-1} \Delta t$$

where

F force in direction indicated by subscripts, lb

M bomb pitching moment, in.-lb

W bomb weight, lb

m bomb mass, W/g, lb-sec<sup>2</sup>/in.

I bomb moment of inertia, lb-sec<sup>2</sup>-in.

$C_{mq}$  damping coefficient =  $\frac{\partial C_m}{\partial \frac{\dot{\theta} l}{2V}}$

$\dot{\theta}$  bomb rotary (angular) velocity, deg/sec

V airstream velocity, in./sec

$\Delta t$  time interval occurring between successive bomb positions

and the subscripts n - 1 denote value from previous point in step-by-step calculations, and 0 denotes zero time.

The geometric and aerodynamic parameters assumed for all cases (full-scale conditions, bomb 3) are as follows:

$$\alpha_{wf} = 4^\circ$$

$$x_0 = 0$$

$$l = 182 \text{ in.}$$

$$C_{L\alpha b} = 0.15$$

$$u_{x_0} = 0$$

$$\frac{l^2}{l} = 0.5$$

$$C_{m\alpha b} = -0.11$$

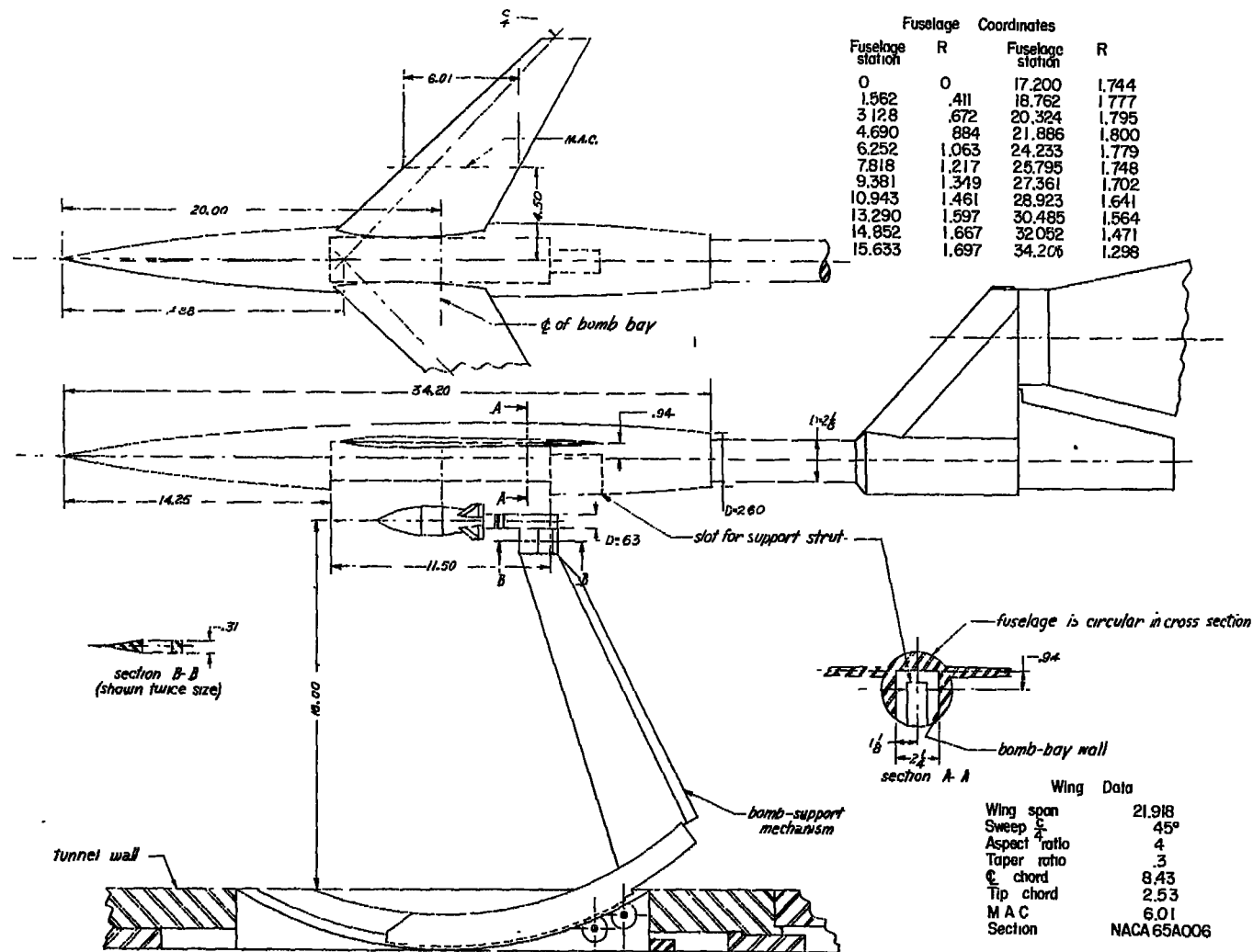
$$S_b = 3.69 \text{ sq ft}$$

## REFERENCES

1. Rainey, Robert W.: A Wind-Tunnel Investigation of Bomb Release at a Mach Number of 1.62. NACA RM L53L29, 1954.
2. Lee, John B., and Carter, Howard S.: An Investigation of Ejection Releases of Submerged and Semisubmerged Dynamically Scaled Stores From a Simulated Bomb Bay of a Fighter-Bomber Airplane at Supersonic Speeds. NACA RM L56I10, 1956.
3. Faget, Maxime A., and Carlson, Harry W.: Experimental Techniques for Predicting Store Motions During Release or Ejection. NACA RM L55L20b, 1956.
4. Alford, William J., Jr.: Effects of Wing-Fuselage Flow Fields on Missile Loads at Subsonic Speeds. NACA RM L55E10a, 1955.
5. Strauss, L. H.: Study of External Store Separation. Aircraft Armaments, Inc., ER-561, Contract NOa(s) 54-679-6. Final Rept. 6-1-54 to 2-28-55.  $M = 0.5$  to  $1.0$ .
6. Smith, Norman F., and Carlson, Harry W.: The Origin and Distribution of Supersonic Store Interference From Measurement of Individual Forces on Several Wing-Fuselage-Store Configurations. III.- Swept-Wing Fighter-Bomber Configuration With Large and Small Stores. Mach Number, 1.61. NACA RM L55H01, 1955.
7. Martin, John C., Diederich, Margaret S., and Bobbitt, Percy J.: A Theoretical Investigation of the Aerodynamics of Wing-Tail Combinations Performing Time-Dependent Motions at Supersonic Speeds. NACA TN 3072, 1954.

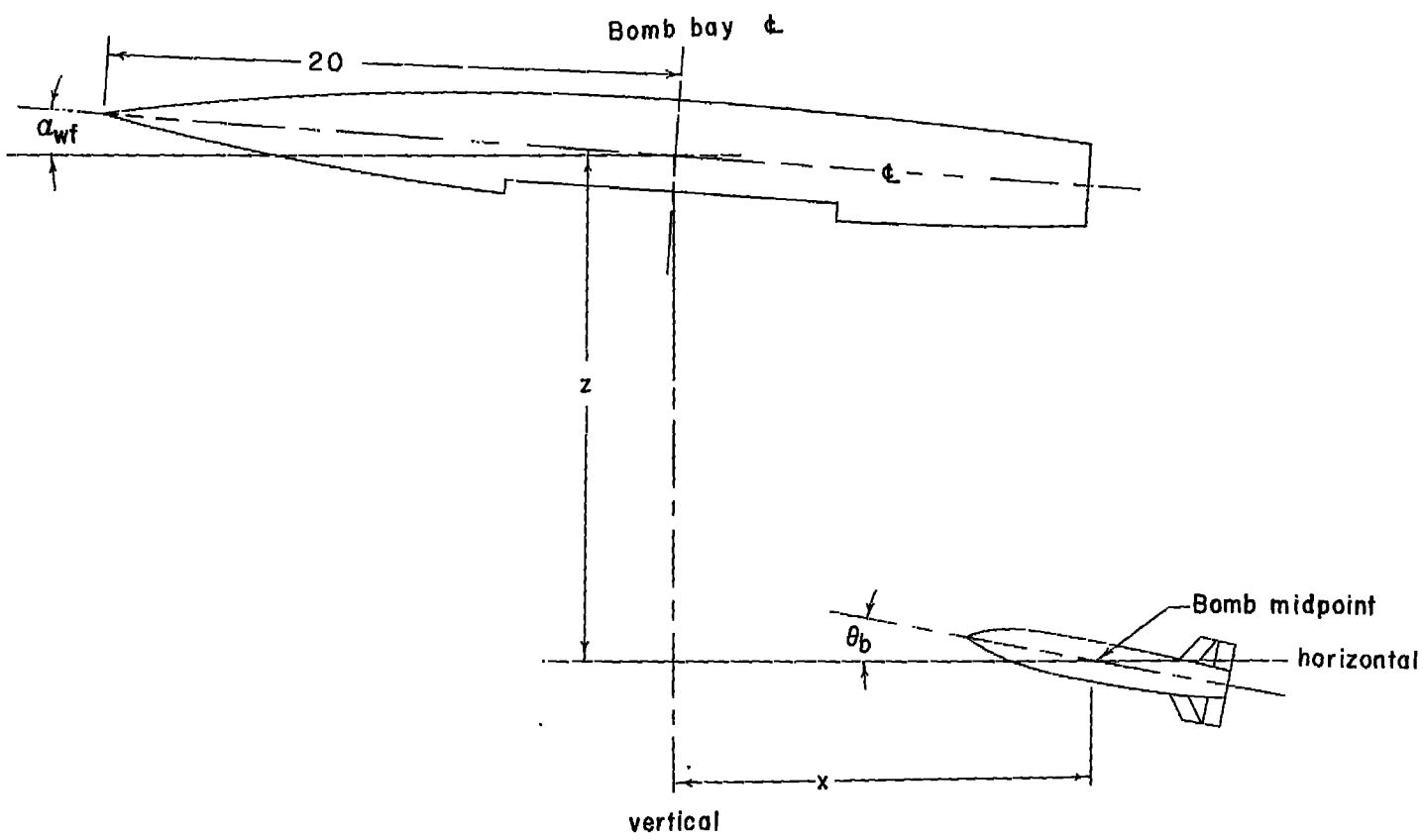
TABLE I  
INDEX TO CONFIGURATIONS

Bomb	Fins	Wing	Basic data figure	Contour-plot figure
1	On	On	7	-----
1	Off	On	8	-----
2	On (large)	On	9	20, 21, 22
2	On (small)	On	10	-----
2	Off	On	11	-----
3	On	On	12	23, 24, 25
3	Off	On	13	-----
3	On	Off	14	-----



(a) Dimensions of components. All dimensions are in inches.

Figure 1.- Layout of model installation.



(b) Sketch showing x- and z-grid-system orientation for bombs.

Figure 1.- Concluded.

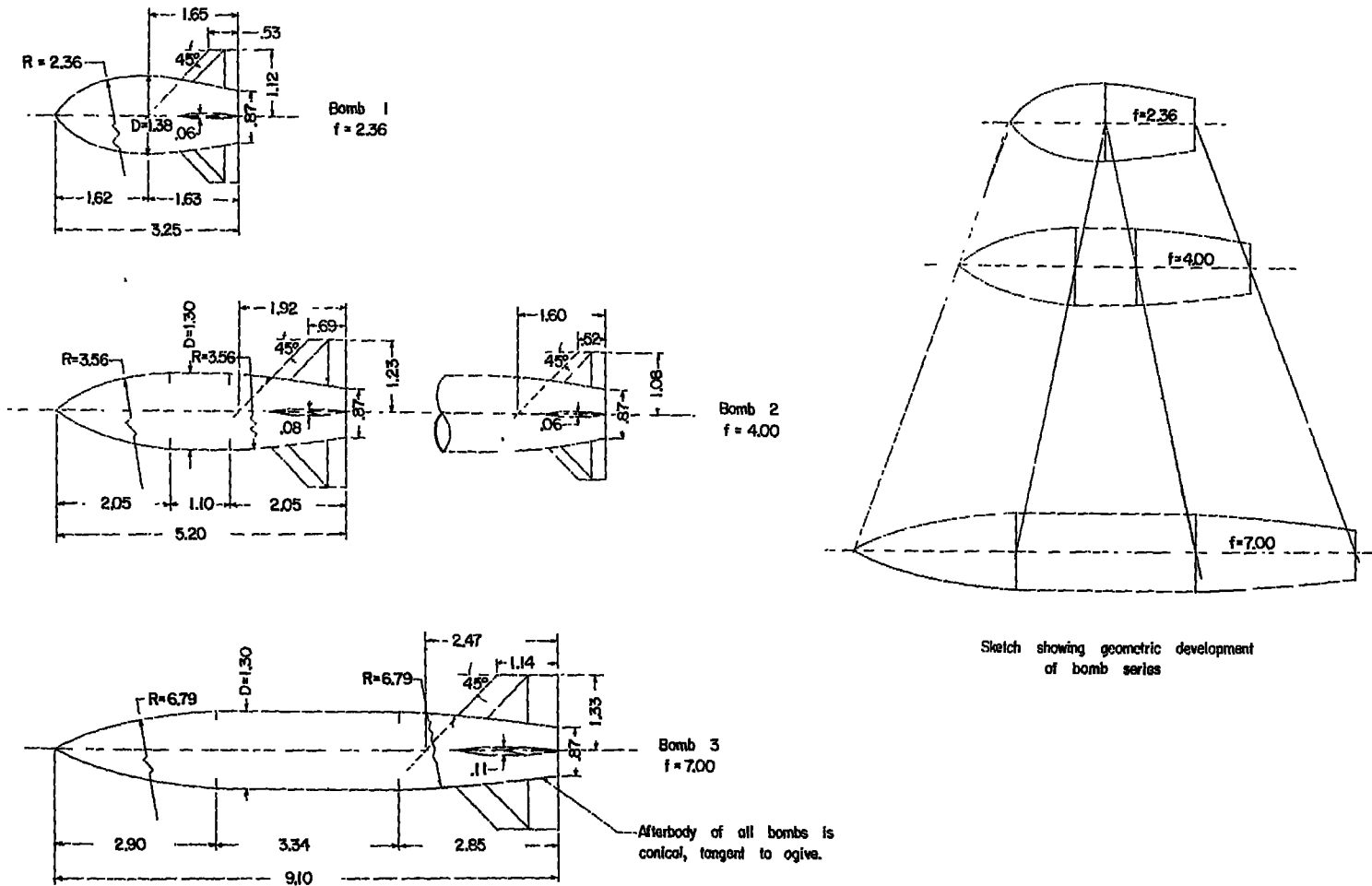
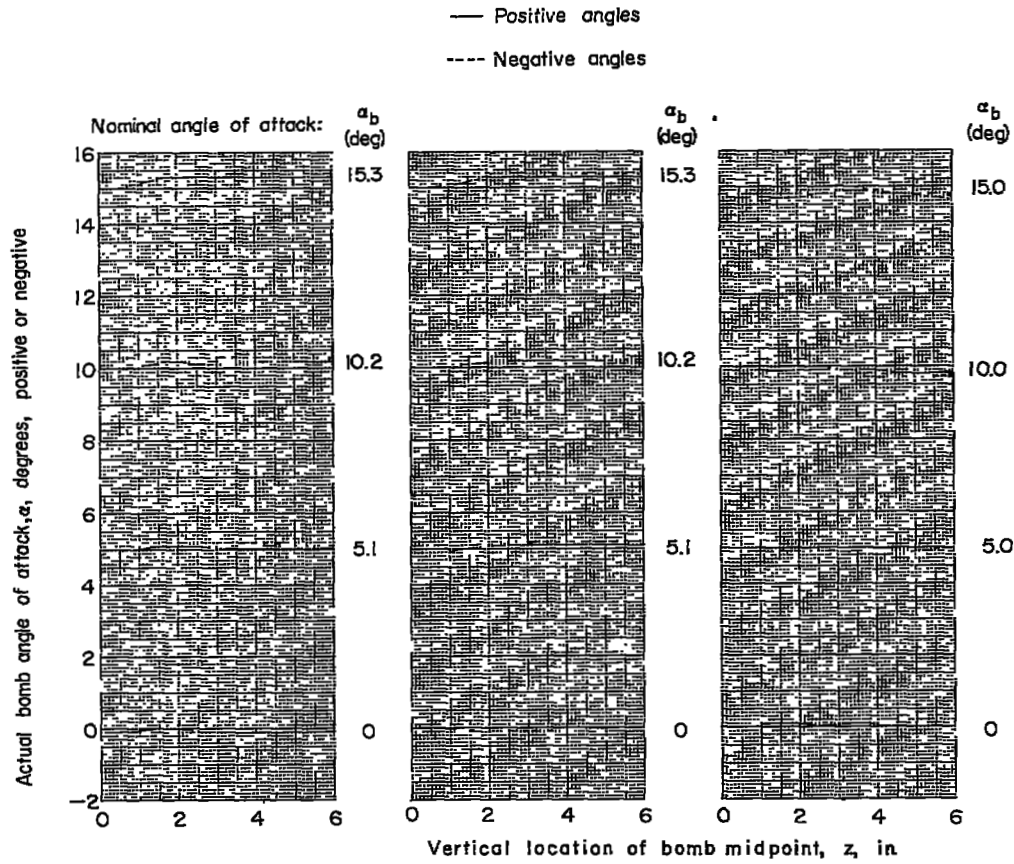


Figure 2.- Details and dimensions of bombs. All dimensions are in inches.



(a) Bomb 1;  $x = -2.55$  inches.      (b) Bomb 2;  $x = -2.55$  inches.      (c) Bomb 3;  $x = -0.15$  inch.

Figure 3.- Actual angles of attack (calculated from deflection calibrations) for three bombs. Nominal values of angle of attack  $\alpha_b$  chosen for use with the corresponding force data are shown.  $\alpha_{wf} = 4^\circ$ .

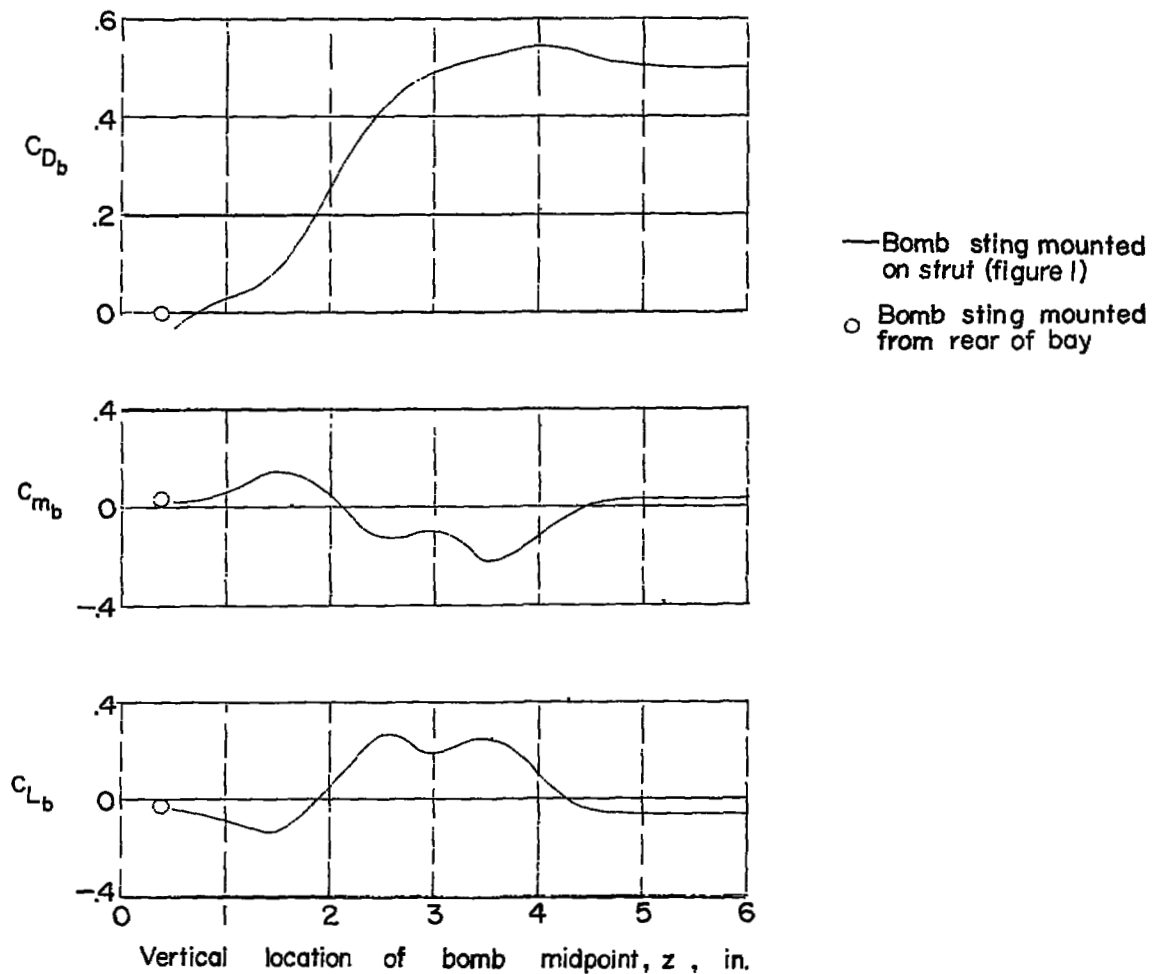


Figure 4.- Comparison of forces measured on bomb with and without bomb-support strut. Bomb 2; large fins;  $x = 0.95$  inch;  $\alpha_{wf} = 0^\circ$ ;  $\alpha_b = 0^\circ$ .

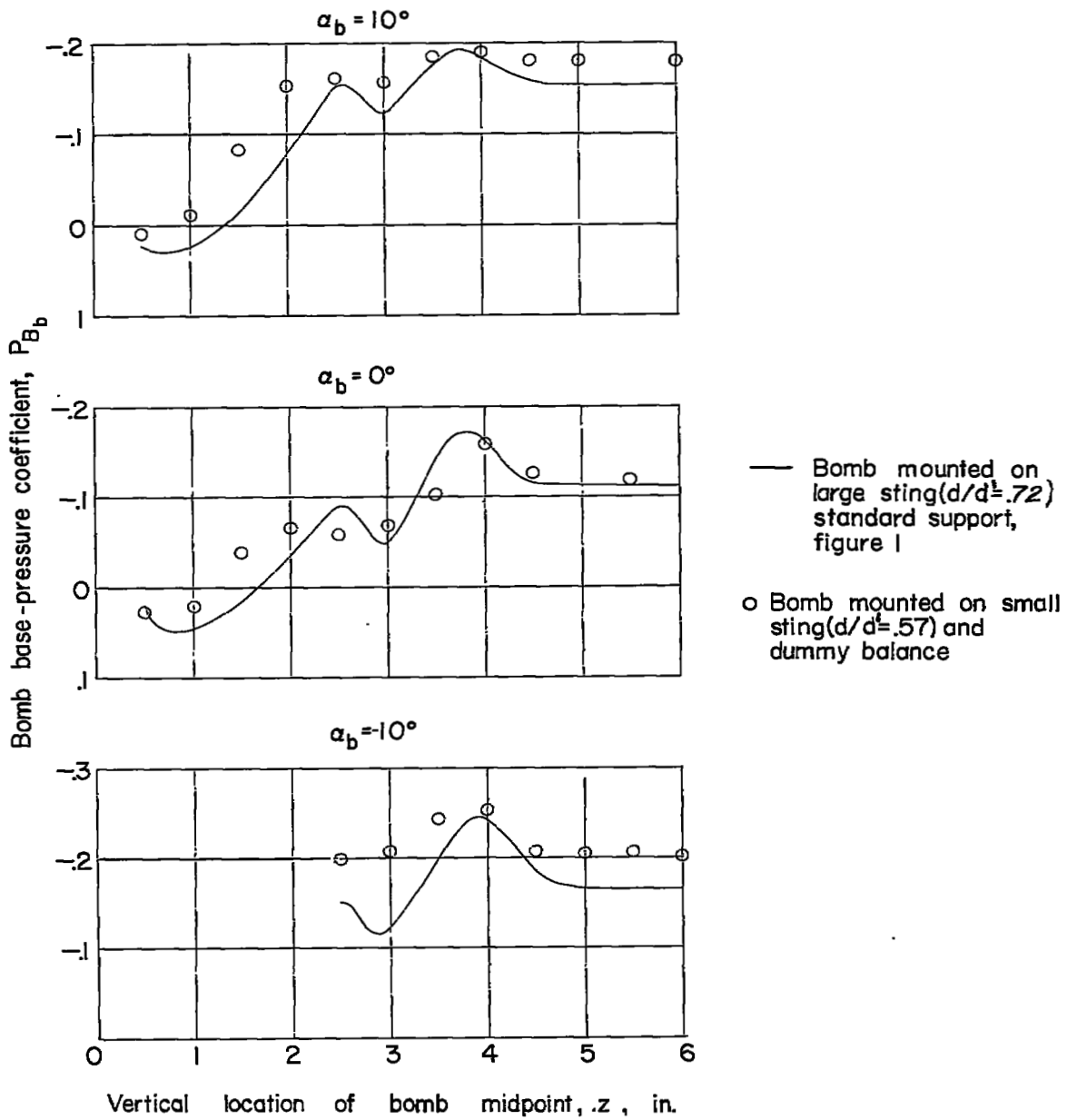
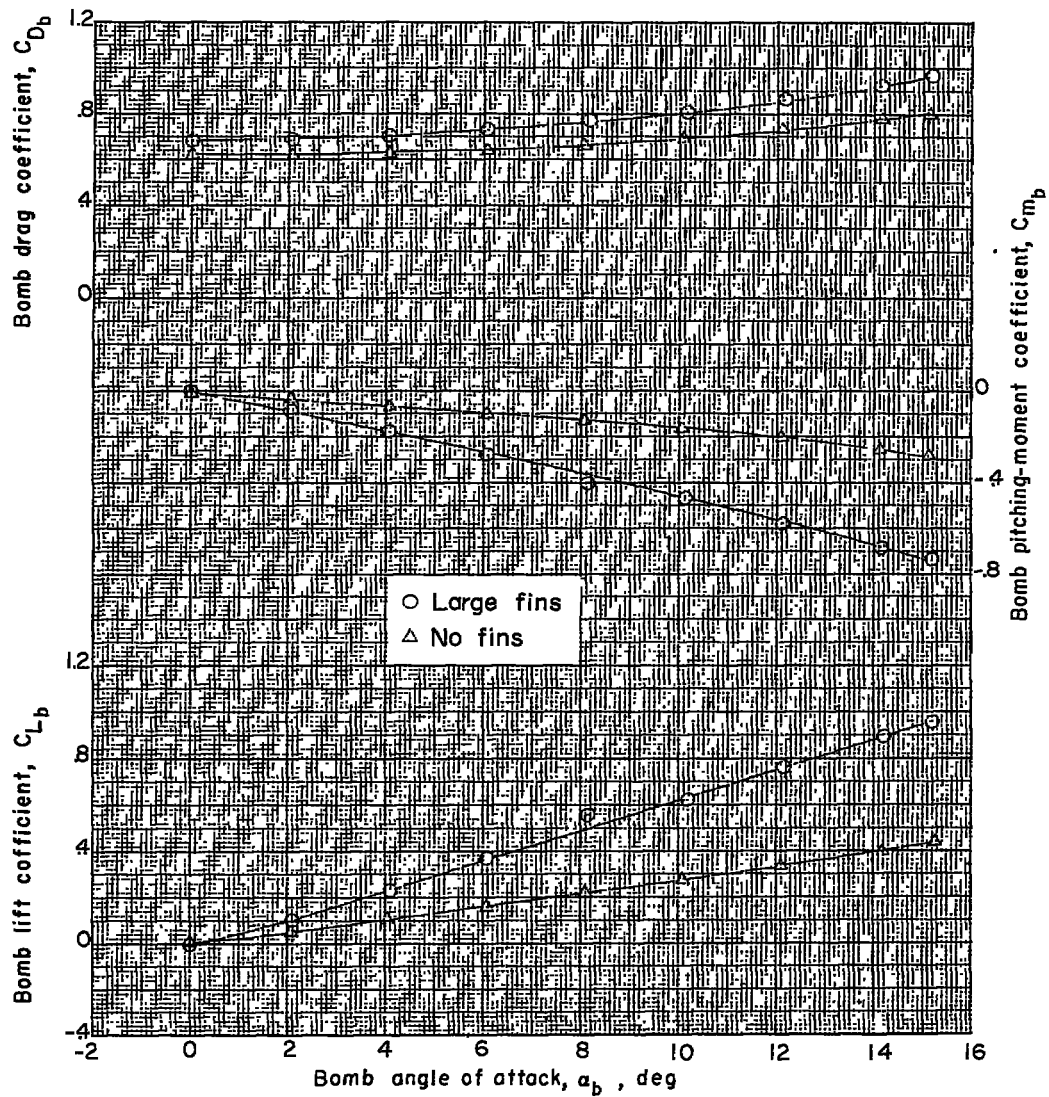
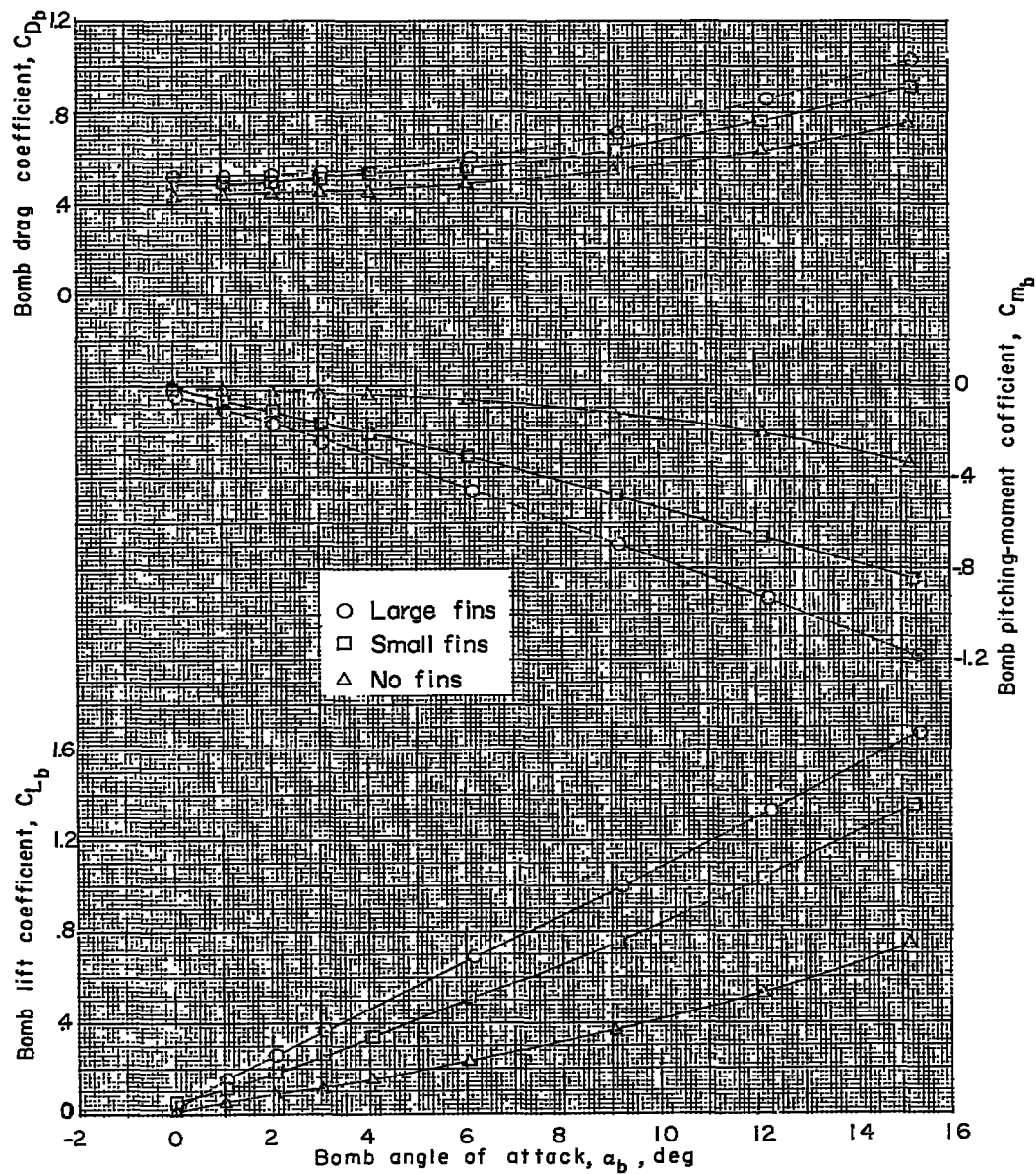


Figure 5.- Comparison of bomb base pressures measured with support stings of large and small diameters.  $x = -2.55$  inches;  $\alpha_{WF} = 40^\circ$ ; bomb 2.



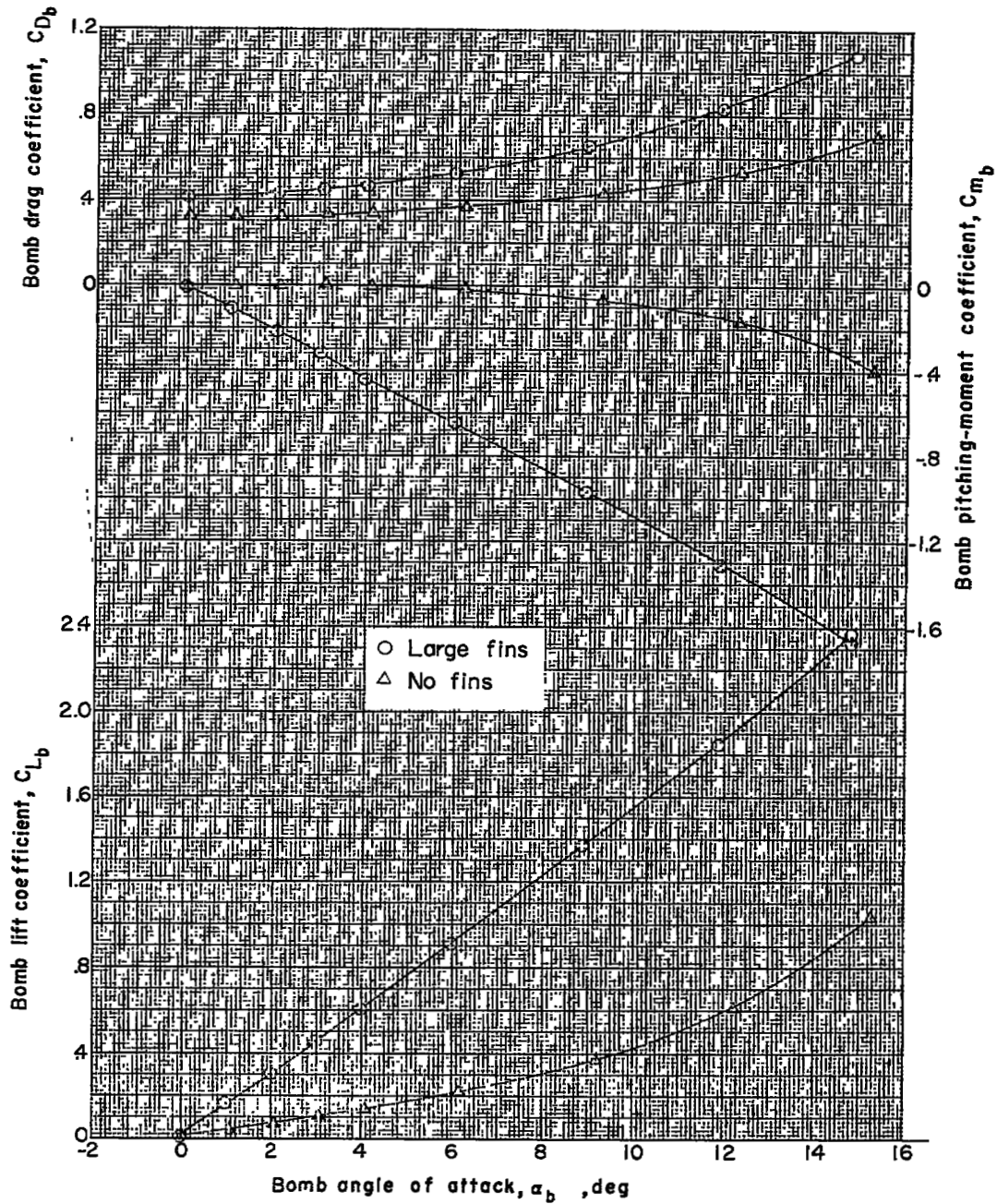
(a) Bomb 1.

Figure 6.- Aerodynamic characteristics of the isolated bomb.



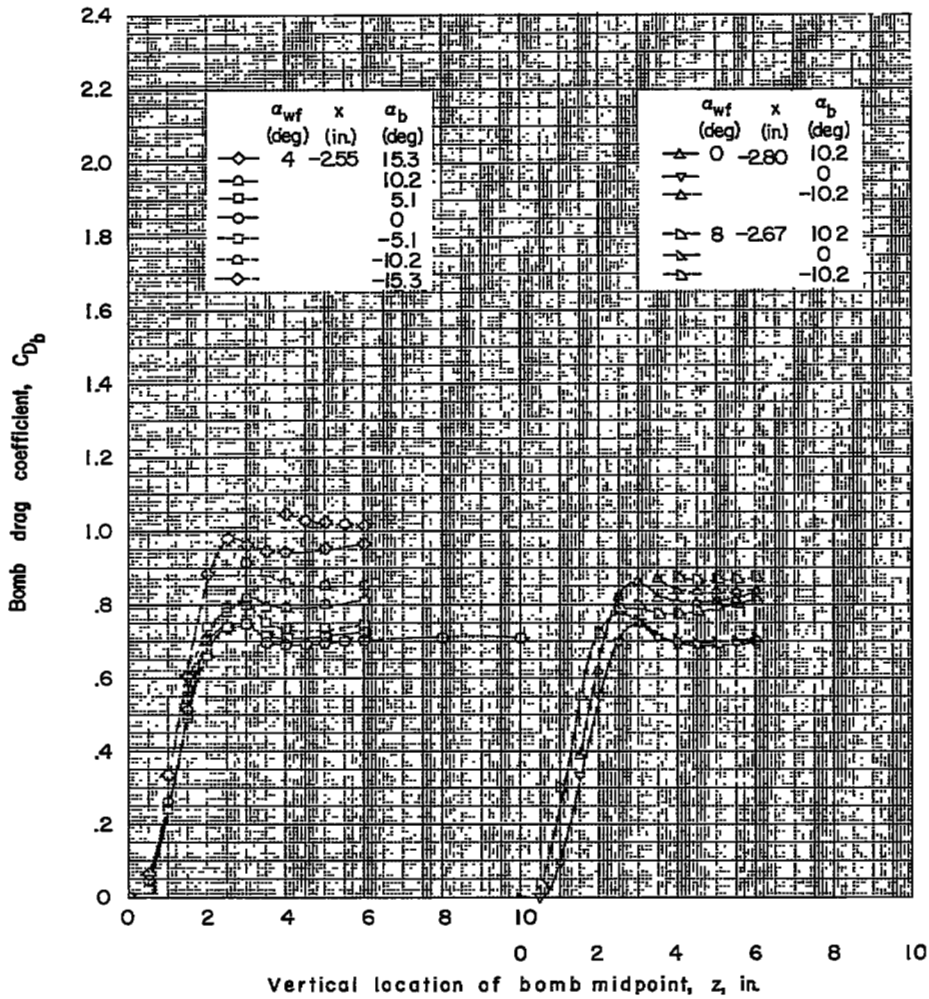
(b) Bomb 2.

Figure 6.- Continued.



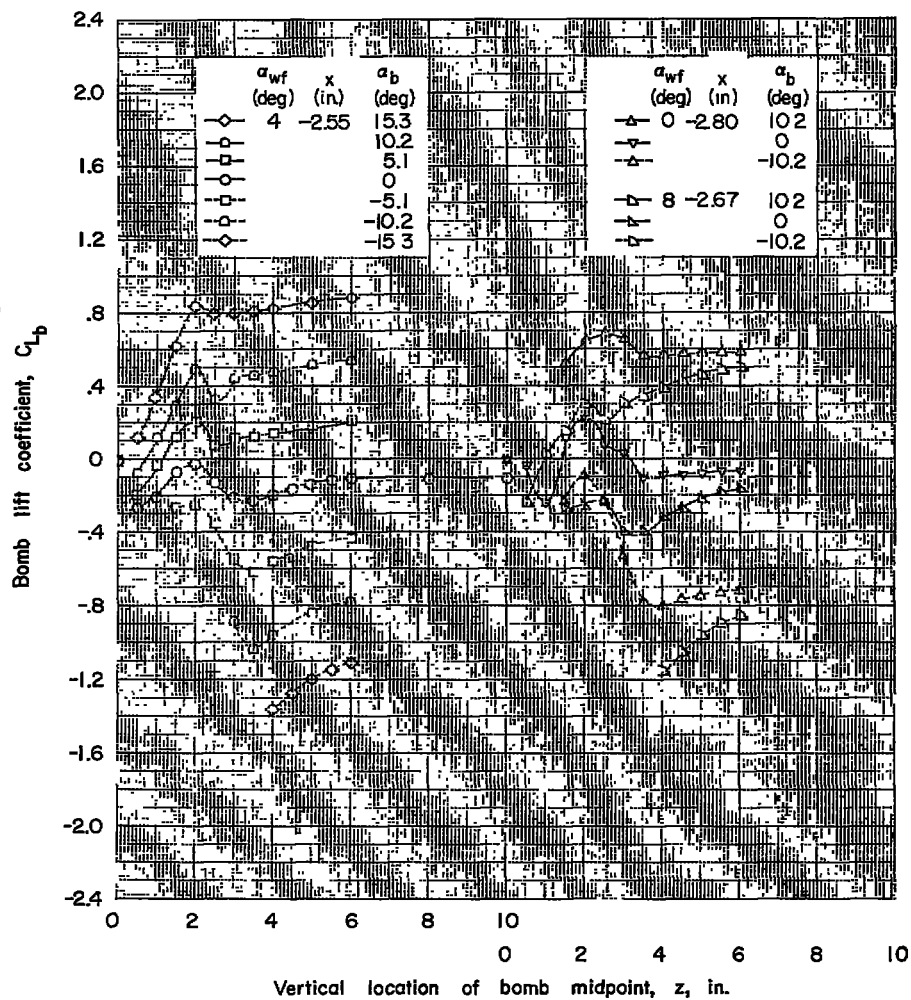
(c) Bomb 3.

Figure 6.- Concluded.



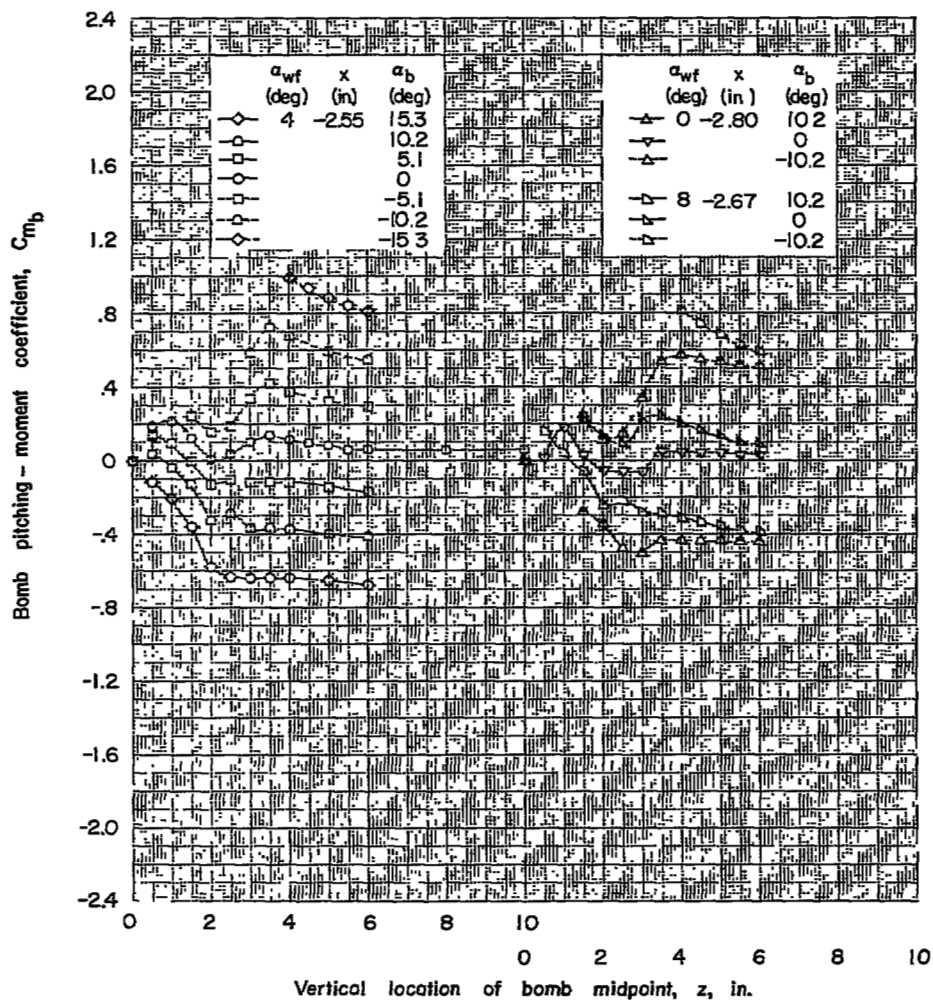
(a)  $x = -2.55$  to  $-2.80$  inches.

Figure 7.- Force data for bomb 1 in presence of wing-fuselage combination. Fins on.



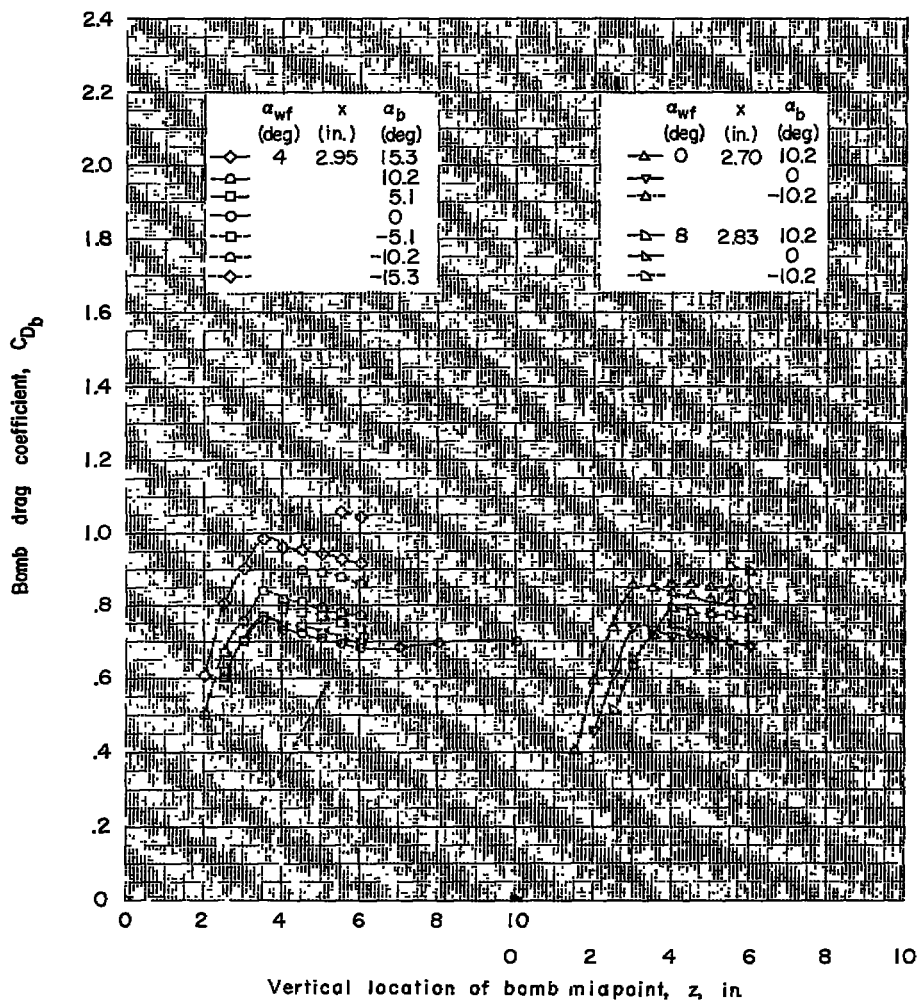
(a) Continued.

Figure 7.- Continued.



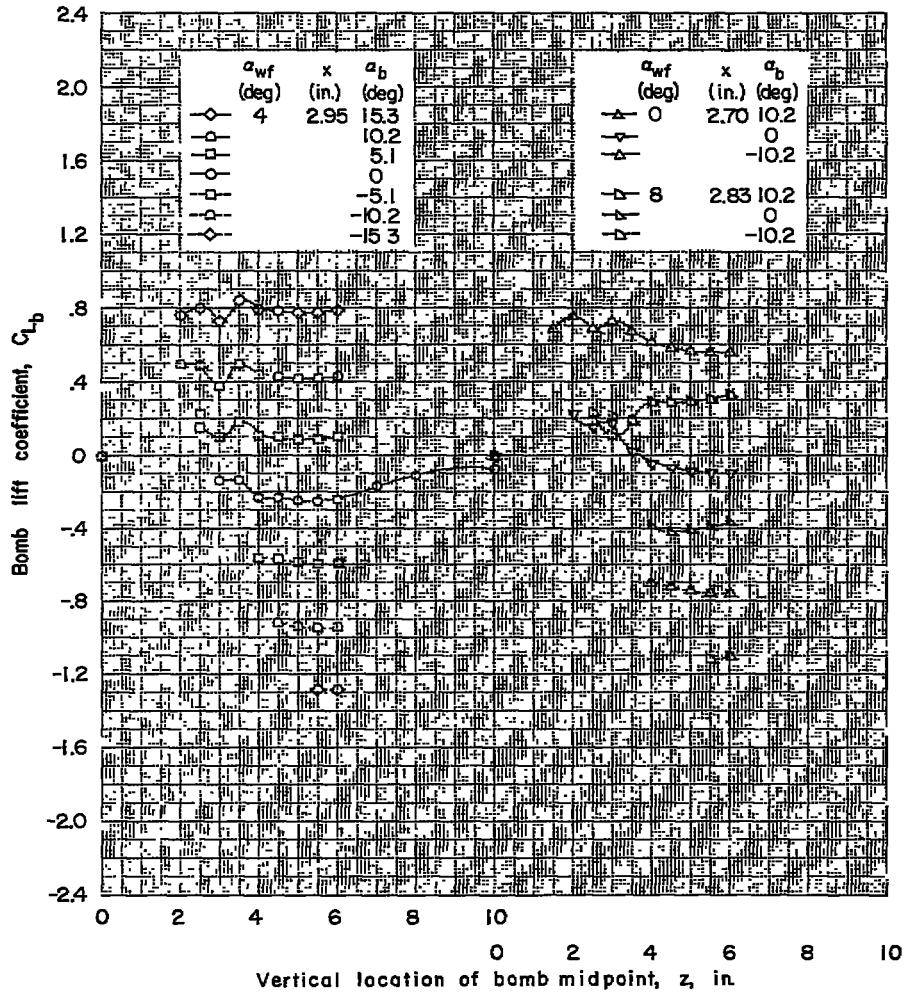
(a) Concluded.

Figure 7.- Continued.



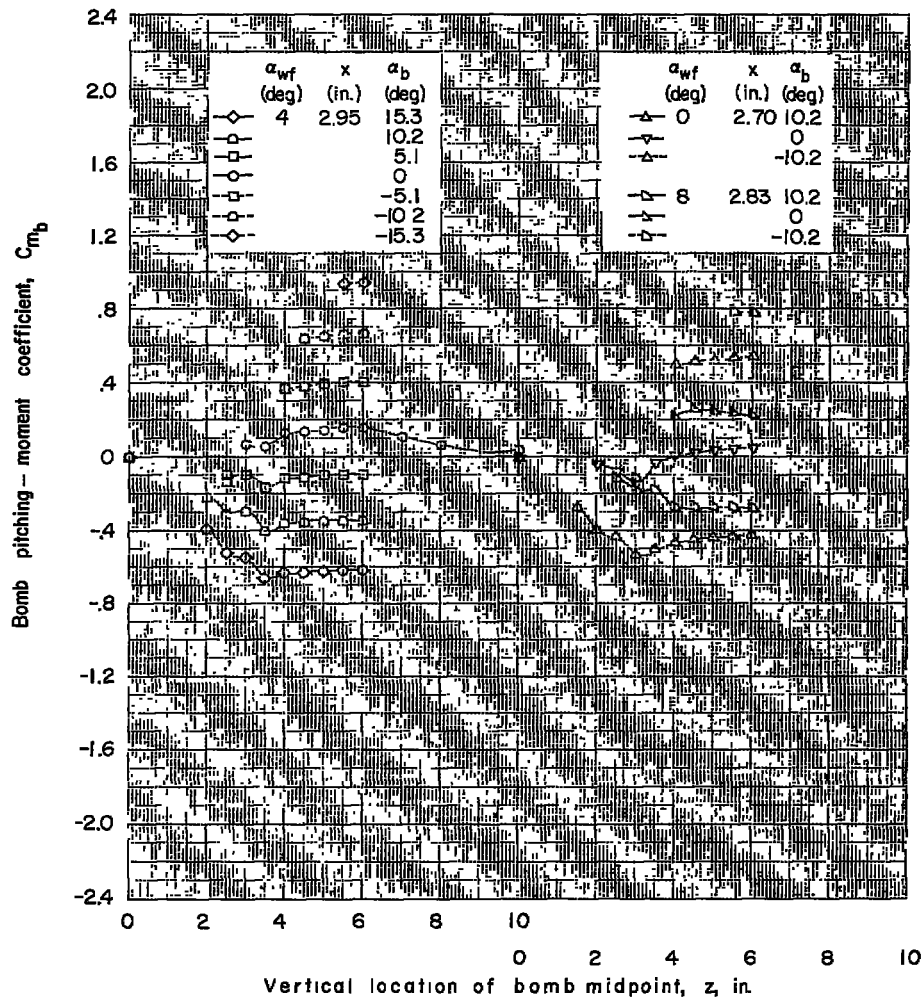
(b)  $x = 2.70$  to  $2.95$  inches.

Figure 7.- Continued.



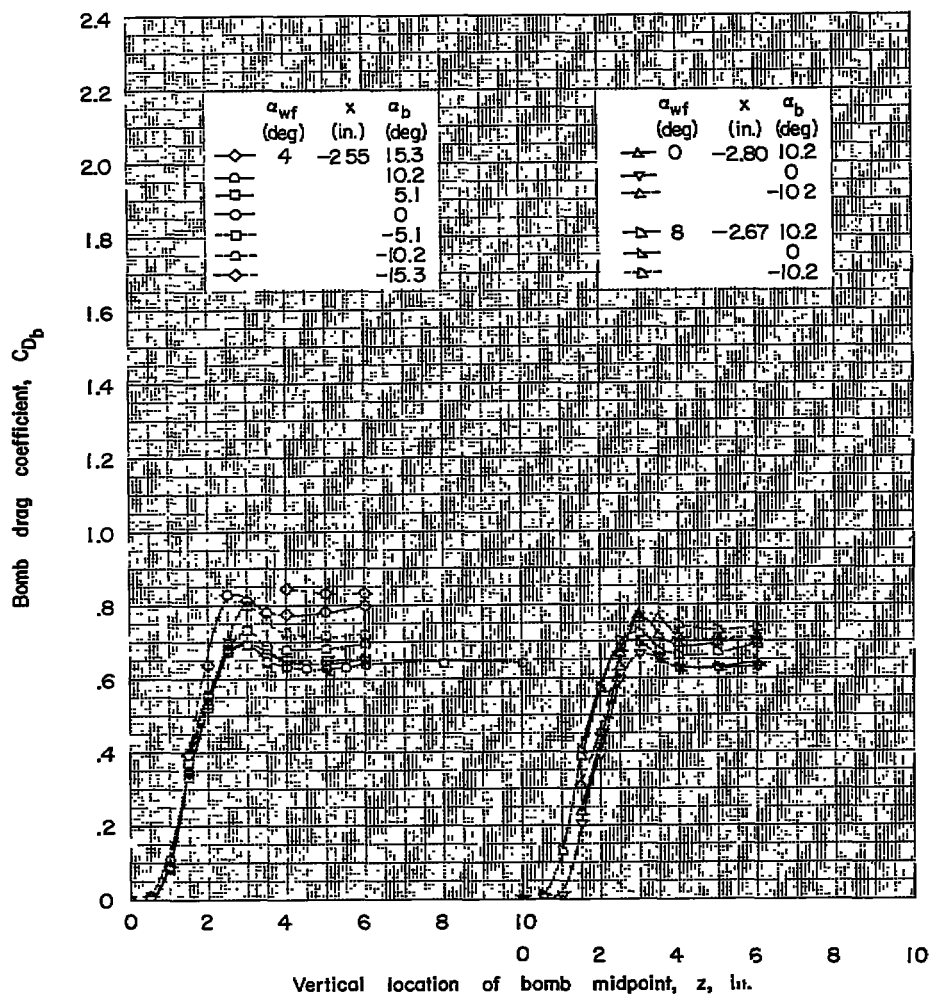
(b) Continued.

Figure 7.- Continued.



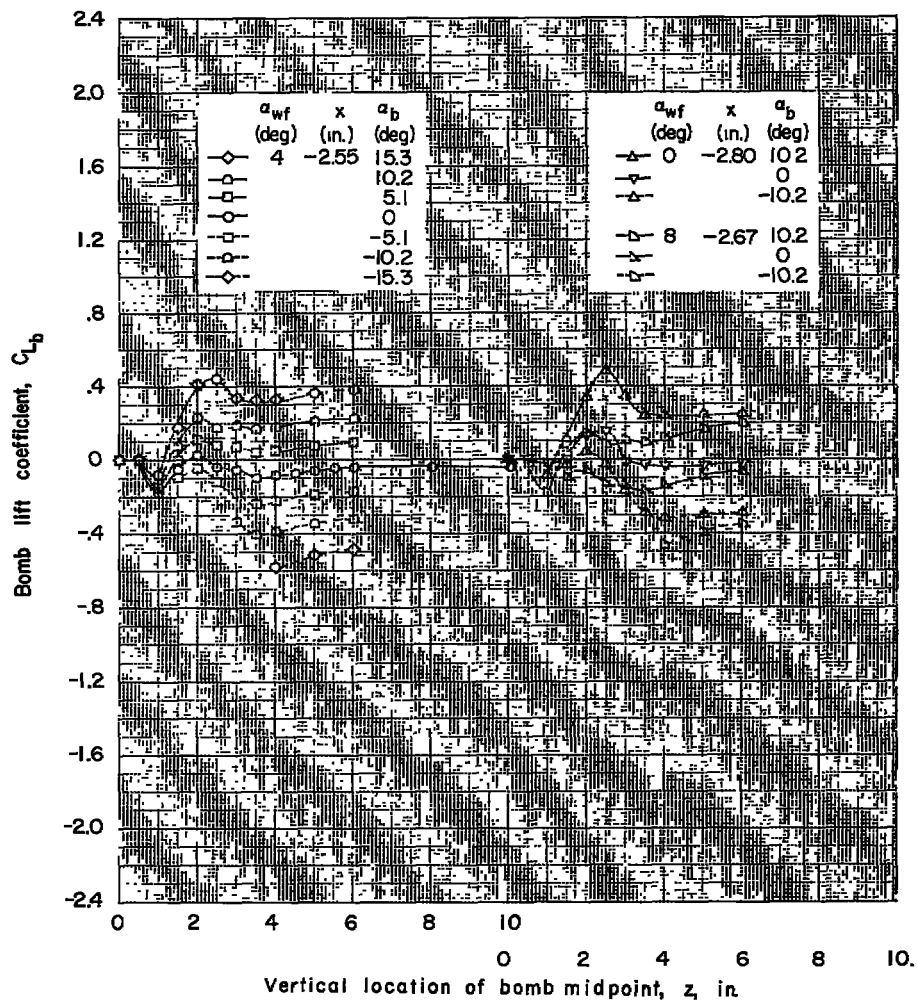
(b) Concluded.

Figure 7.- Concluded.



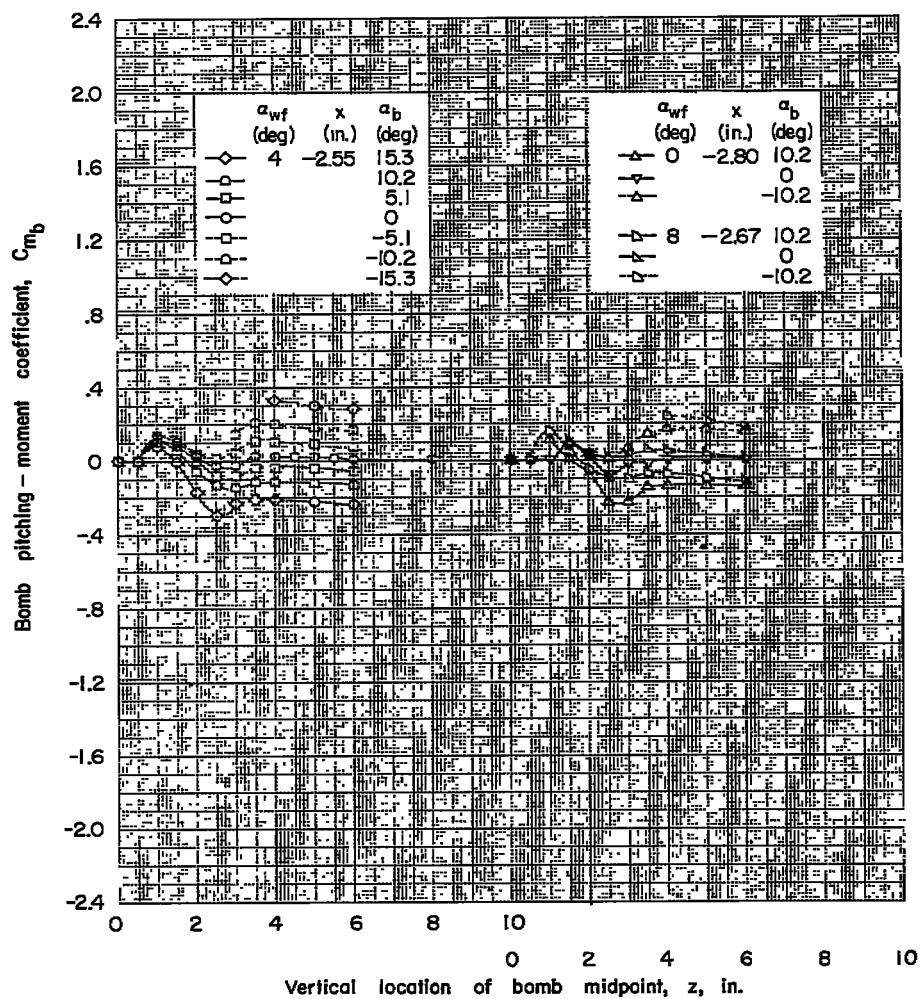
(a)  $x = -2.55$  to  $-2.80$  inches.

Figure 8.- Force data for bomb 1 in presence of wing-fuselage combination. Fins off.



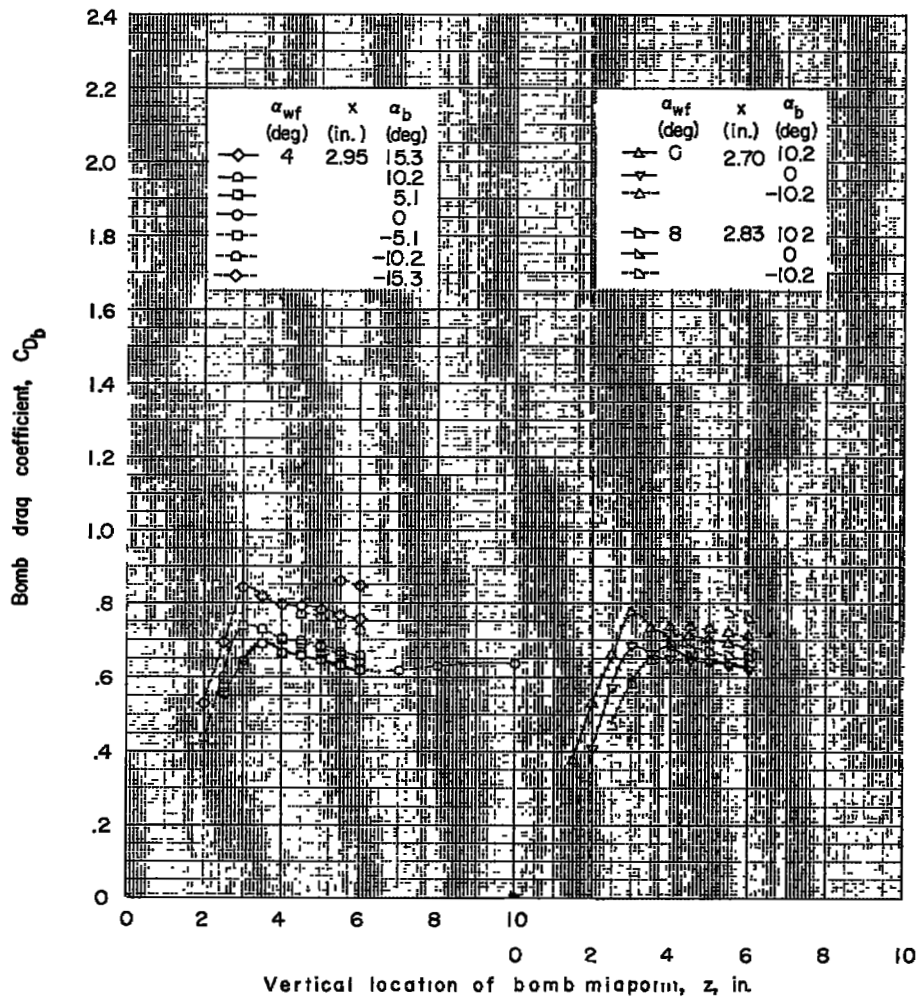
(a) Continued.

Figure 8.- Continued.



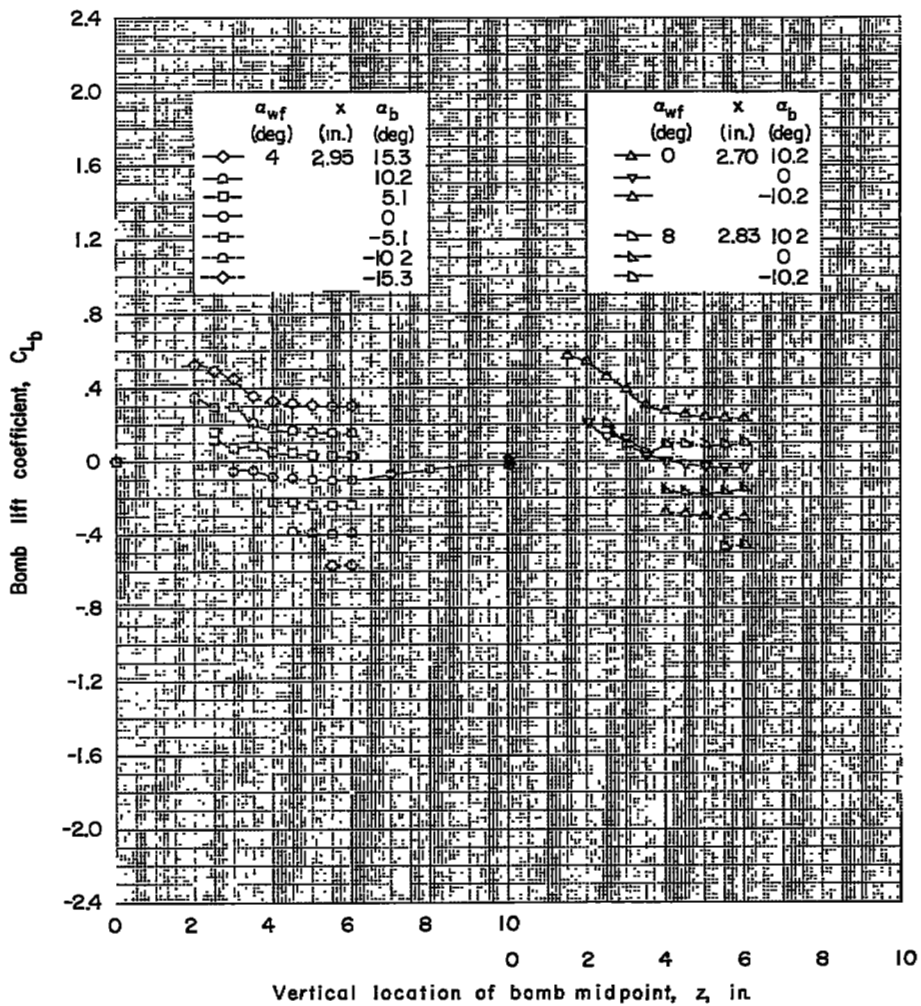
(a) Concluded.

Figure 8.- Continued.



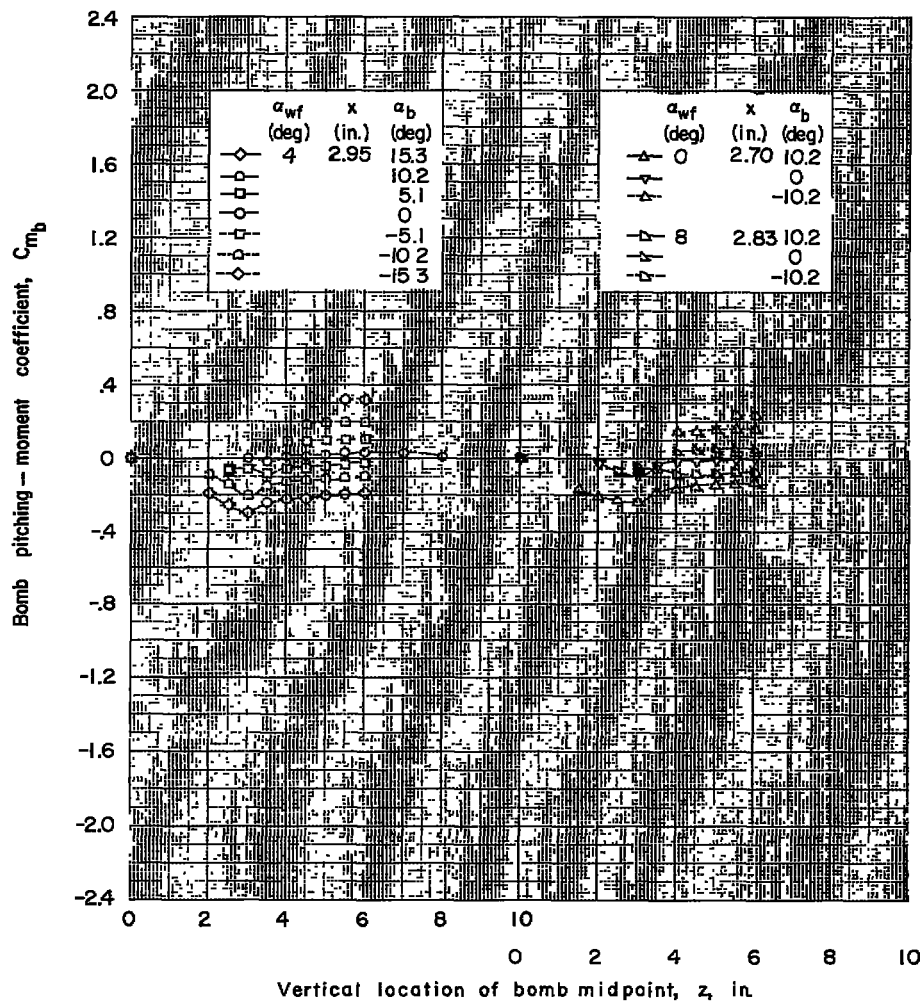
(b)  $x = 2.70$  to  $2.95$  inches.

Figure 8.- Continued.



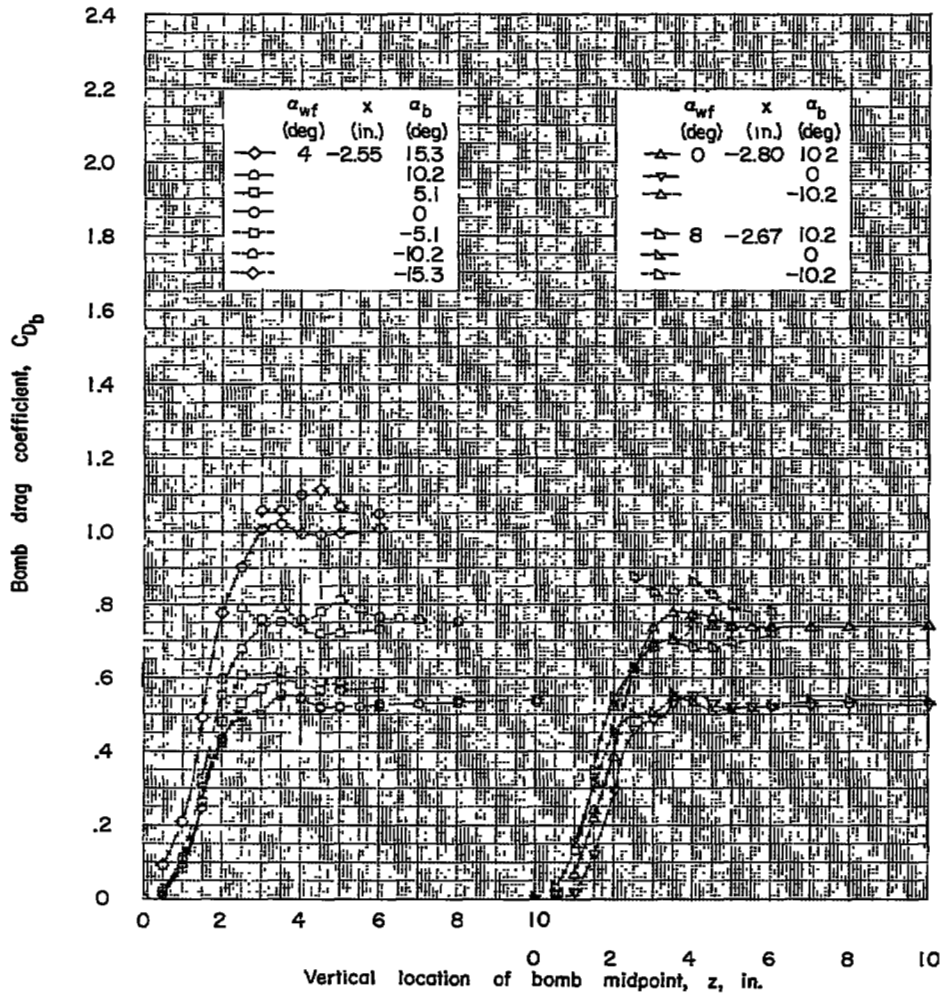
(b) Continued.

Figure 8.- Continued.



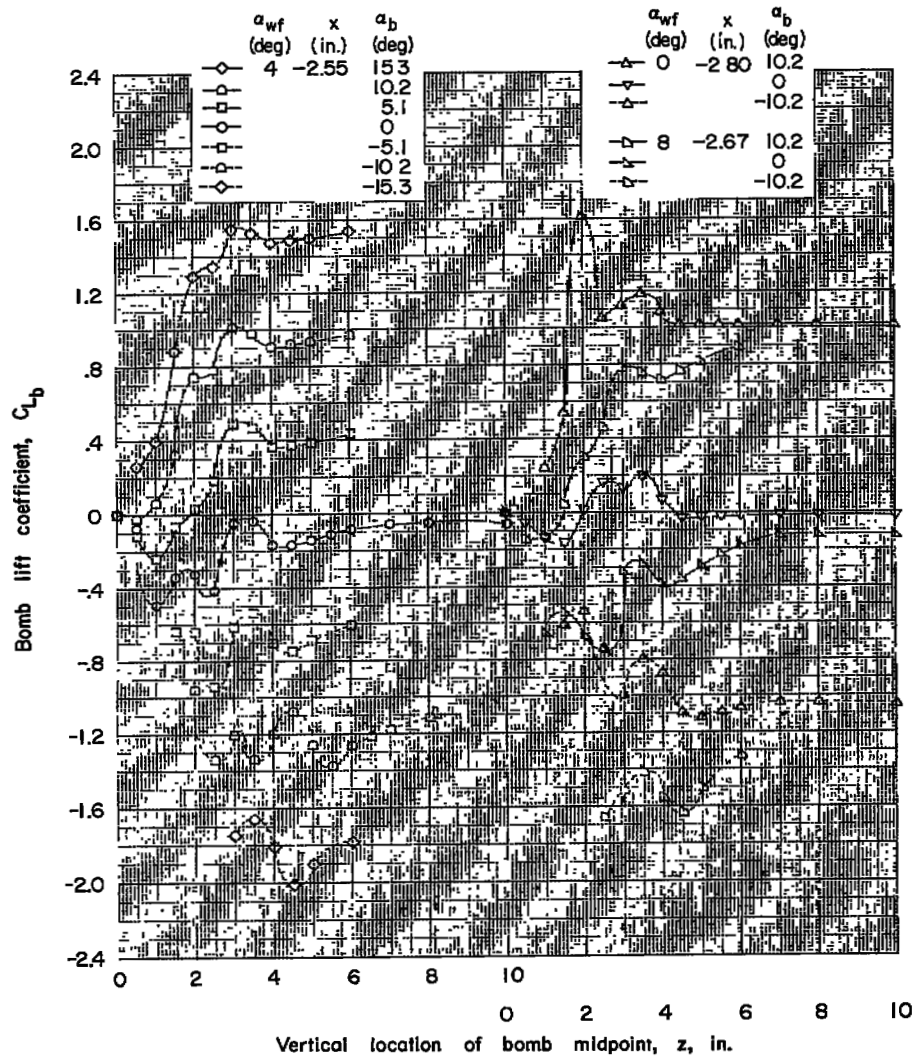
(b) Concluded.

Figure 8.- Concluded.



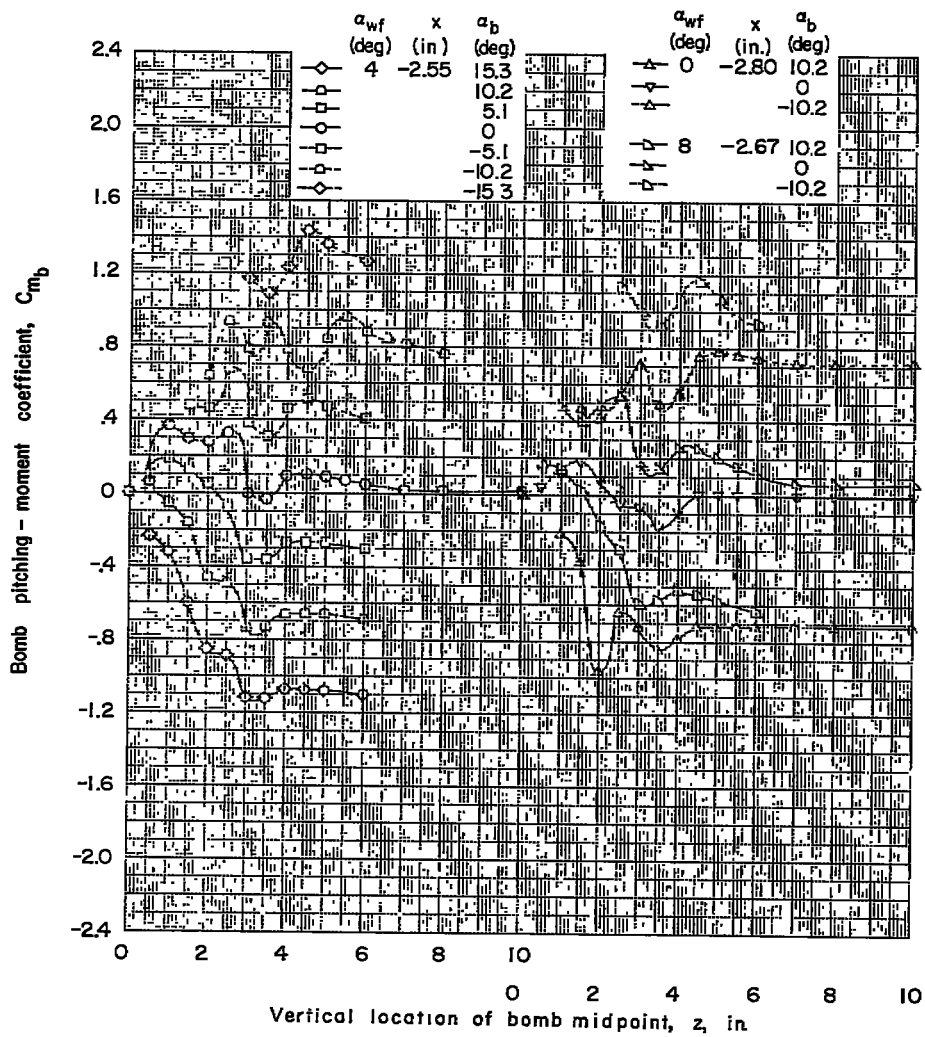
(a)  $x = -2.55$  to  $-2.80$  inches.

Figure 9.- Force data for bomb 2 in presence of wing-fuselage combination. Fins on.



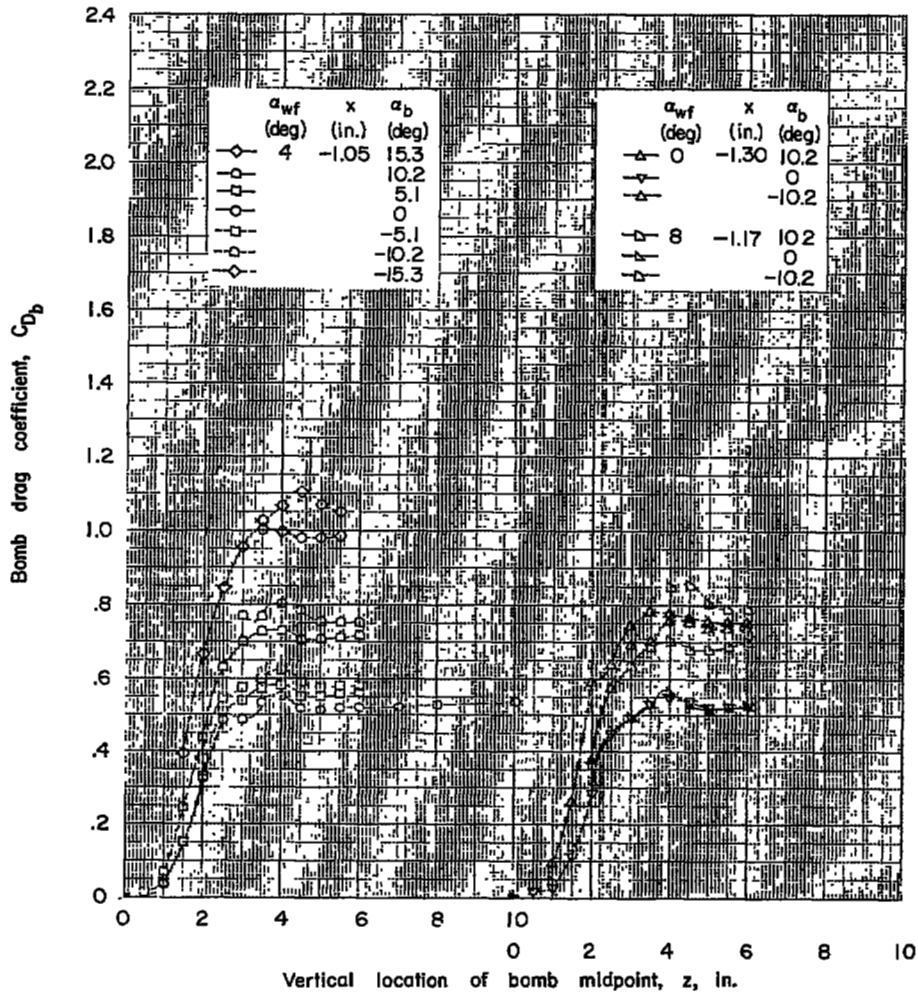
(a) Continued.

Figure 9.- Continued.



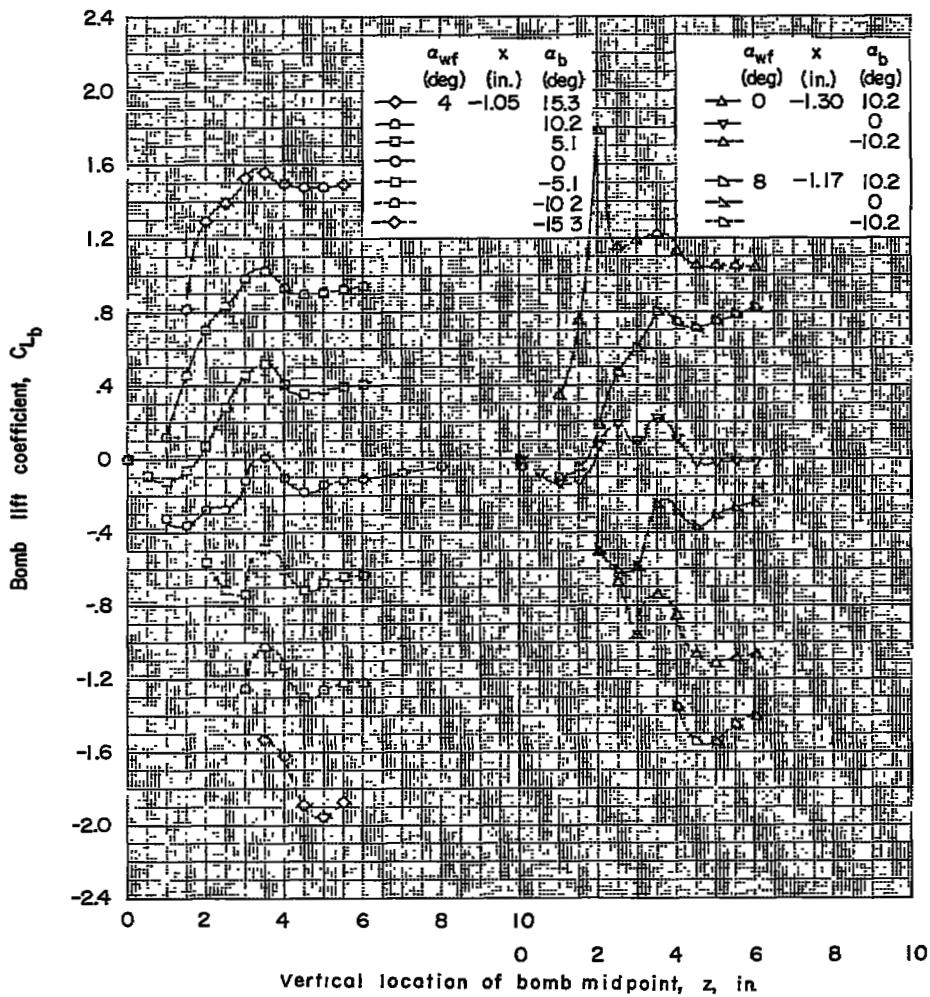
(a) Concluded.

Figure 9.- Continued.



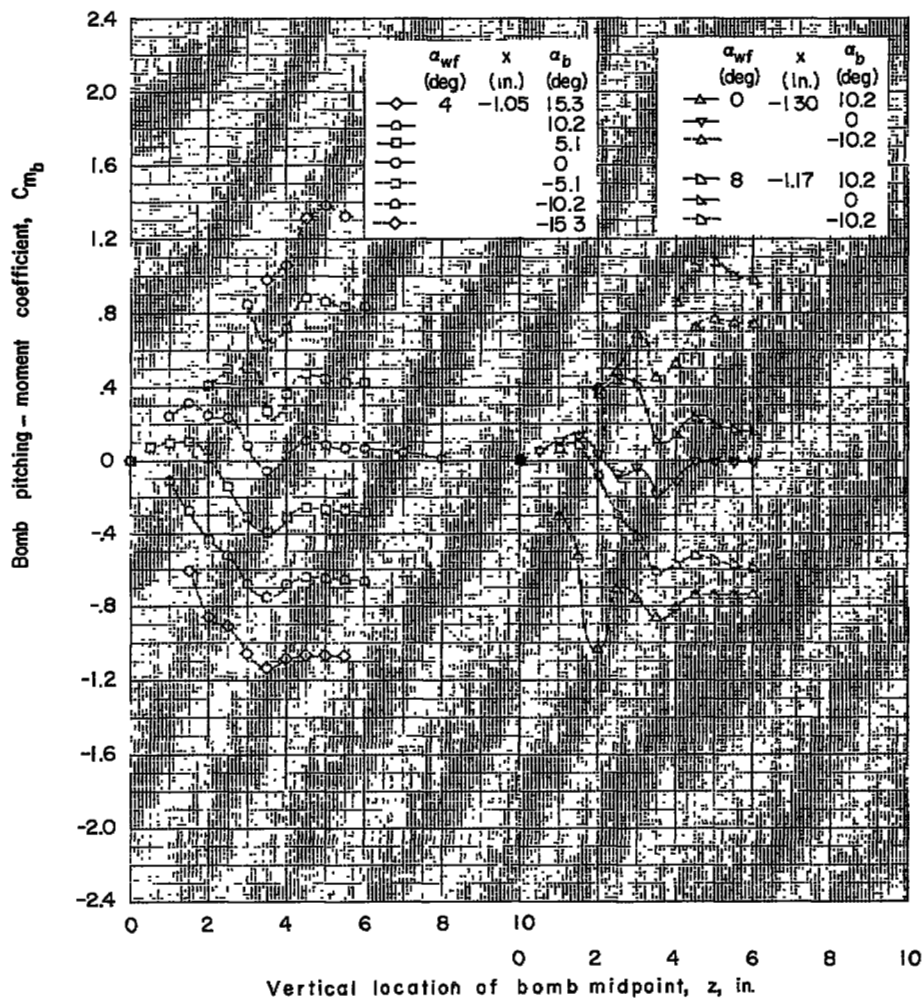
(b)  $x = -1.05$  to  $-1.30$  inches.

Figure 9.- Continued.



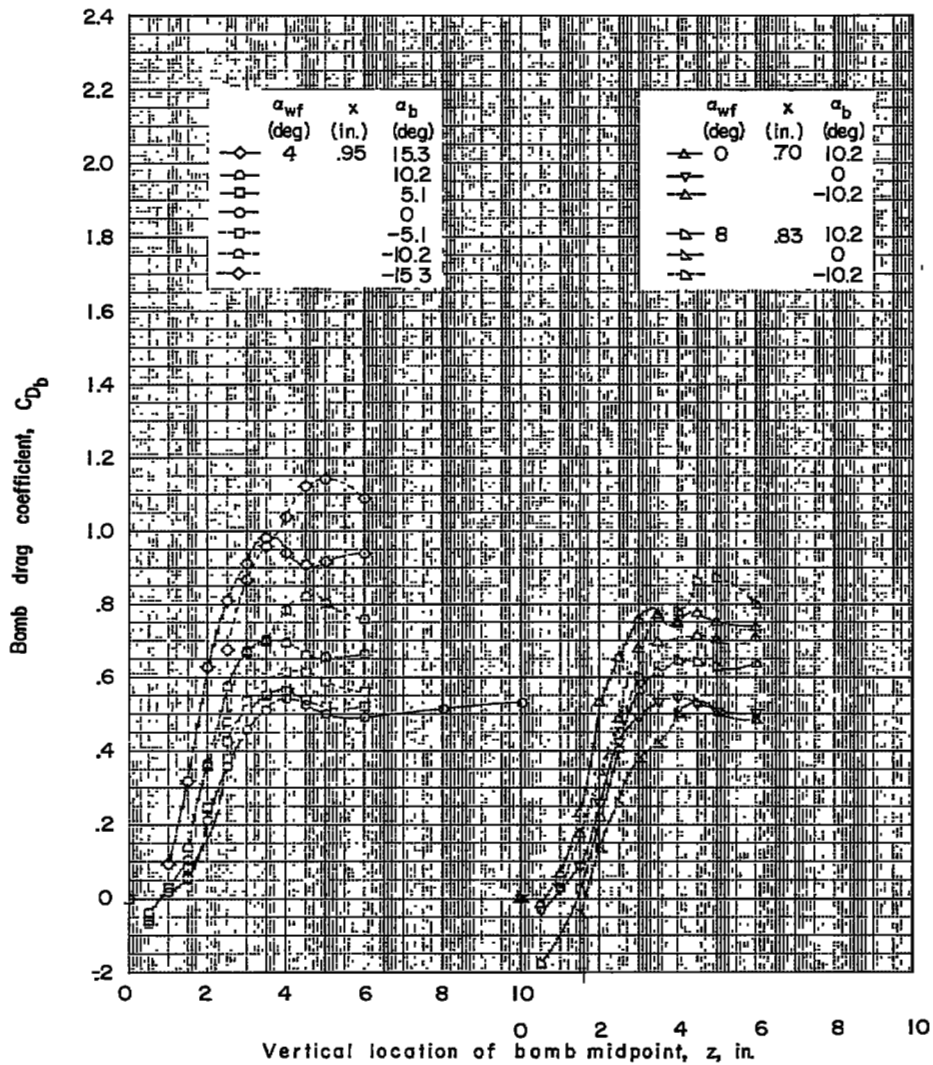
(b) Continued.

Figure 9.- Continued.



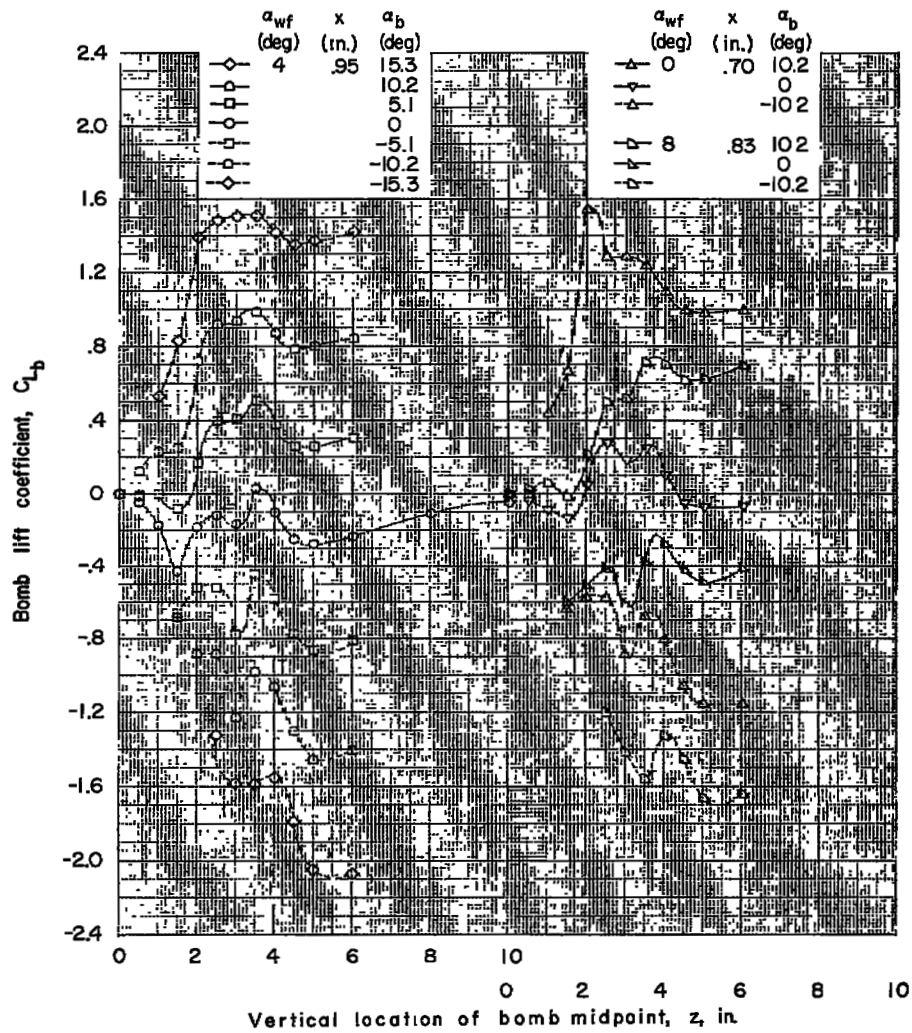
(b) Concluded.

Figure 9.- Continued.



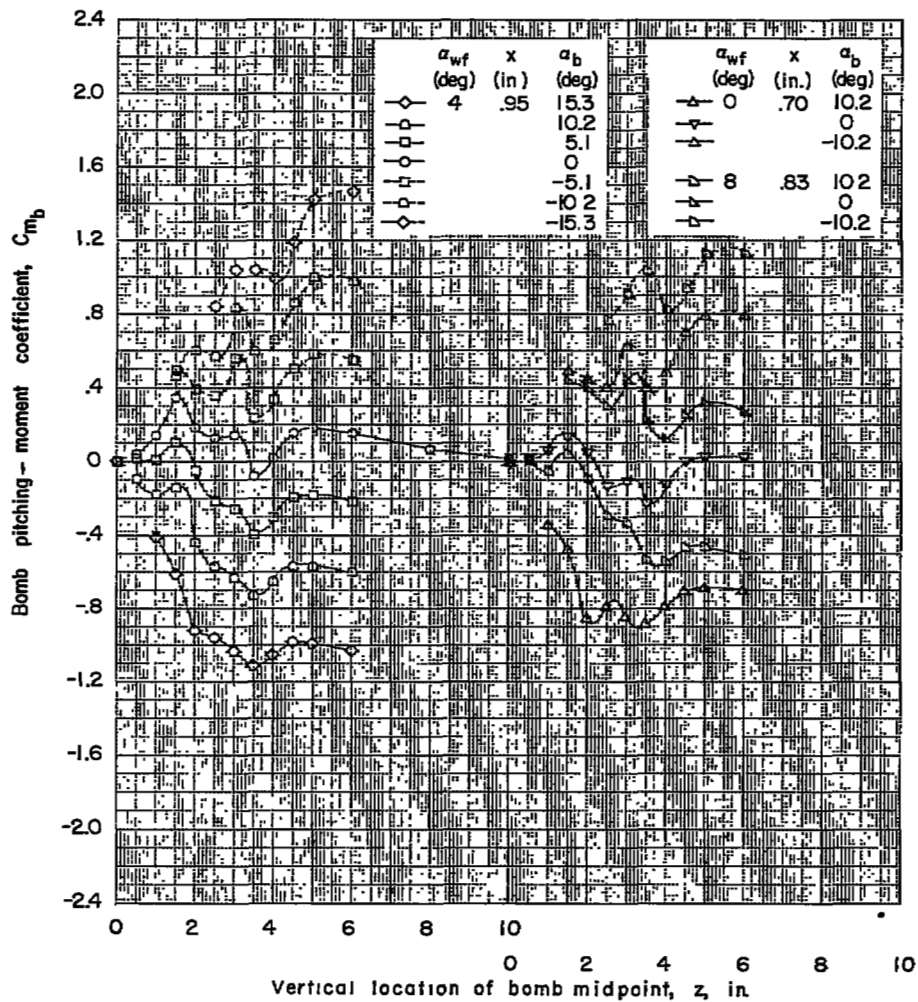
(c)  $x = 0.70$  to  $0.95$  inch.

Figure 9.- Continued.



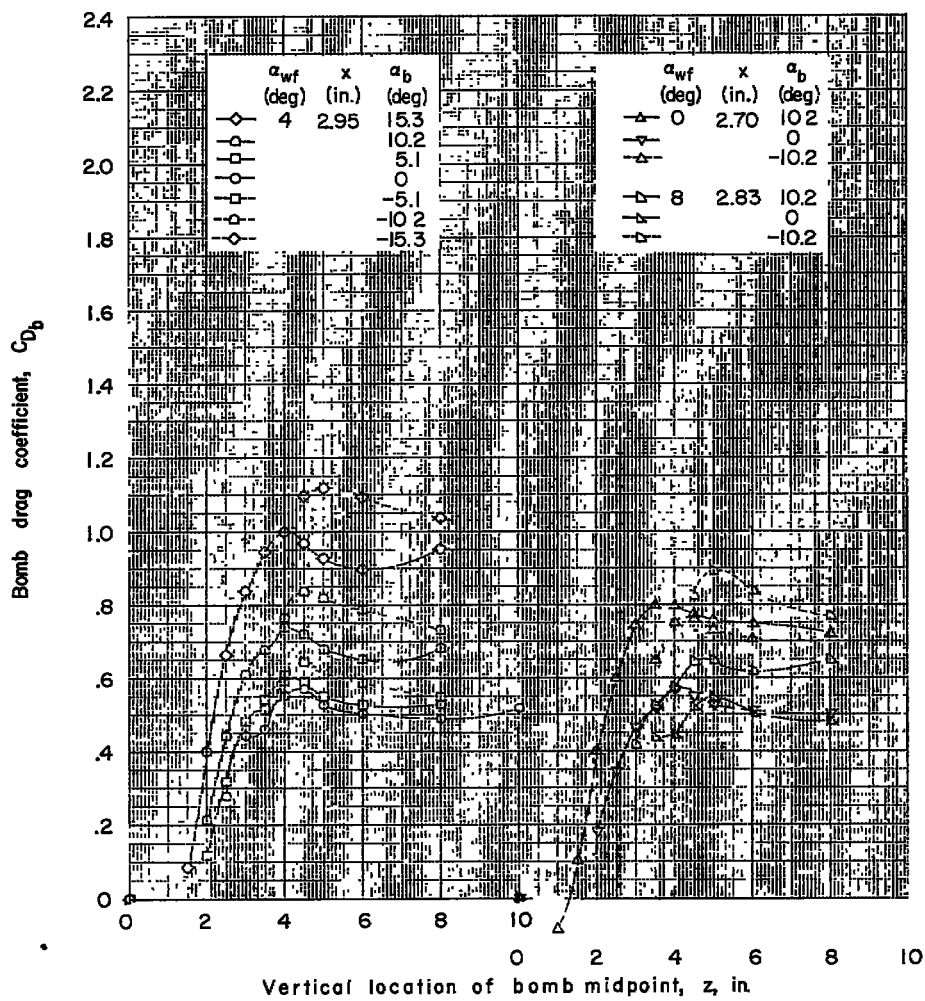
(c) Continued.

Figure 9.- Continued.



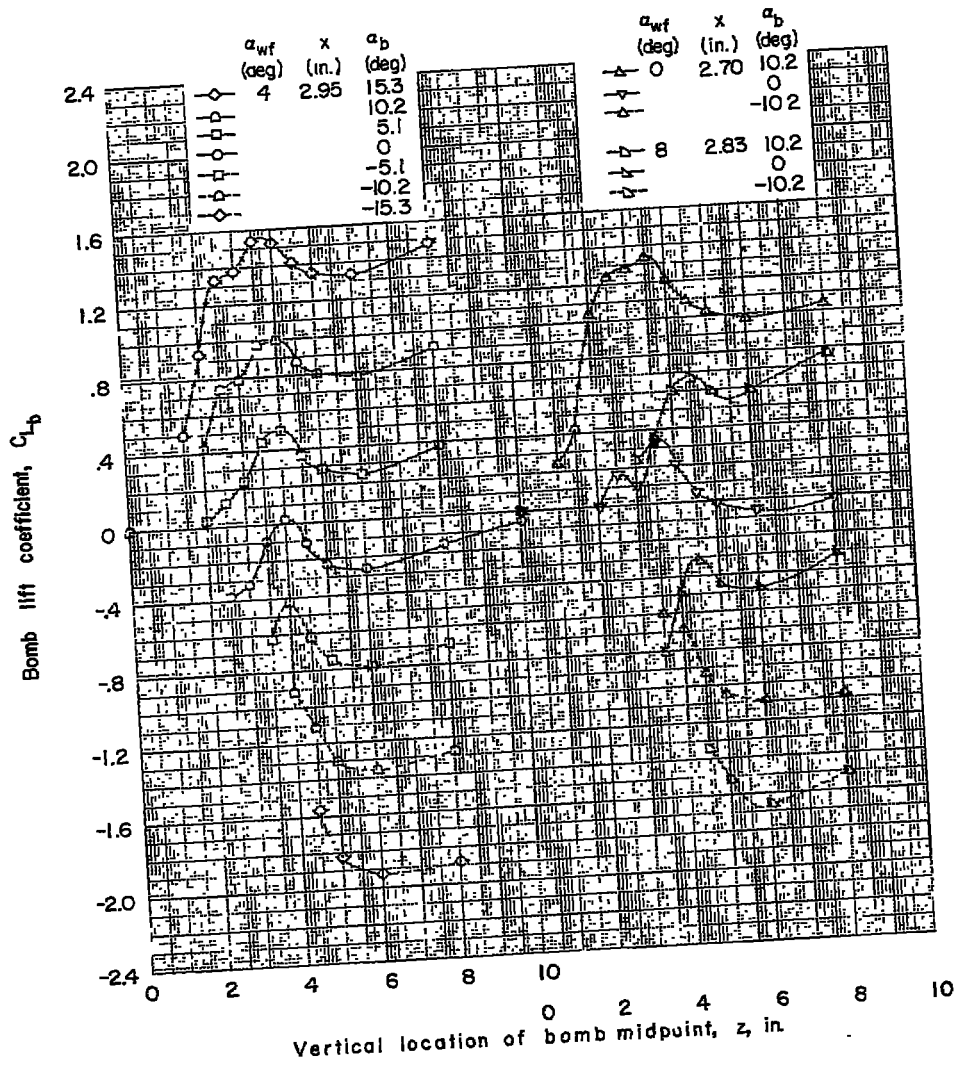
(c) Concluded.

Figure 9.- Continued.



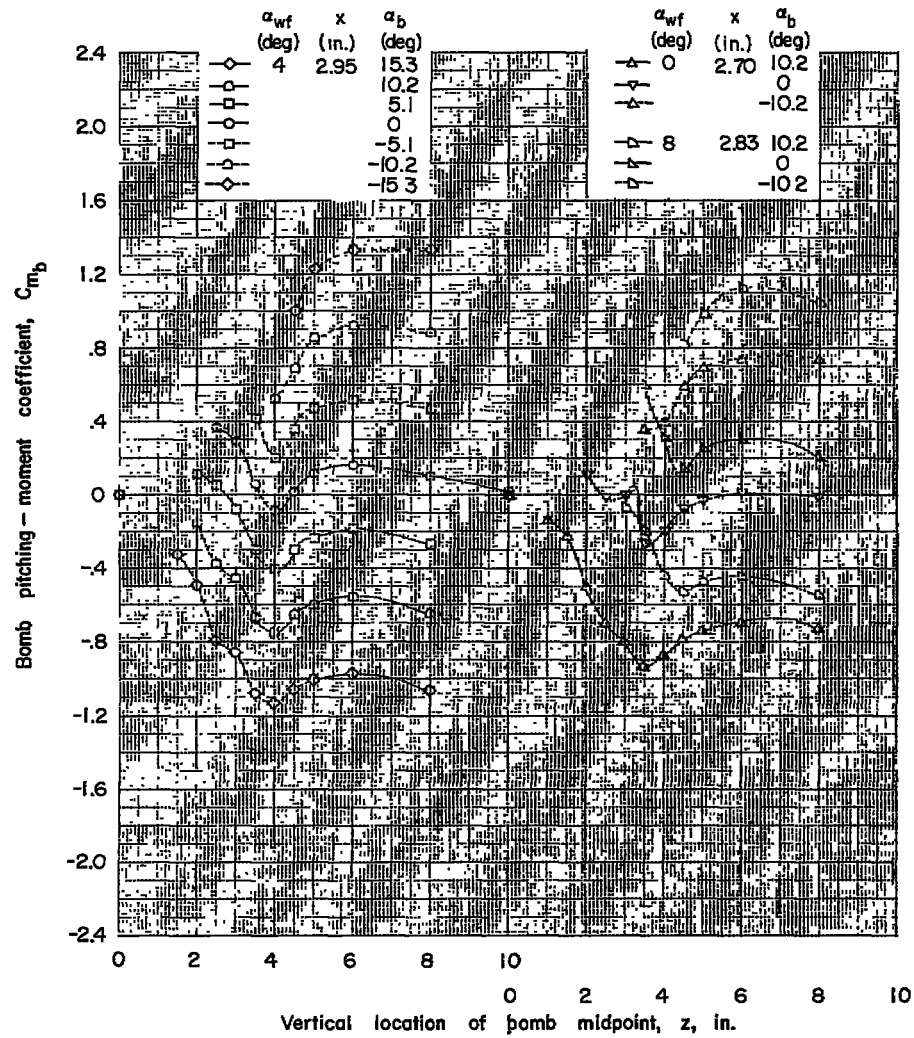
(d)  $x = 2.70$  to  $2.95$  inches.

Figure 9.- Continued.



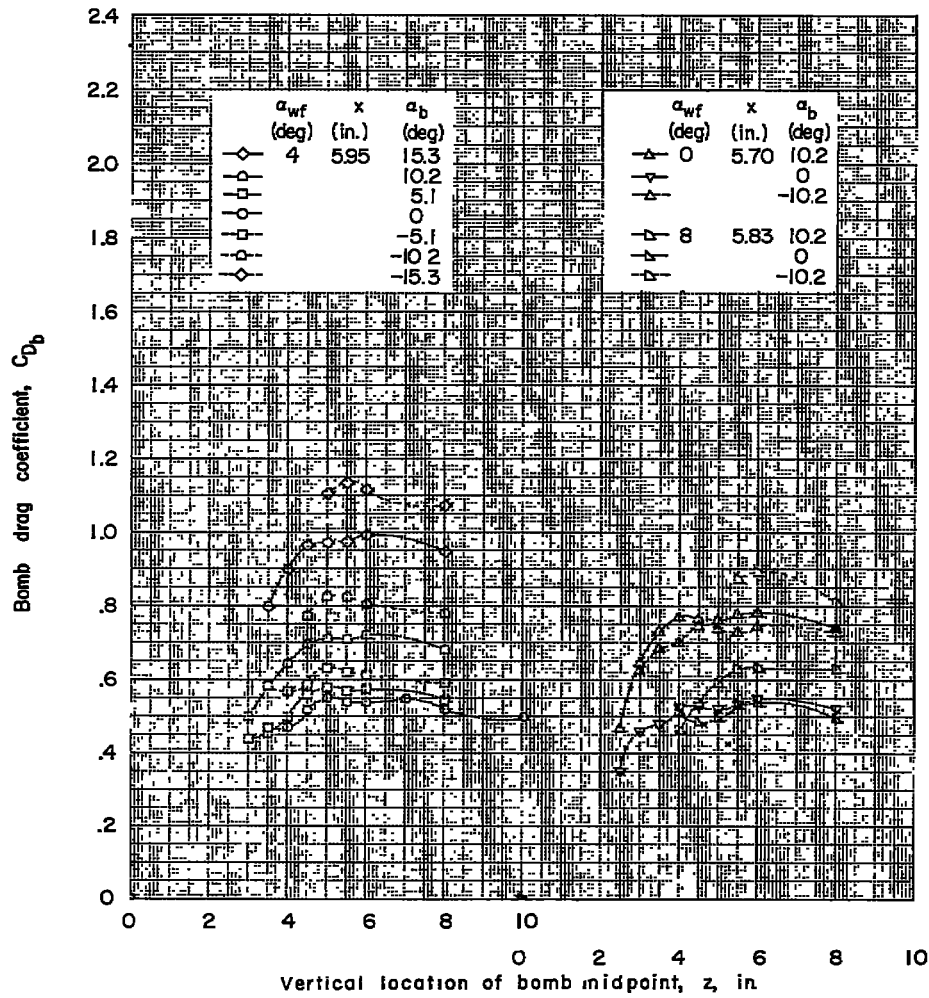
(d) Continued.

Figure 9.- Continued.



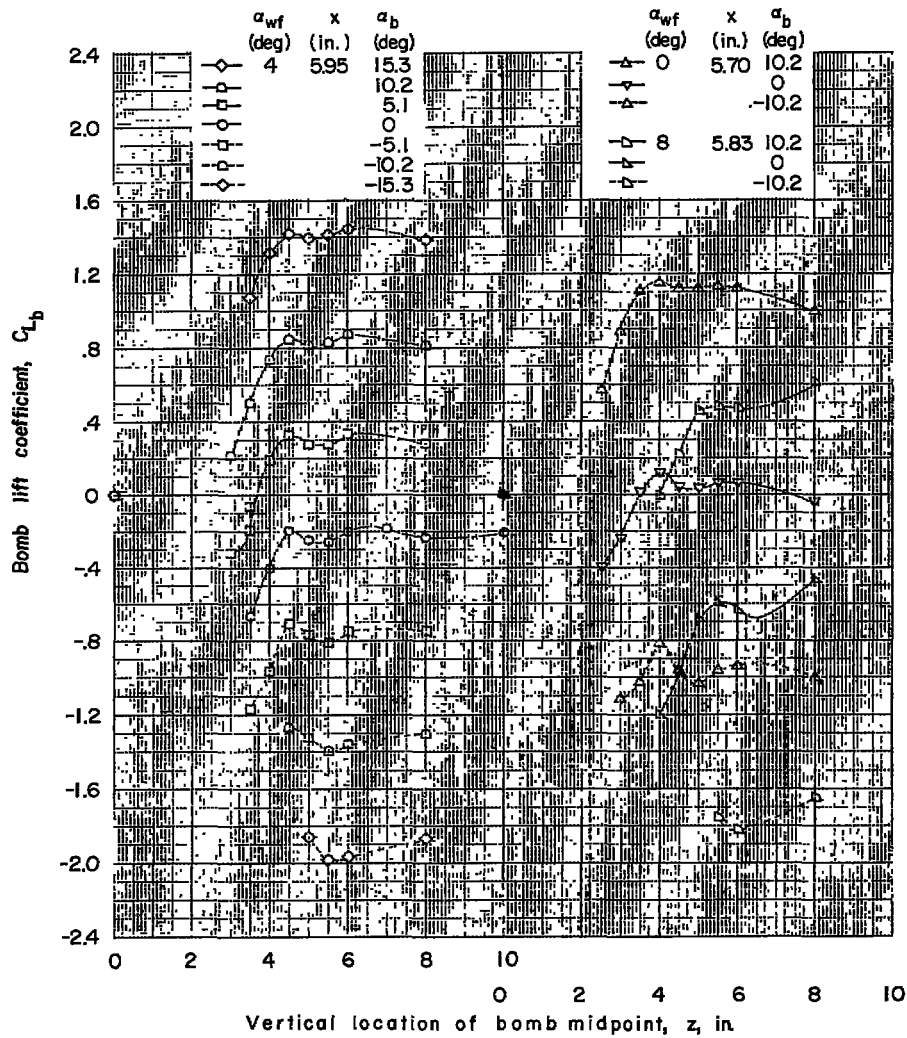
(d) Concluded.

Figure 9.- Continued.



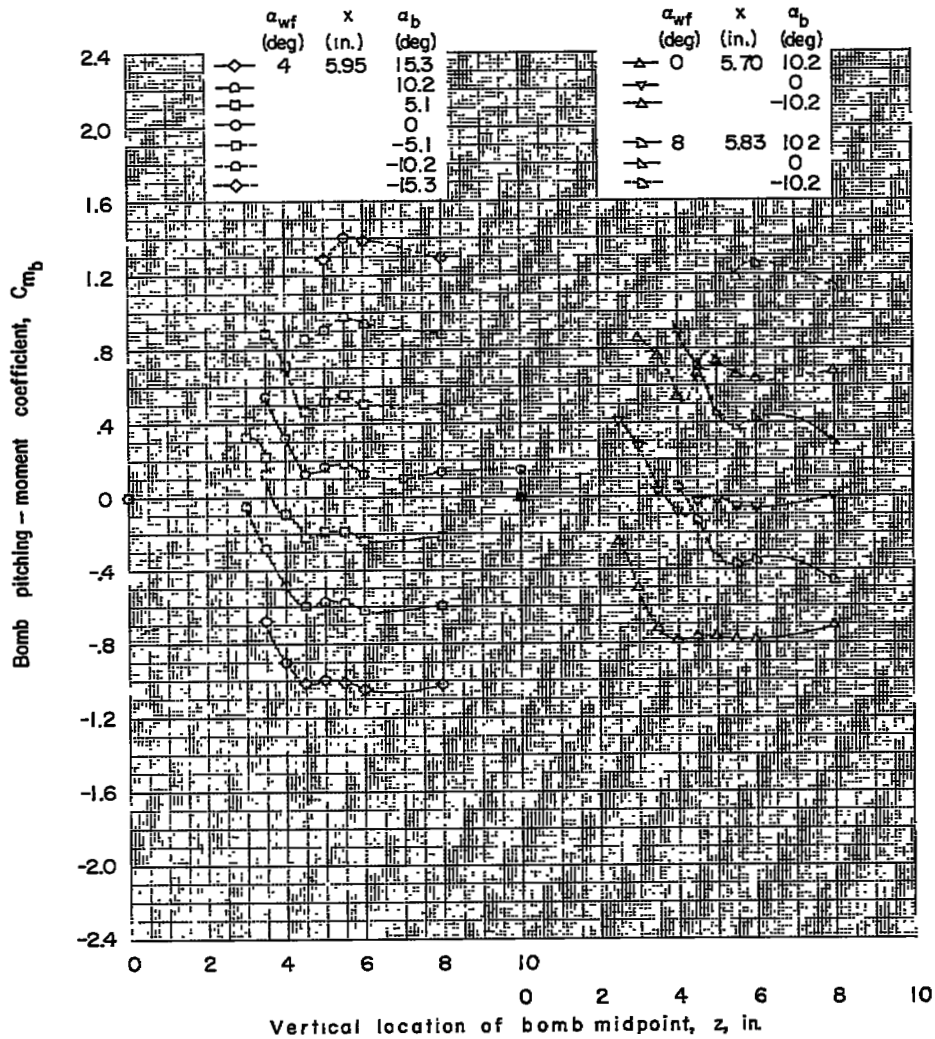
(e)  $x = 5.70$  to  $5.95$  inches.

Figure 9.- Continued.



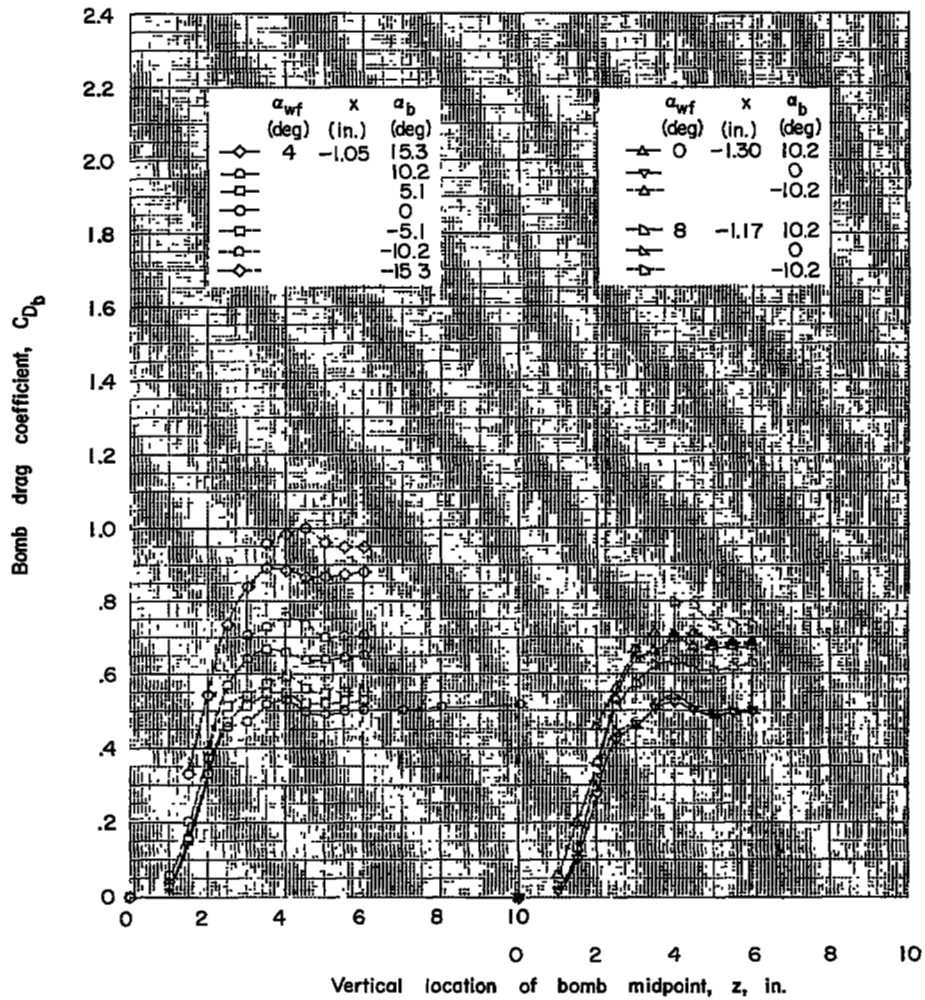
(e) Continued.

Figure 9.- Continued.



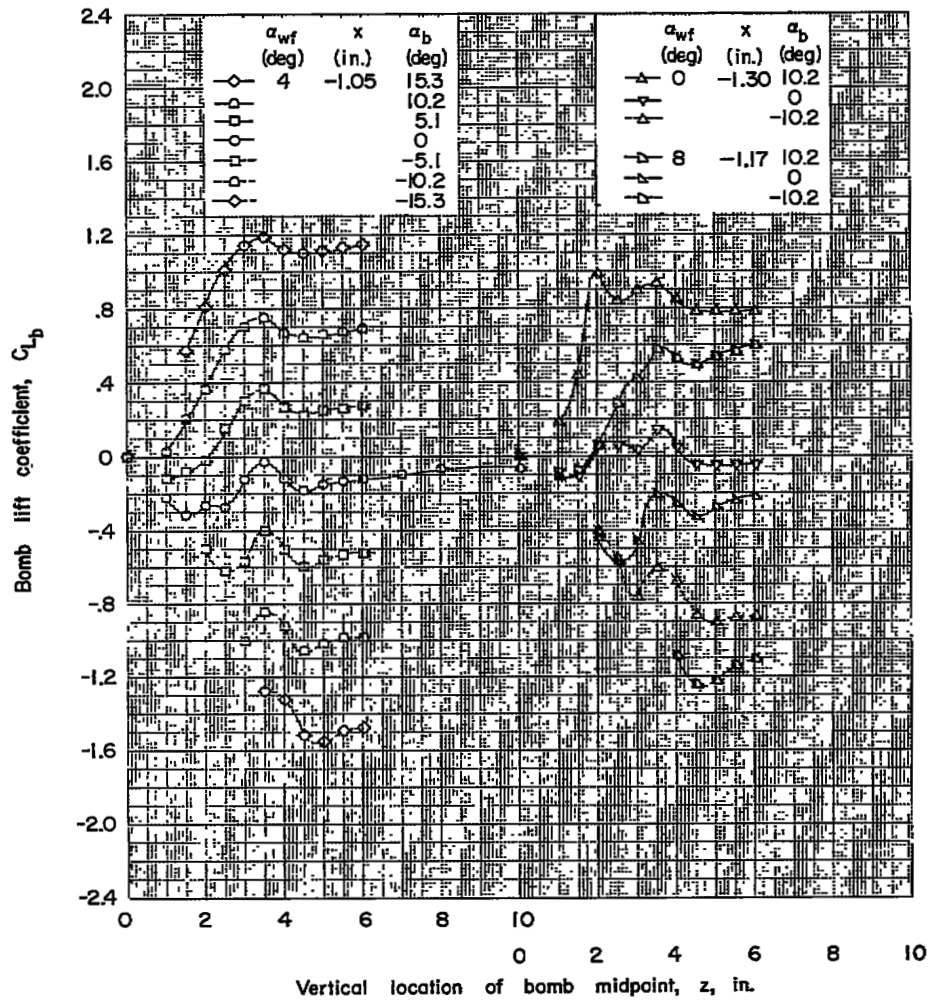
(e) Concluded.

Figure 9.- Concluded.



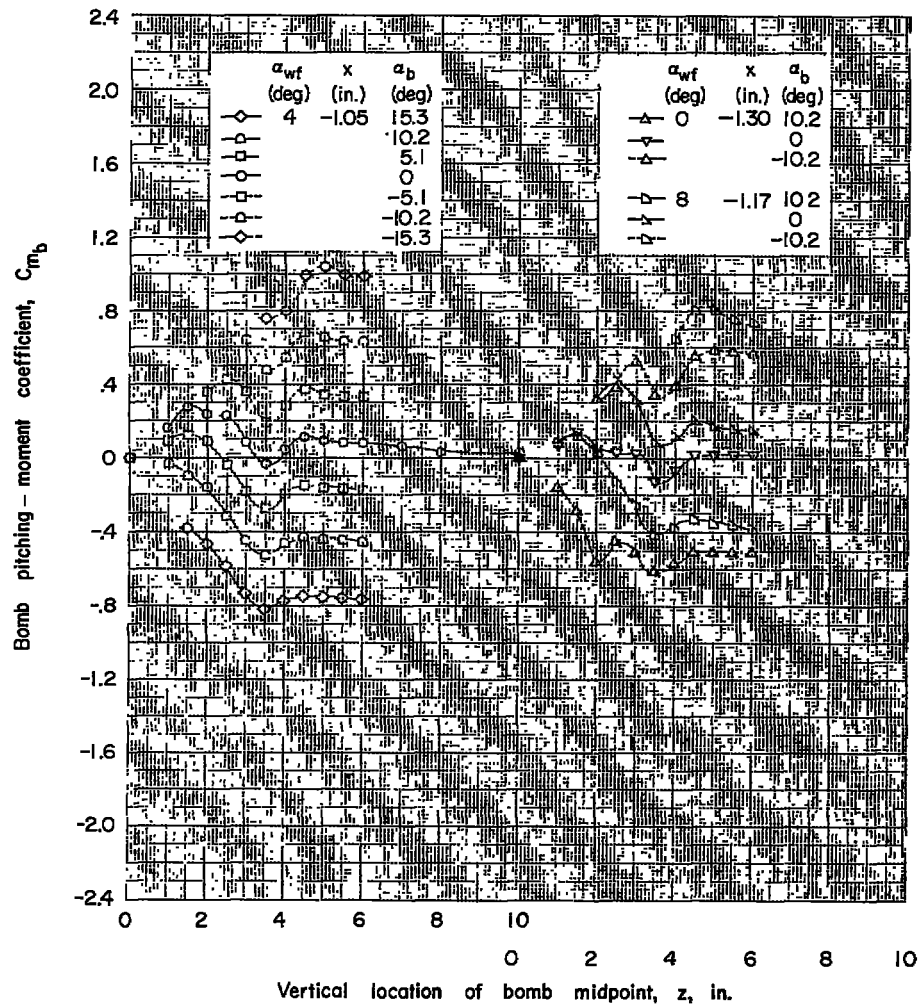
(a)  $x = -1.05$  to  $-1.30$  inches.

Figure 10.- Force data for bomb 2 in presence of wing-fuselage combination. Small fins on.



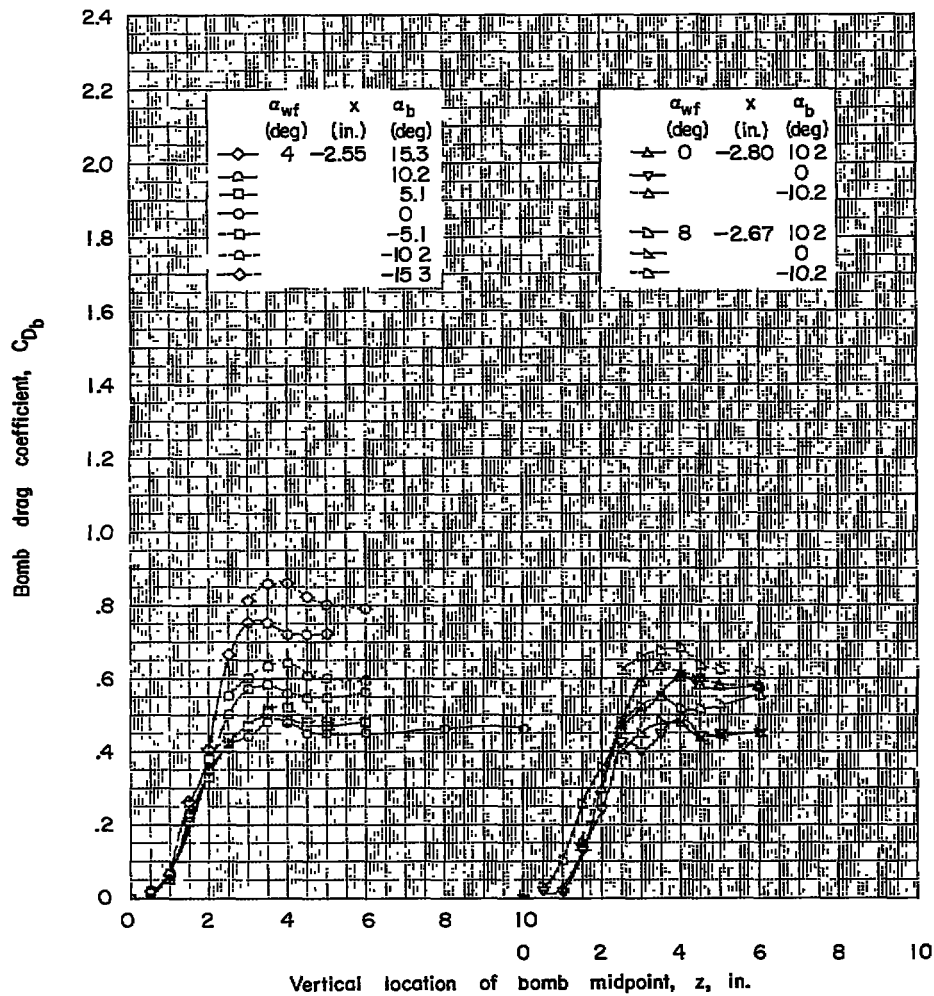
(a) Continued.

Figure 10.- Continued.



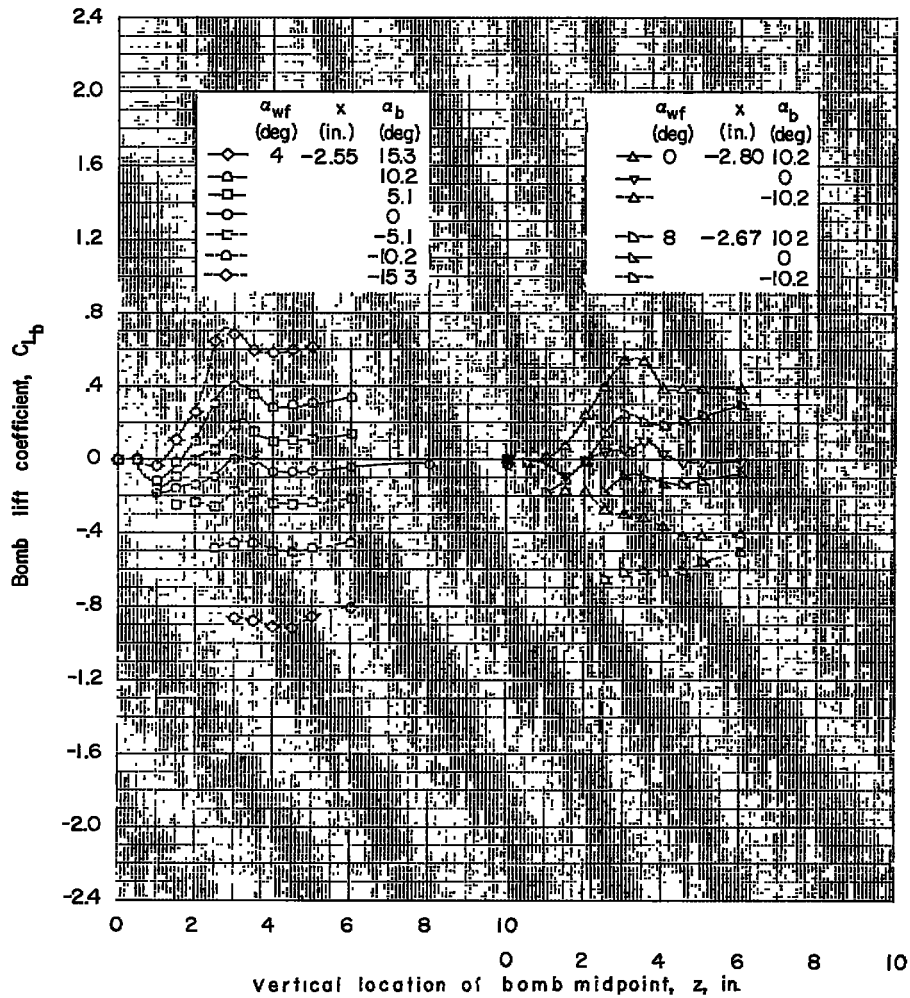
(a) Concluded.

Figure 10.- Concluded.



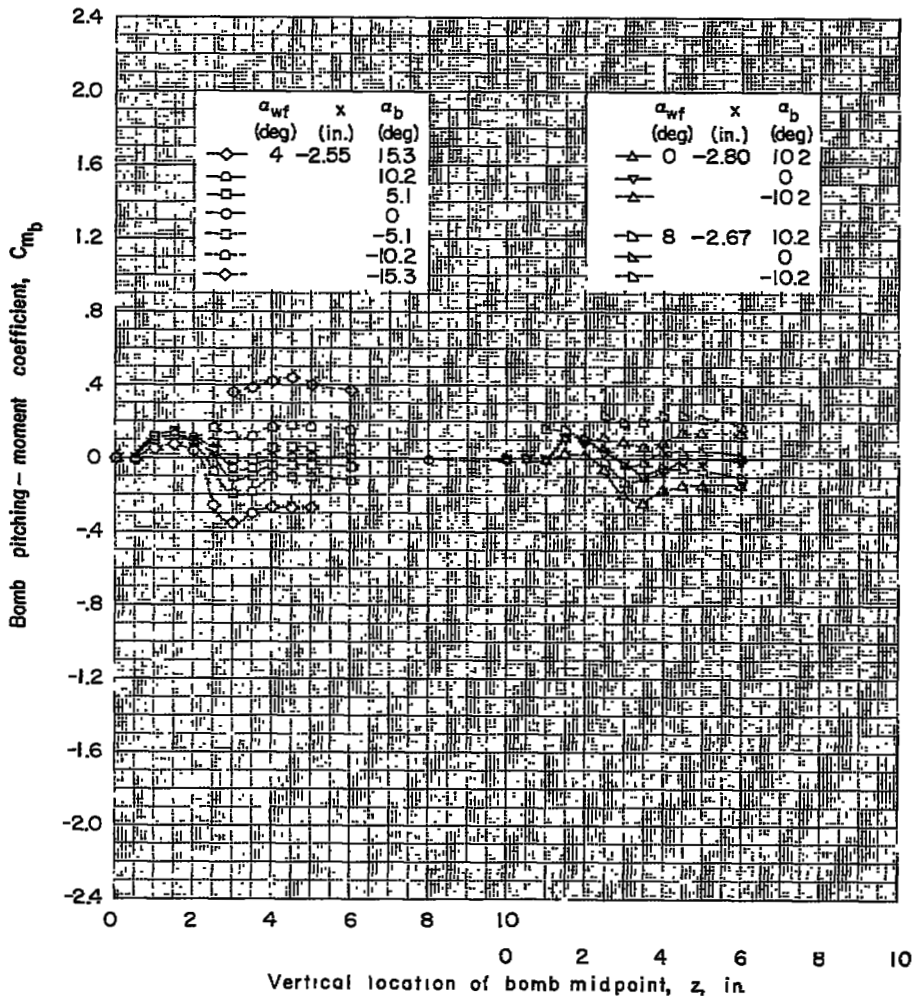
(a)  $x = -2.55$  to  $-2.80$  inches.

Figure 11.- Force data for bomb 2 in presence of wing-fuselage combination. Fins off.



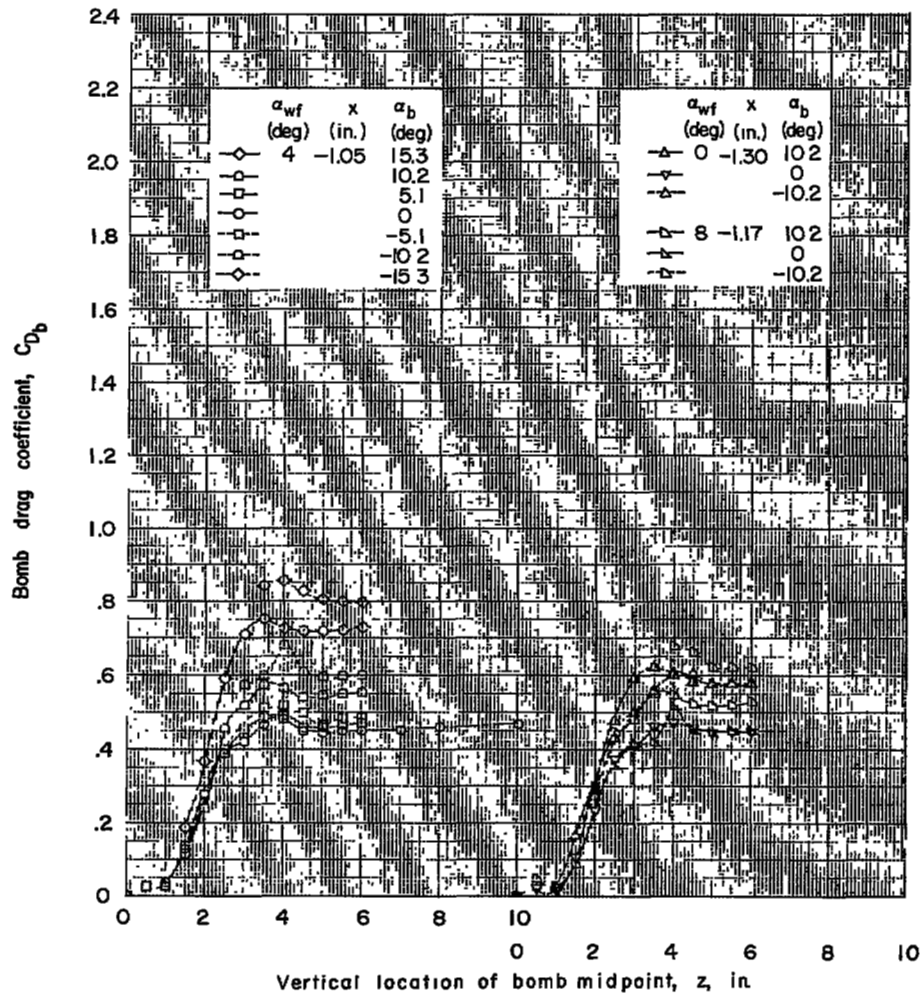
(a) Continued.

Figure 11.- Continued.



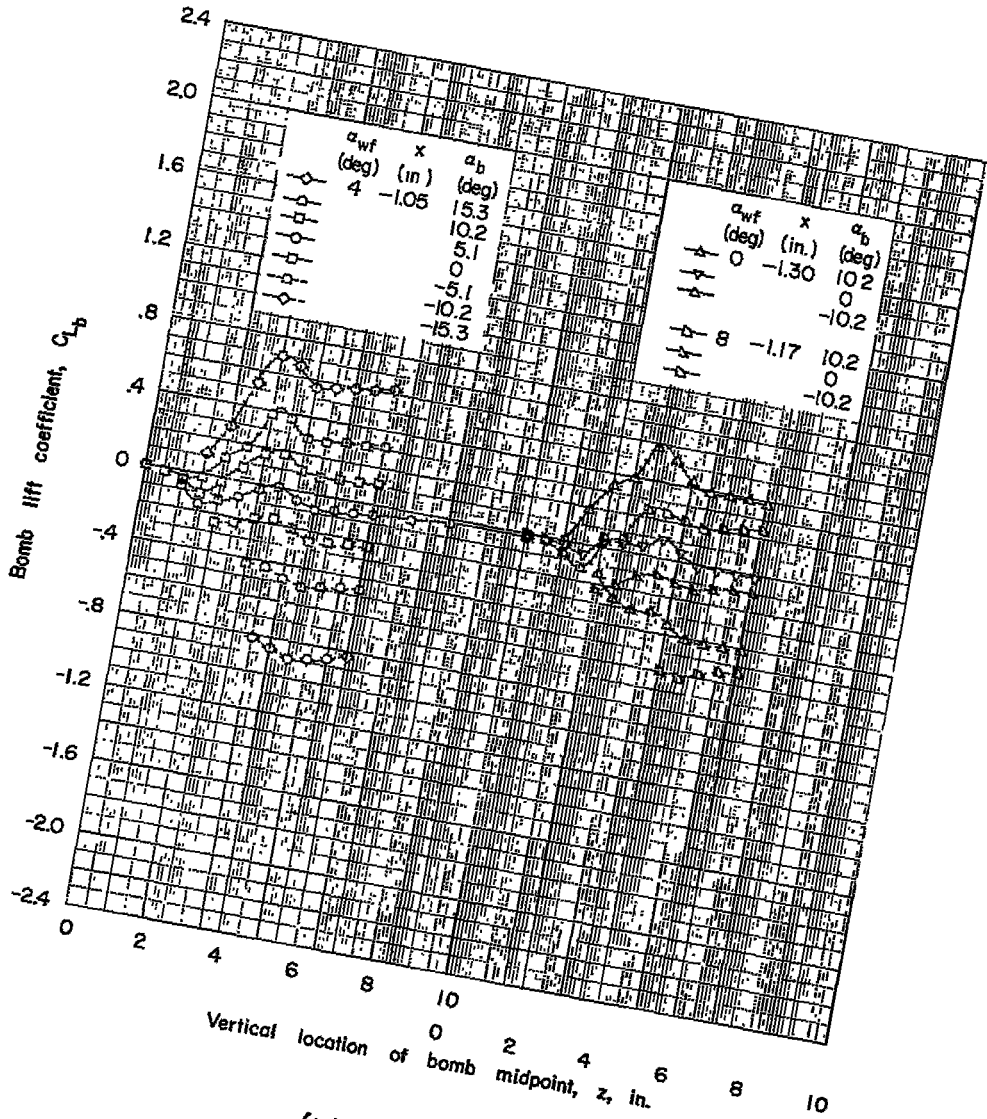
(a) Concluded.

Figure 11.- Continued.



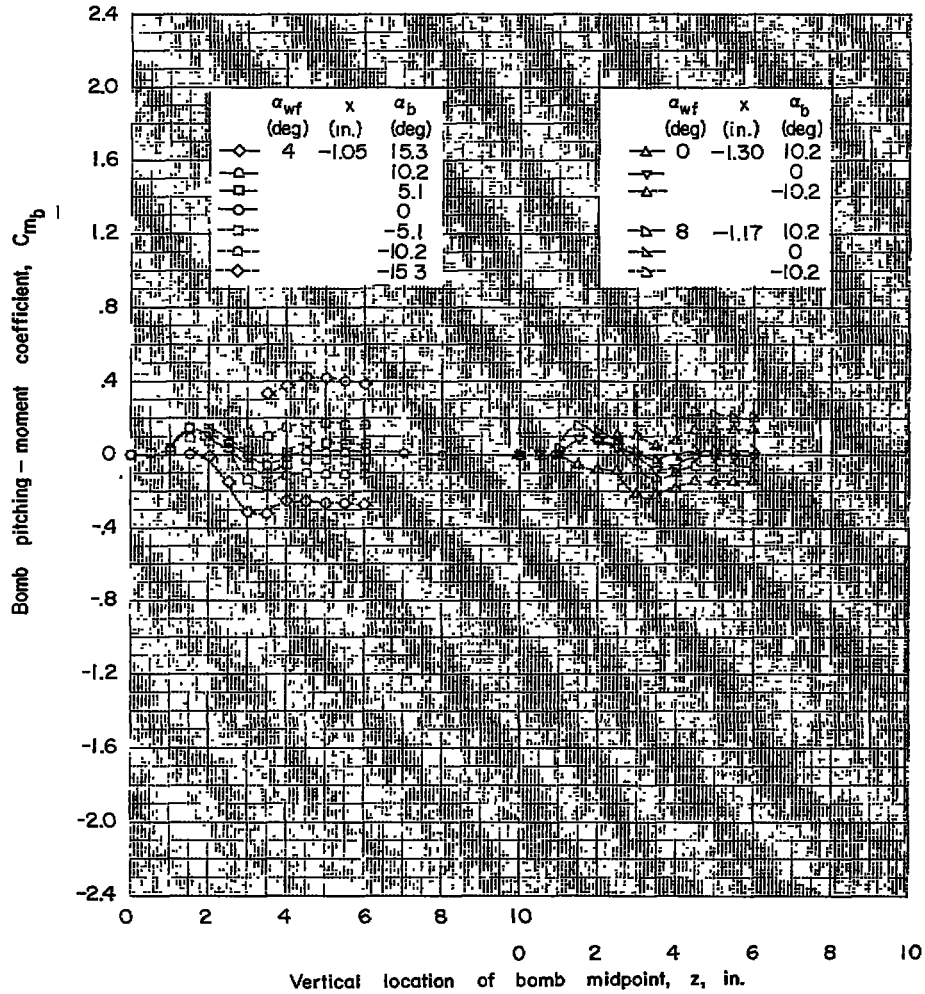
(b)  $x = -1.05$  to  $-1.30$  inches.

Figure 11.- Continued.



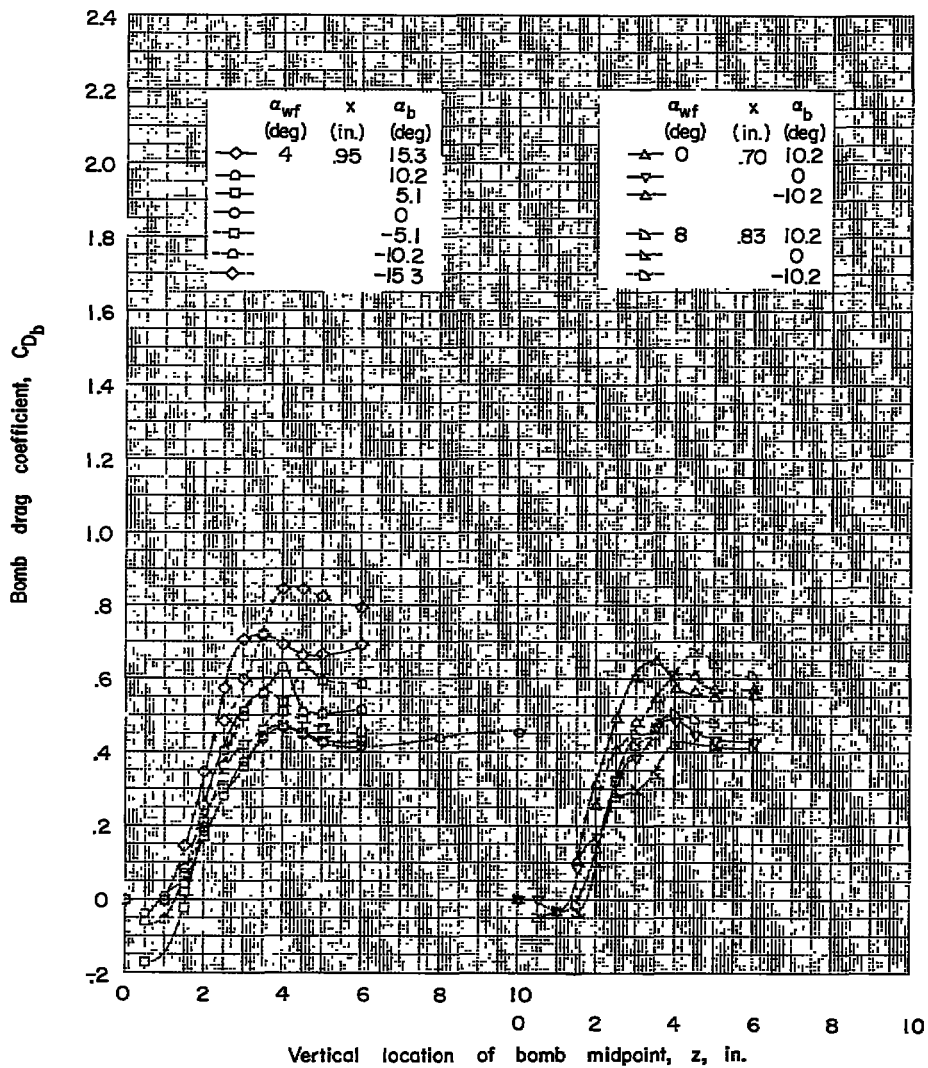
(b) Continued.

Figure 11.- Continued.



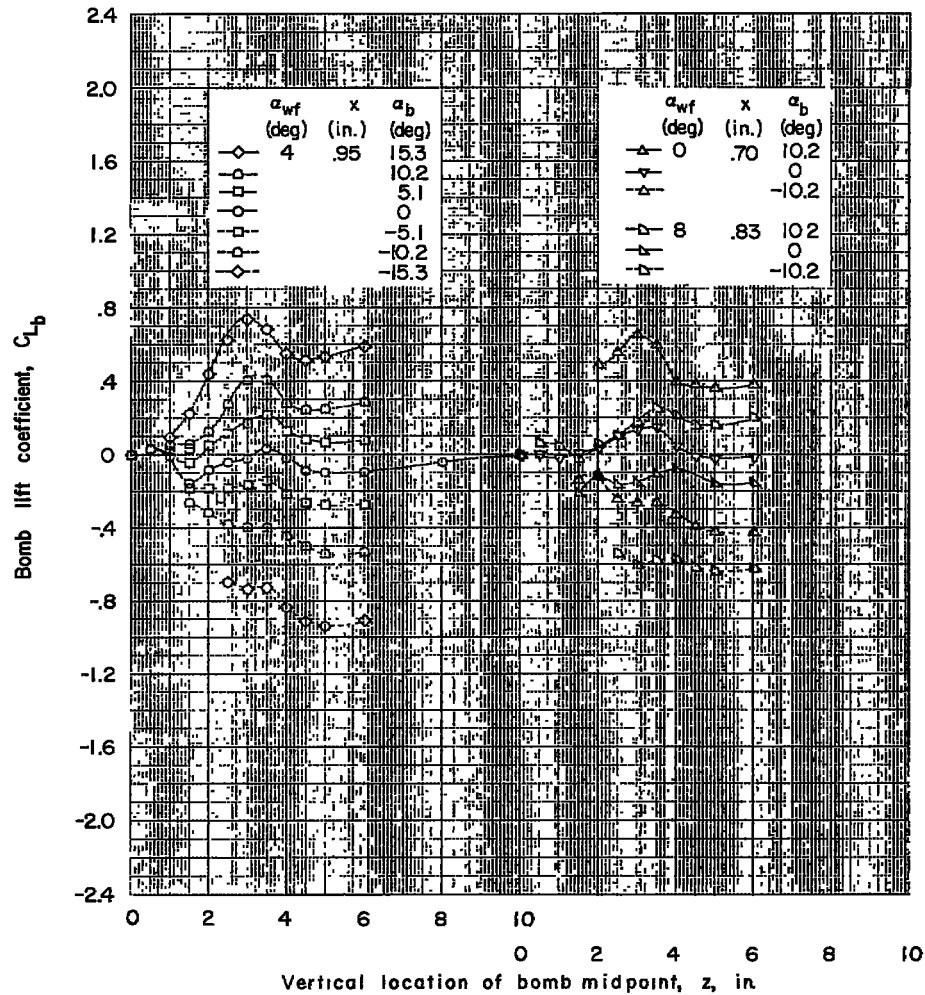
(b) Concluded.

Figure 11.- Continued.



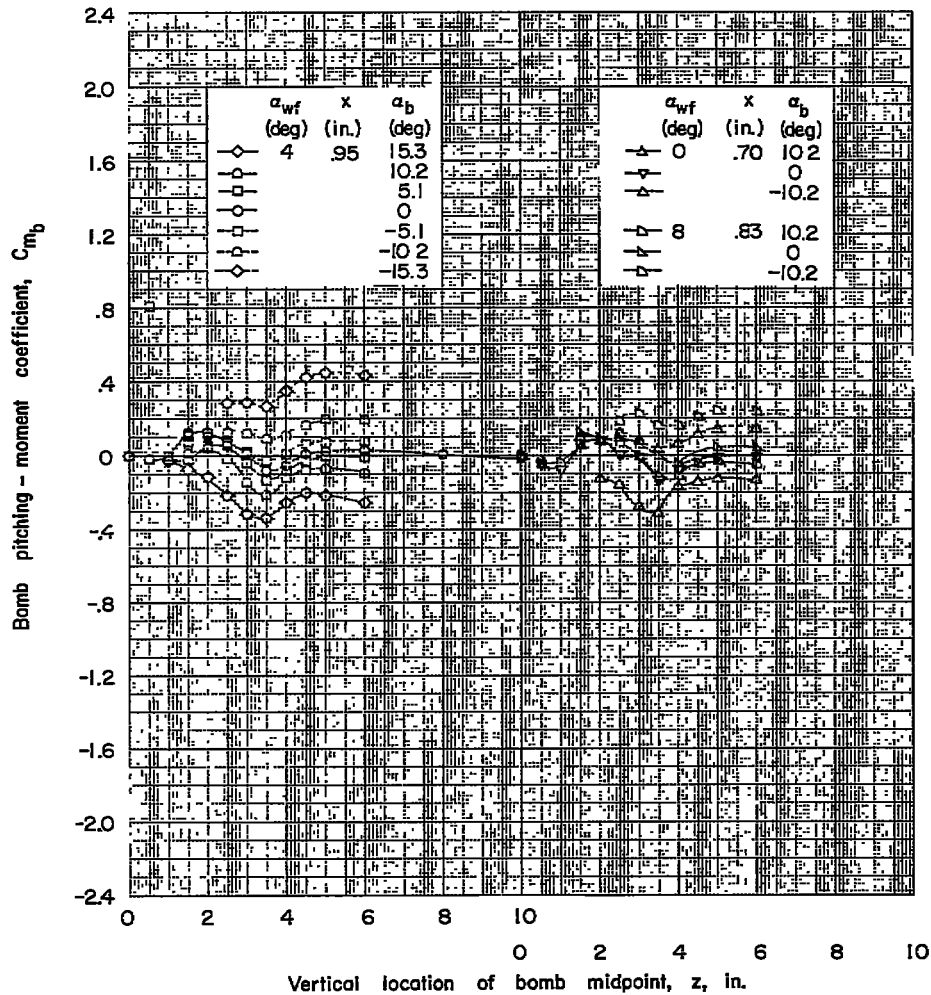
(c)  $x = 0.70$  to  $0.95$  inch.

Figure 11.- Continued.



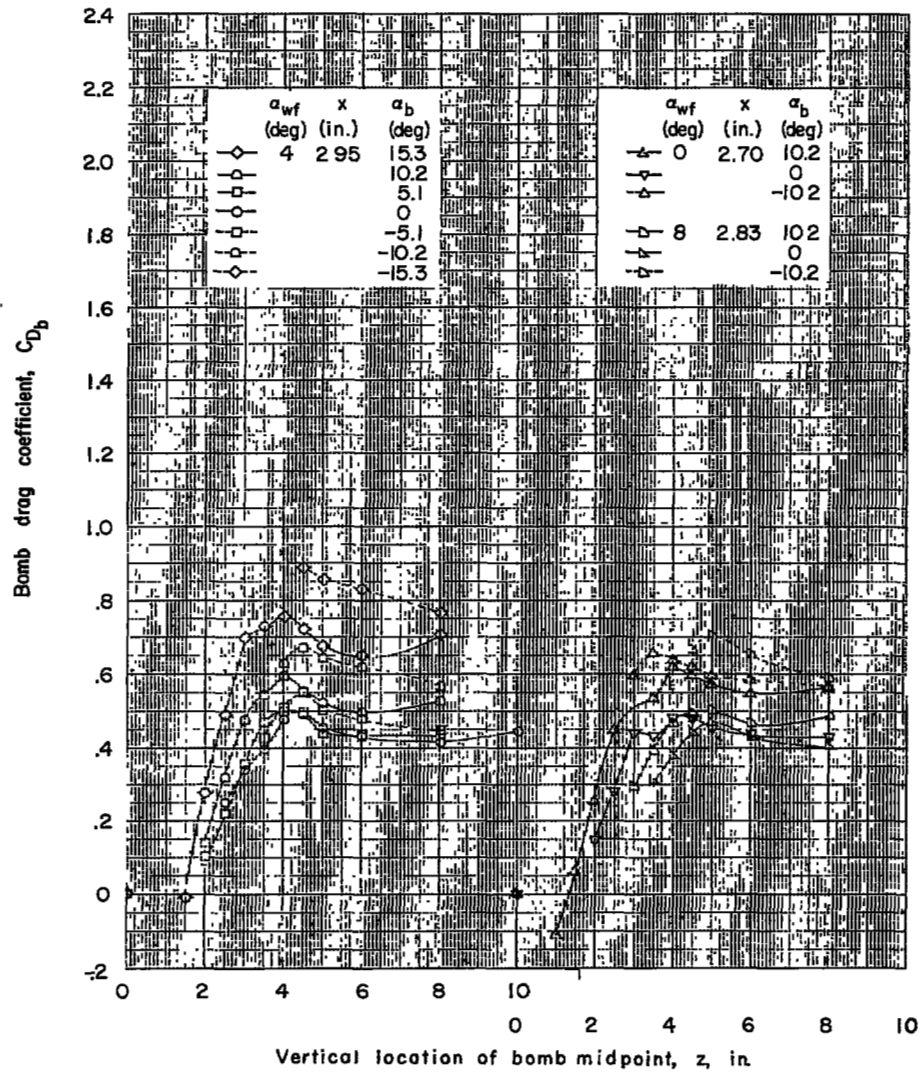
(c) Continued.

Figure 11.- Continued.



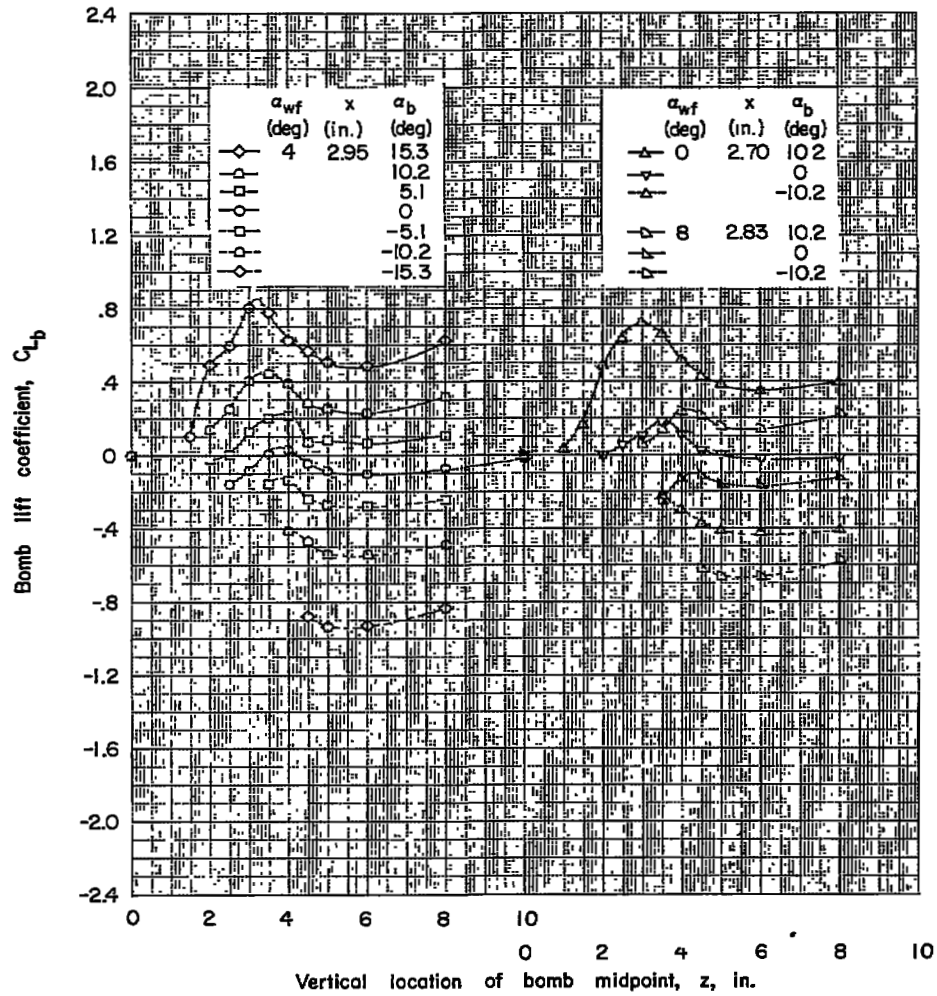
(c) Concluded.

Figure 11.- Continued.



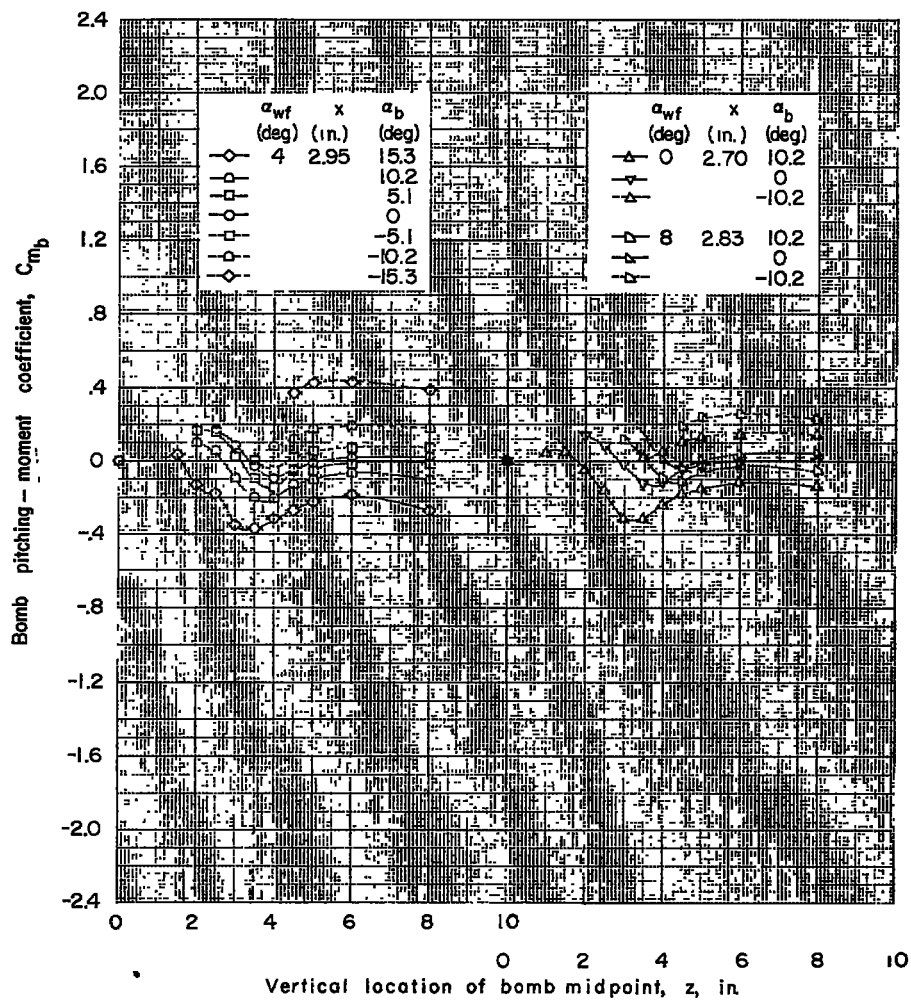
(d)  $x = 2.70$  to  $2.95$  inches.

Figure 11.- Continued.



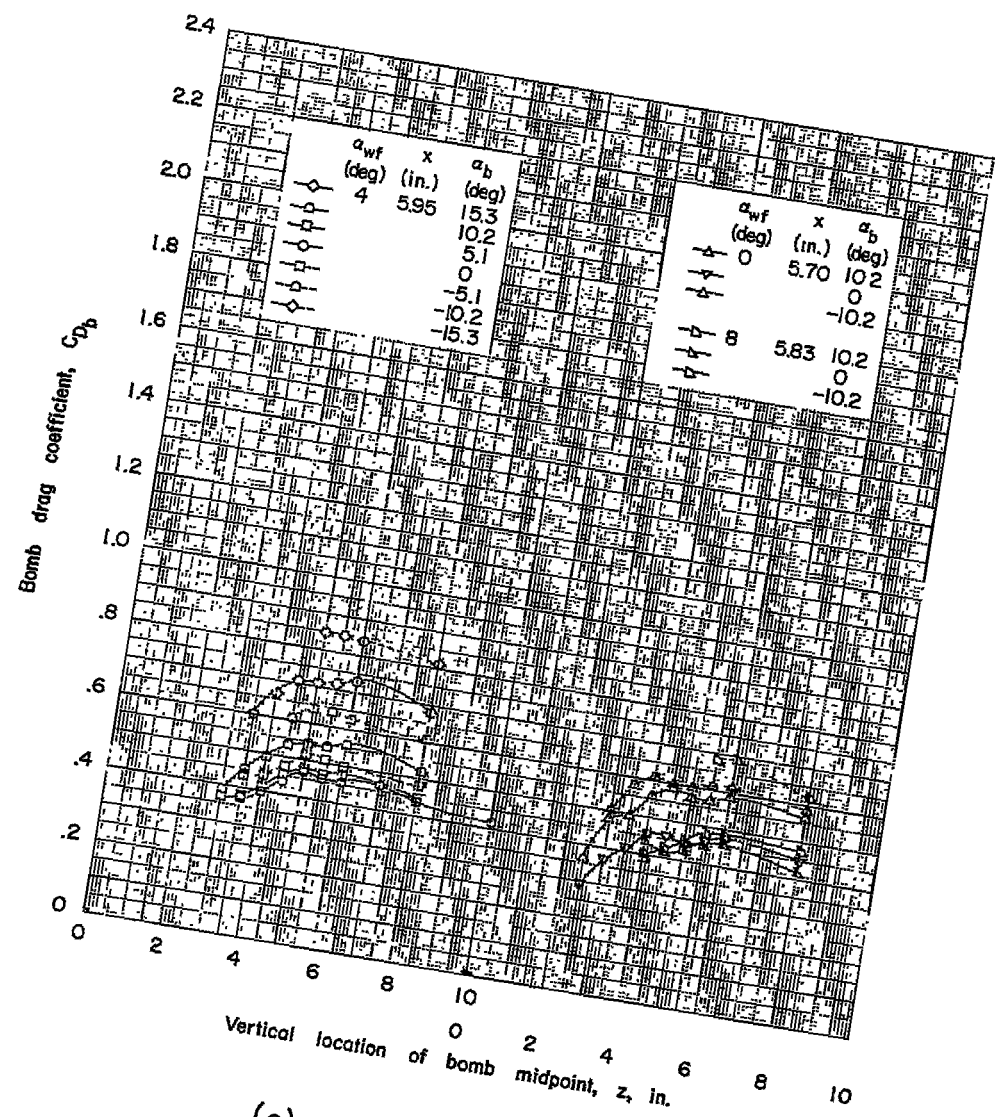
(d) Continued.

Figure 11.- Continued.



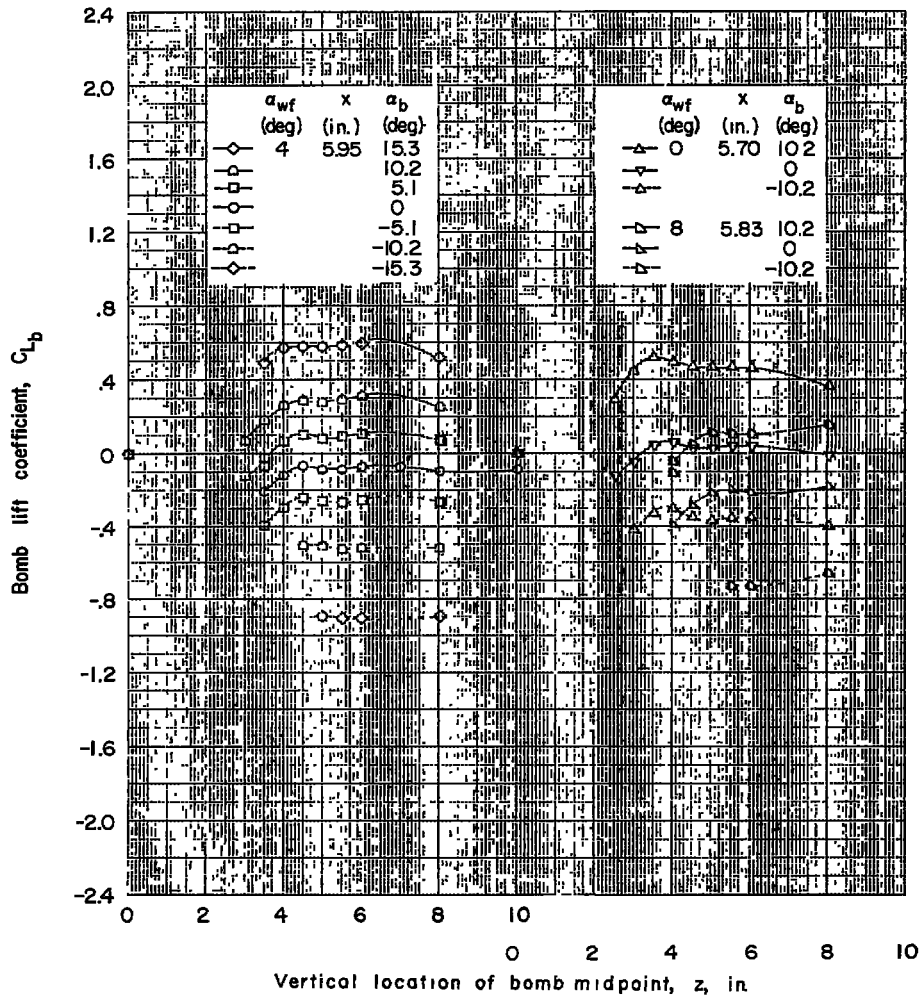
(d) Concluded.

Figure 11.- Continued.



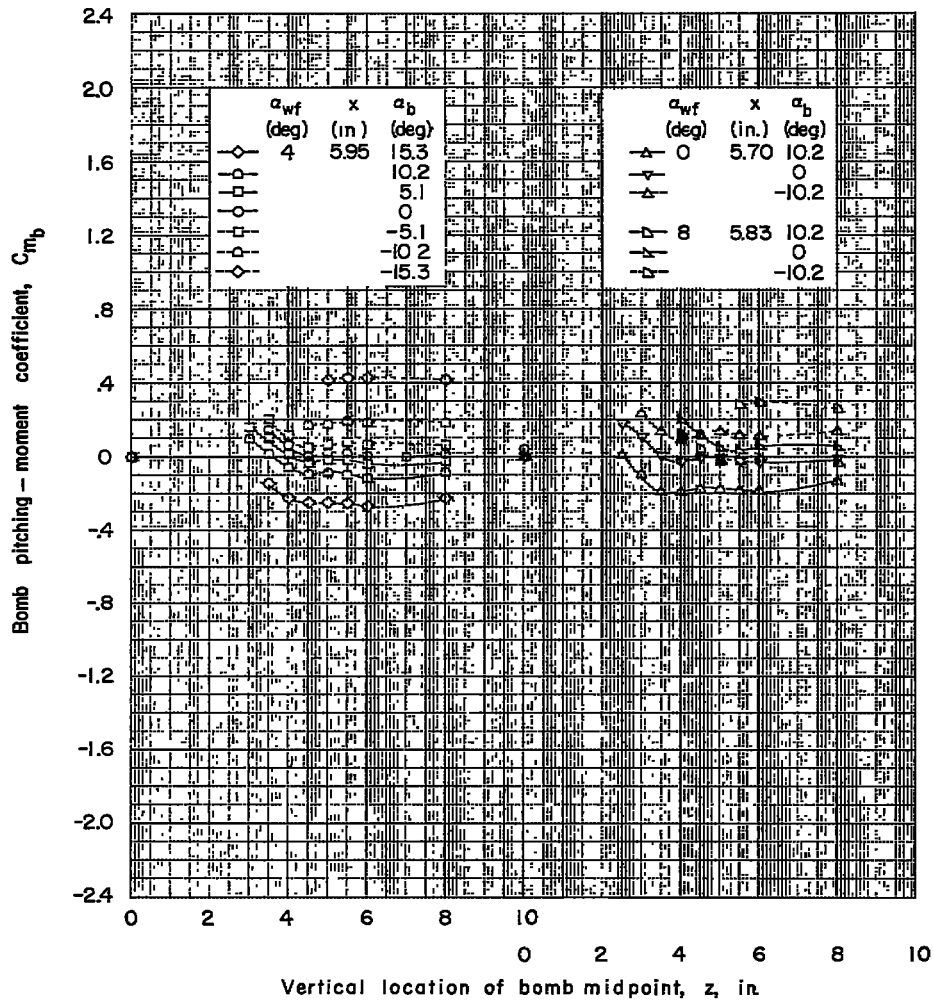
(e)  $x = 5.70$  to  $5.95$  inches.

Figure 11.- Continued.



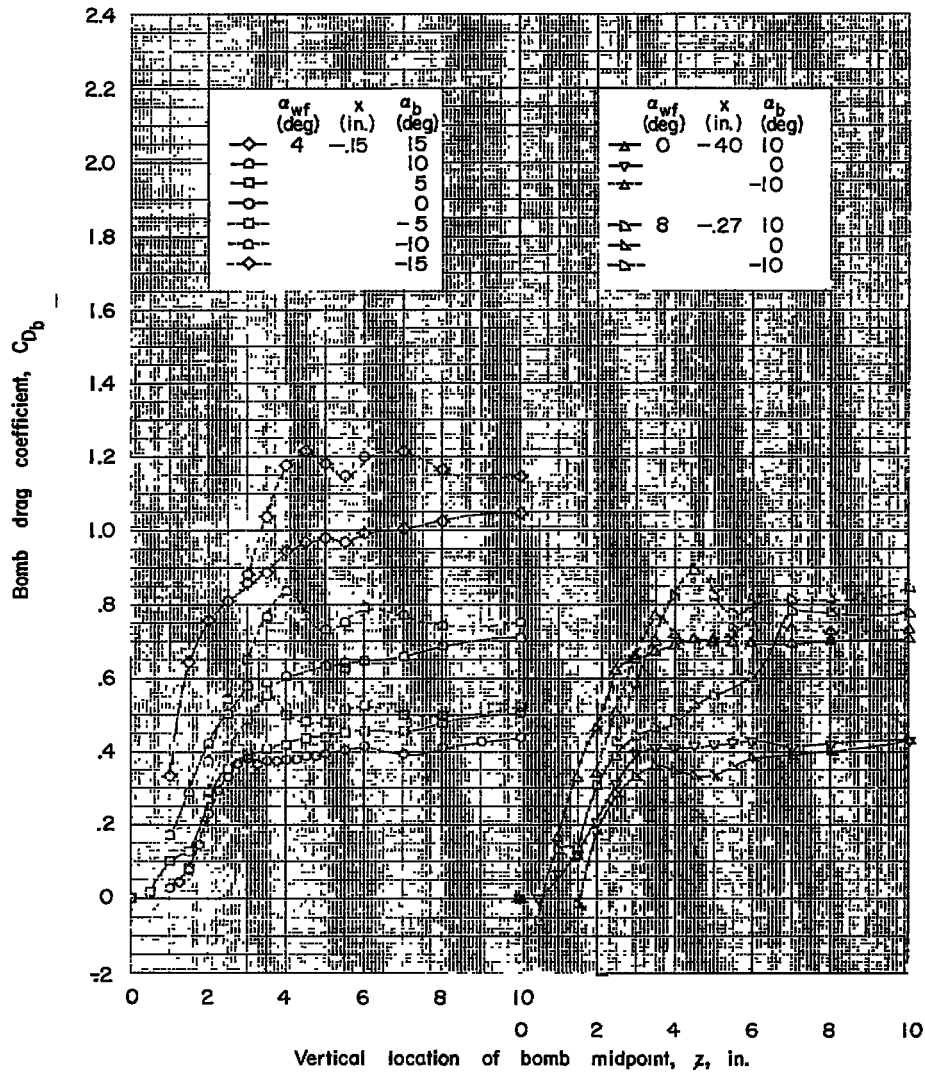
(e) Continued.

Figure 11.- Continued.



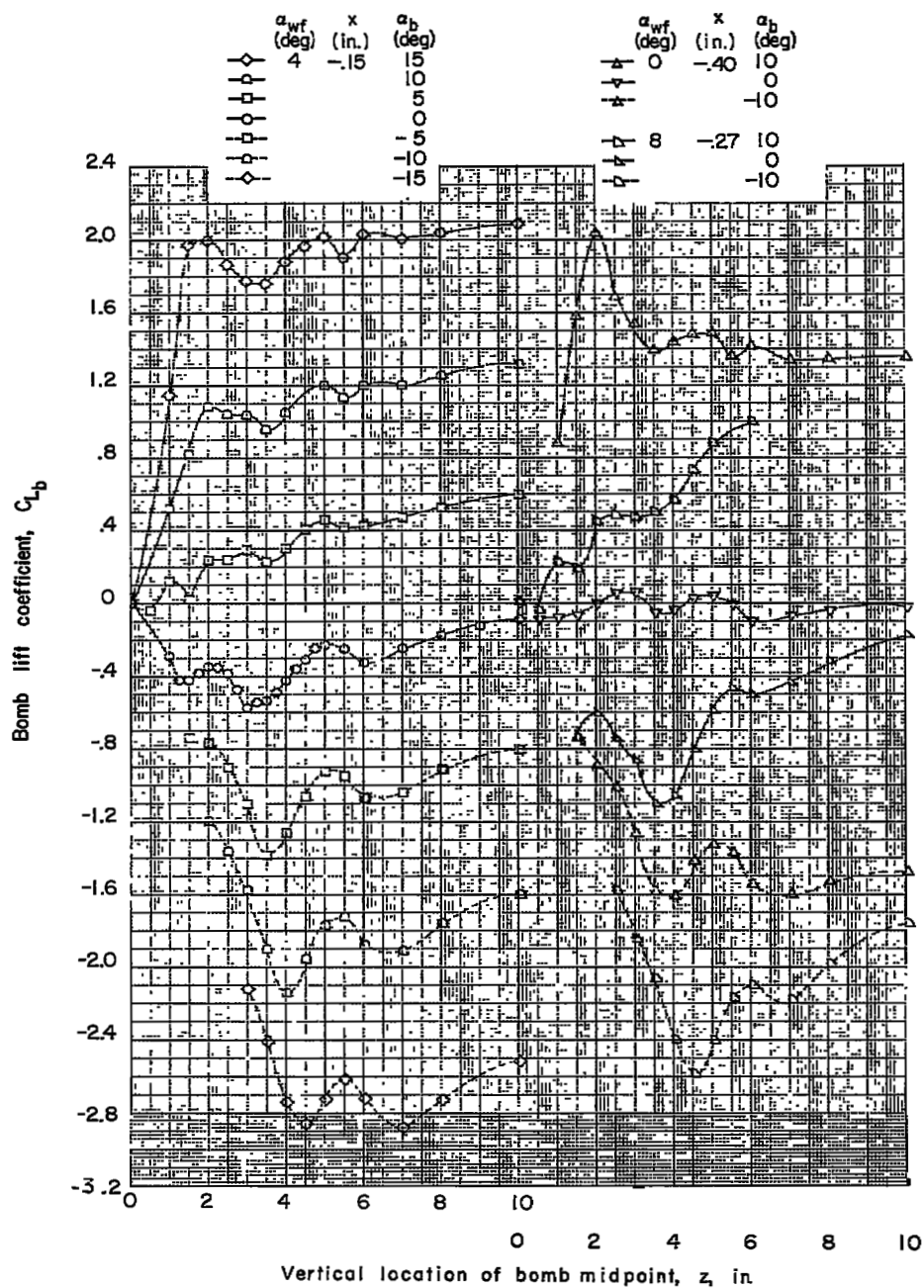
(e) Concluded.

Figure 11.- Concluded.



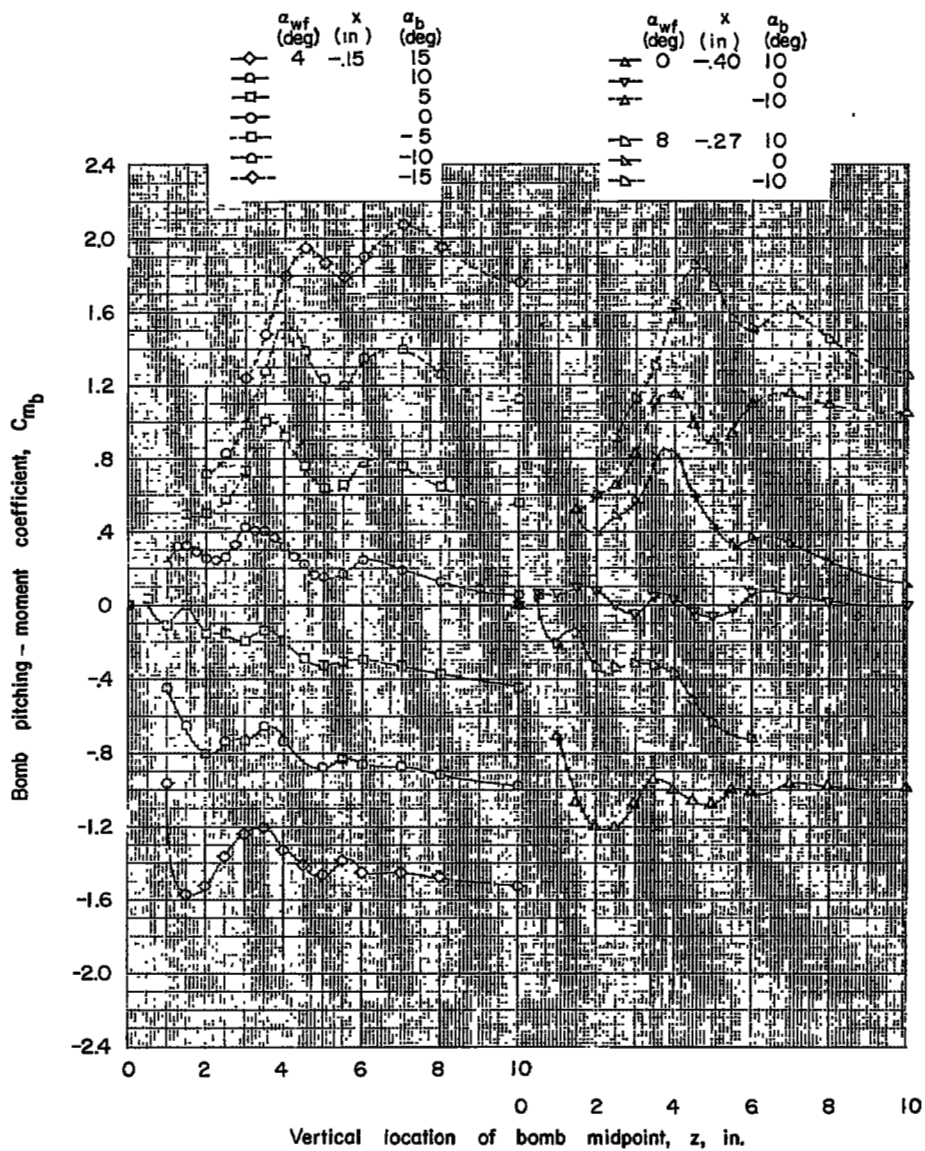
(a)  $x = -0.15$  to  $-0.40$  inch.

Figure 12.- Force data for bomb 3 in presence of wing-fuselage combination. Fins on.



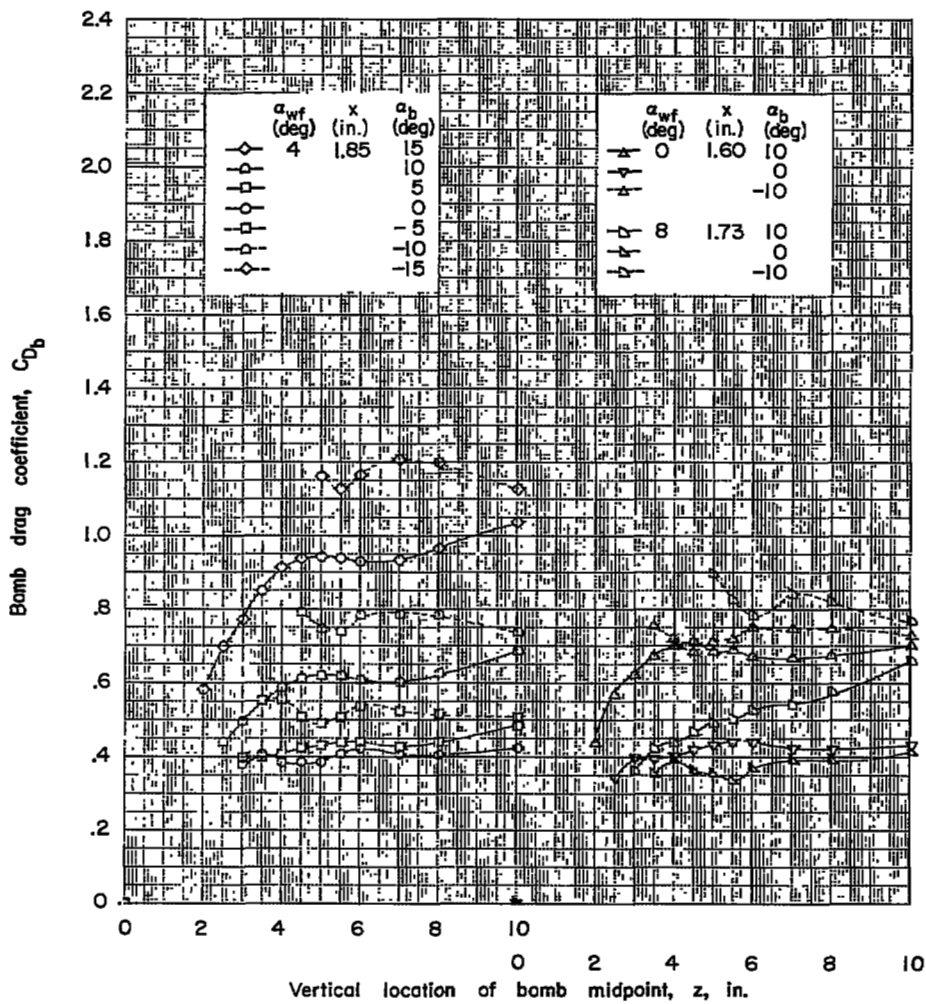
(a) Continued.

Figure 12.- Continued.



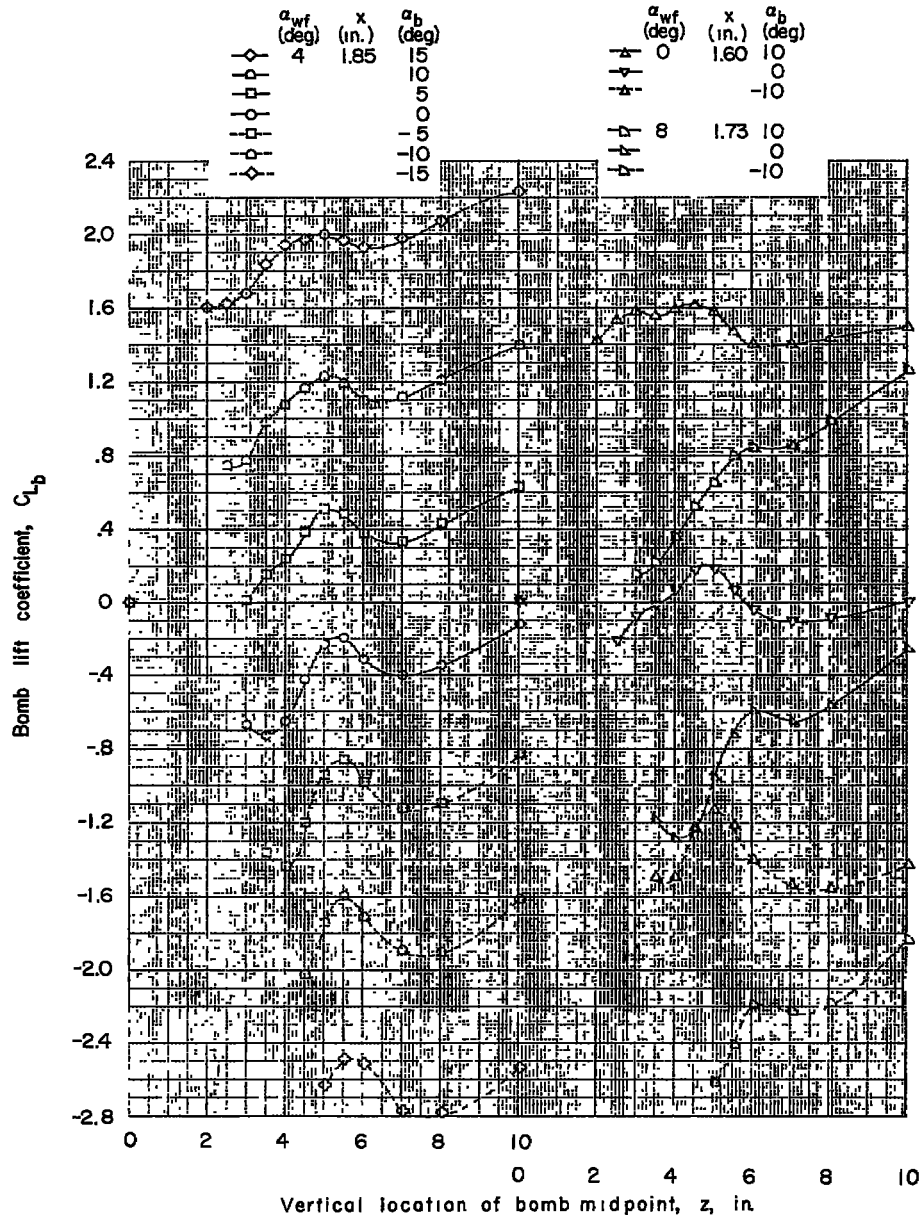
(a) Concluded.

Figure 12.- Continued.



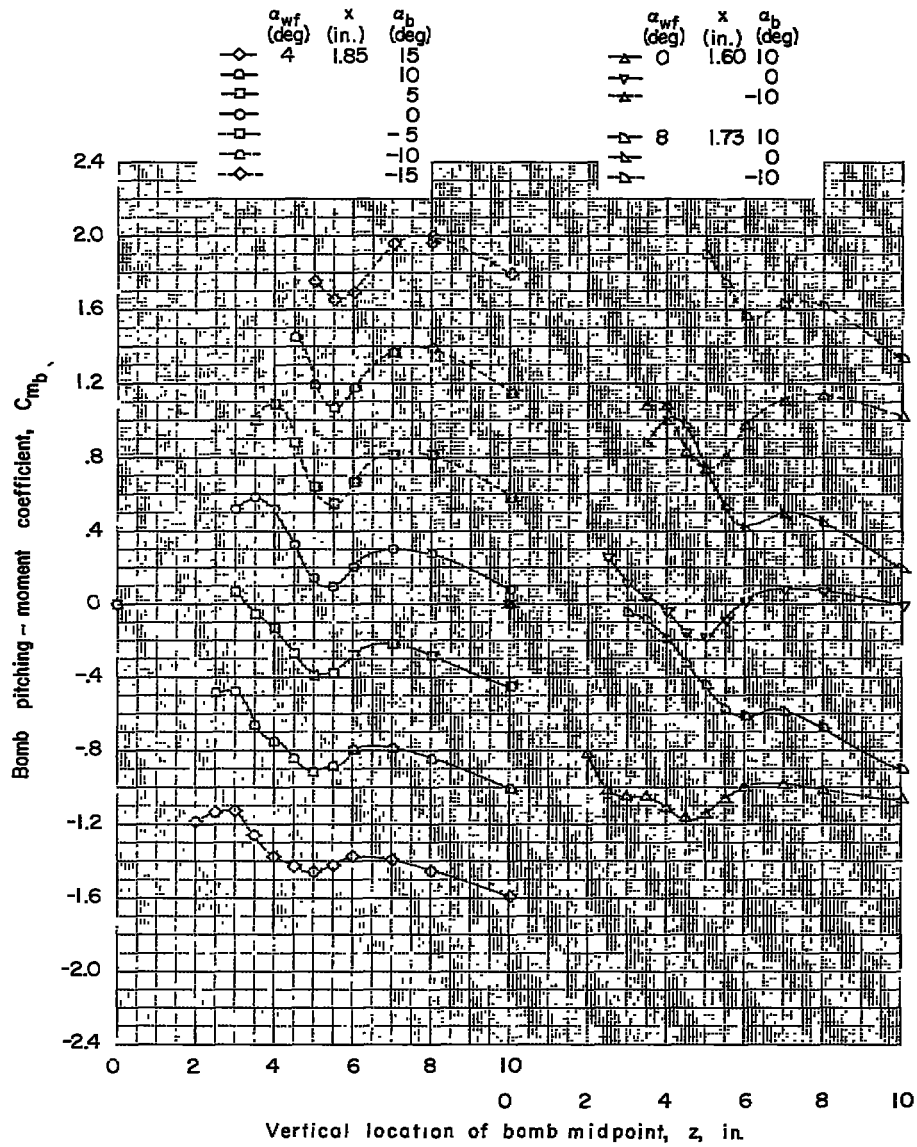
(b)  $x = 1.60$  to  $1.85$  inches.

Figure 12.- Continued.



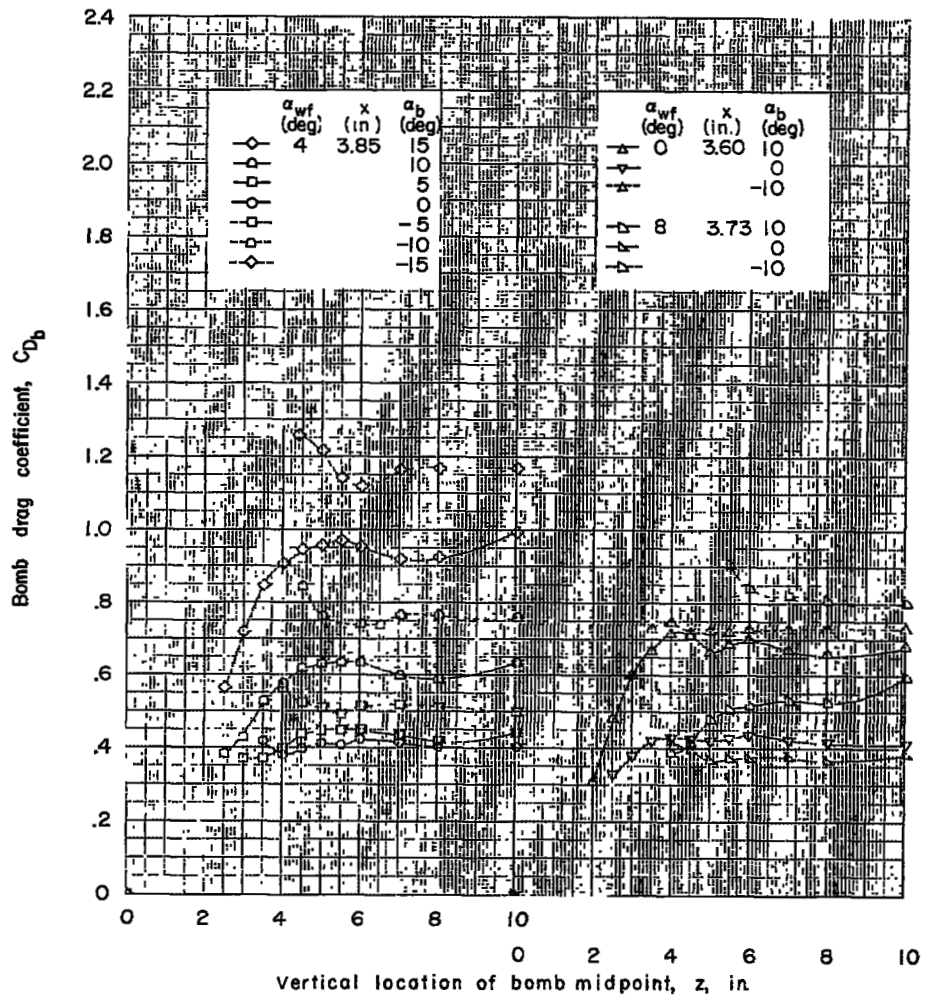
(b) Continued.

Figure 12.- Continued.



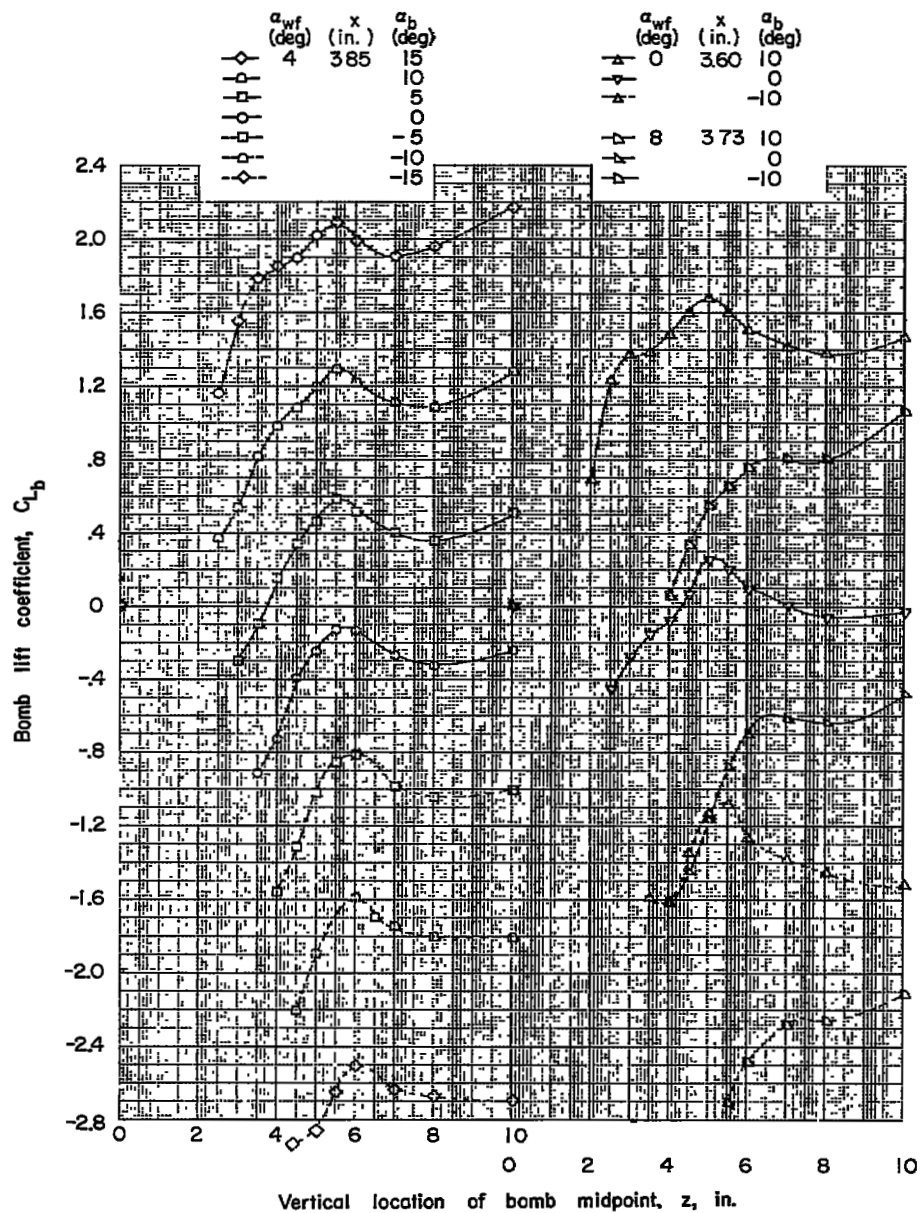
(b) Concluded.

Figure 12.- Continued.



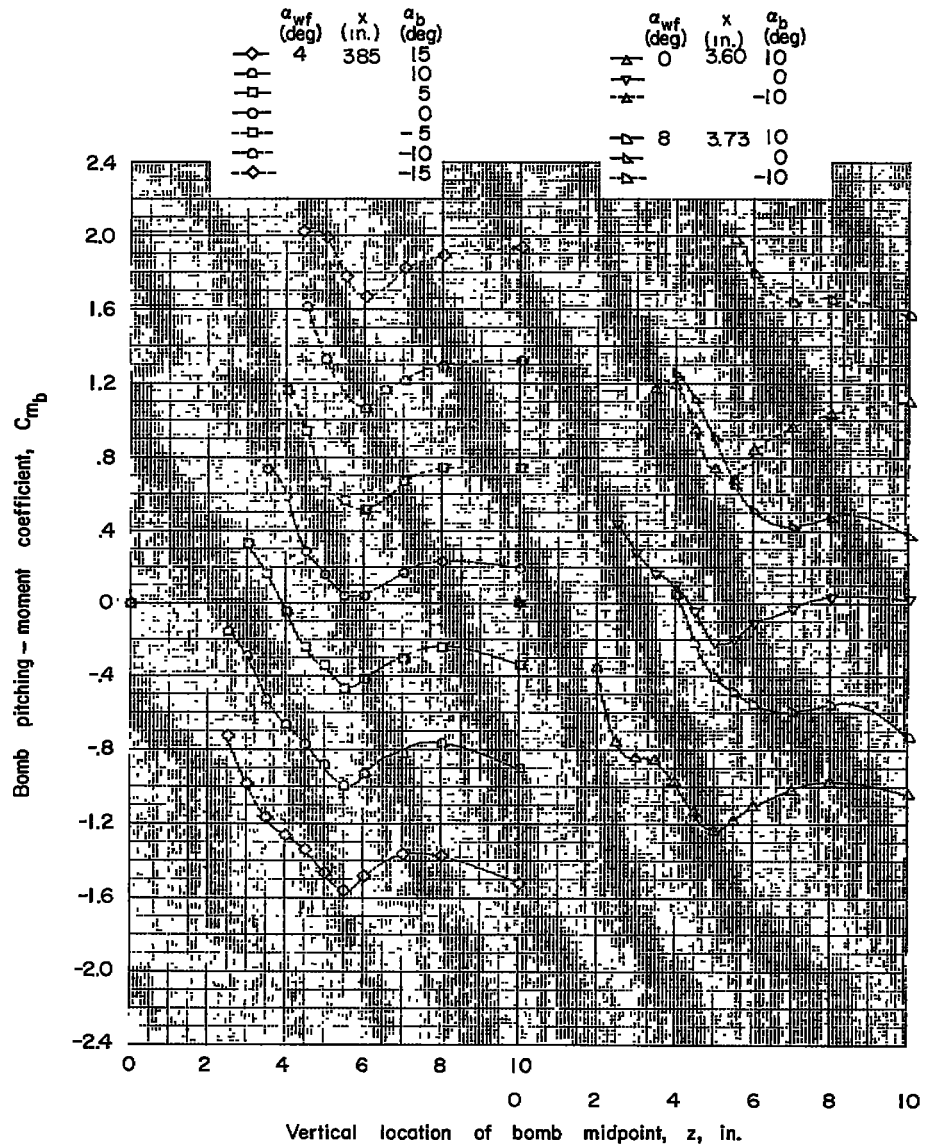
(c)  $x = 3.60$  to  $3.85$  inches.

Figure 12.- Continued.



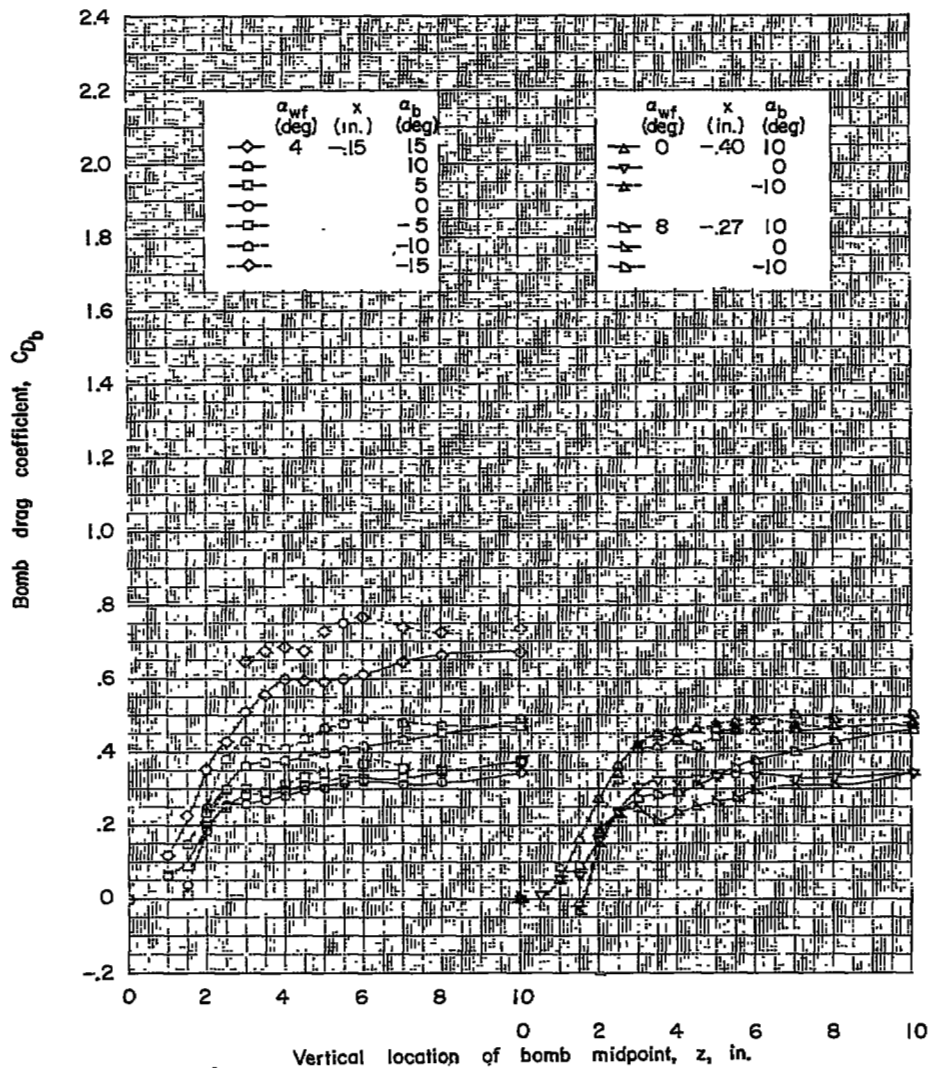
(c) Continued.

Figure 12.- Continued.



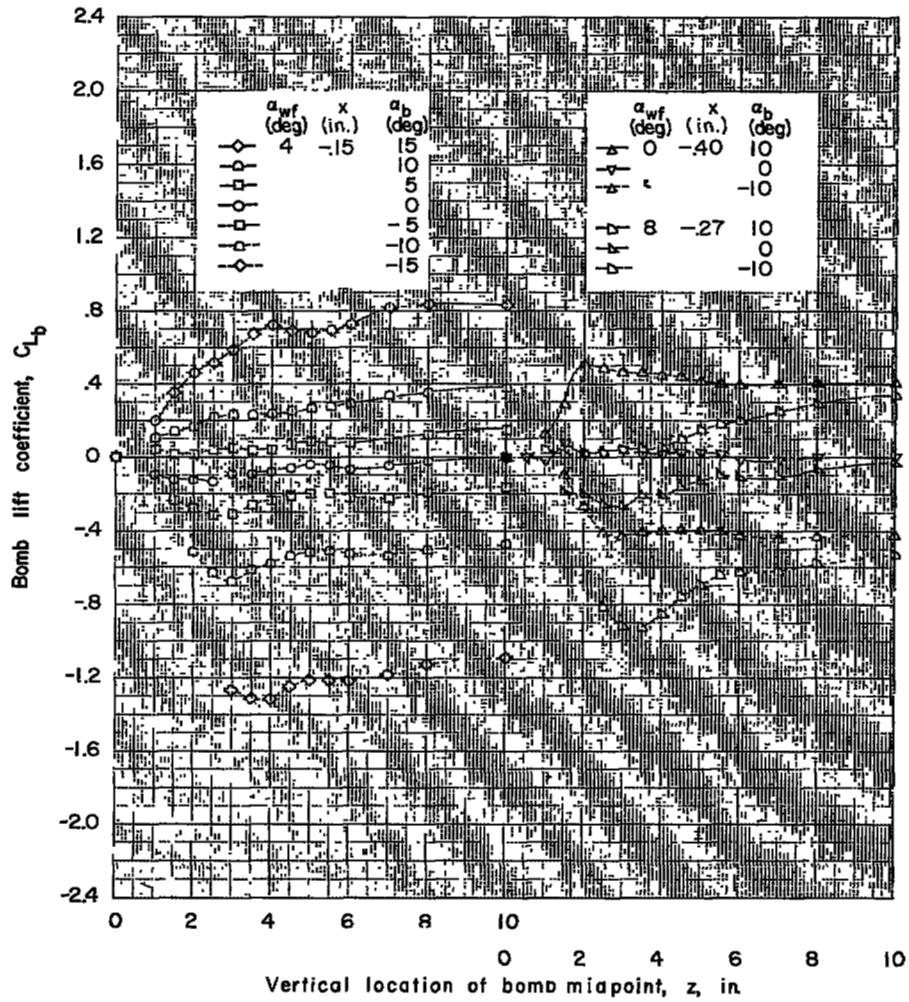
(c) Concluded.

Figure 12.- Concluded.



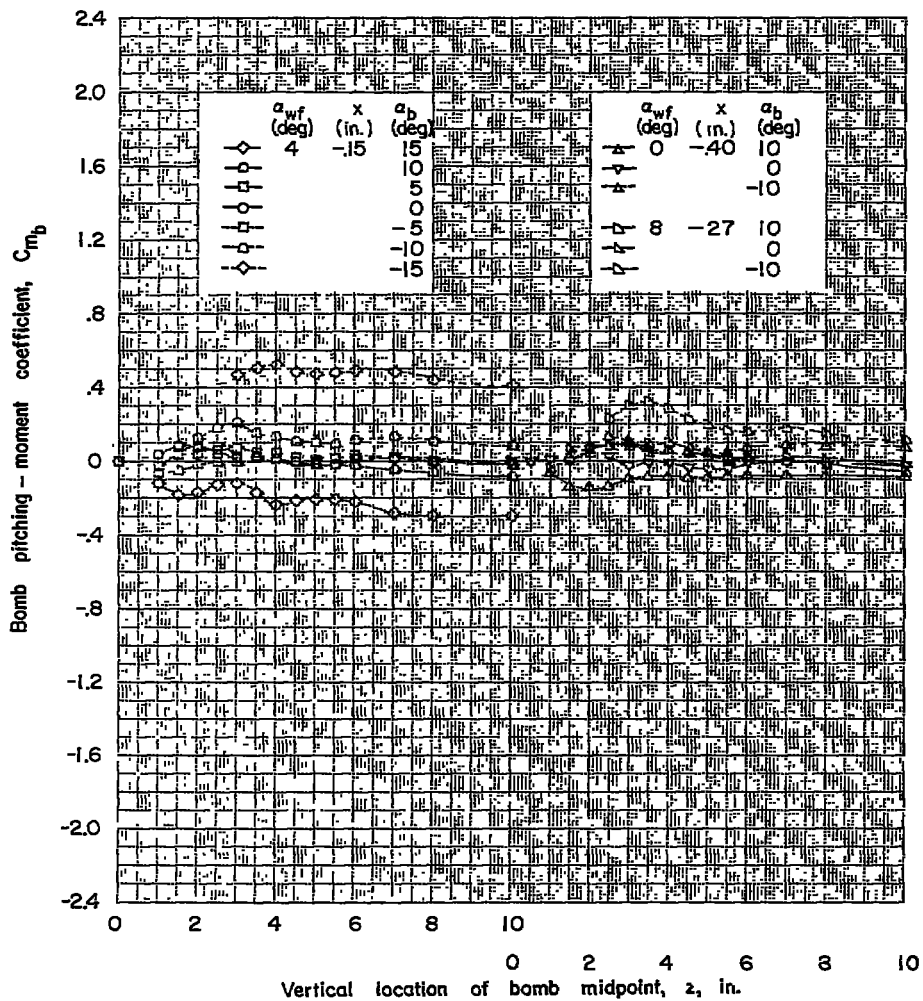
(a)  $x = -0.15$  to  $-0.40$  inch.

Figure 13.- Force data for bomb 3 in presence of wing-fuselage combination. Fins off.



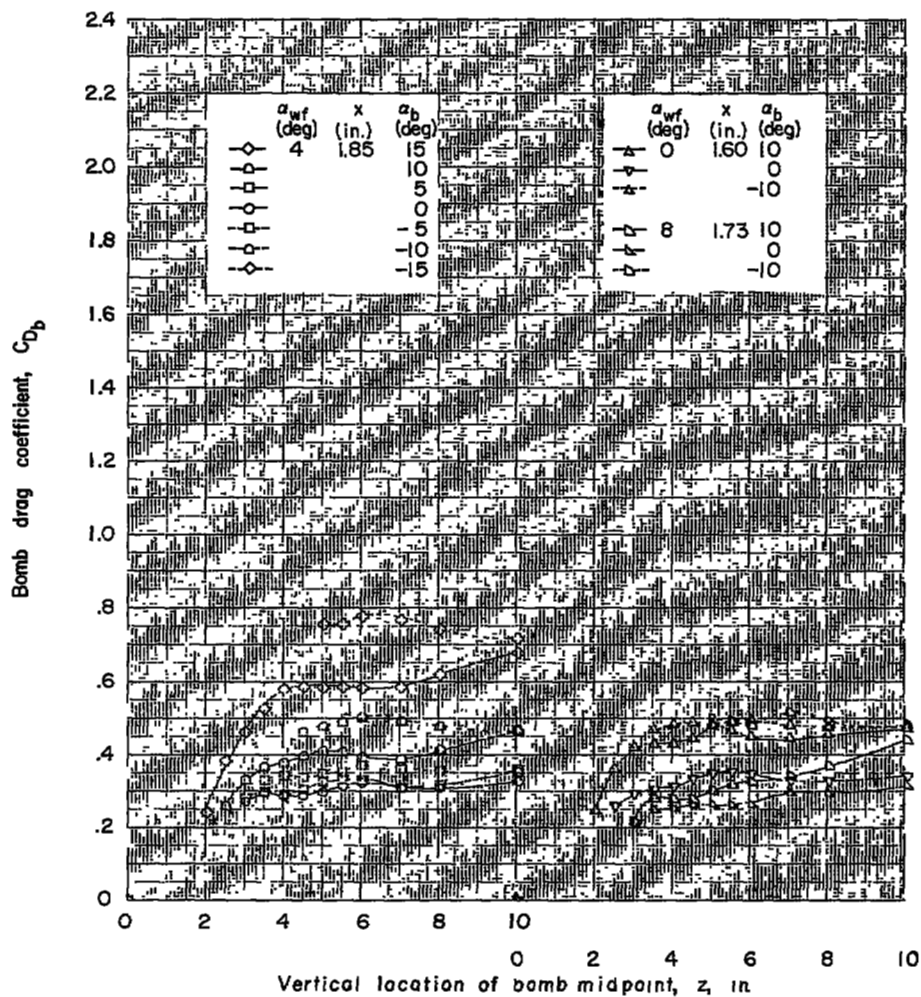
(a) Continued.

Figure 13.- Continued.



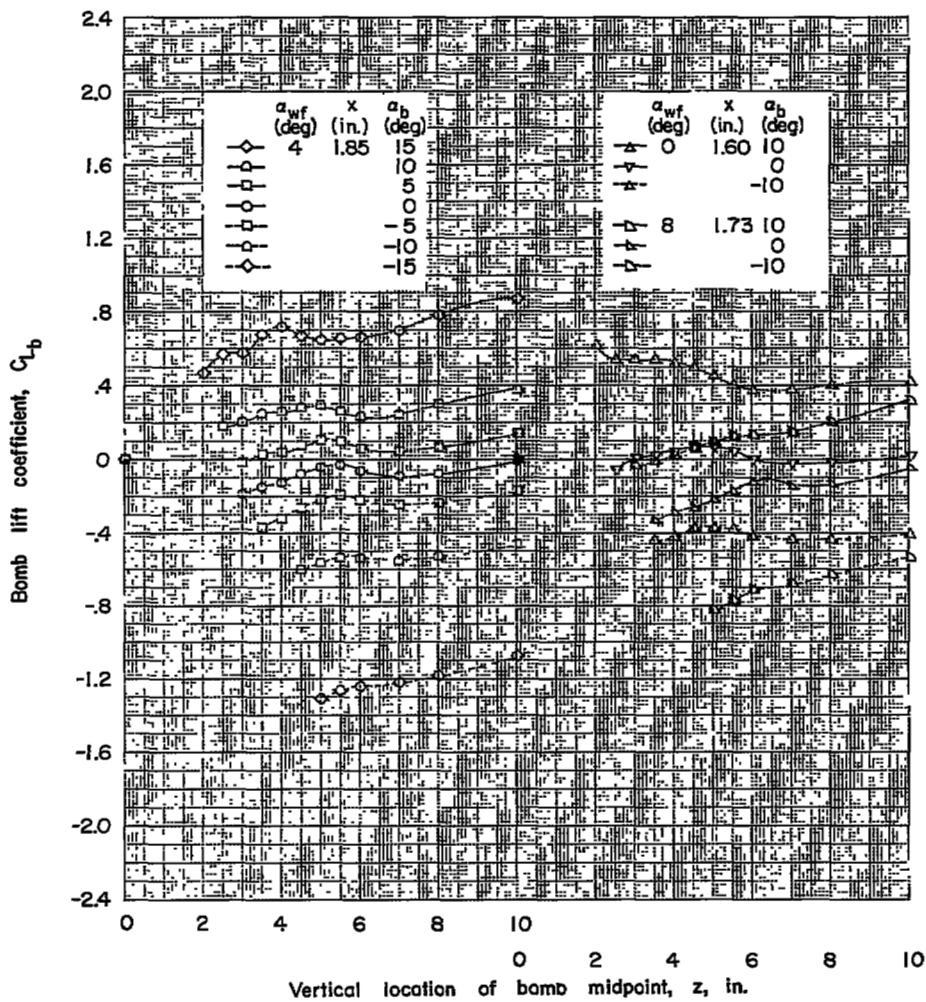
(a) Concluded.

Figure 13.- Continued.



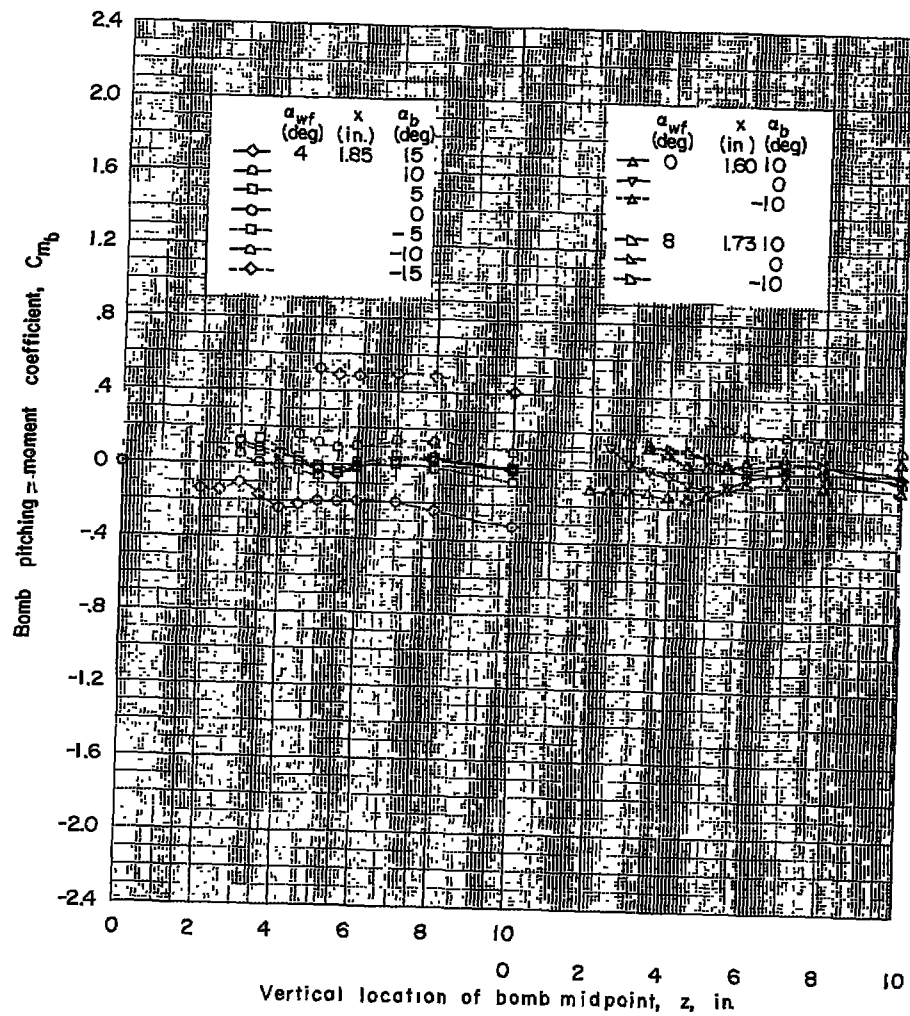
(b)  $x = 1.60$  to  $1.85$  inches.

Figure 13.- Continued.



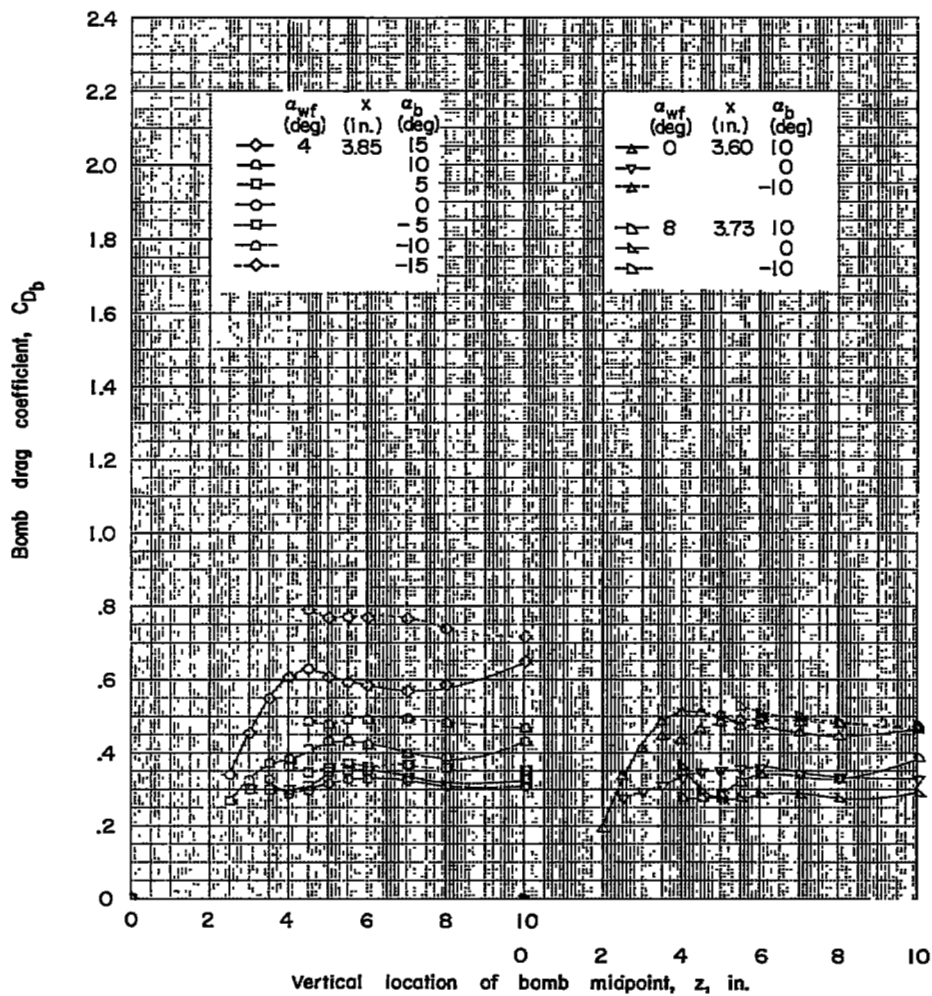
(b) Continued.

Figure 13.- Continued.



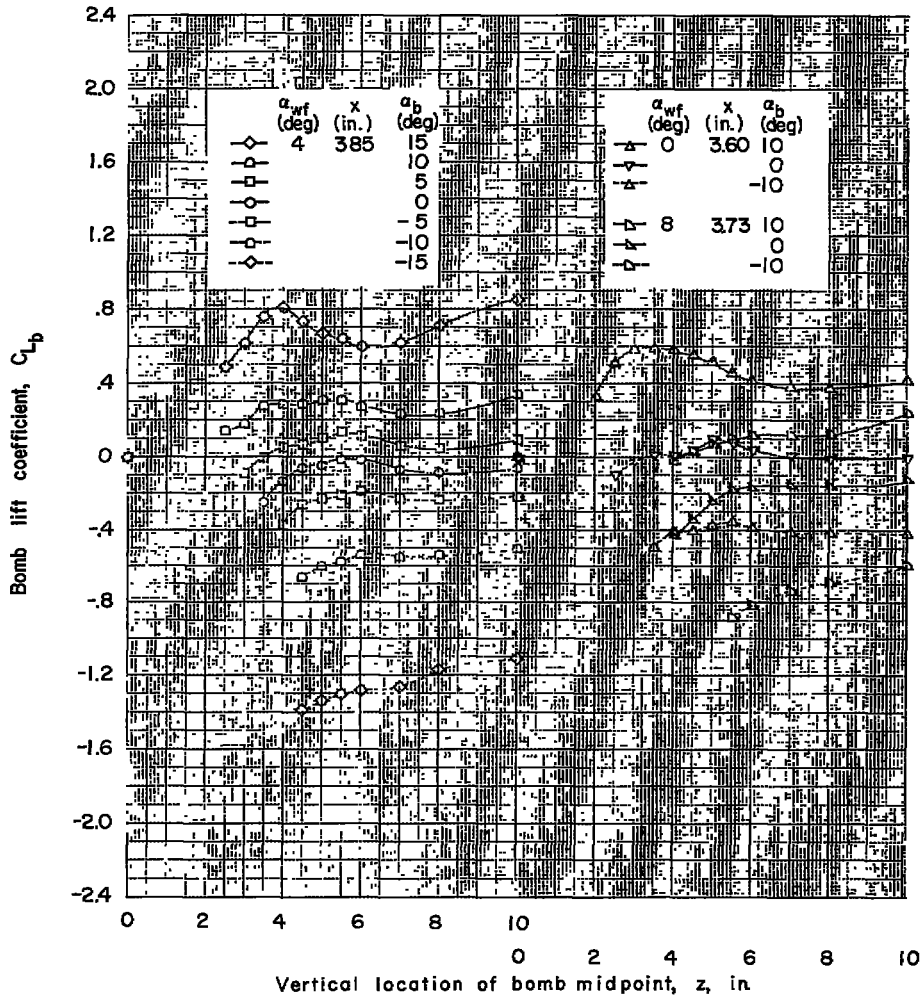
(b) Concluded.

Figure 13.- Continued.



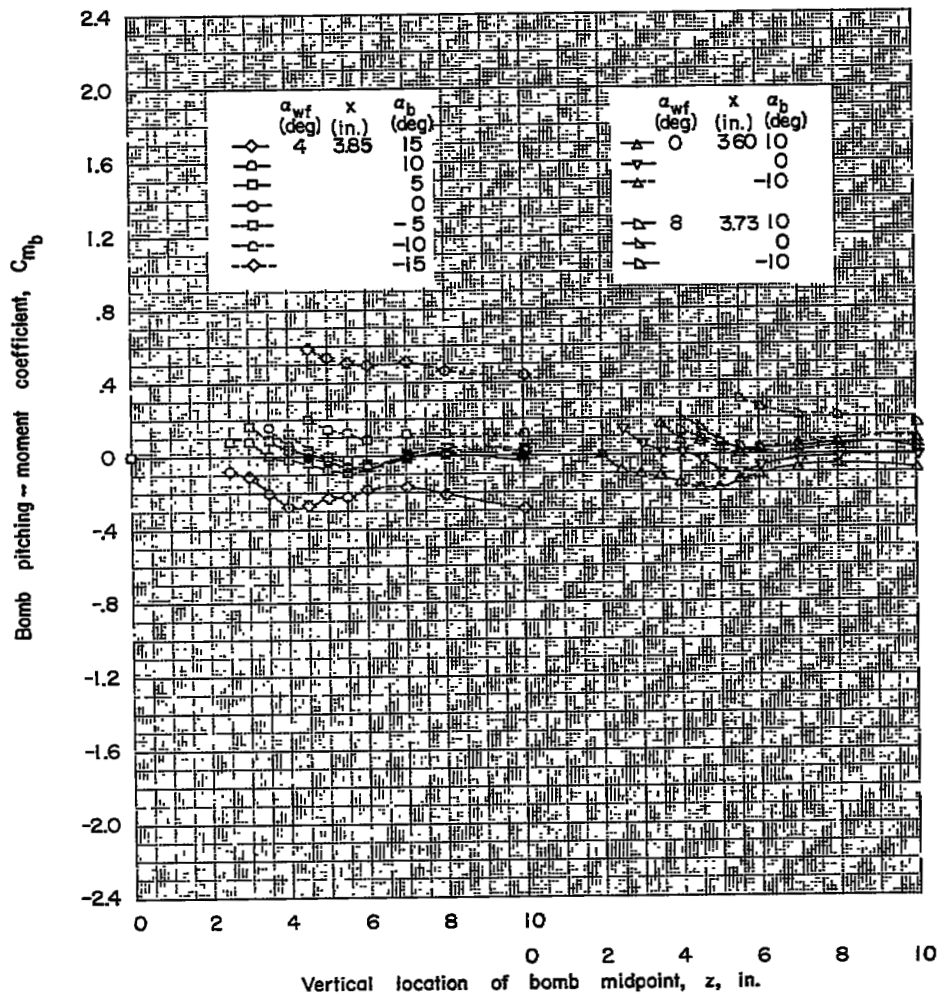
(c)  $x = 3.60$  to  $3.85$  inches.

Figure 13.- Continued.



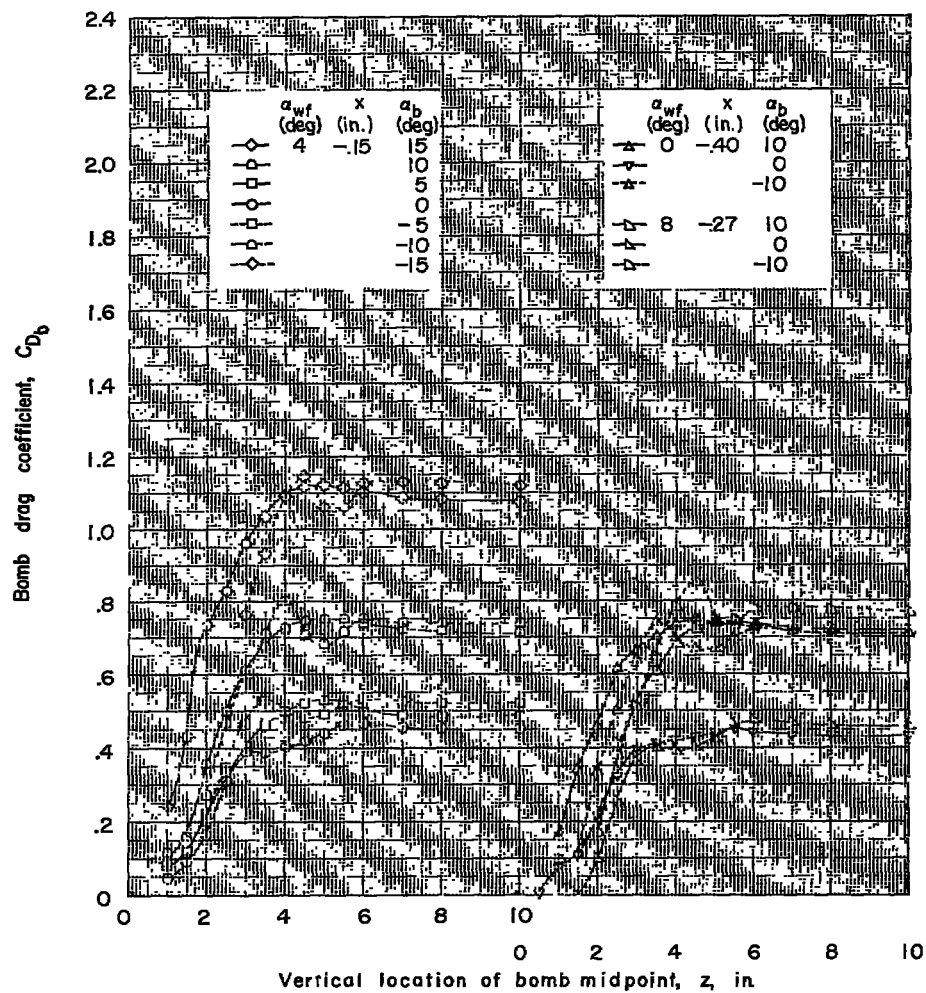
(c) Continued.

Figure 13.- Continued.



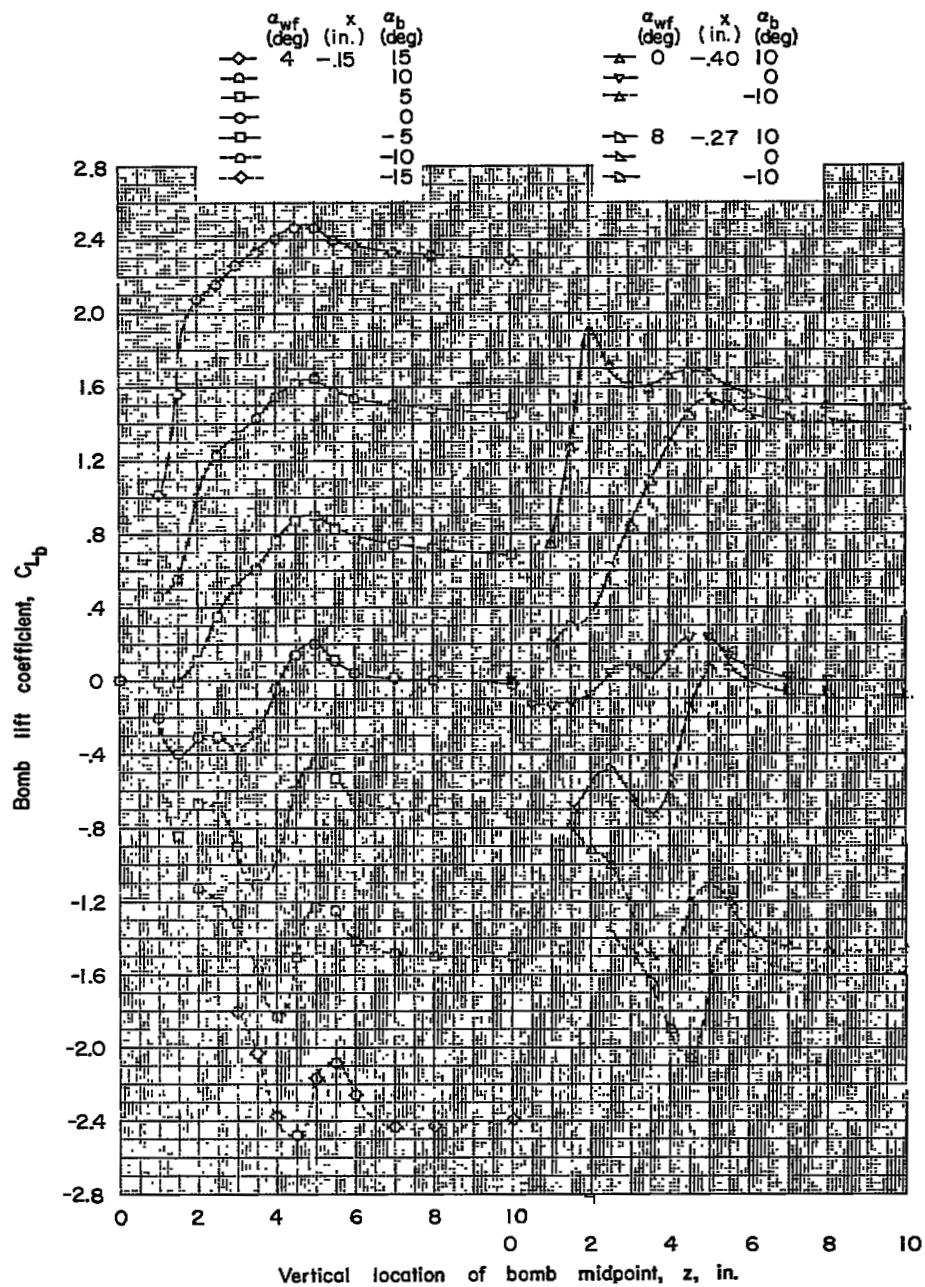
(c) Concluded.

Figure 13.- Concluded.



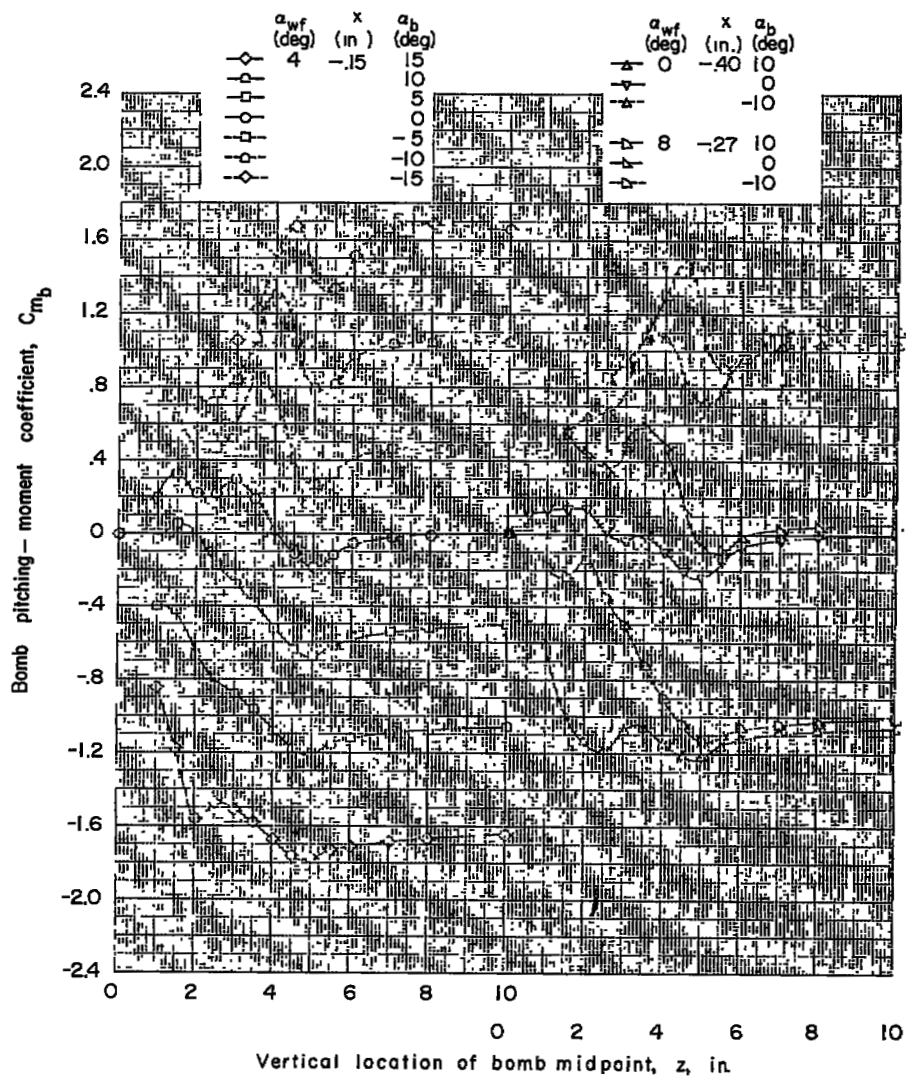
(a)  $x = -0.15$  to  $-0.40$  inch.

Figure 14.- Force data for bomb 3 in presence of fuselage. Fins on; wing off.



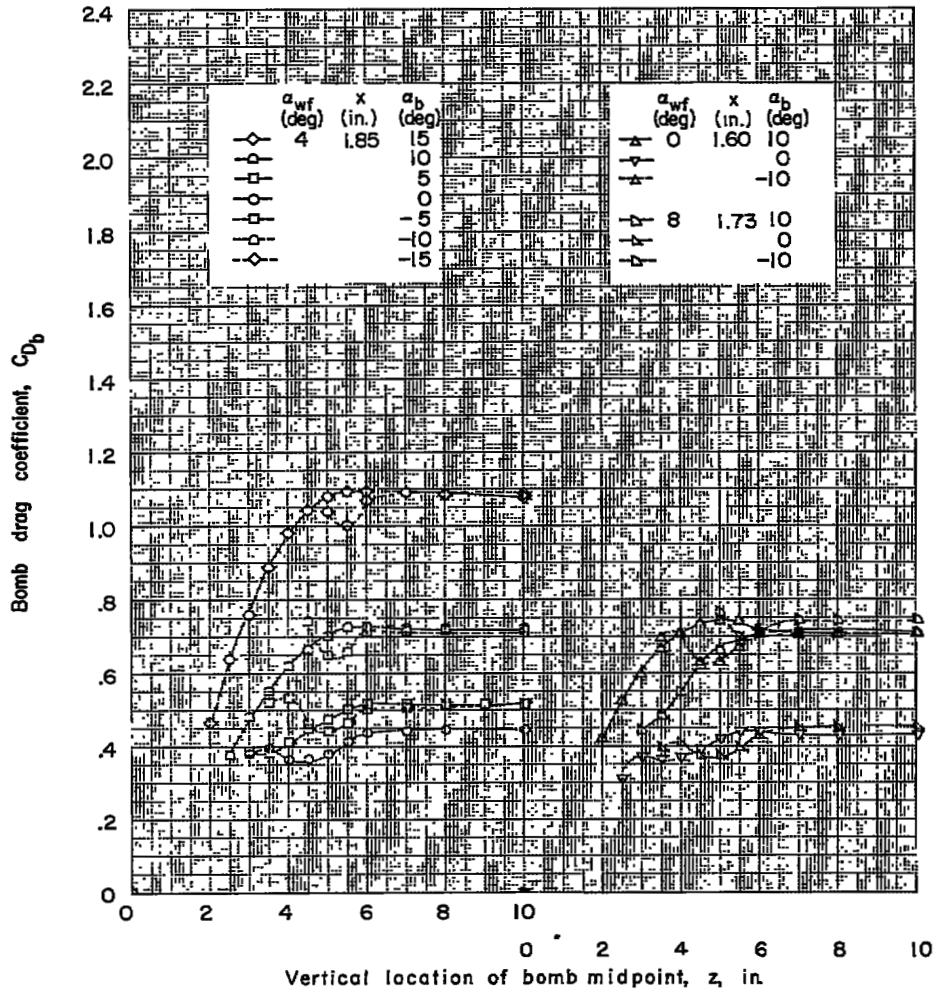
(a) Continued.

Figure 14.- Continued.



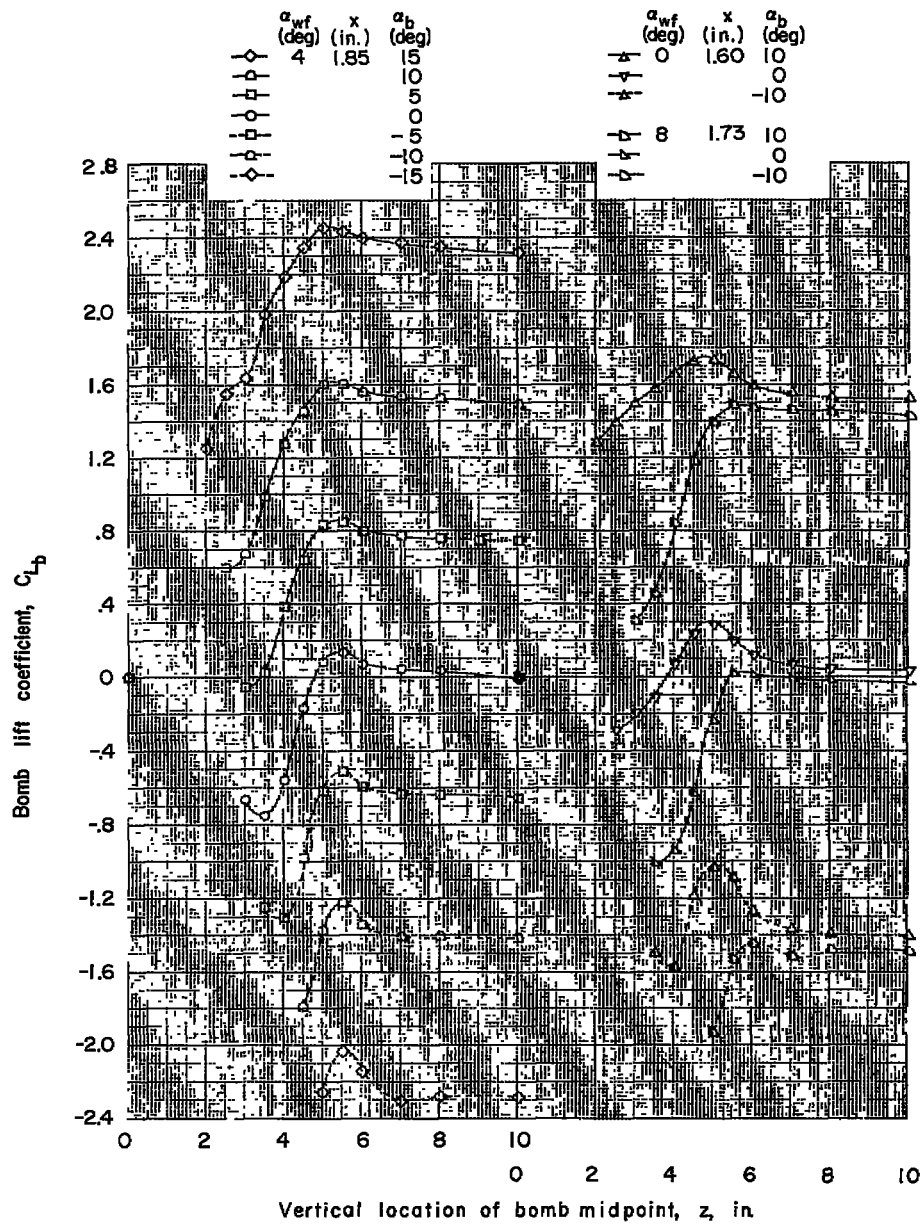
(a) Concluded.

Figure 14.- Continued.



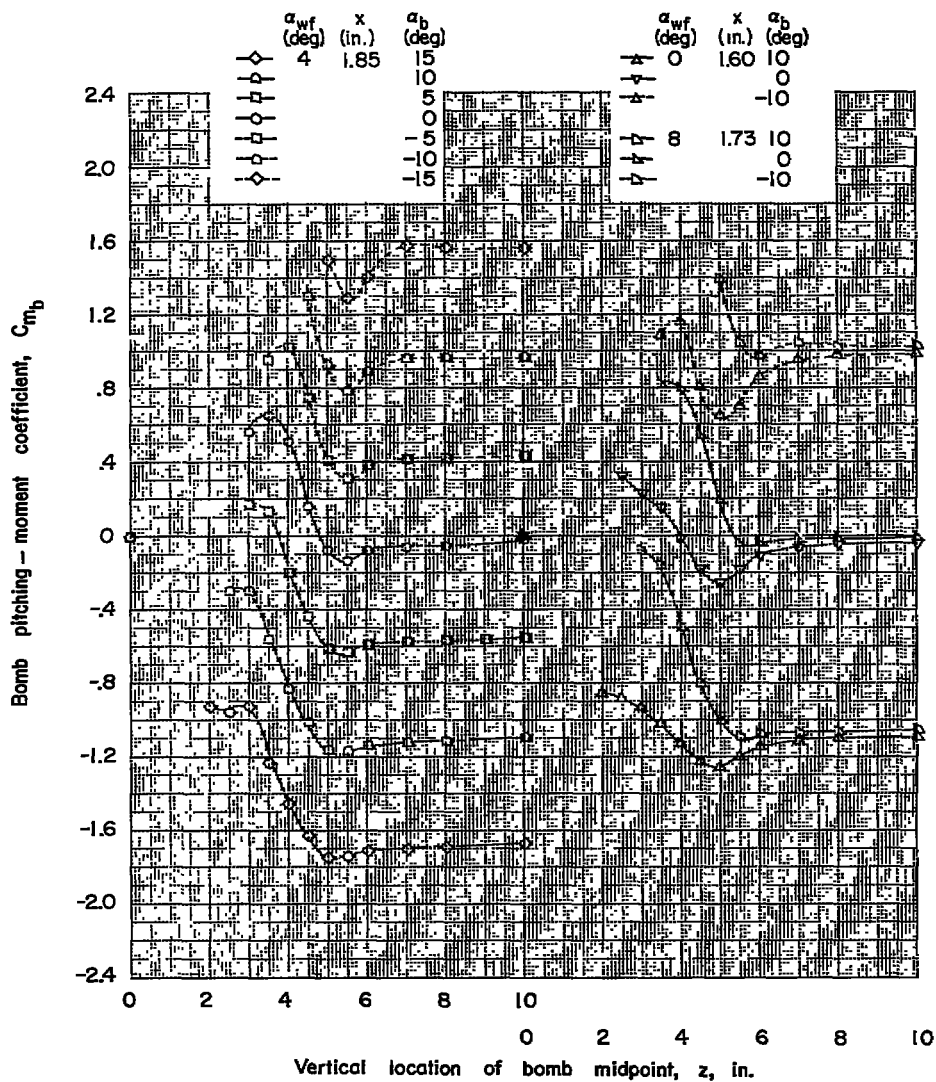
(b)  $x = 1.60$  to  $1.85$  inches.

Figure 14.- Continued.



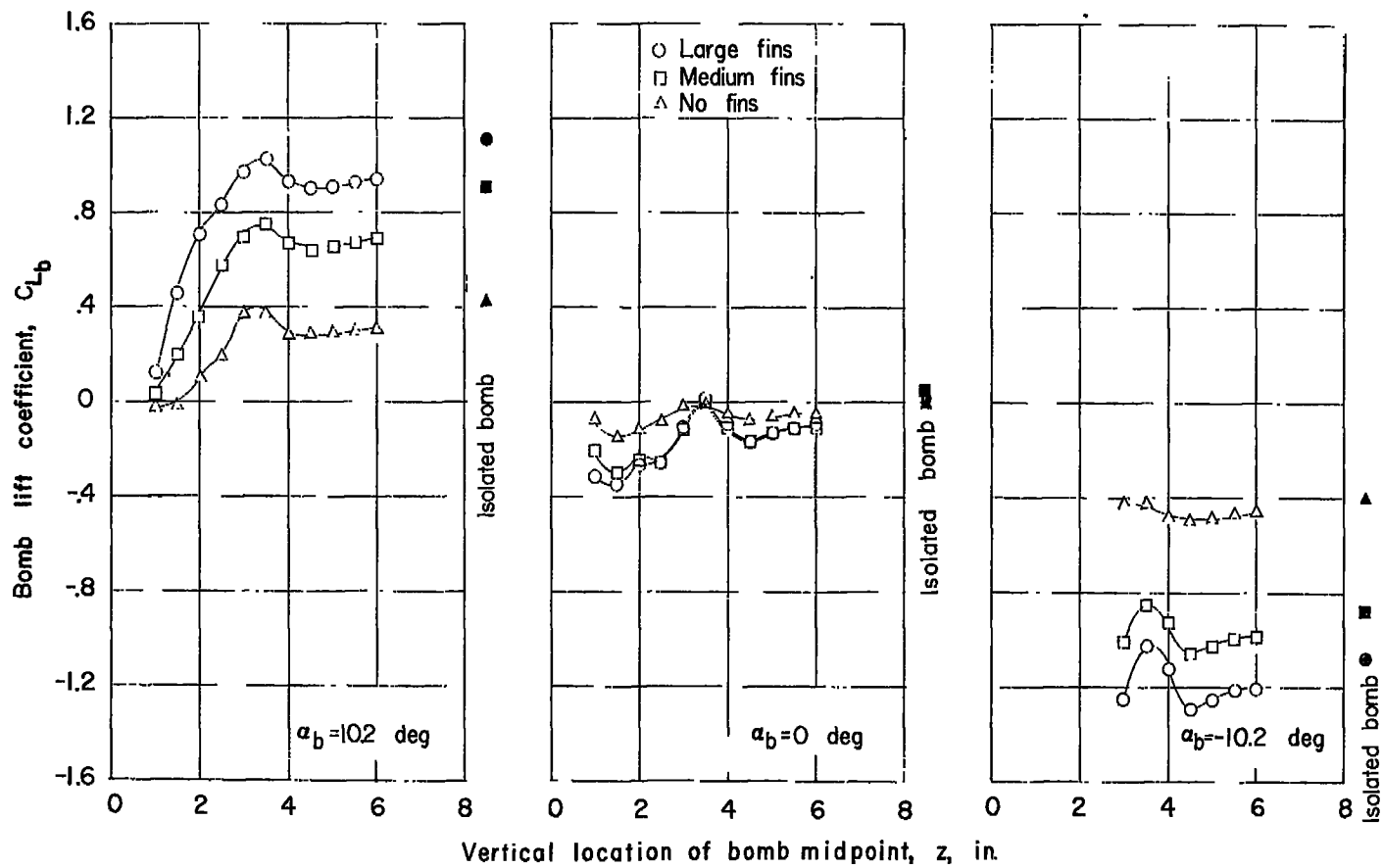
(b) Continued.

Figure 14.- Continued.



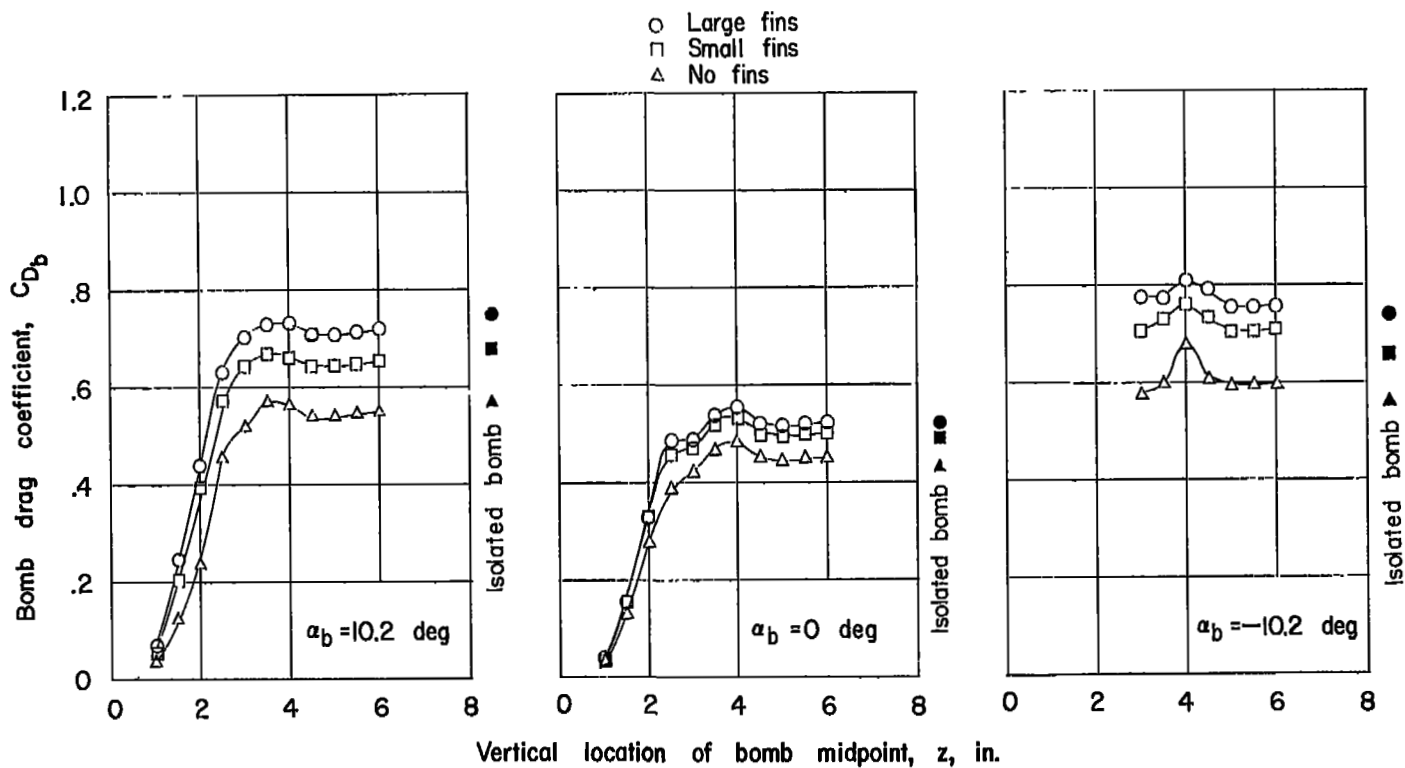
(b) Concluded.

Figure 14.- Concluded.



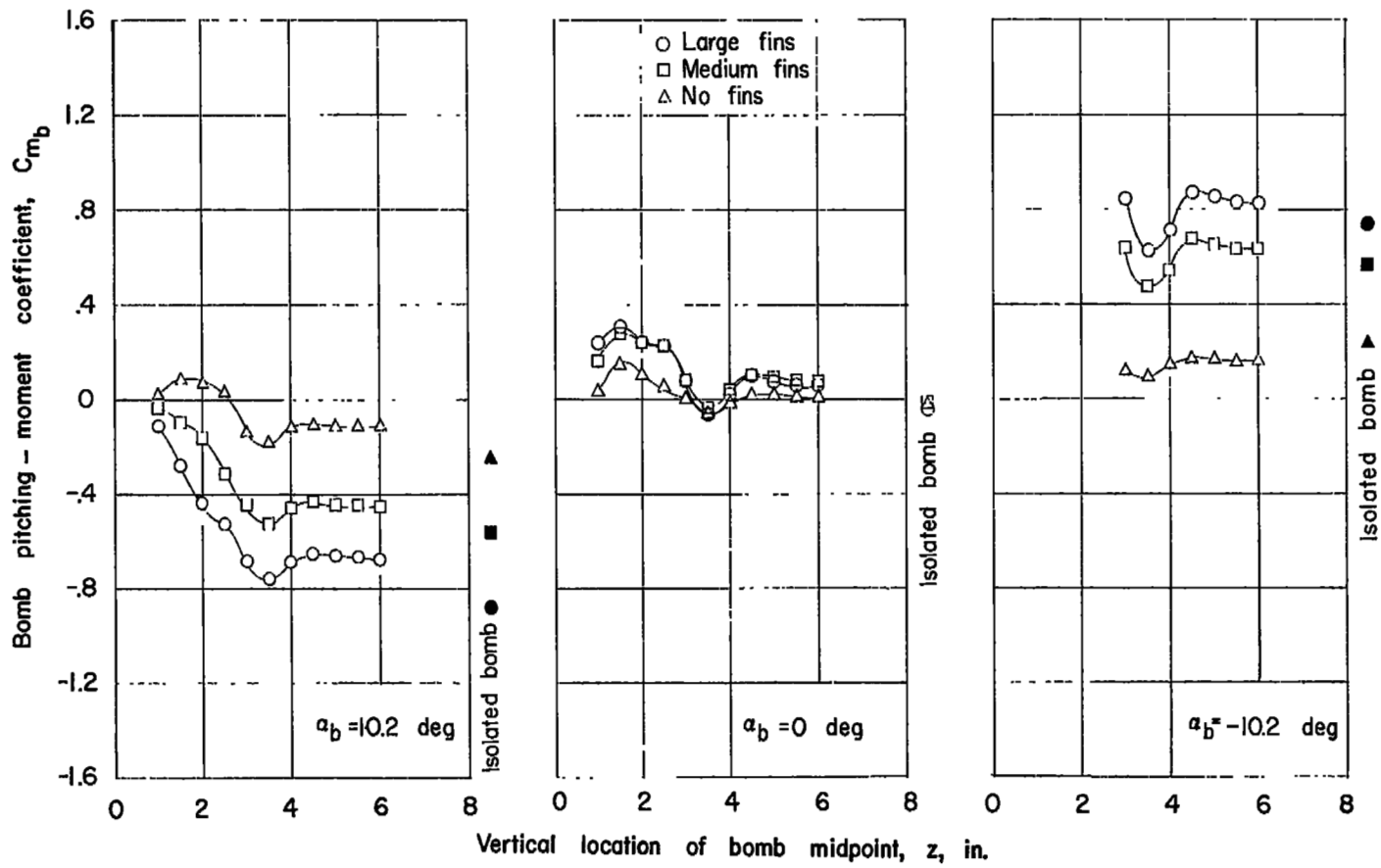
(a) Lift.

Figure 15.- Effect of tail fins on the forces on bomb 2.  $\alpha_{wI} = 4^\circ$ ;  
 $x = -1.05$  inches.



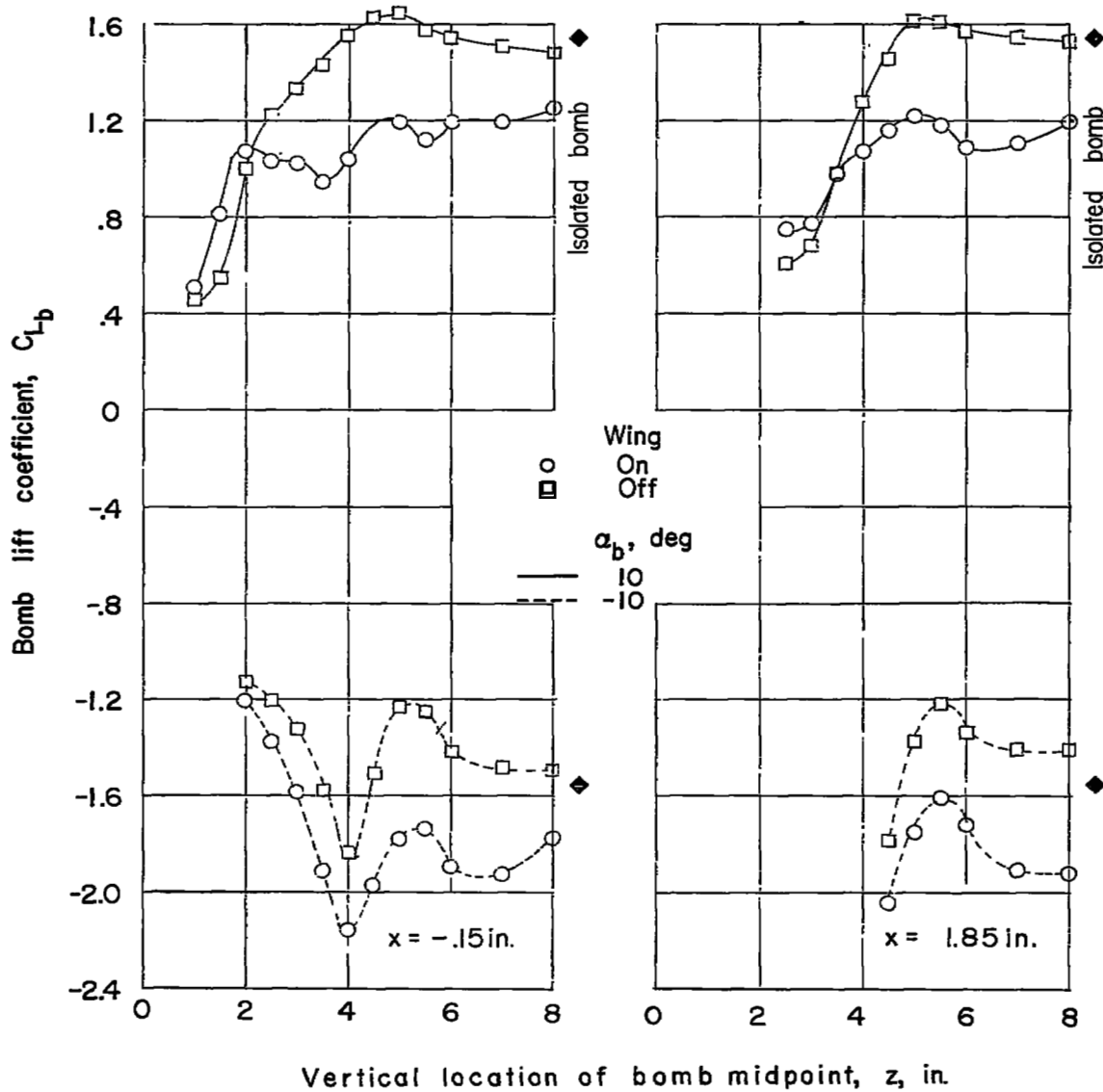
(b) Drag.

Figure 15.- Continued.



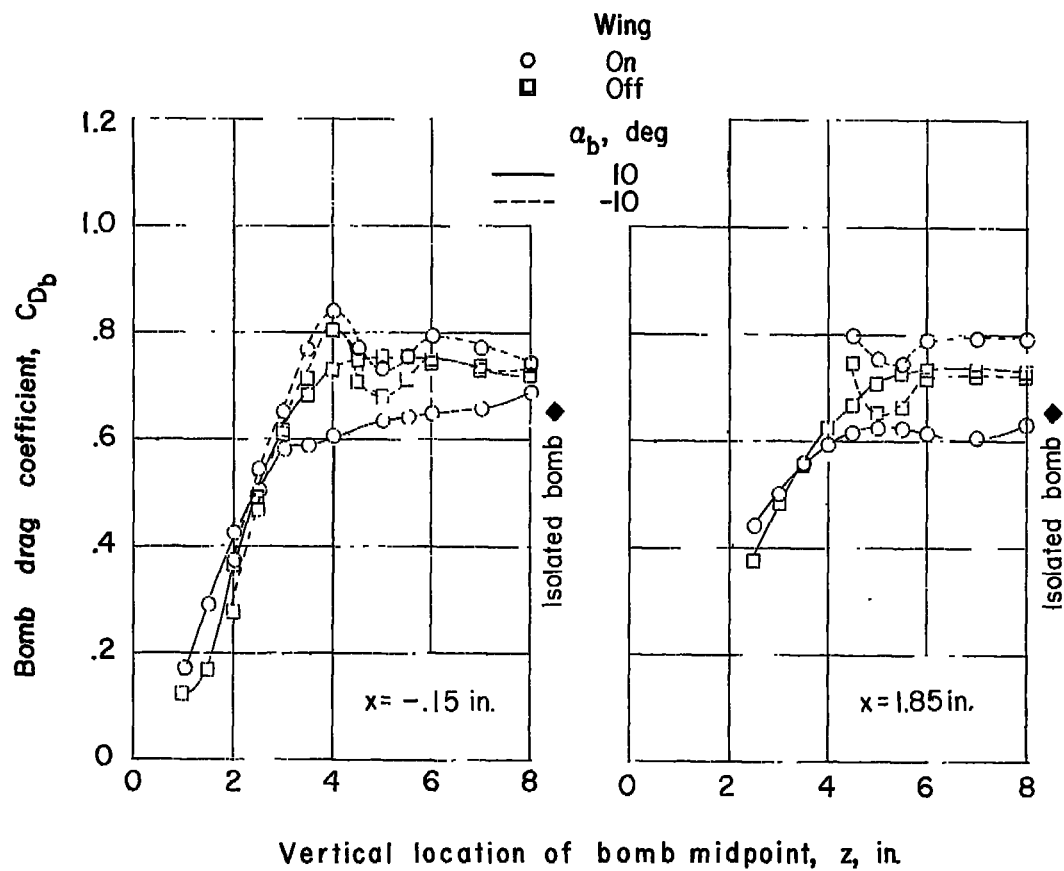
(c) Pitching moment.

Figure 15.- Concluded.



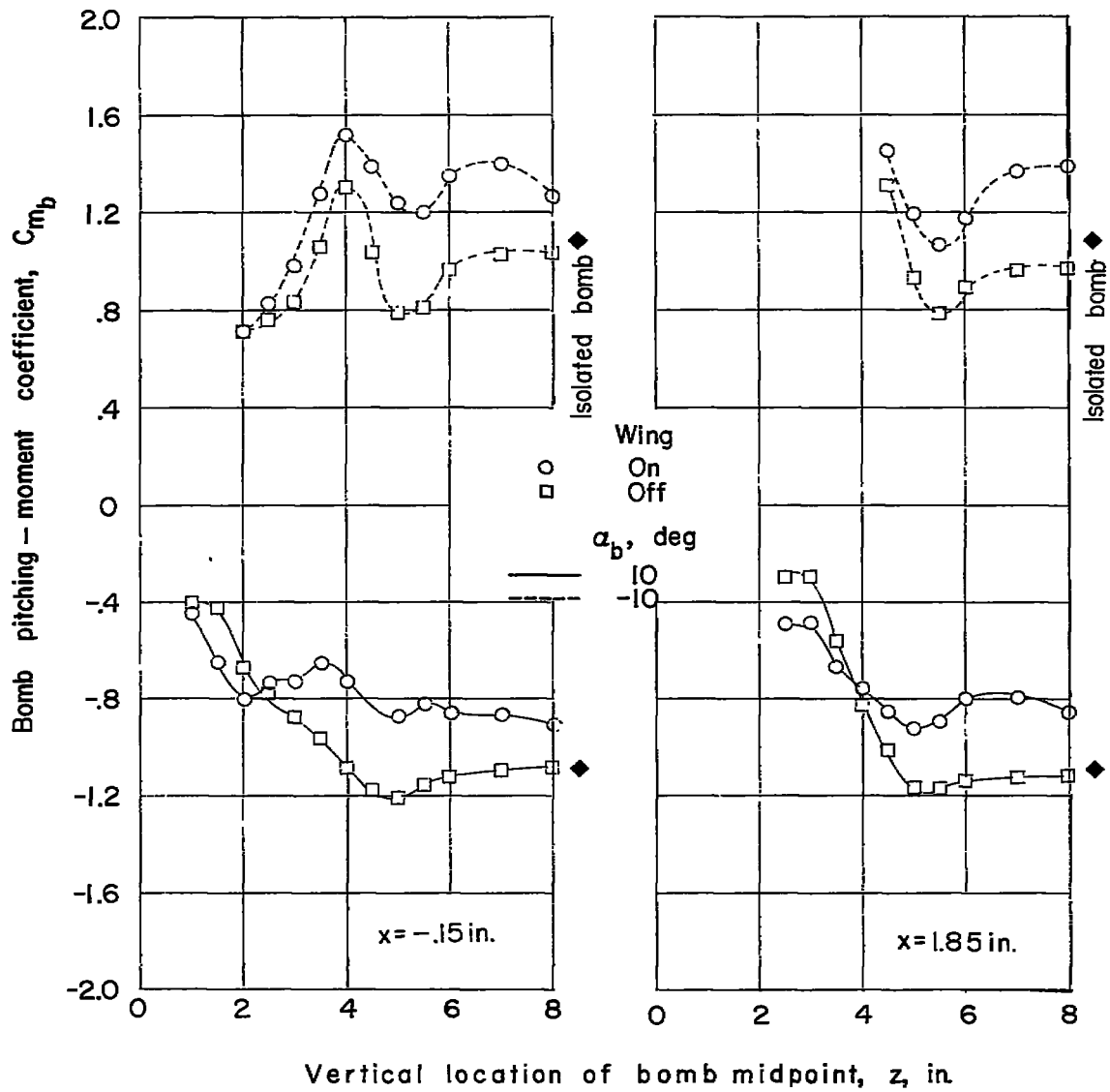
(a) Lift.

Figure 16.- Effect of wing on the forces on bomb 3.  $\alpha_{wf} = 4^\circ$ .



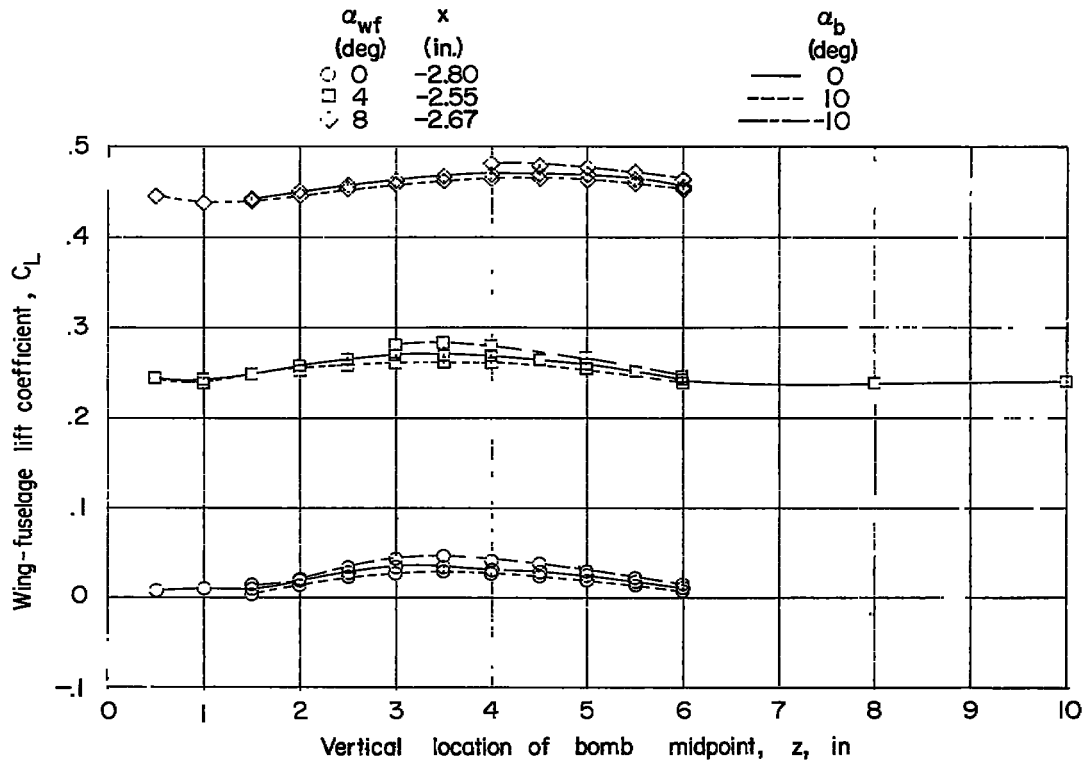
(b) Drag.

Figure 16.- Continued.



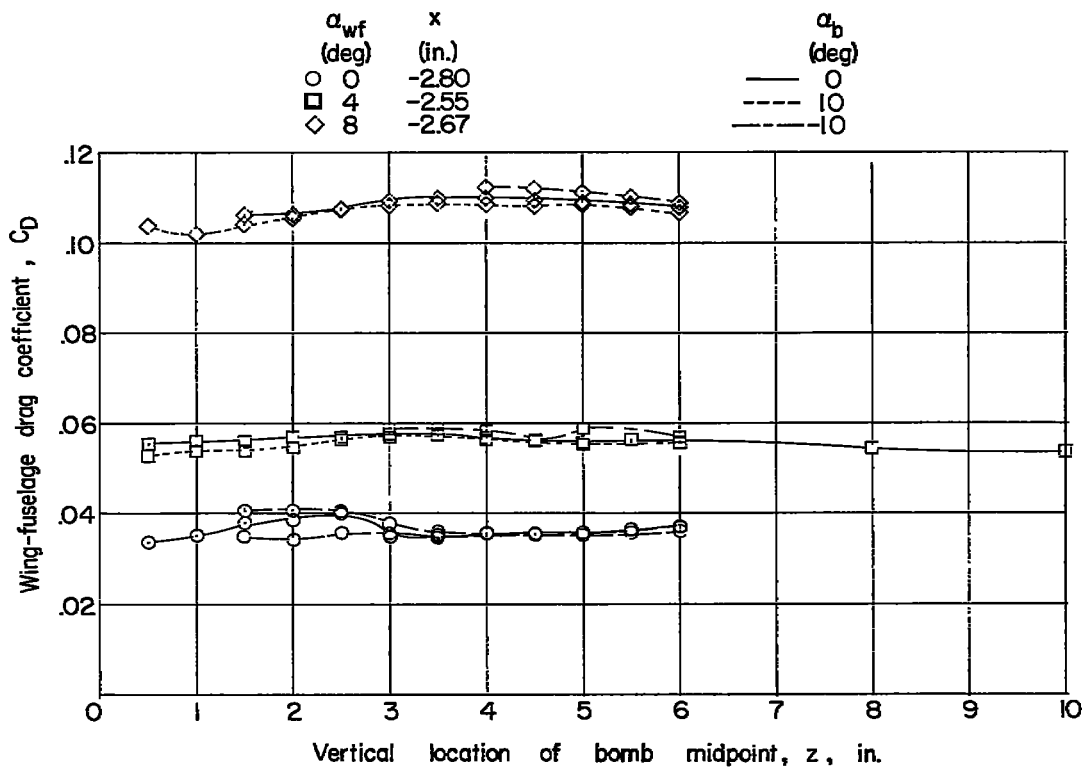
(c) Pitching moment.

Figure 16.- Concluded.



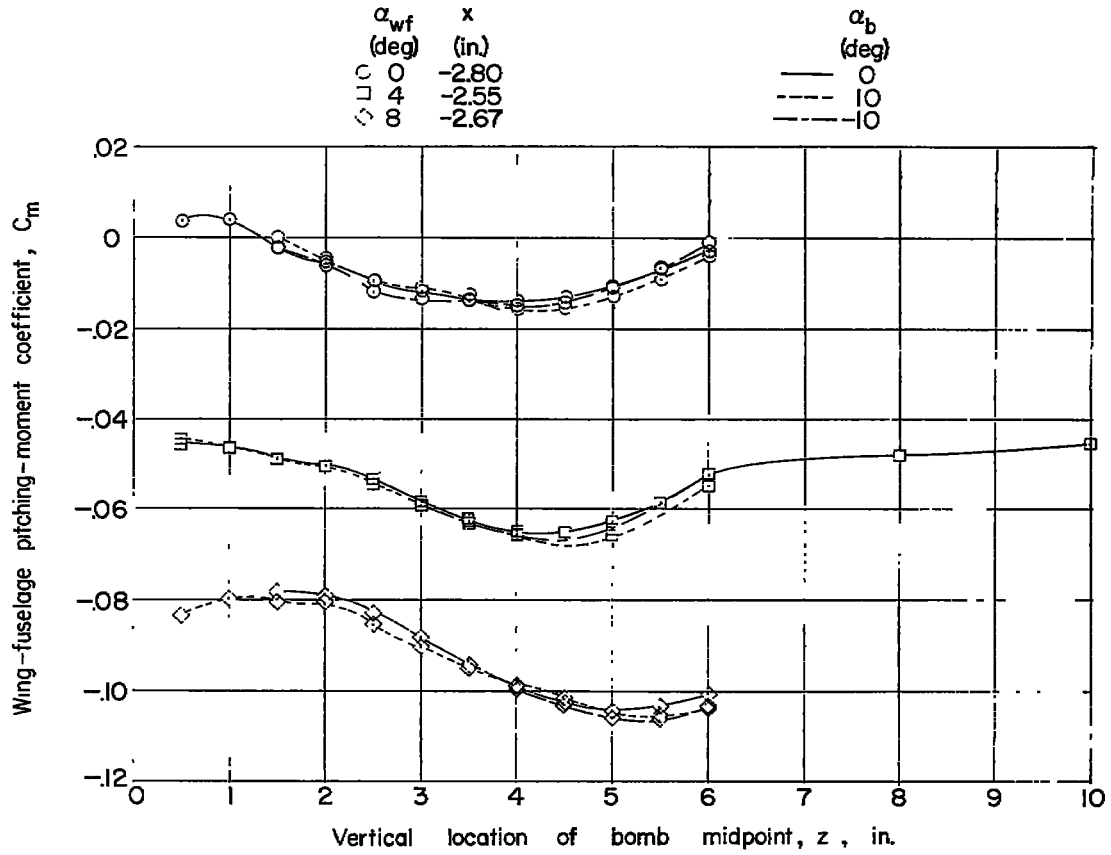
(a) Lift.

Figure 17.- Force data for wing-fuselage combination in presence of bomb 1.



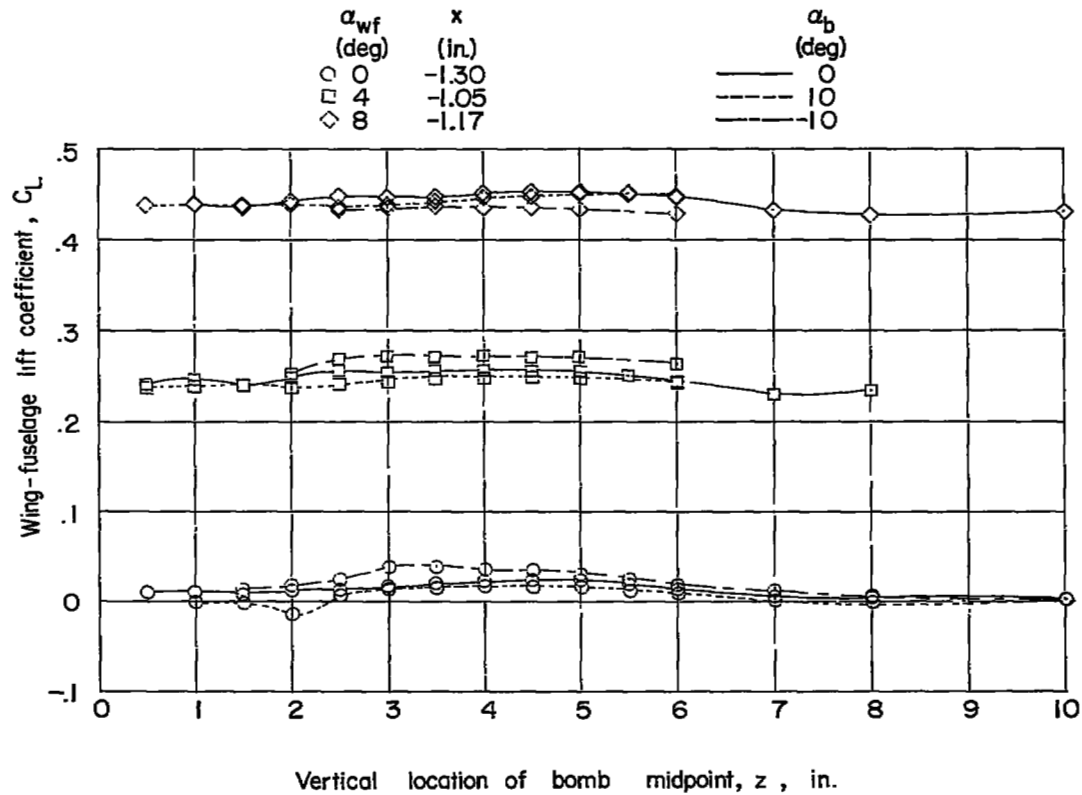
(b) Drag.

Figure 17.- Continued.



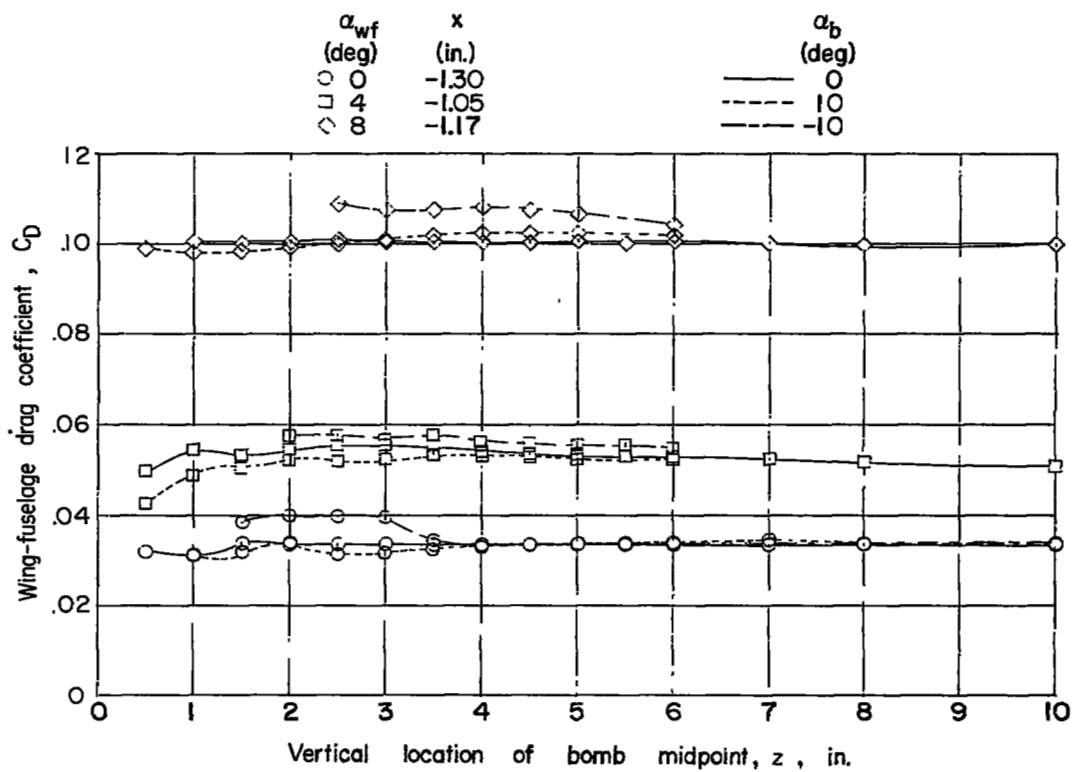
(c) Pitching moment.

Figure 17.- Concluded.



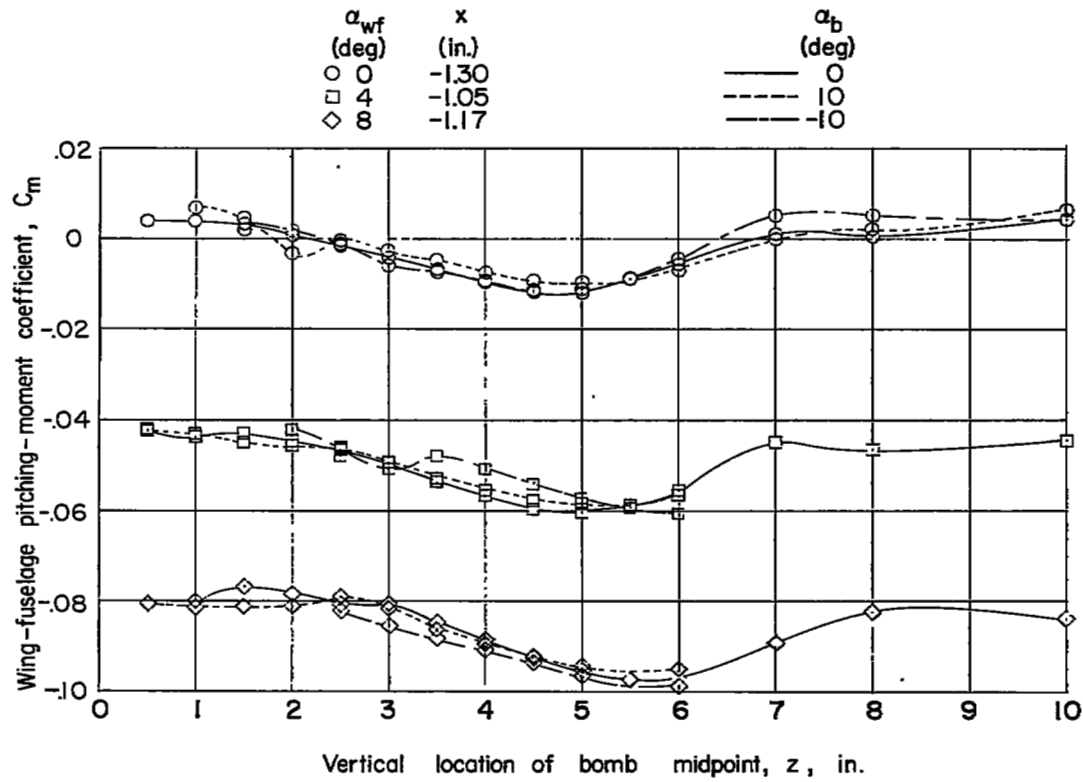
(a) Lift.

Figure 18.- Force data for wing-fuselage combination in presence of bomb 2.



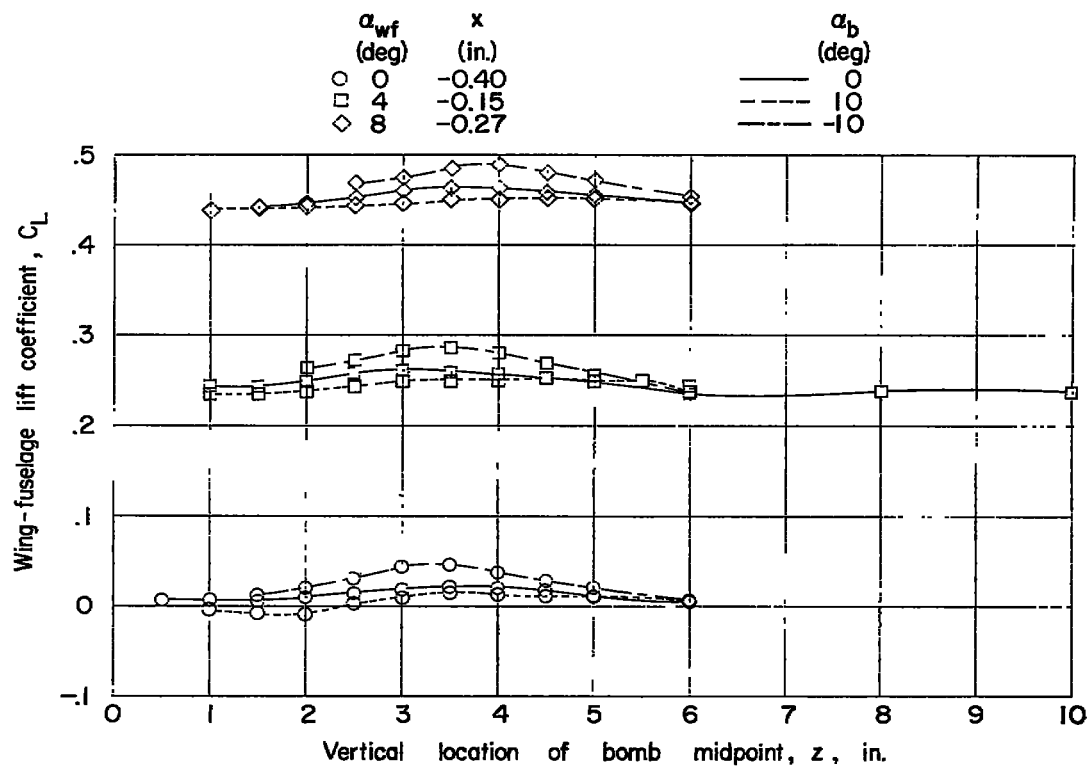
(b) Drag.

Figure 18.- Continued.



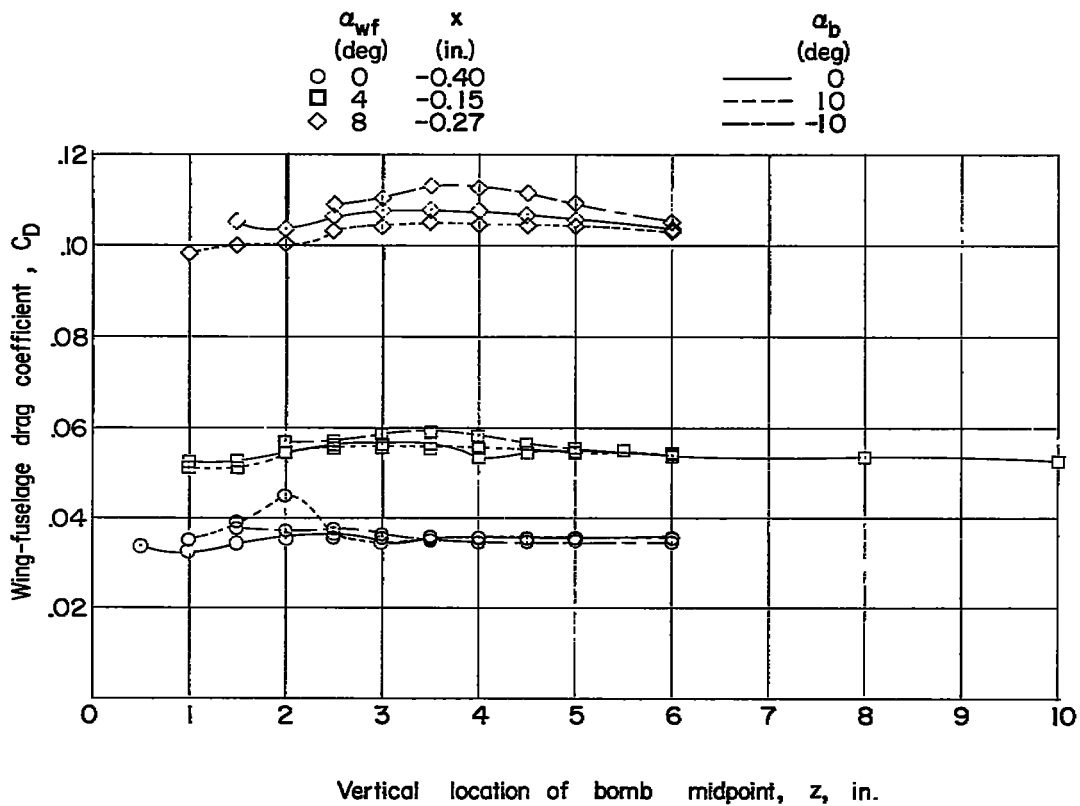
(c) Pitching moment.

Figure 18.- Concluded.



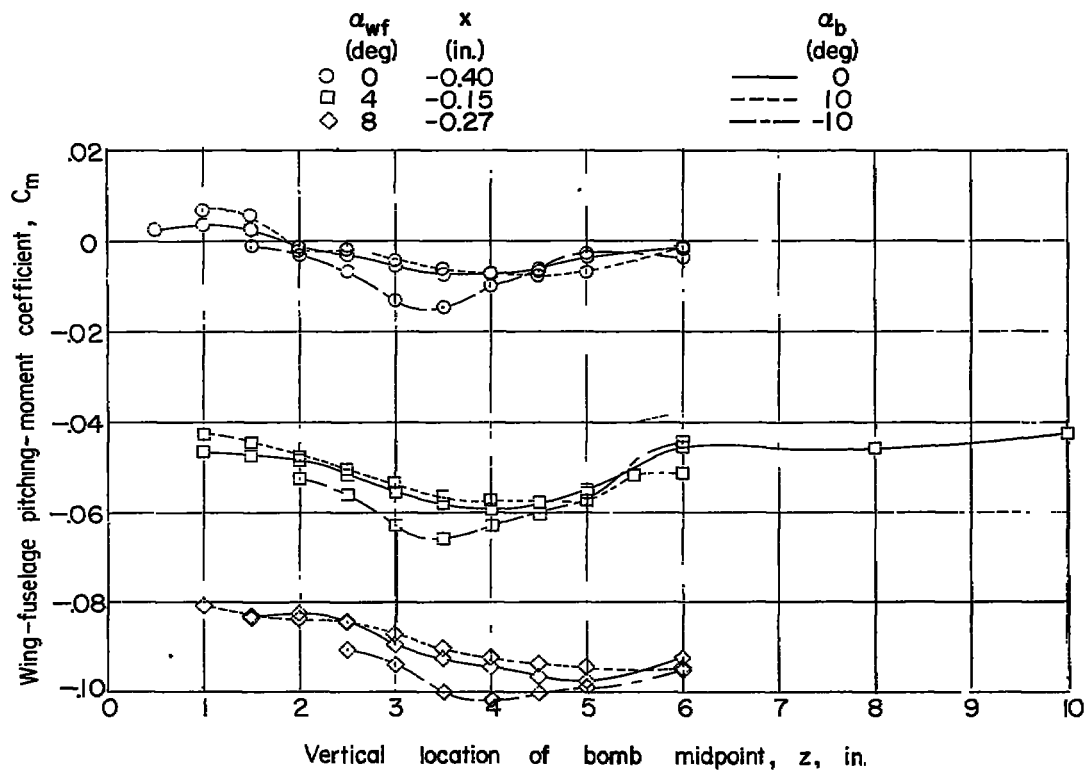
(a) Lift.

Figure 19.- Force data for wing-fuselage combination in presence of bomb 3.



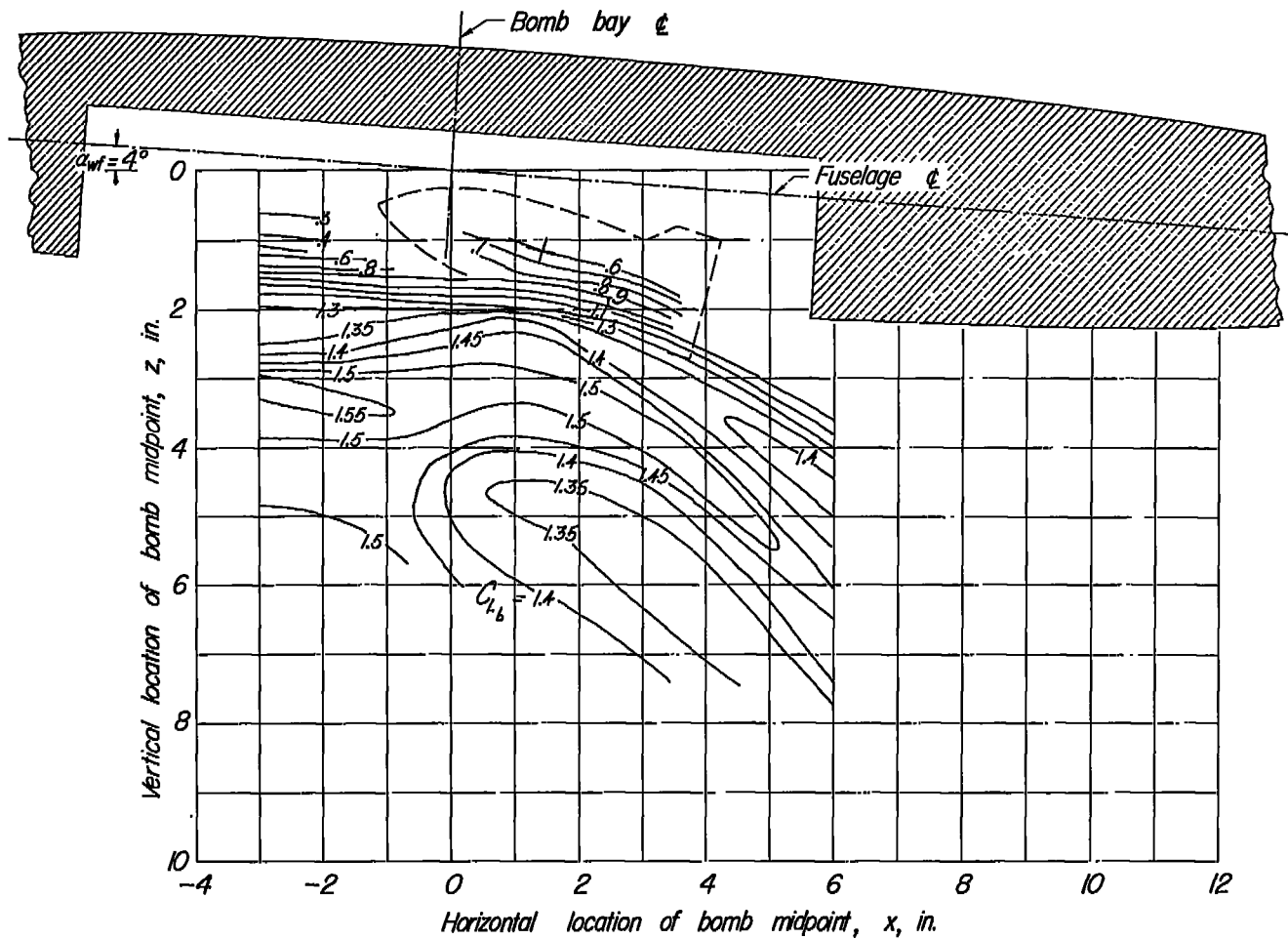
(b) Drag.

Figure 19.- Continued.



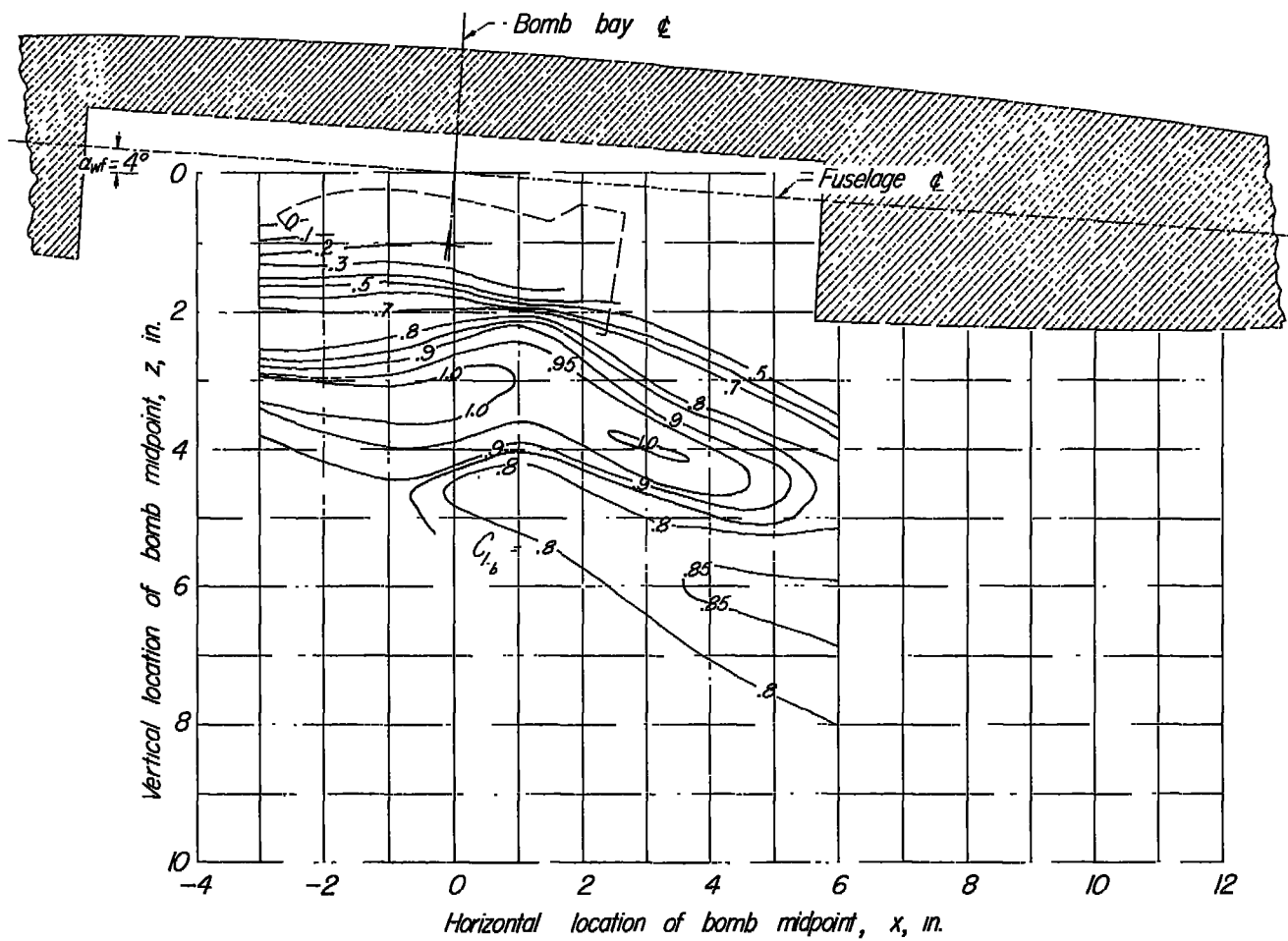
(c) Pitching moment.

Figure 19.- Concluded.



(a)  $\alpha_b = 15^\circ$ .

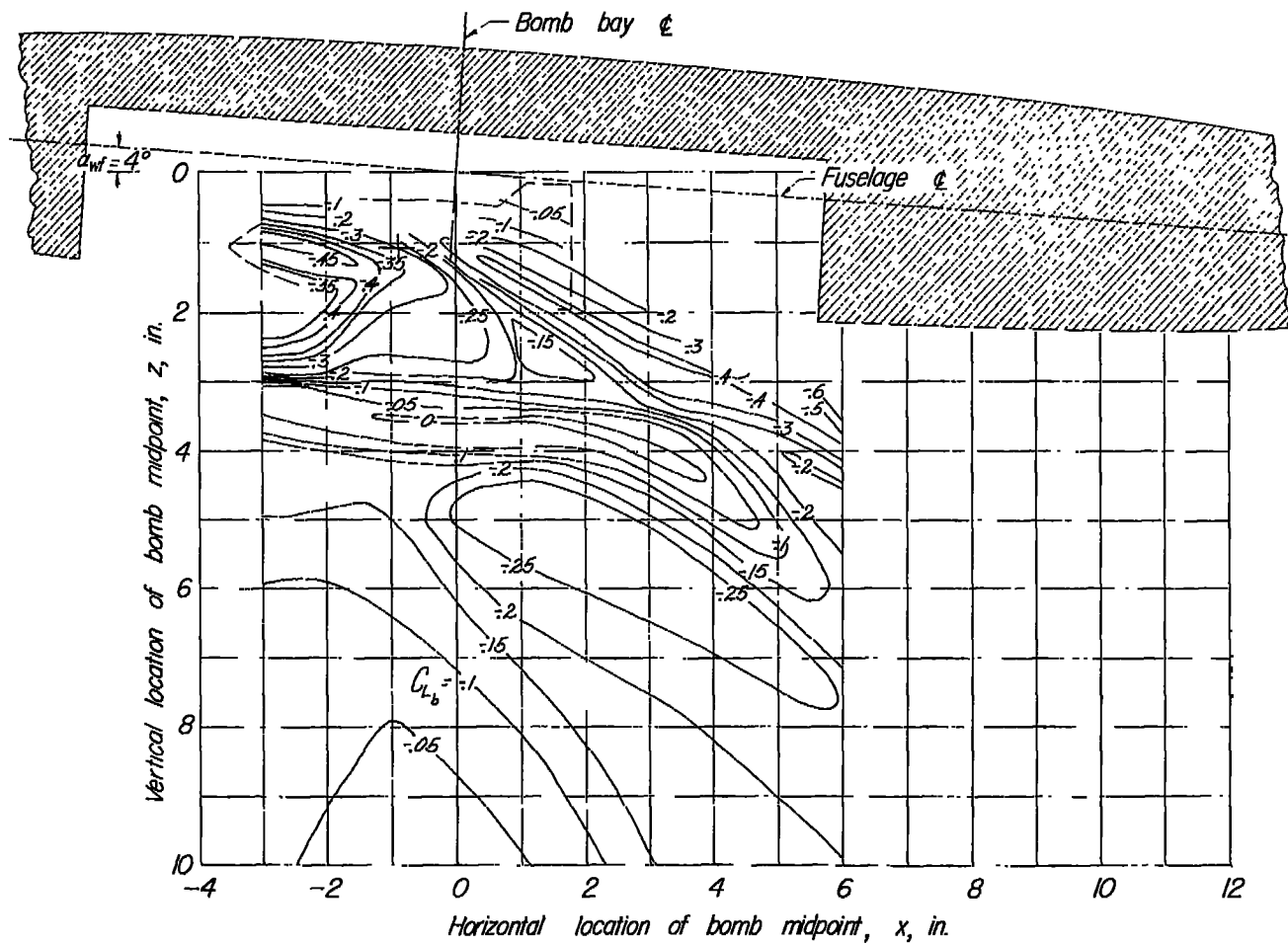
Figure 20.- Contour plot of the lift of bomb 2 in presence of the wing-fuselage combination.  $\alpha_{wf} = 4^\circ$ .



(b)  $\alpha_b = 10^\circ$ .

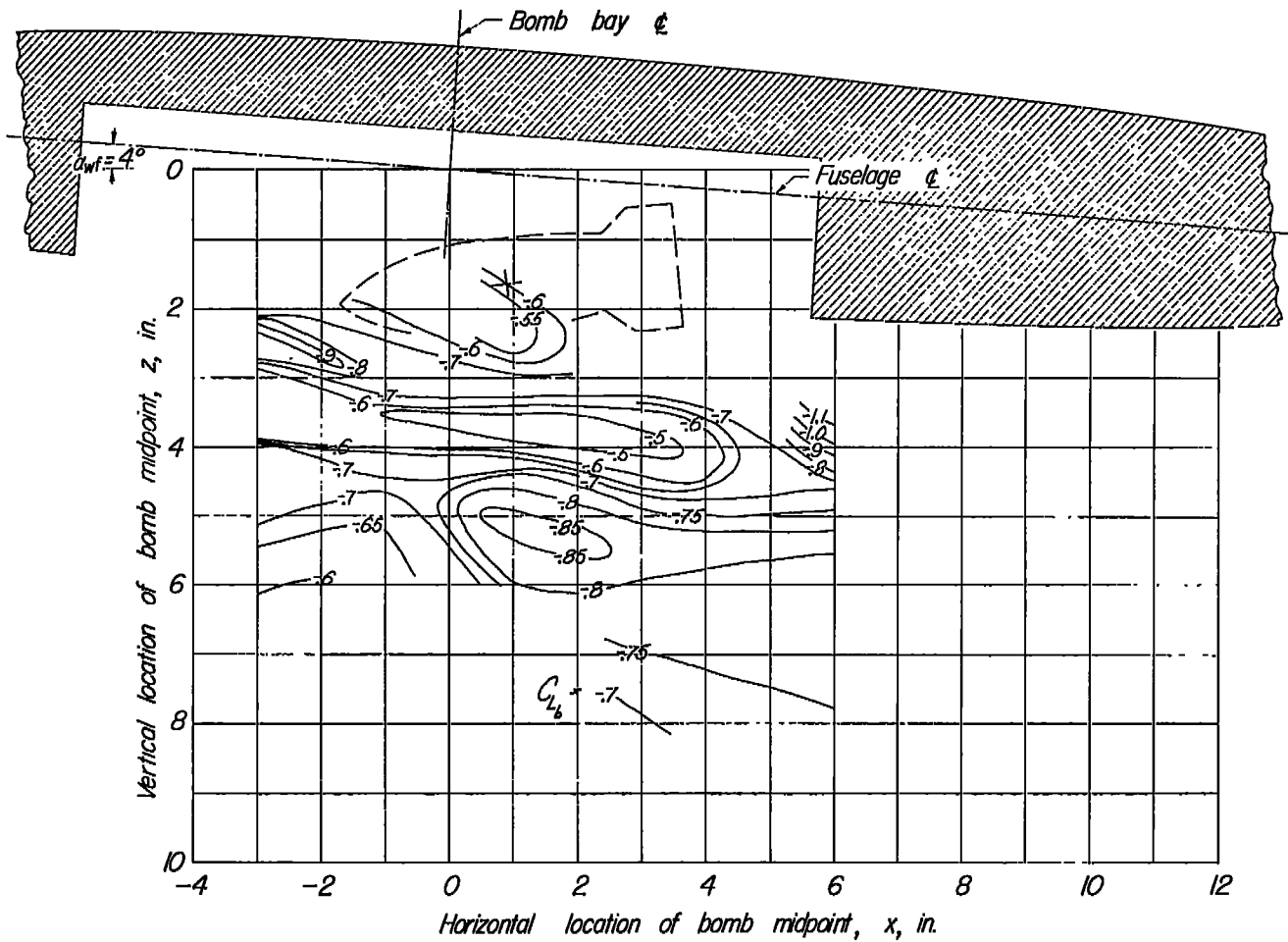
Figure 20.- Continued.





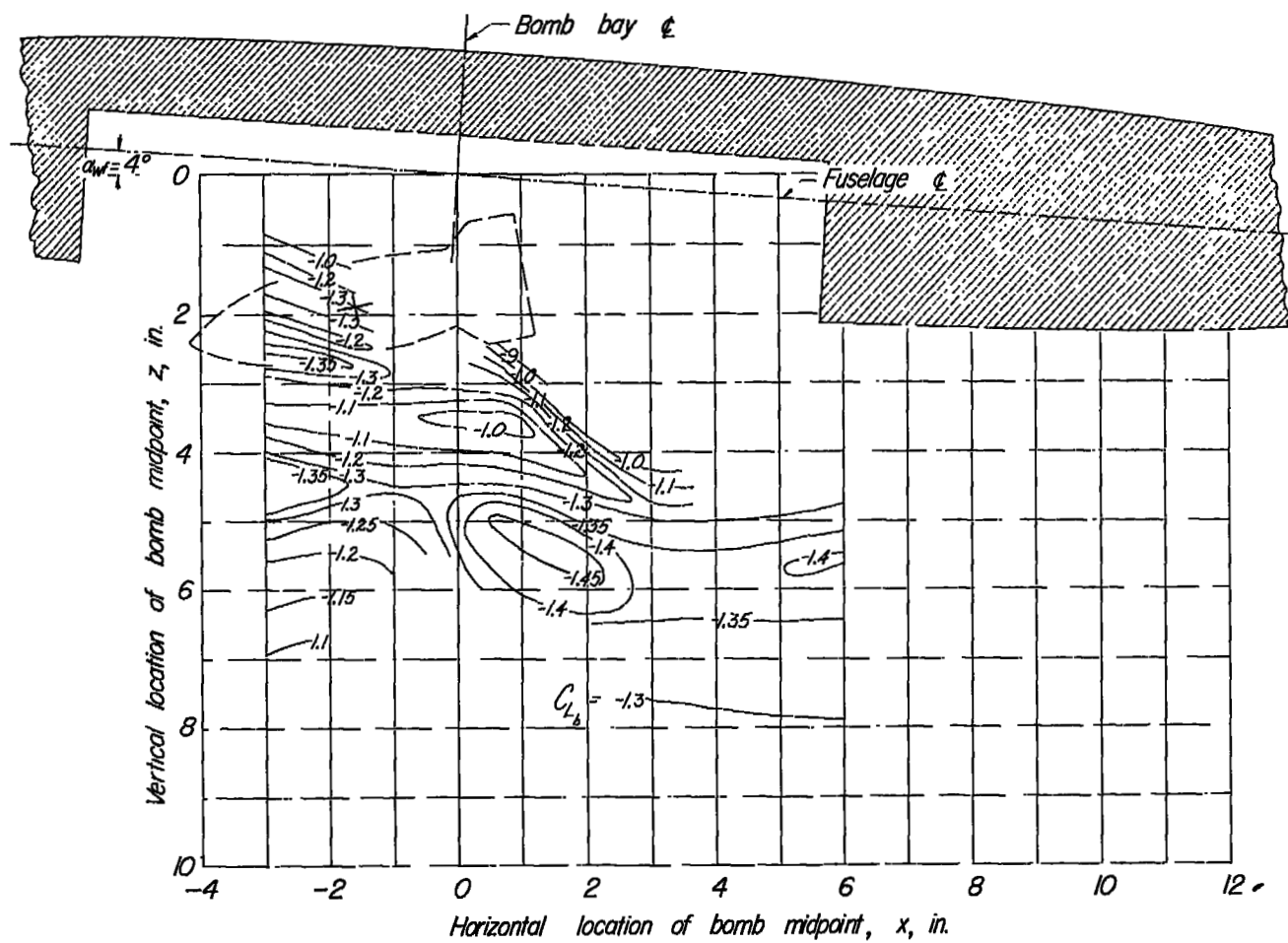
(d)  $\alpha_b = 0^\circ$ .

Figure 20.- Continued.



(e)  $\alpha_b = -5^\circ$ .

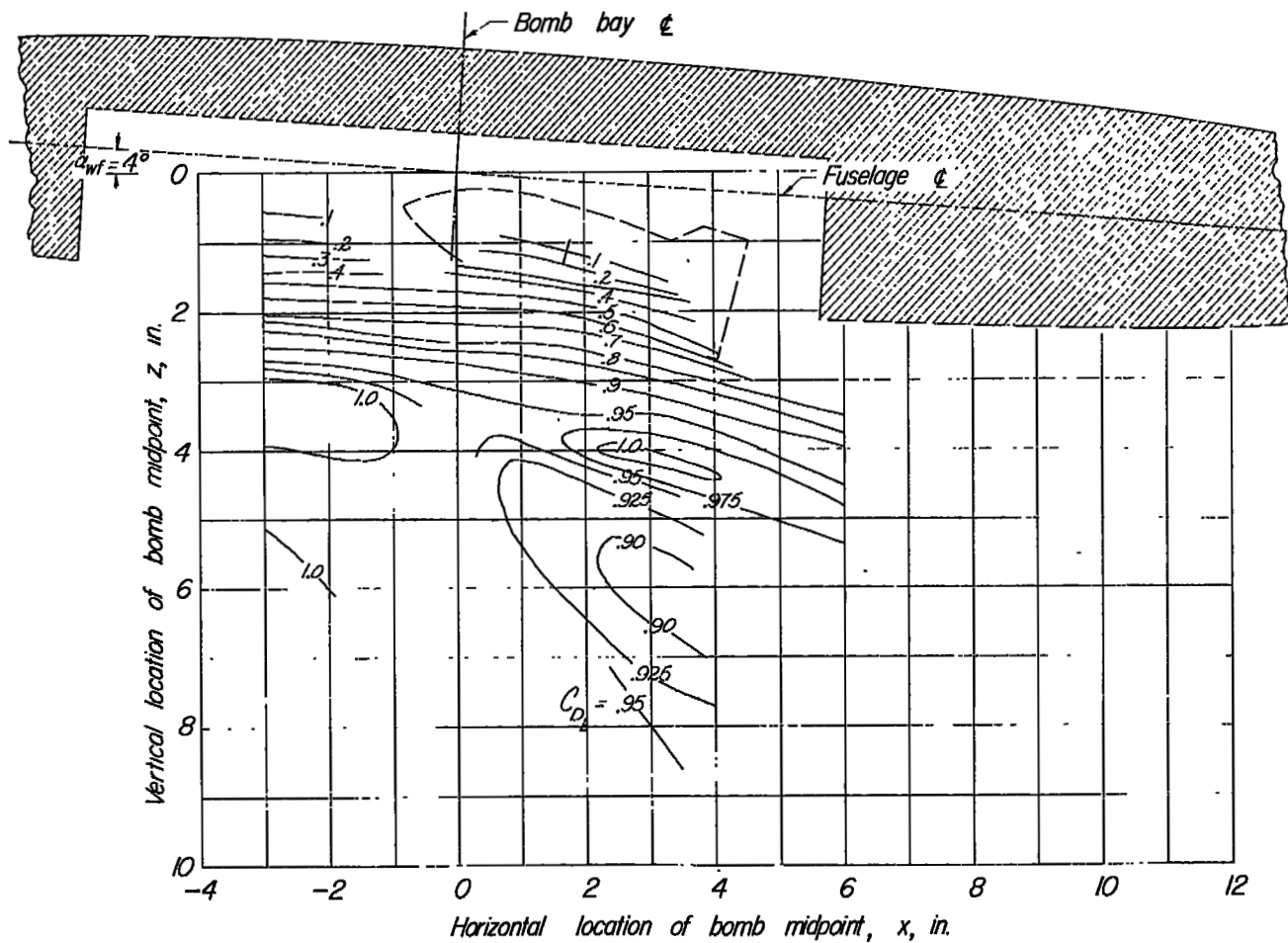
Figure 20.- Continued.



$$(f) \alpha_b = -10^\circ.$$

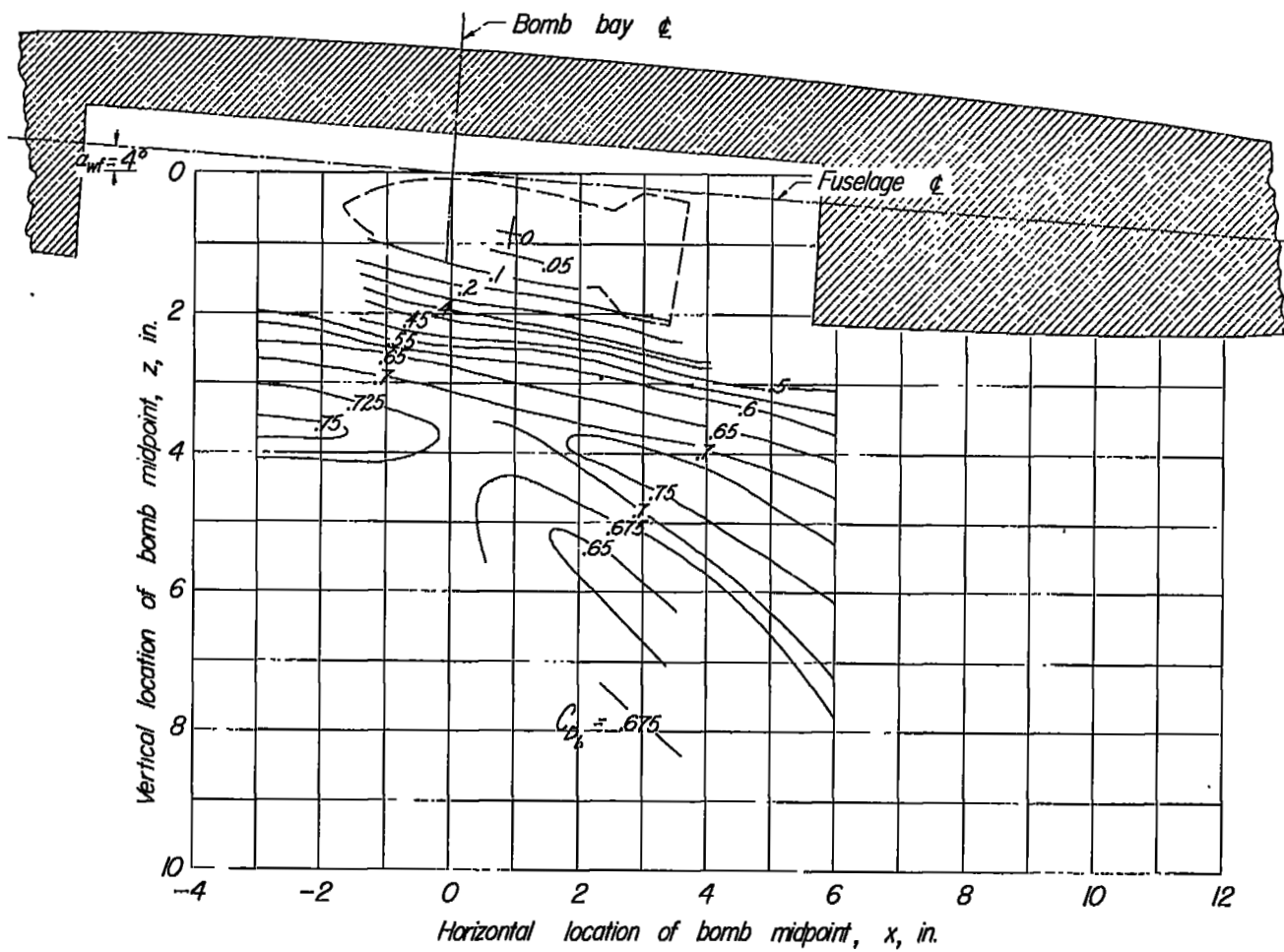
Figure 20.- Continued.





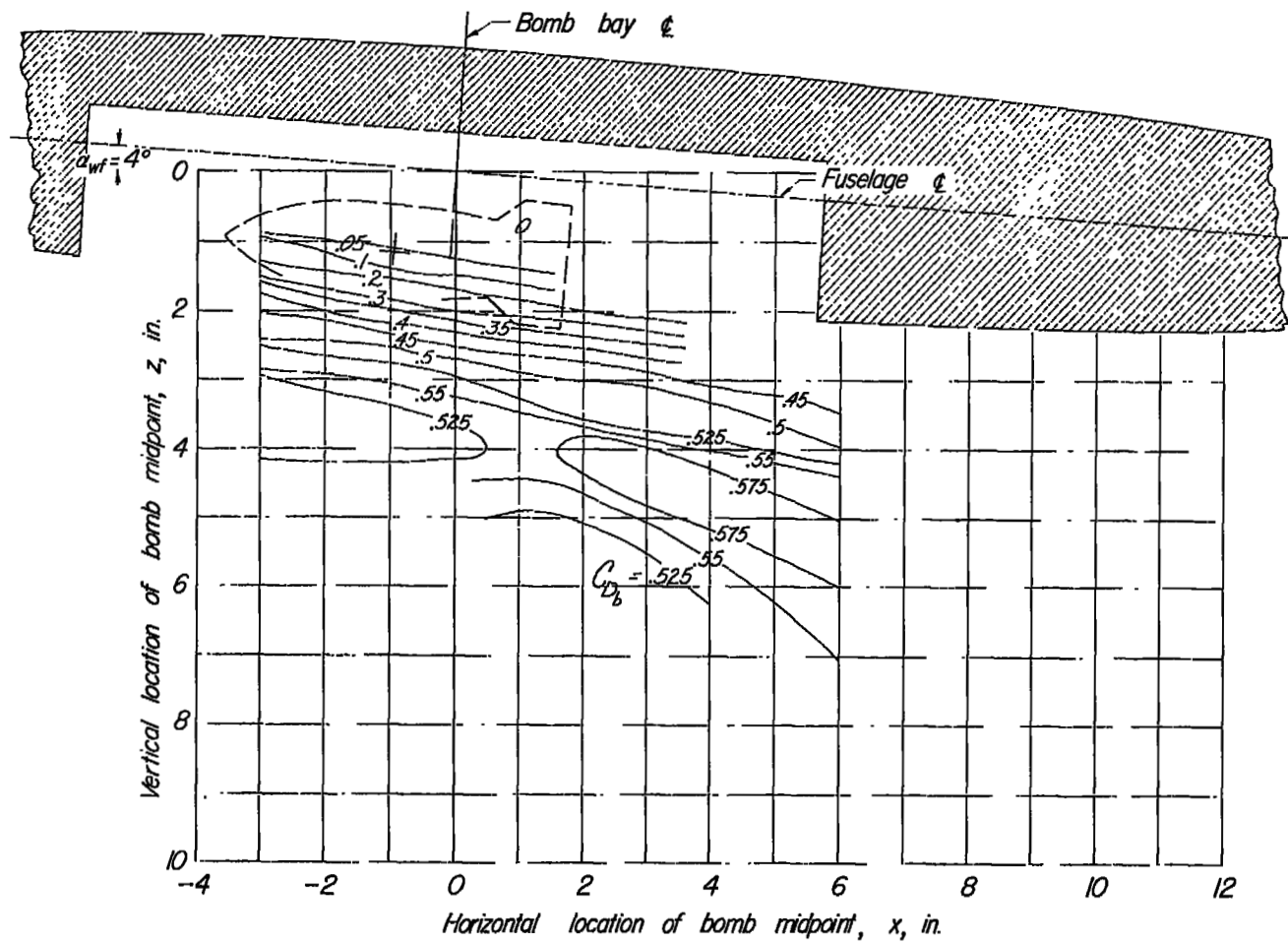
(a)  $\alpha_b = 15^\circ$ .

Figure 21.- Contour plot of the drag of bomb 2 in presence of the wing-fuselage combination.  $\alpha_{wf} = 4^\circ$ .



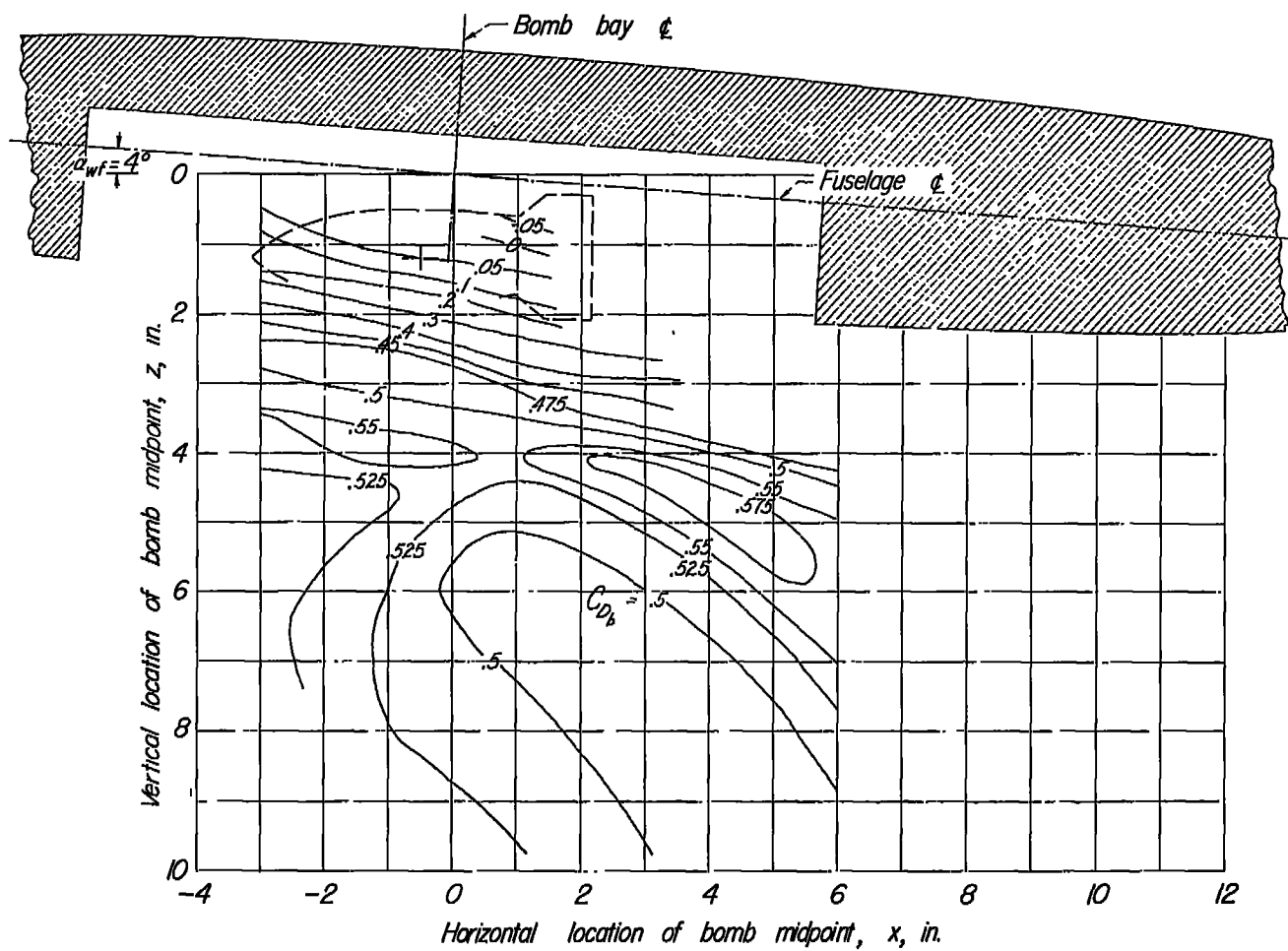
(b)  $\alpha_b = 10^\circ$ .

Figure 21.- Continued.



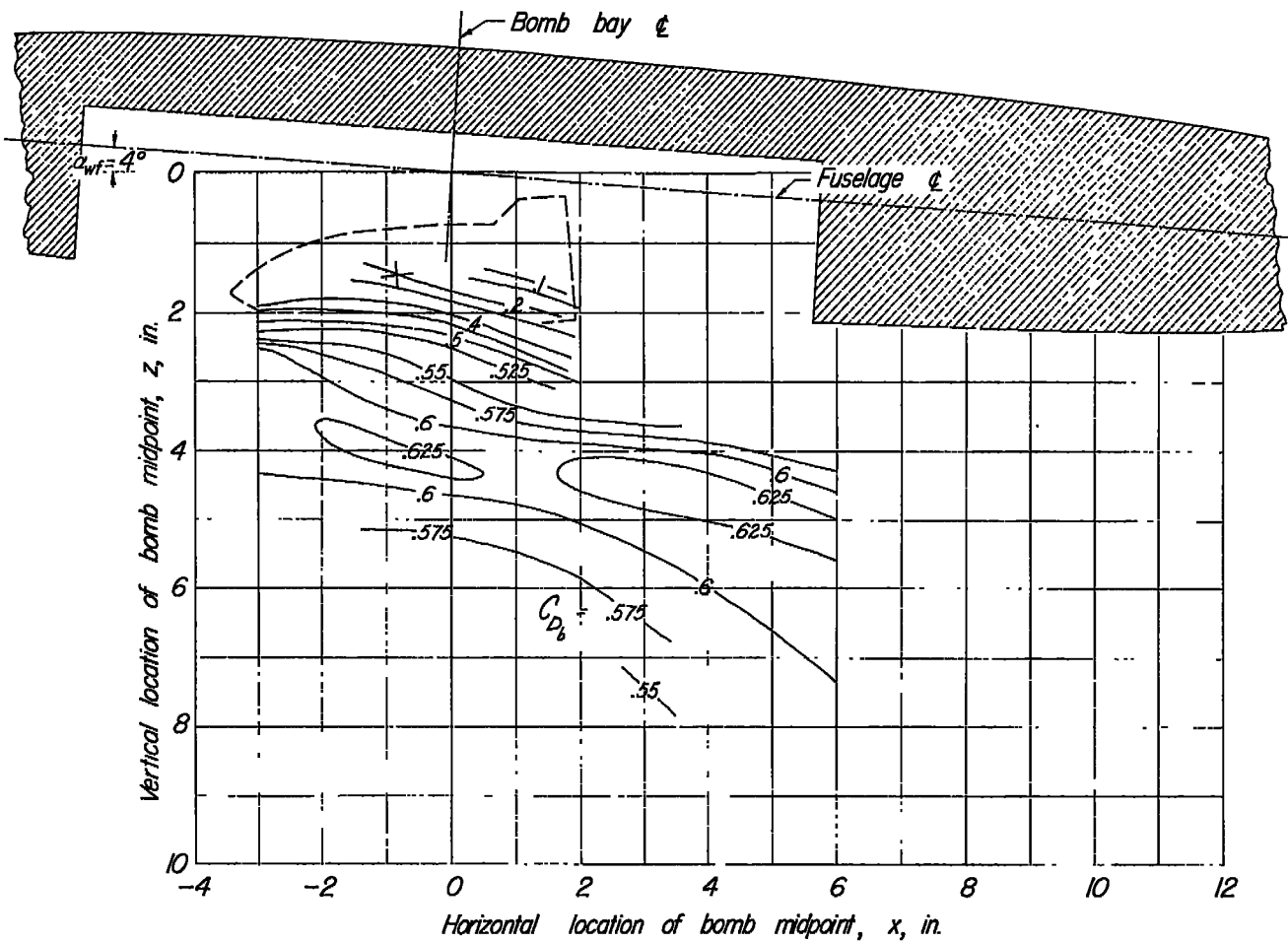
(c)  $\alpha_b = 5^\circ$ .

Figure 21.- Continued.



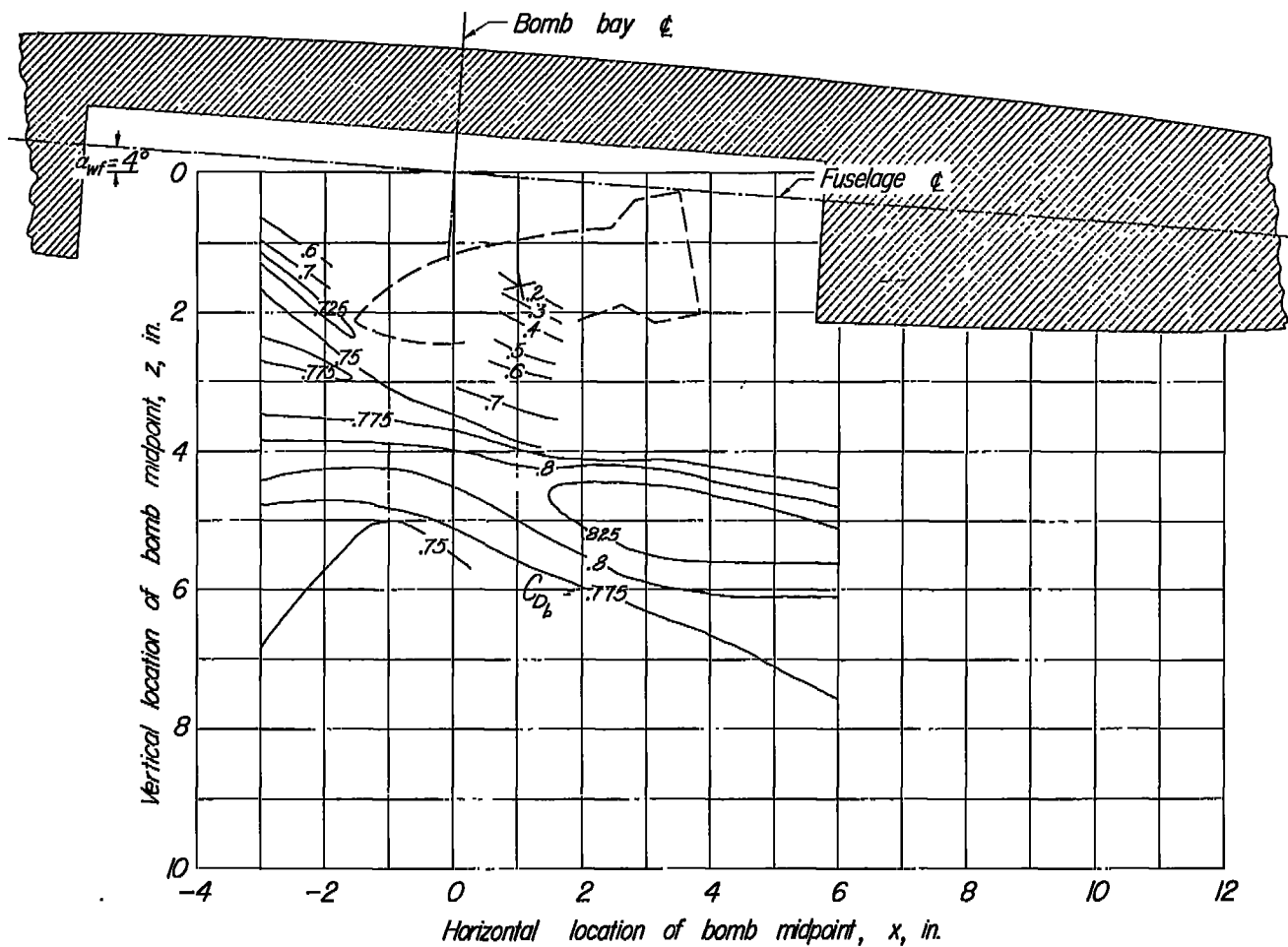
(d)  $\alpha_b = 0^\circ$ .

Figure 21.- Continued.



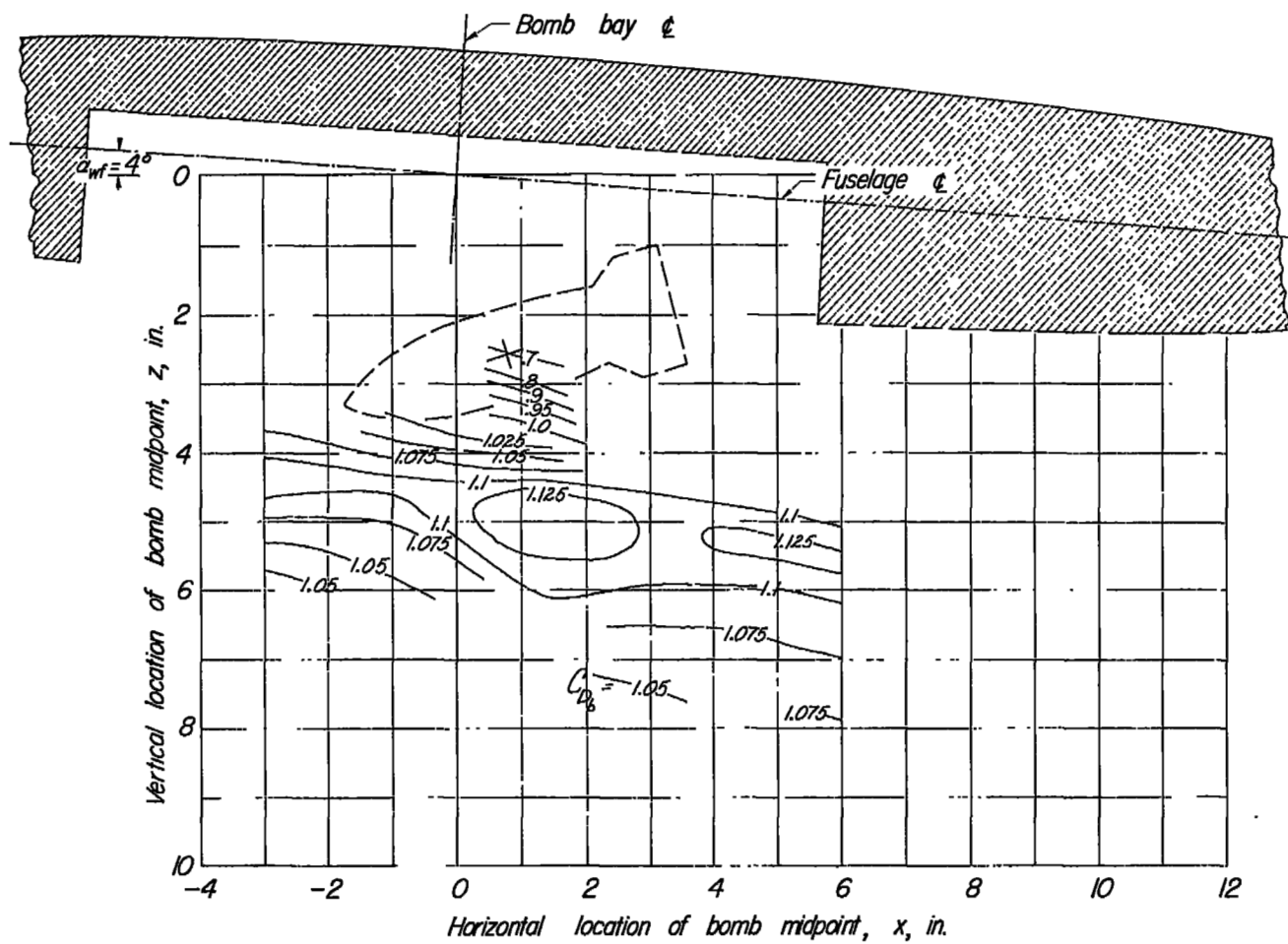
(e)  $\alpha_0 = -5^\circ$ .

Figure 21.- Continued.



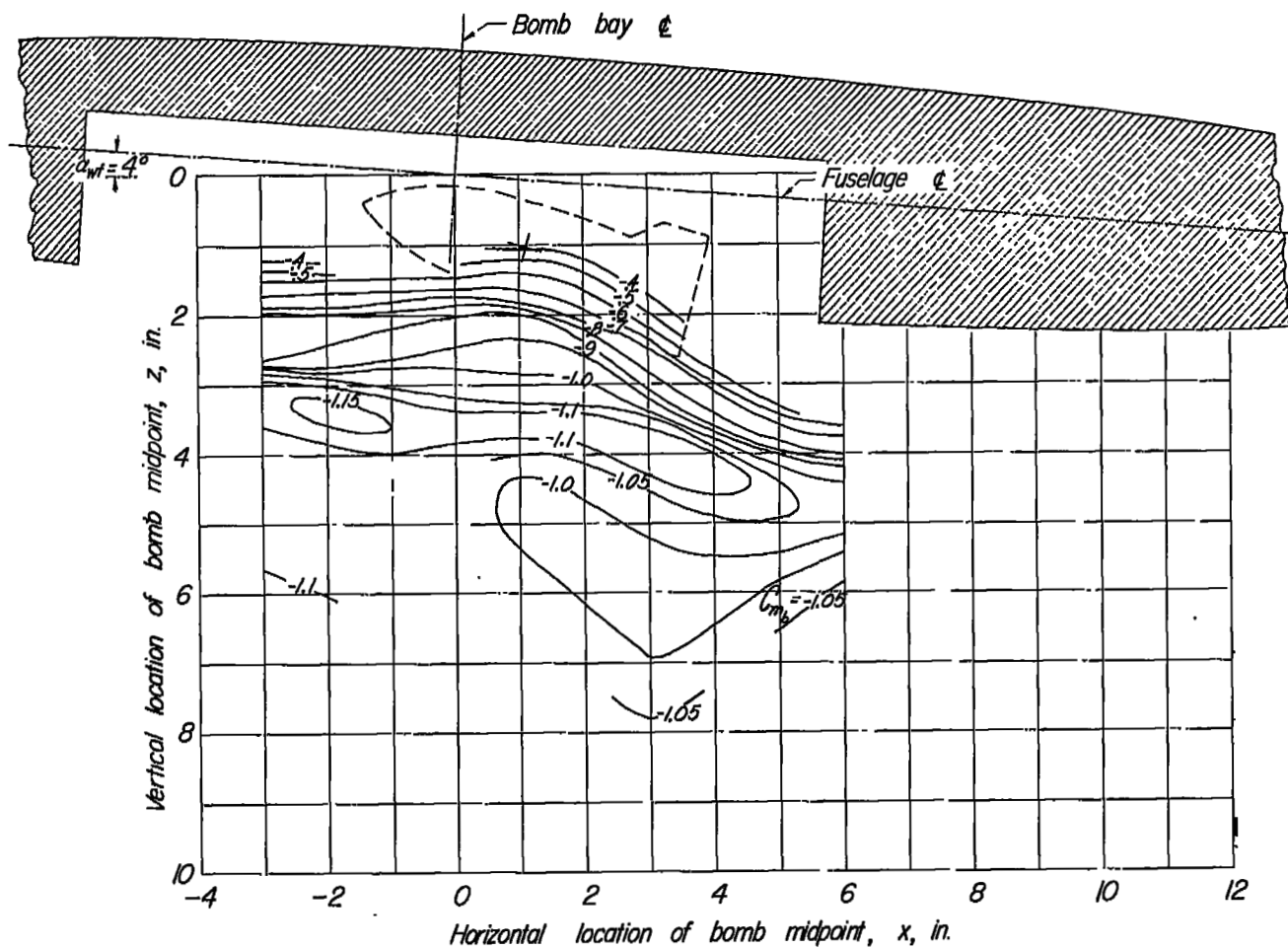
(f)  $\alpha_b = -10^\circ$ .

Figure 21.- Continued.



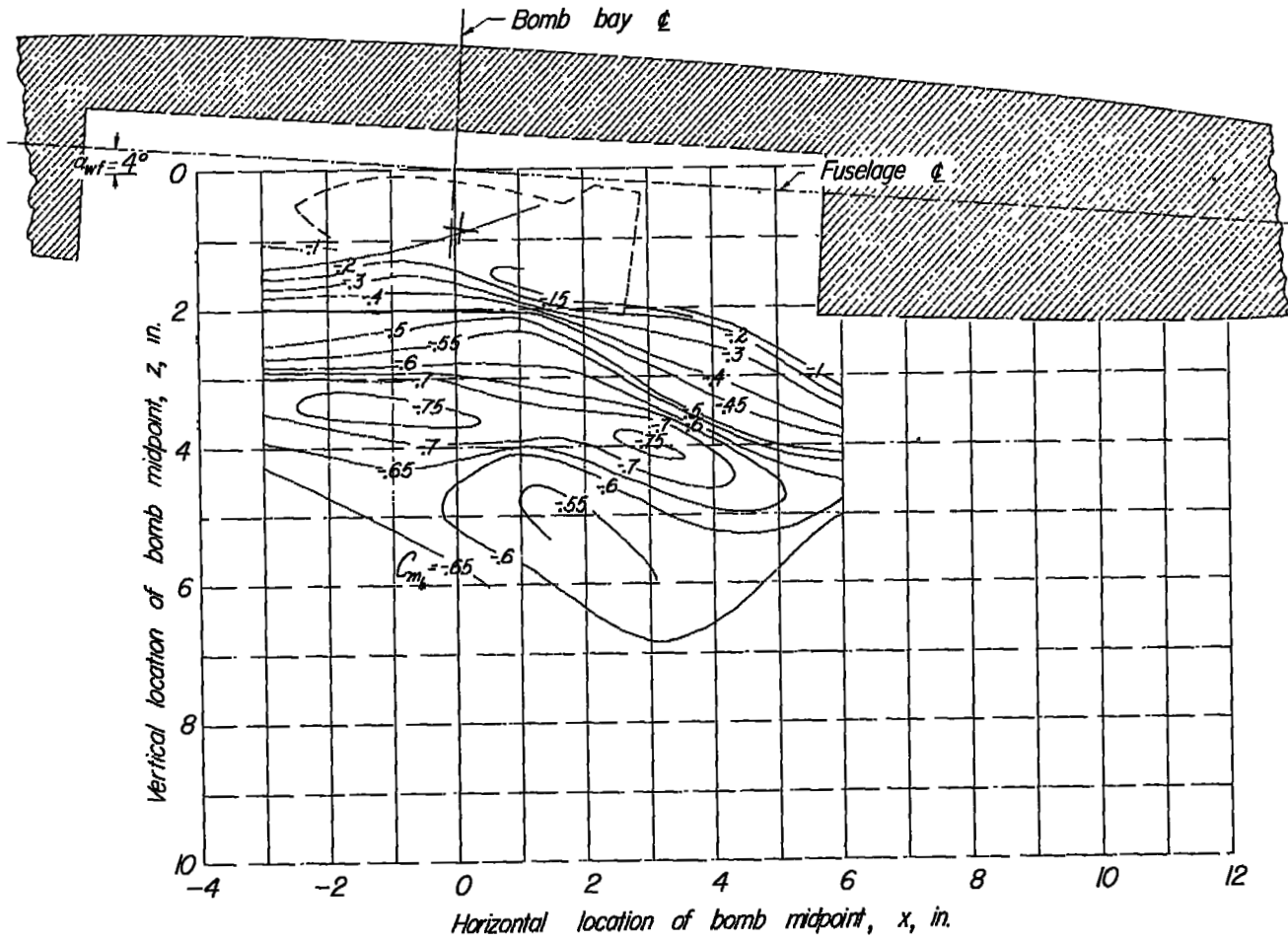
(g)  $\alpha_b = -15^\circ$ .

Figure 21.- Concluded.



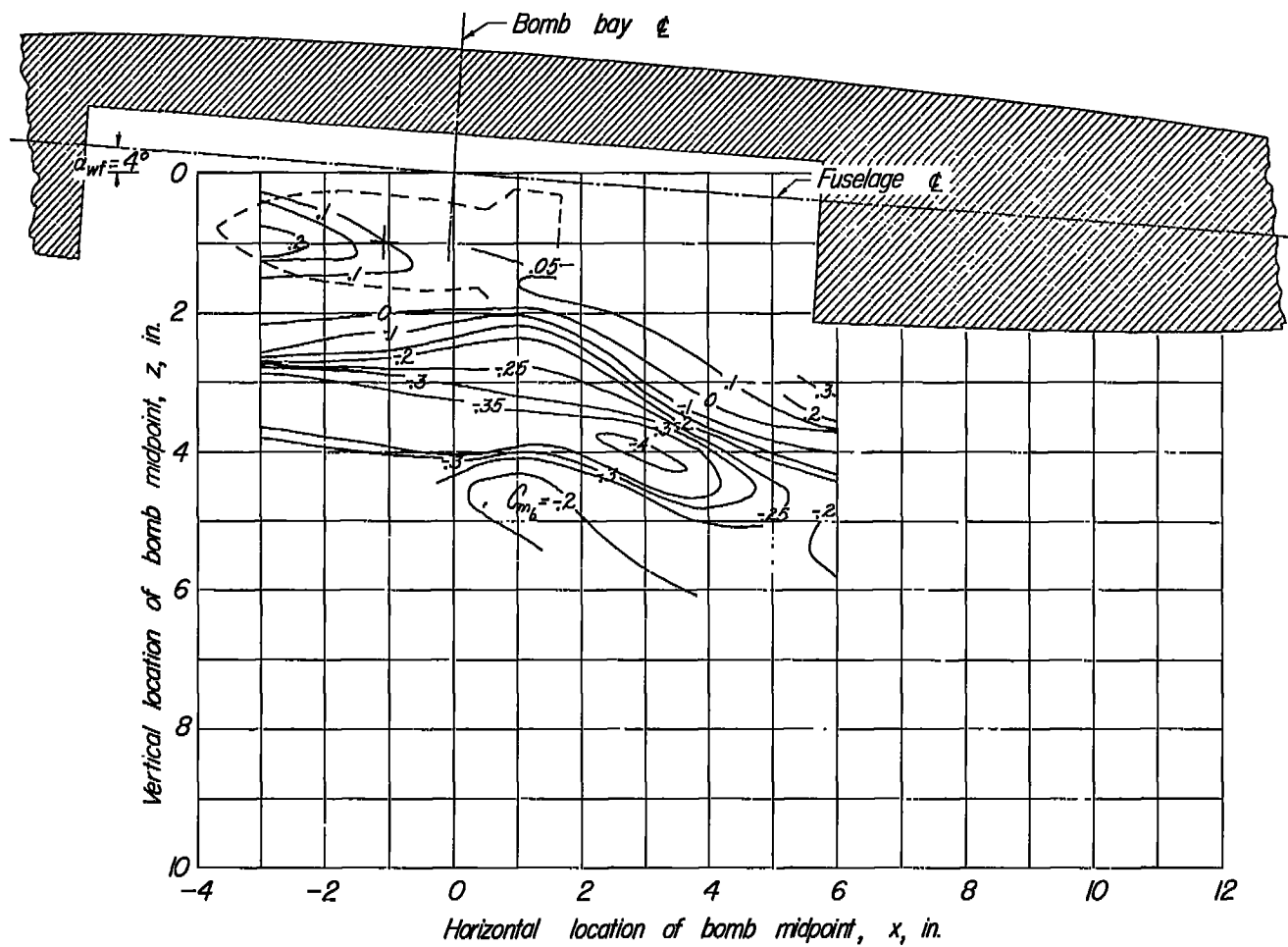
(a)  $\alpha_b = 15^\circ$ .

Figure 22.- Contour plot of the pitching moment of bomb 2 in presence of the wing-fuselage combination.  $\alpha_{wf} = 4^\circ$ .



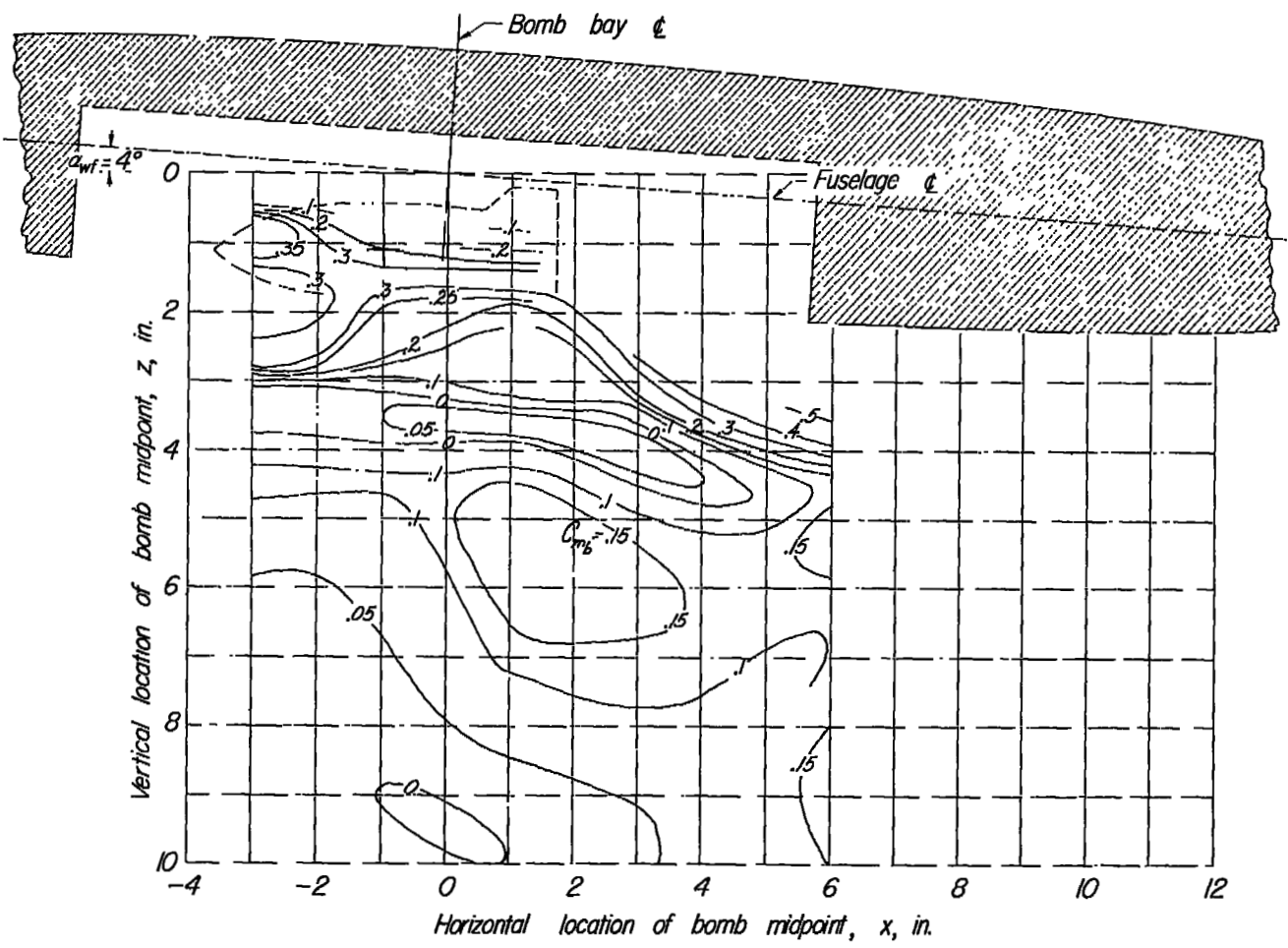
(b)  $\alpha_0 = 10^\circ$ .

Figure 22.- Continued.



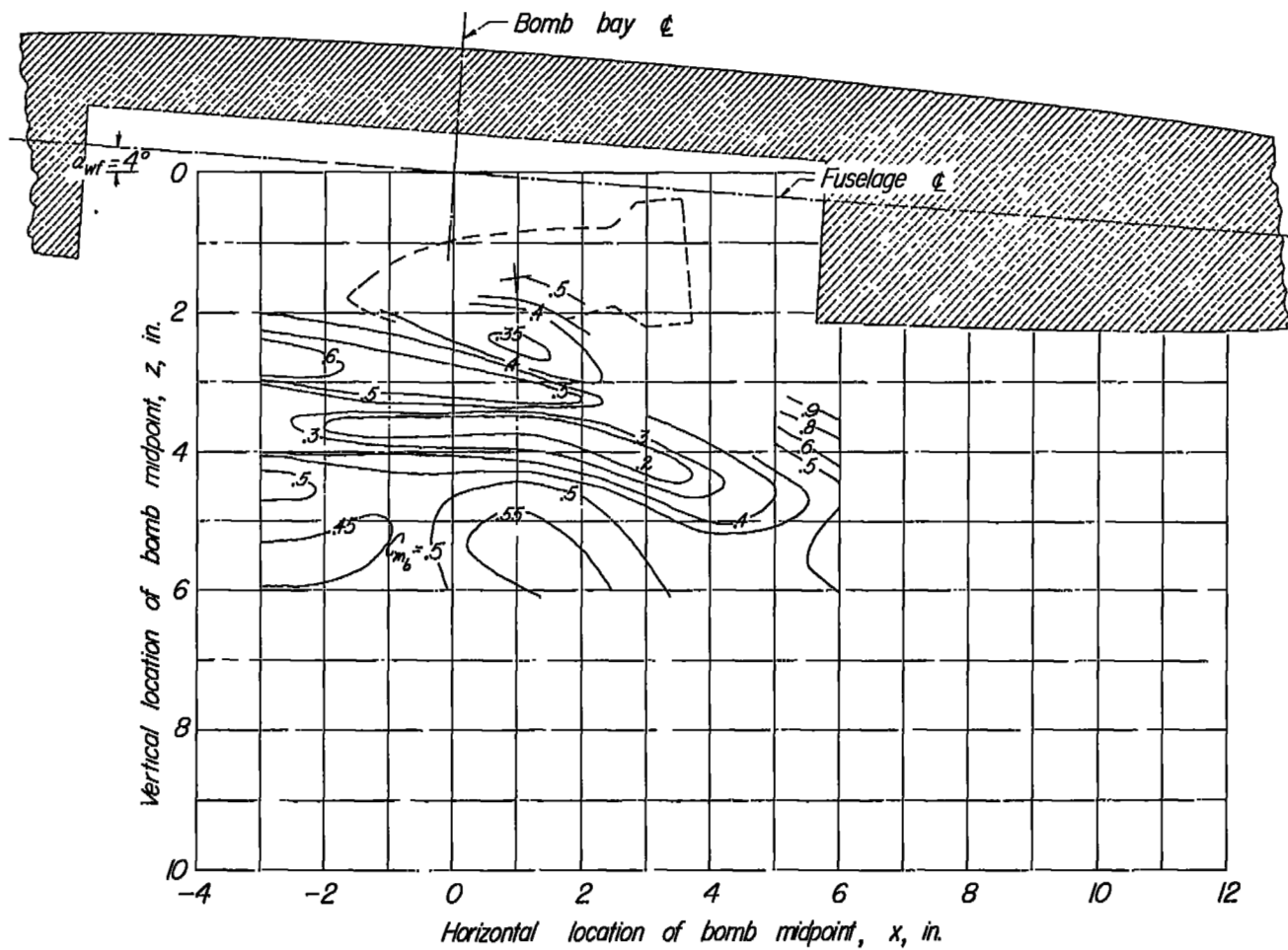
(c)  $\alpha_b = 5^\circ$ .

Figure 22.- Continued.



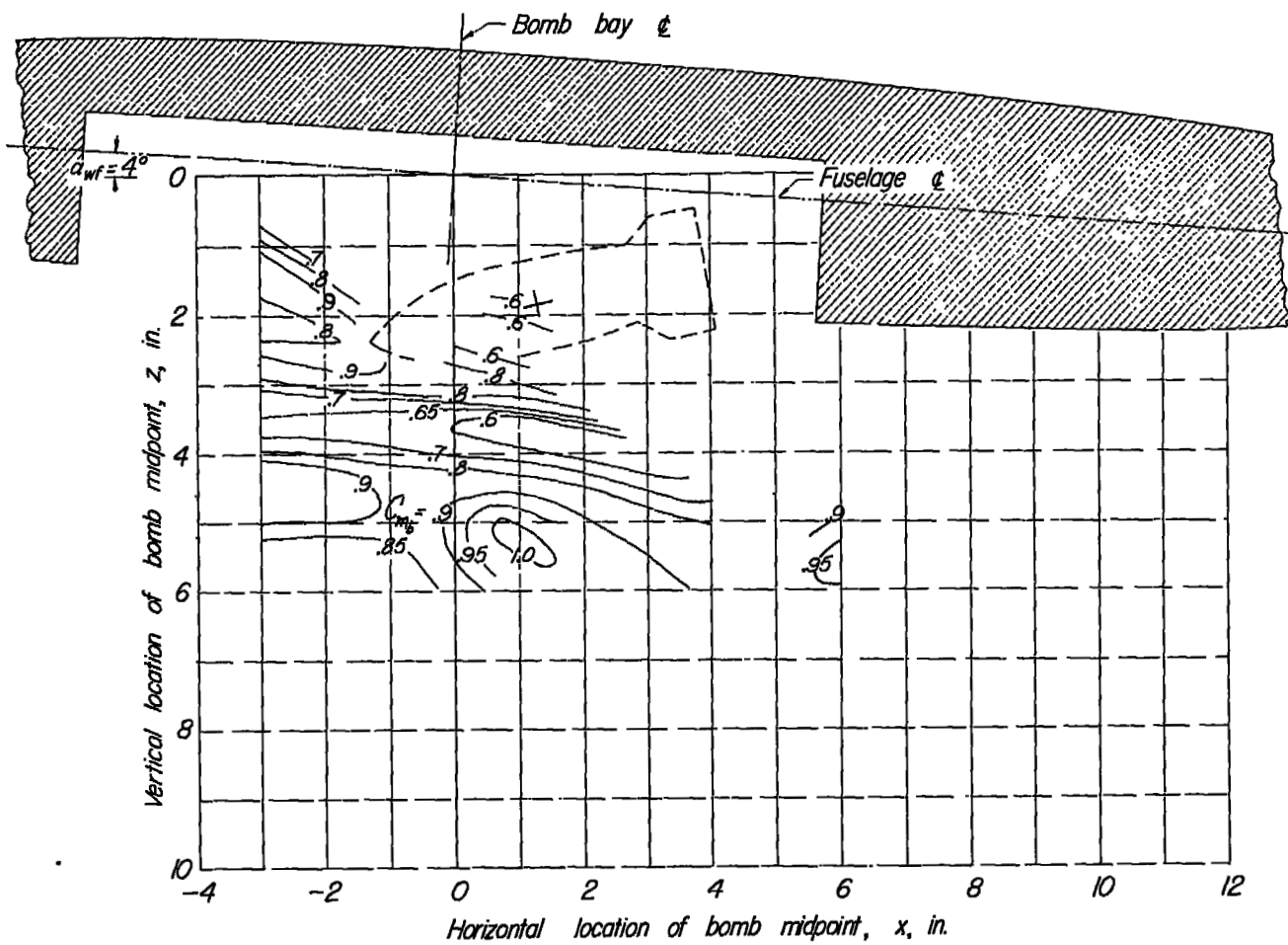
(d)  $\alpha_b = 0^\circ$ .

Figure 22.- Continued.



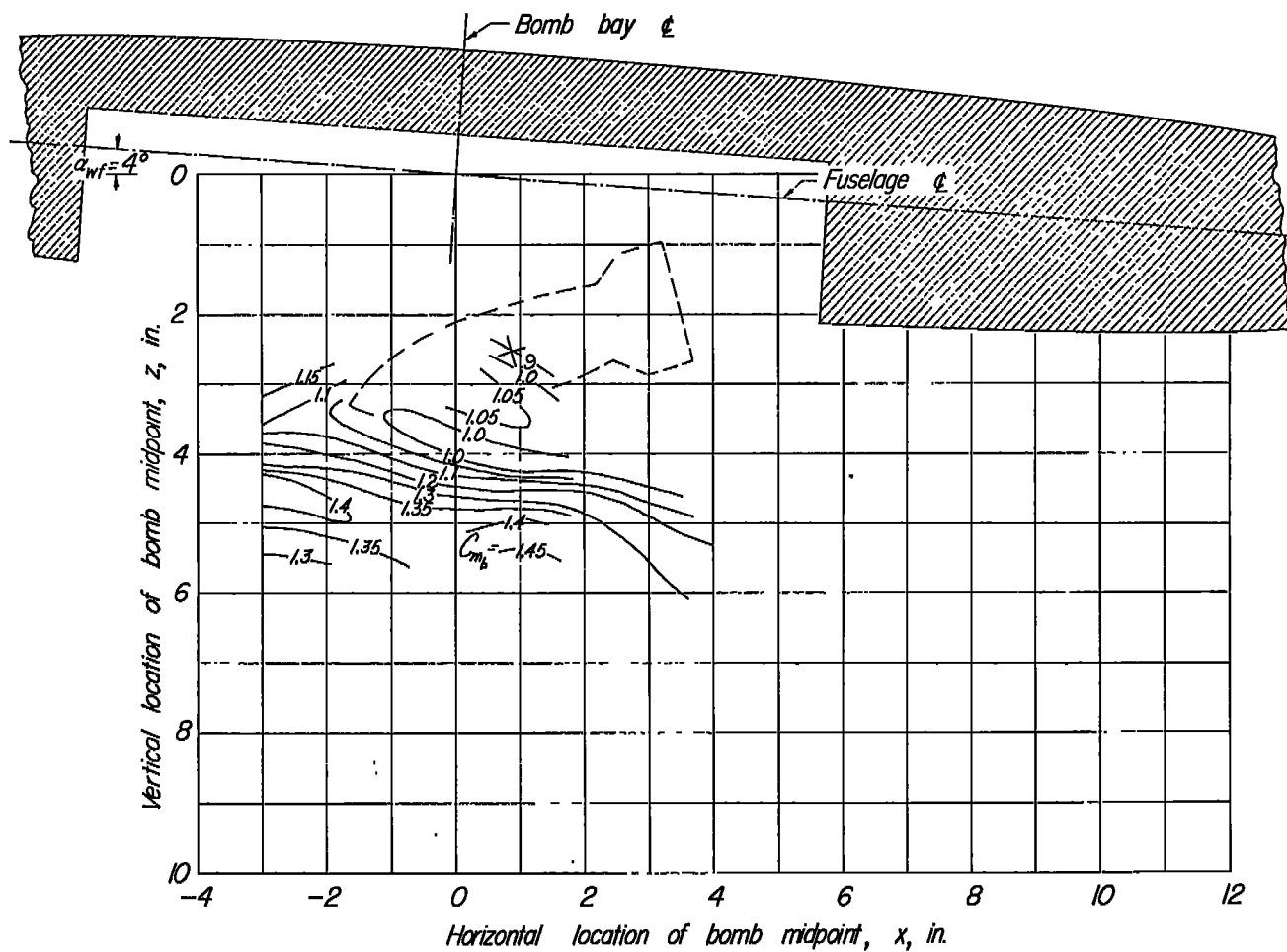
(e)  $\alpha_b = -5^\circ$ .

Figure 22.- Continued.



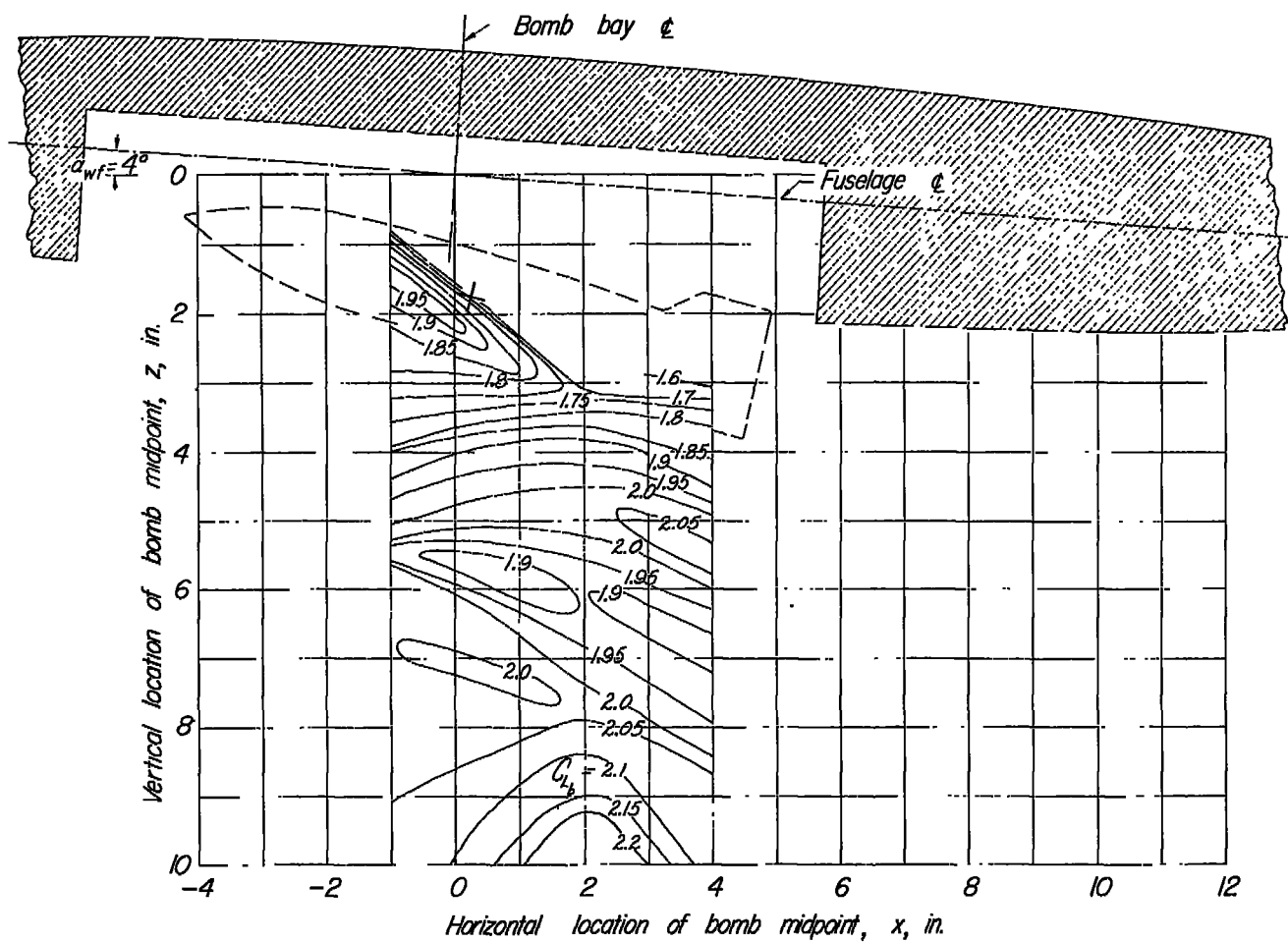
(f)  $\alpha_b = -10^\circ$ .

Figure 22.- Continued.



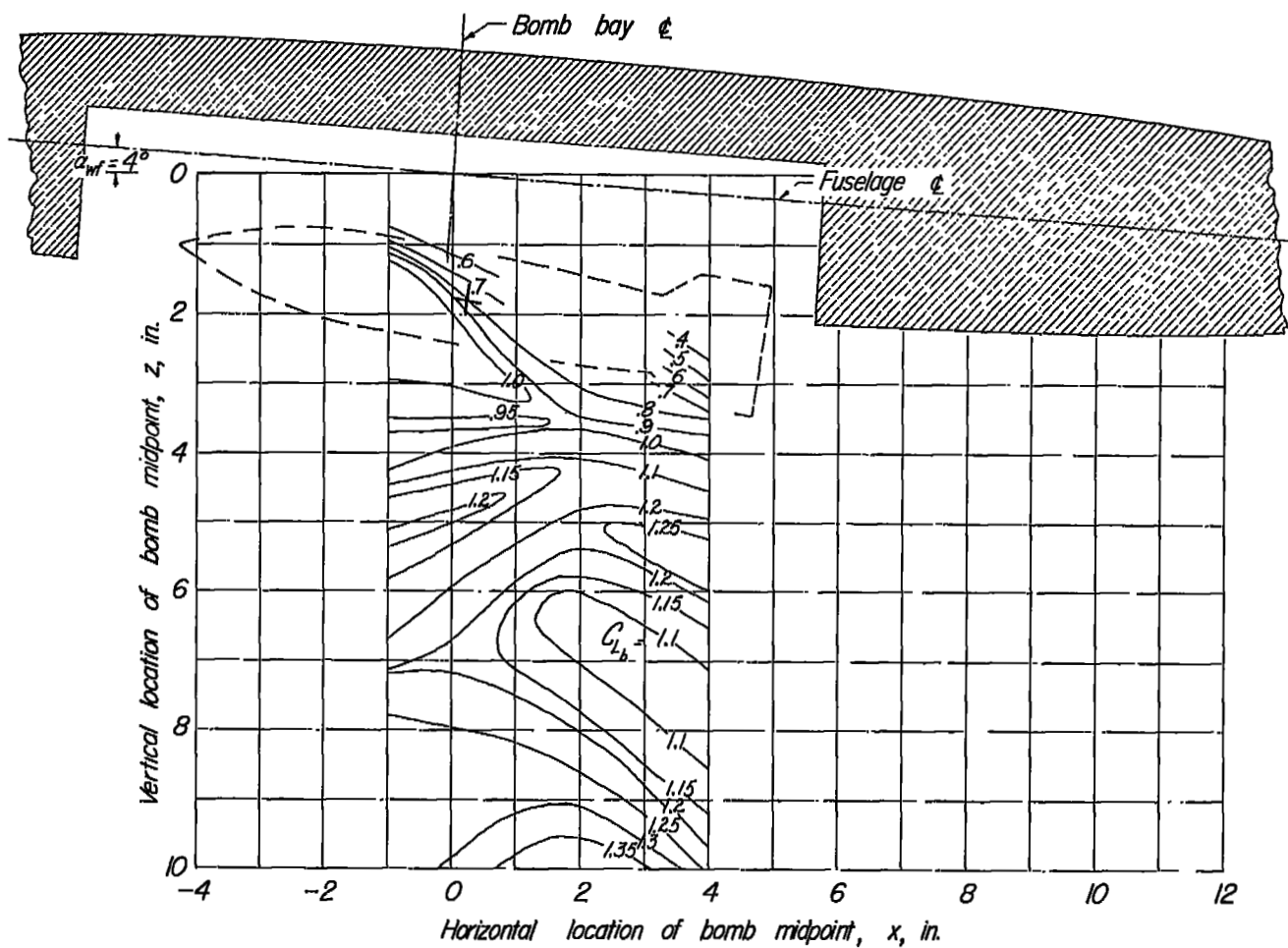
(g)  $\alpha_b = -15^\circ$ .

Figure 22.- Concluded.



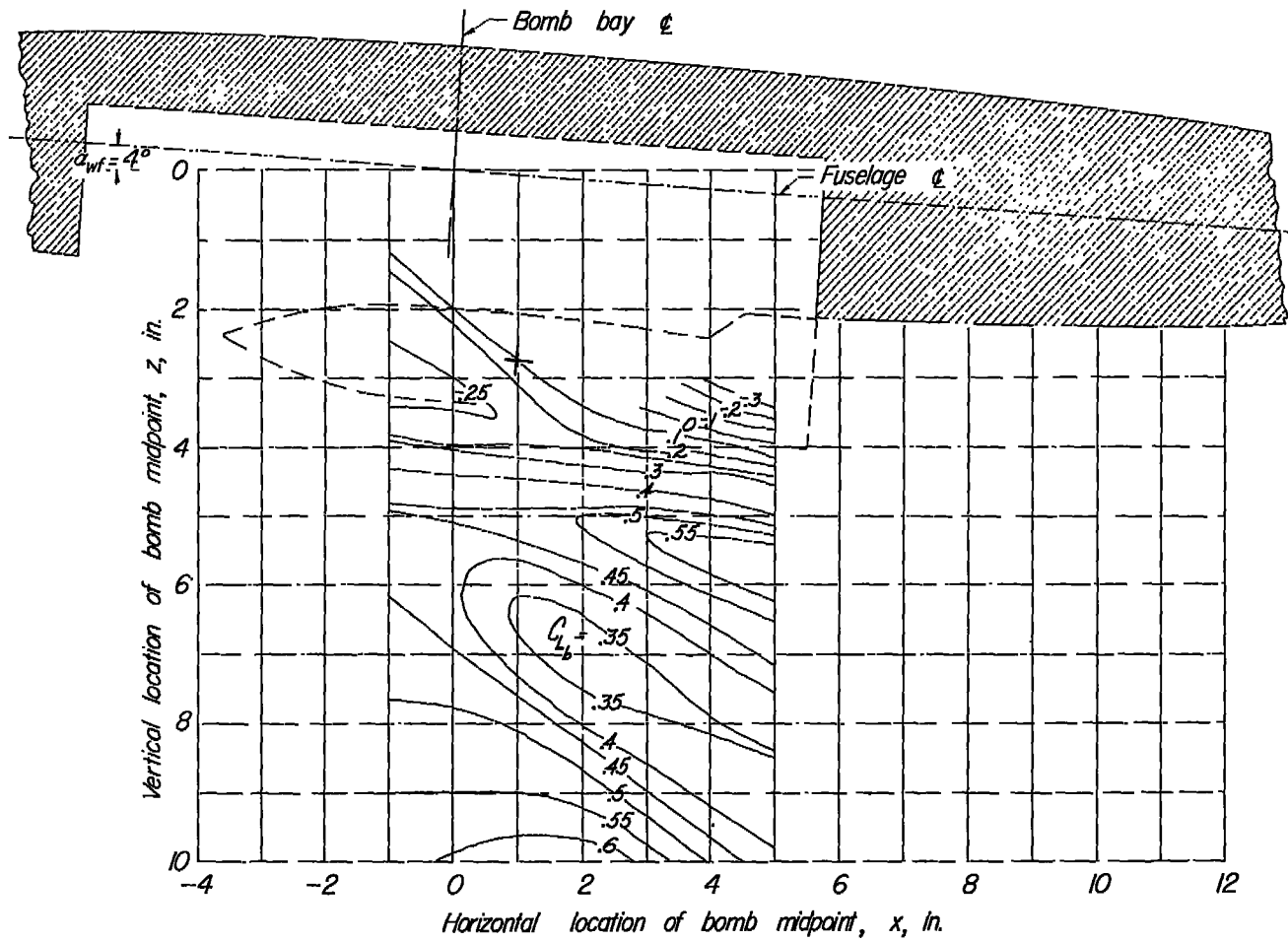
(a)  $\alpha_b = 15^\circ$ .

Figure 23.- Contour plot of the lift of bomb 3 in presence of the wing-fuselage combination.  $\alpha_{wf} = 4^\circ$ .



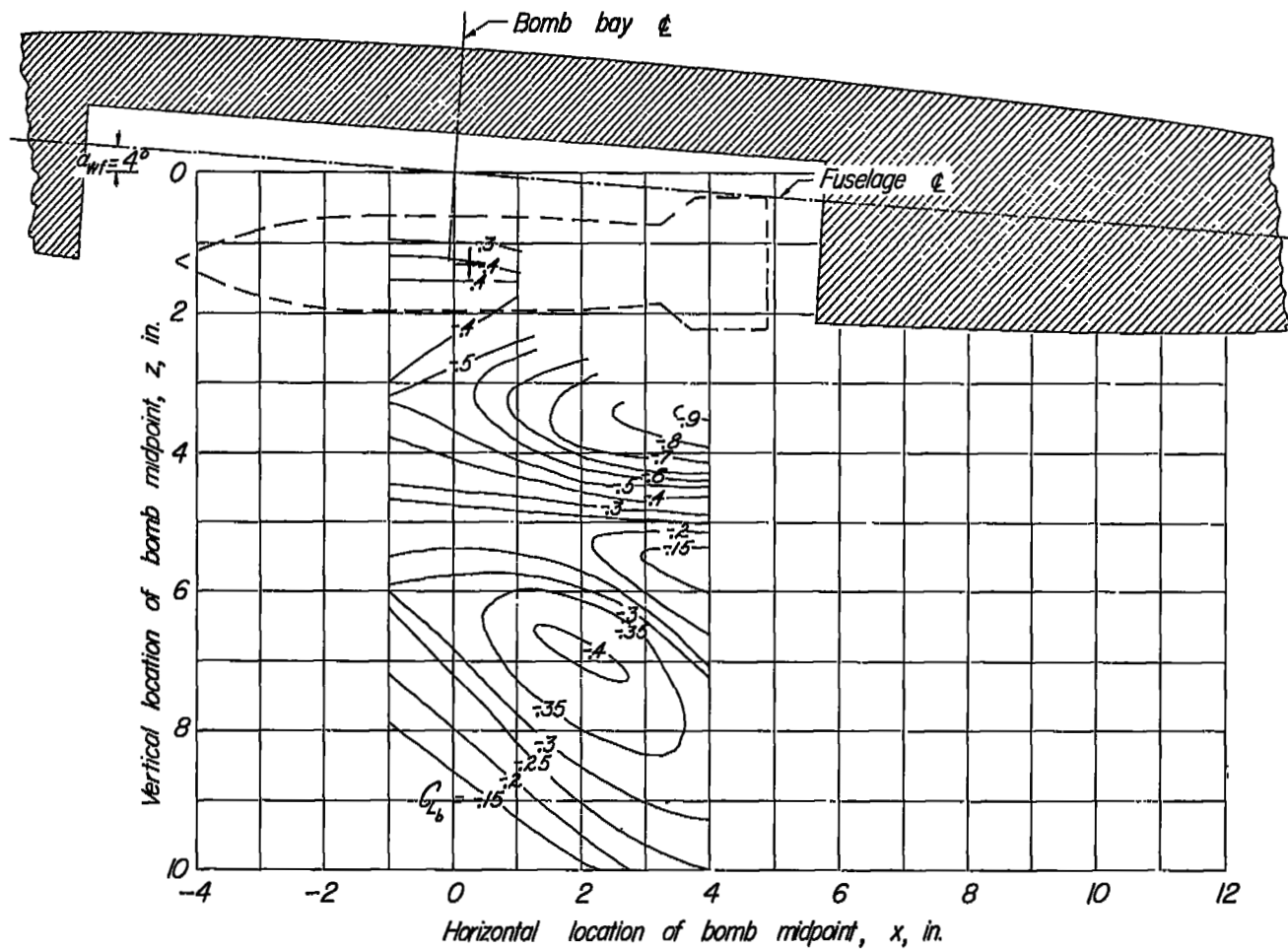
(b)  $\alpha_b = 10^\circ$ .

Figure 23.- Continued.



(c)  $\alpha_b = 5^\circ$ .

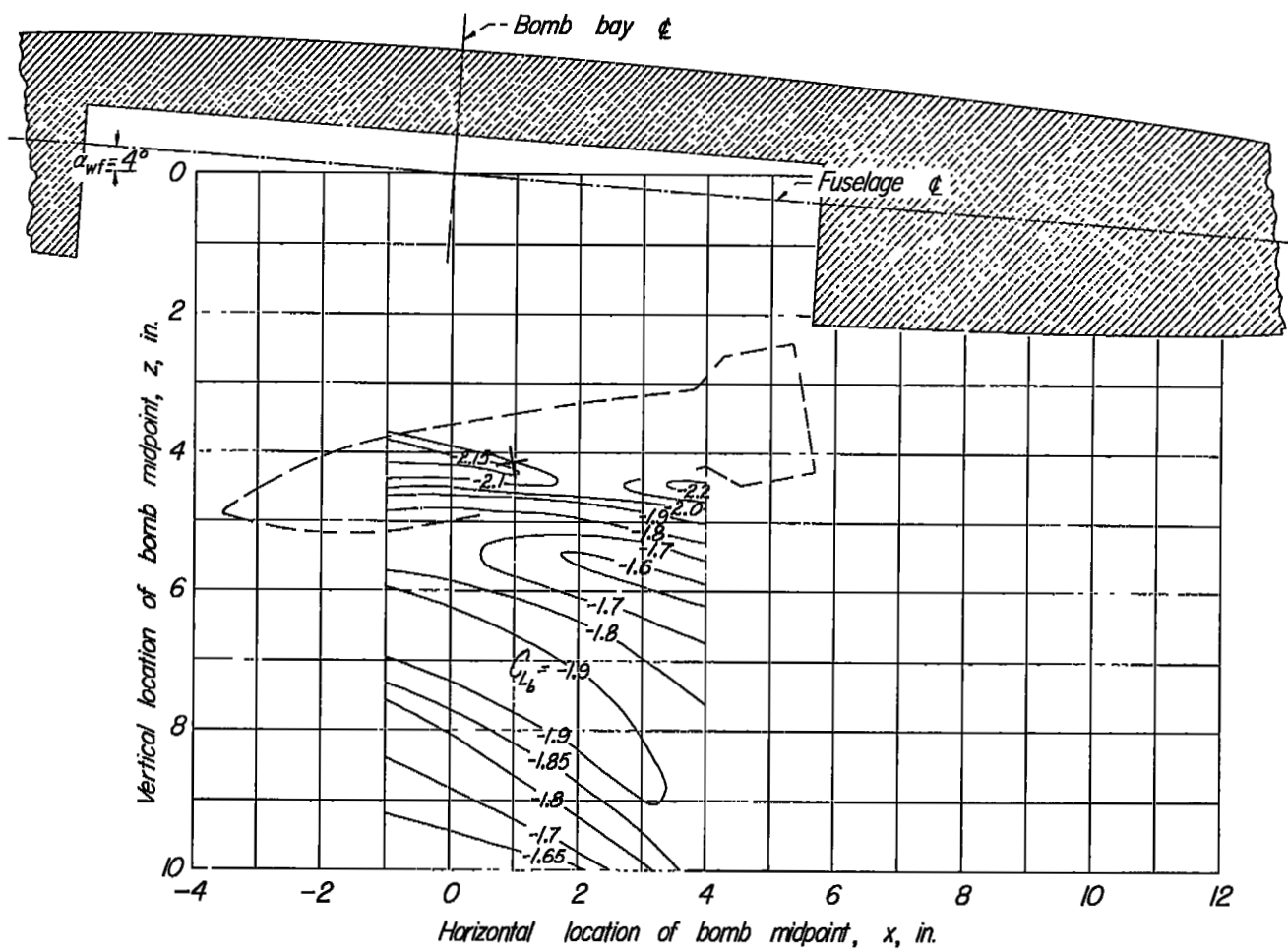
Figure 23.- Continued.



(d)  $\alpha_b = 0^\circ$ .

Figure 23.- Continued.

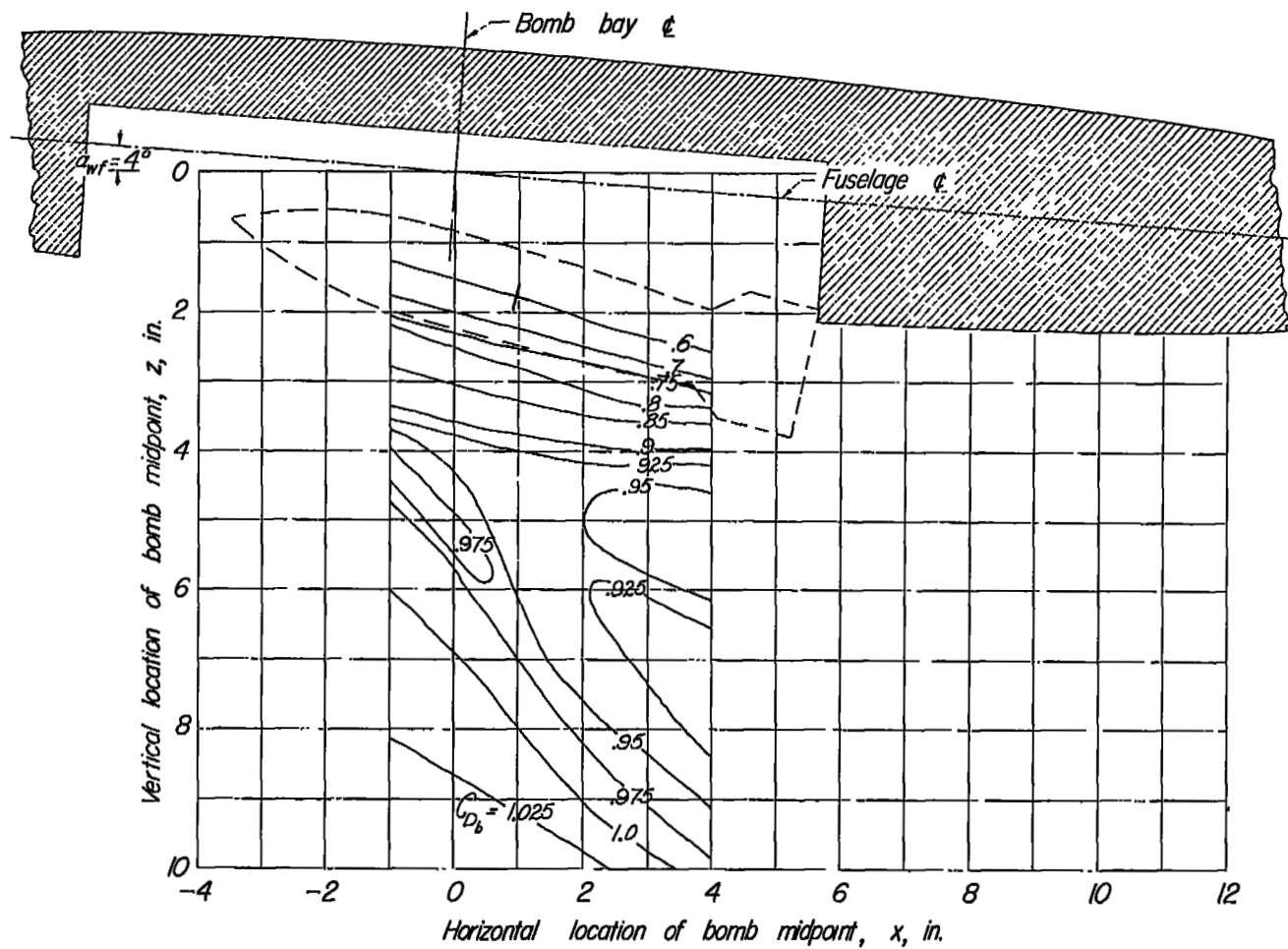




(f)  $\alpha_b = -10^\circ$ .

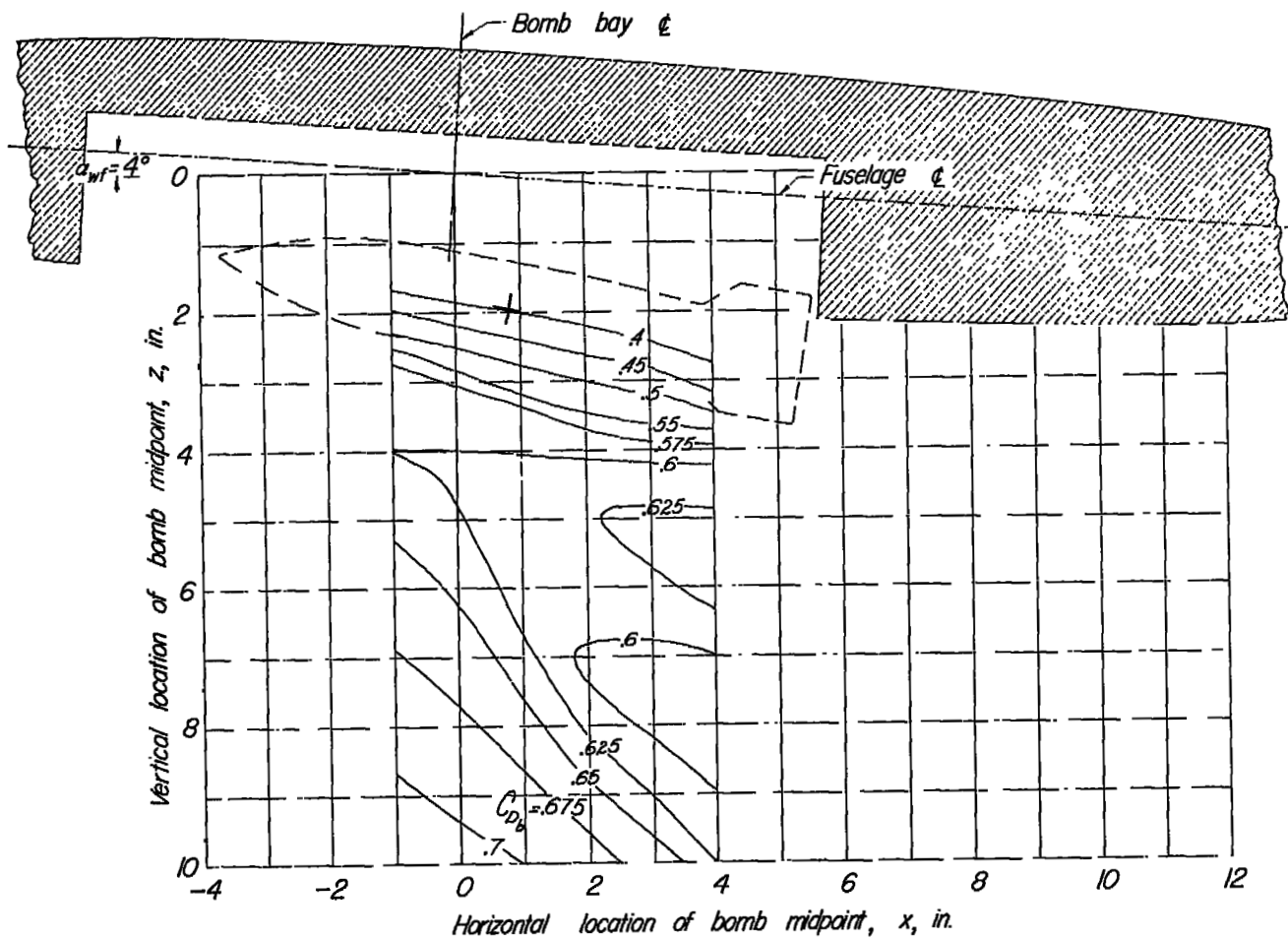
Figure 23.- Continued.





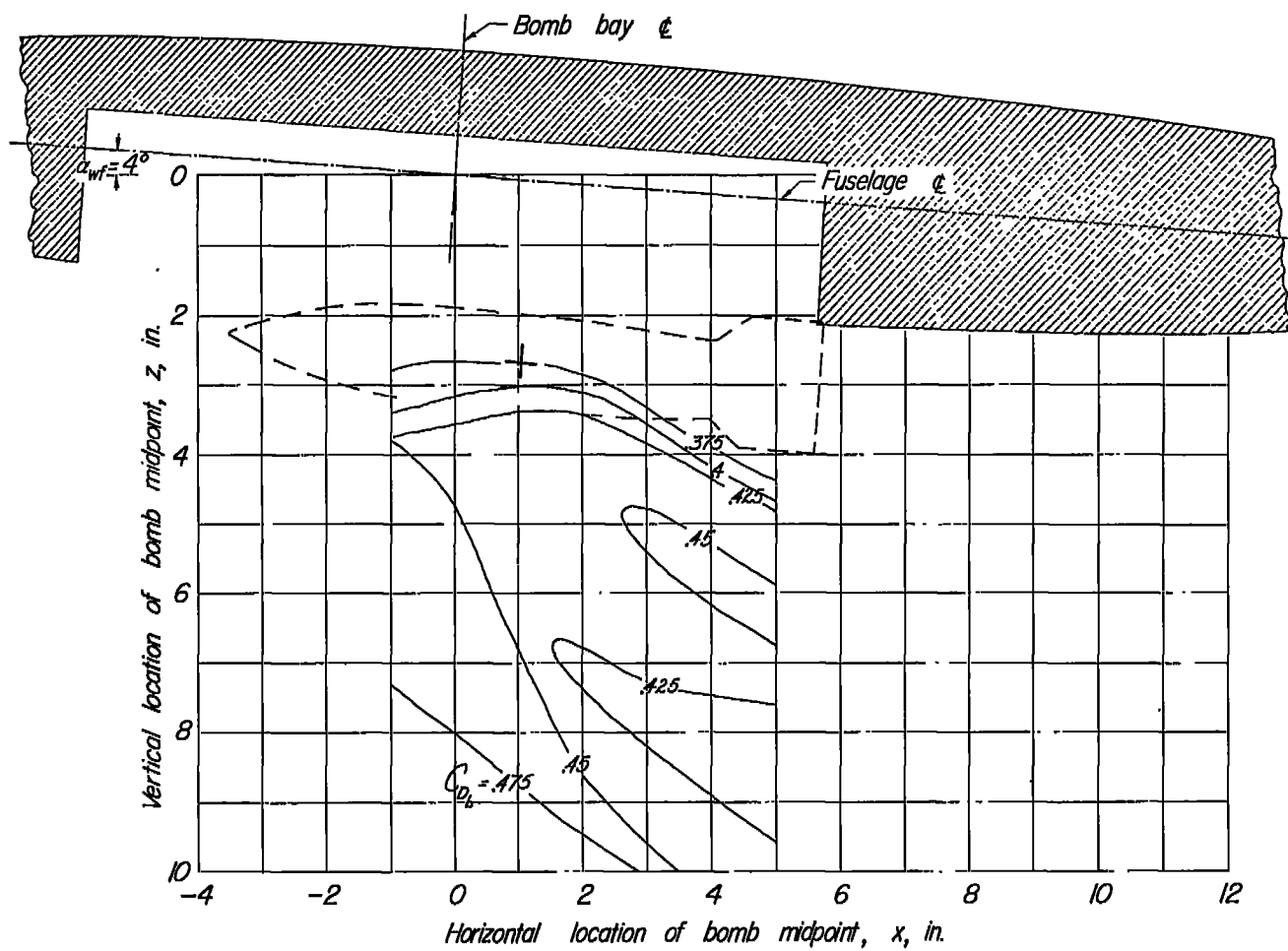
(a)  $\alpha_b = 15^\circ$ .

Figure 24.- Contour plot of the drag of bomb 3 in presence of the wing-fuselage combination.  $\alpha_{wf} = 4^\circ$ .



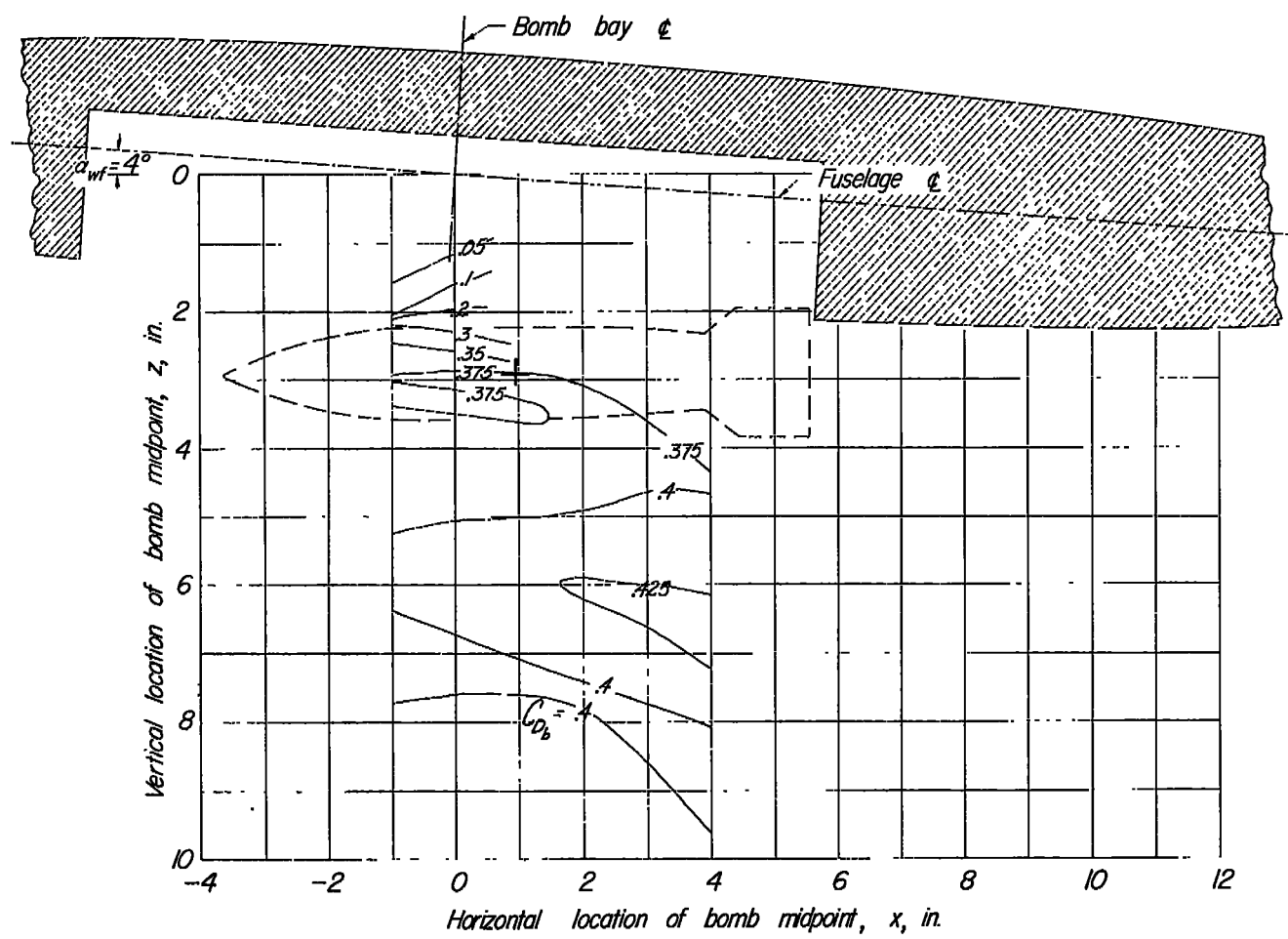
(b)  $\alpha_b = 10^\circ$ .

Figure 24.- Continued.



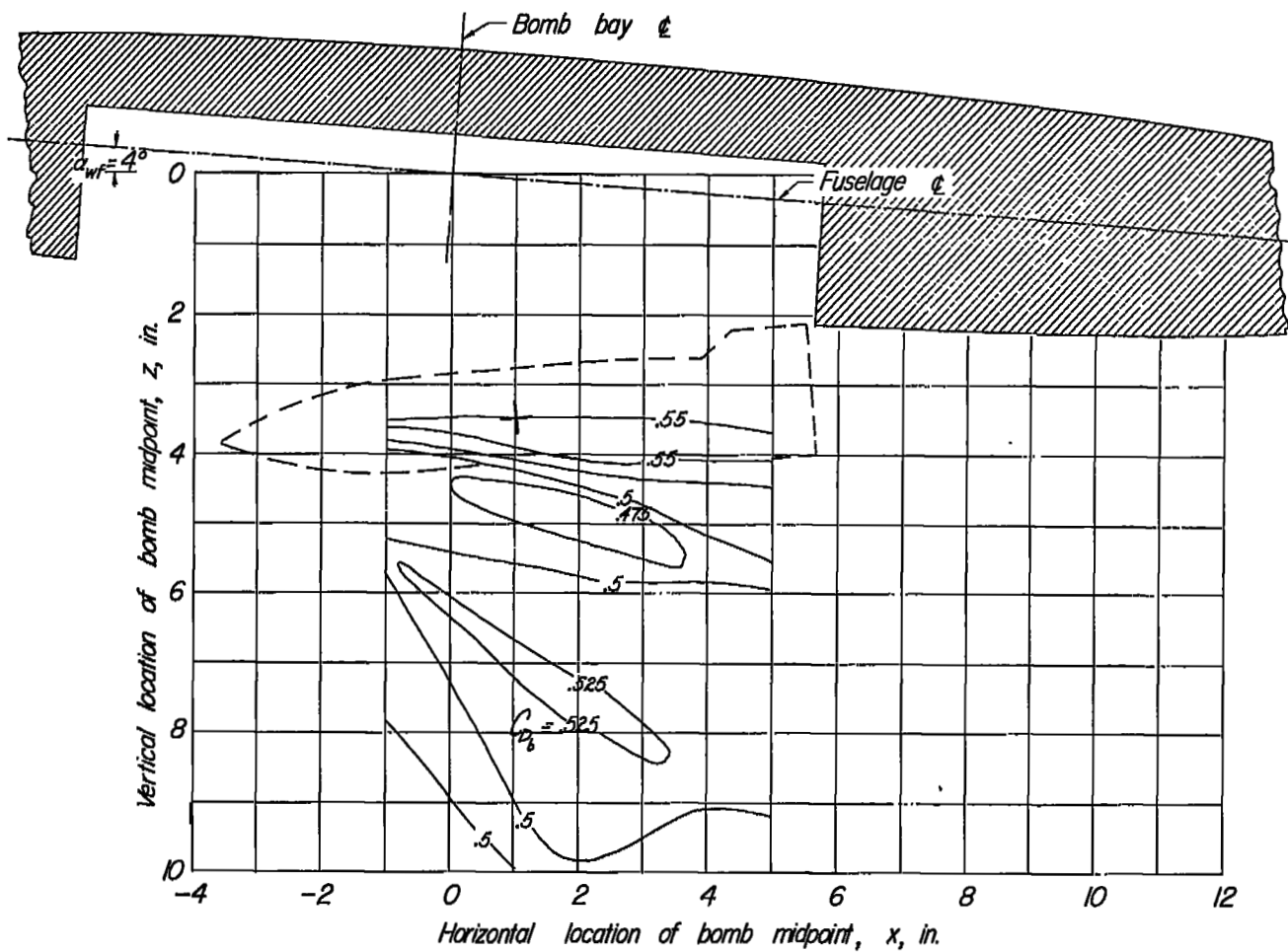
(c)  $\alpha_b = 5^\circ$ .

Figure 24.- Continued.



(d)  $\alpha_b = 0^\circ$ .

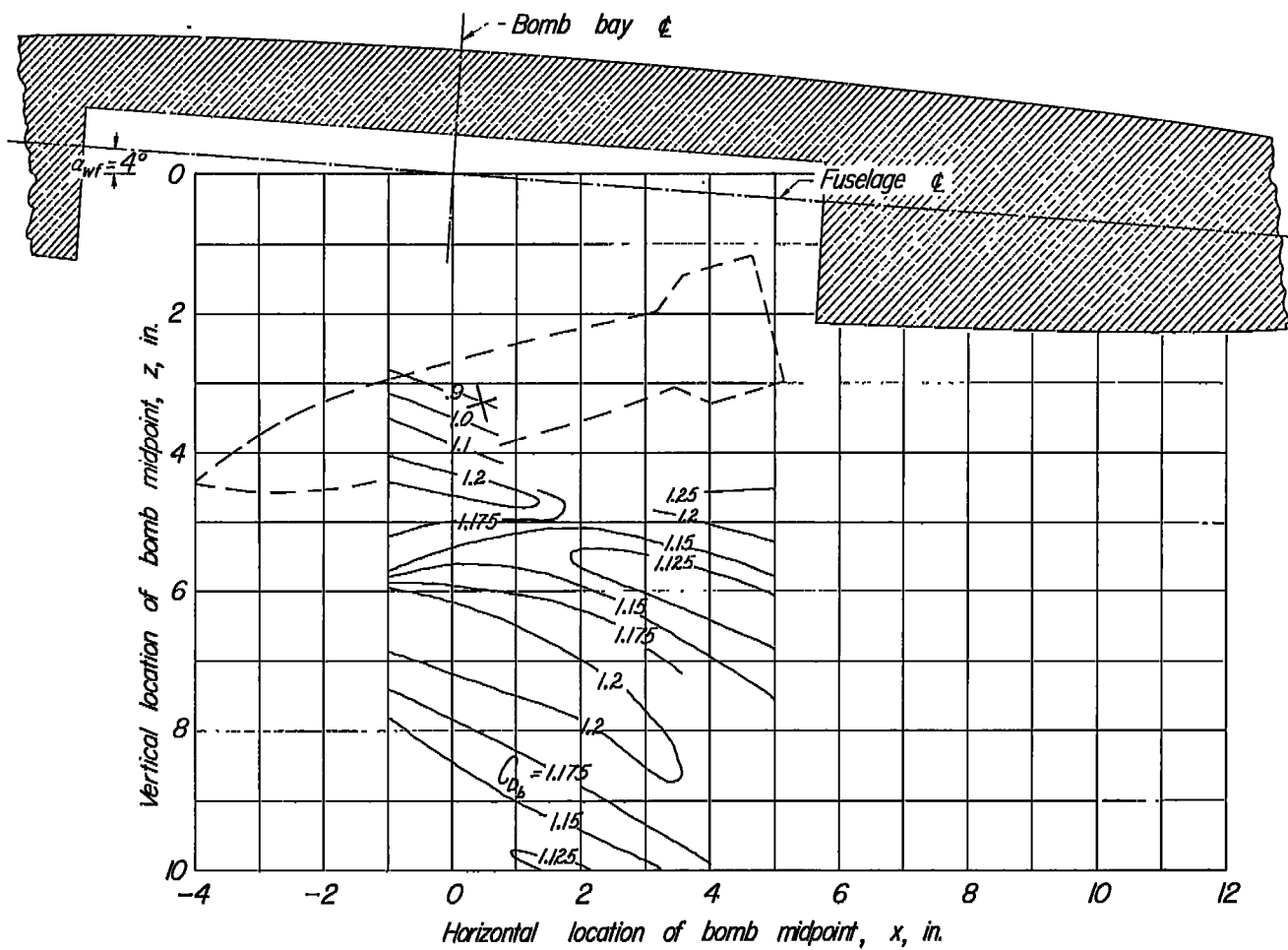
Figure 24.- Continued.



(e)  $\alpha_b = -5^\circ$ .

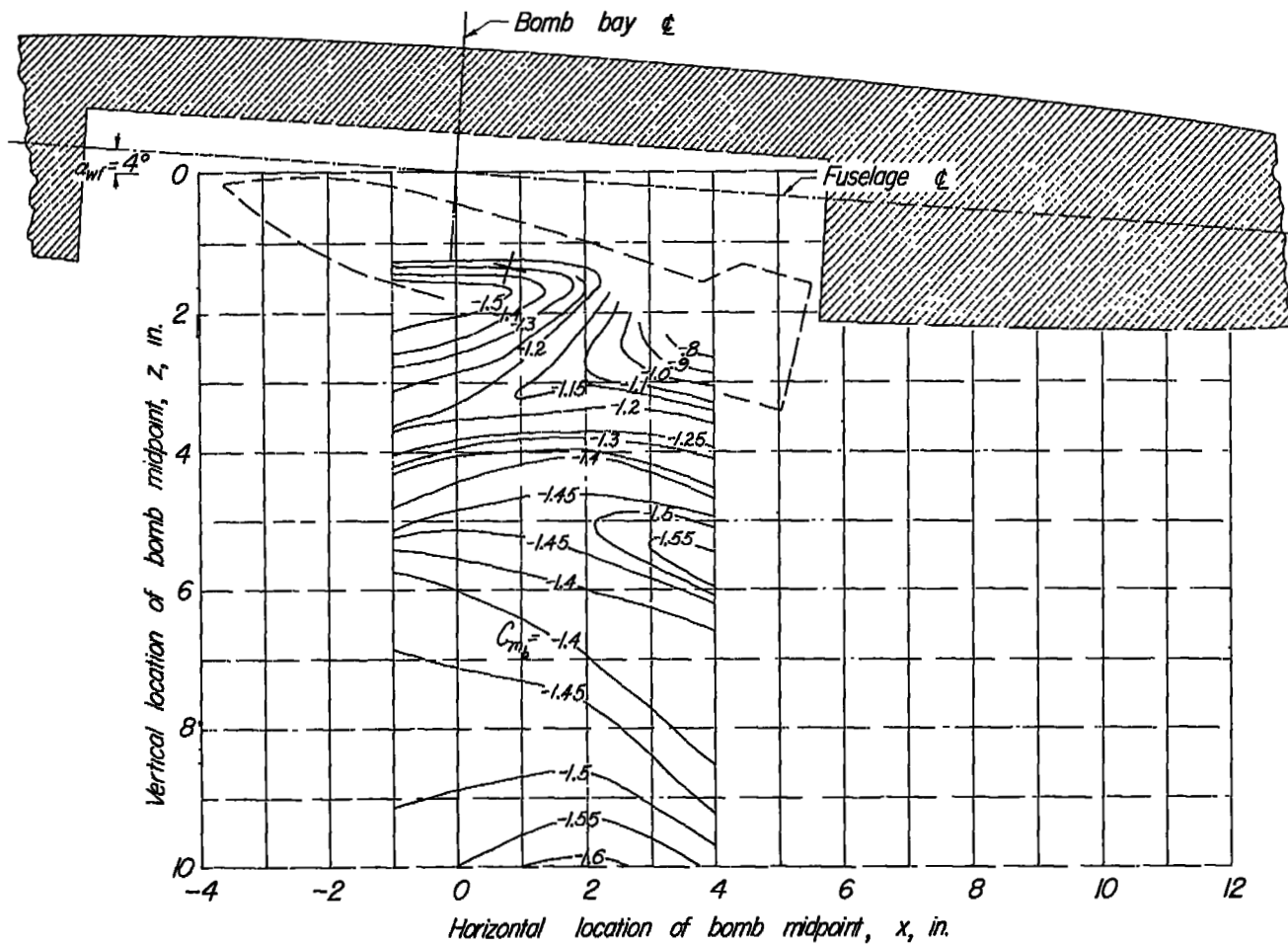
Figure 24.- Continued.





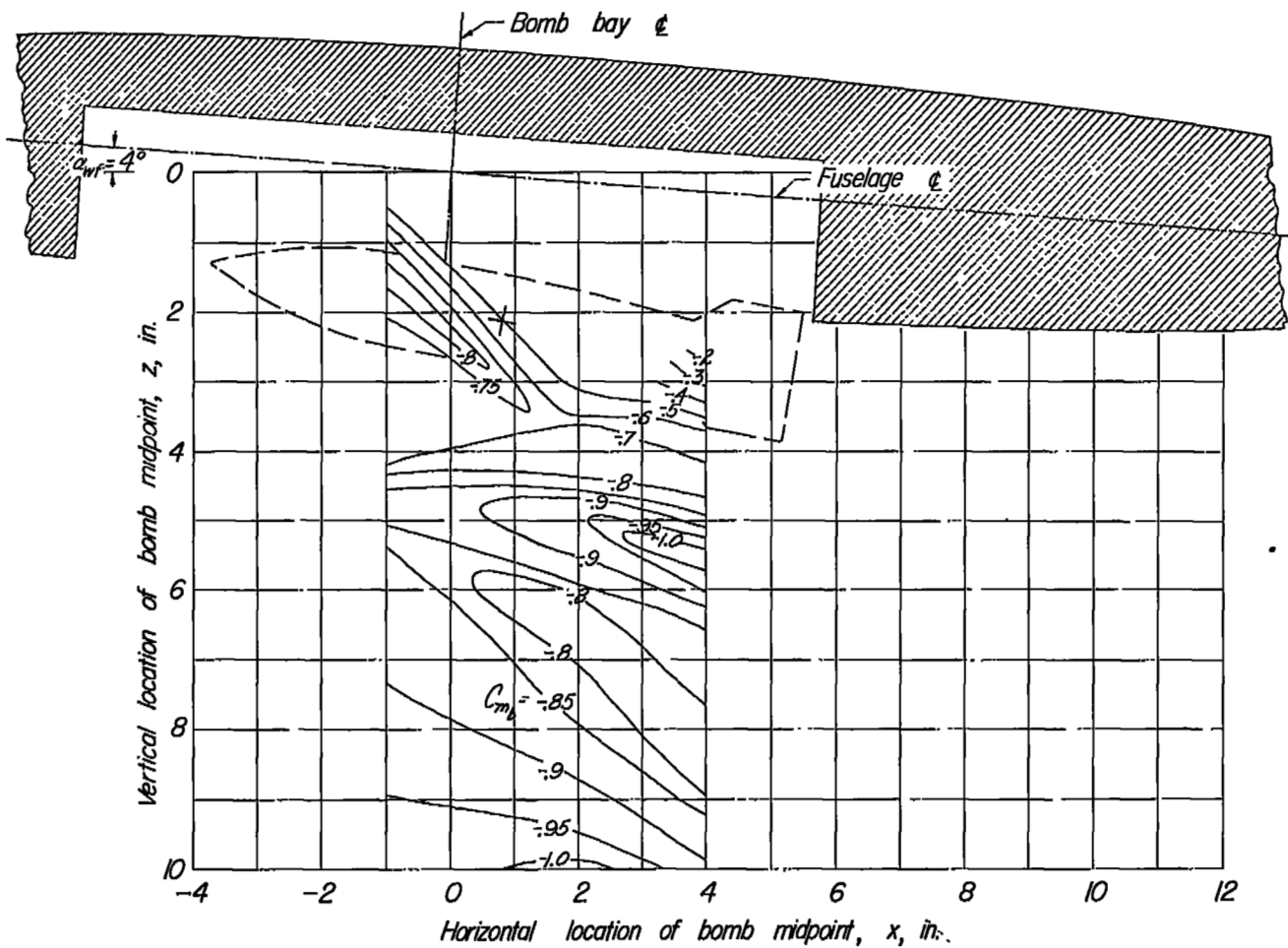
(g)  $\alpha_0 = -15^\circ$ .

Figure 24.- Concluded.



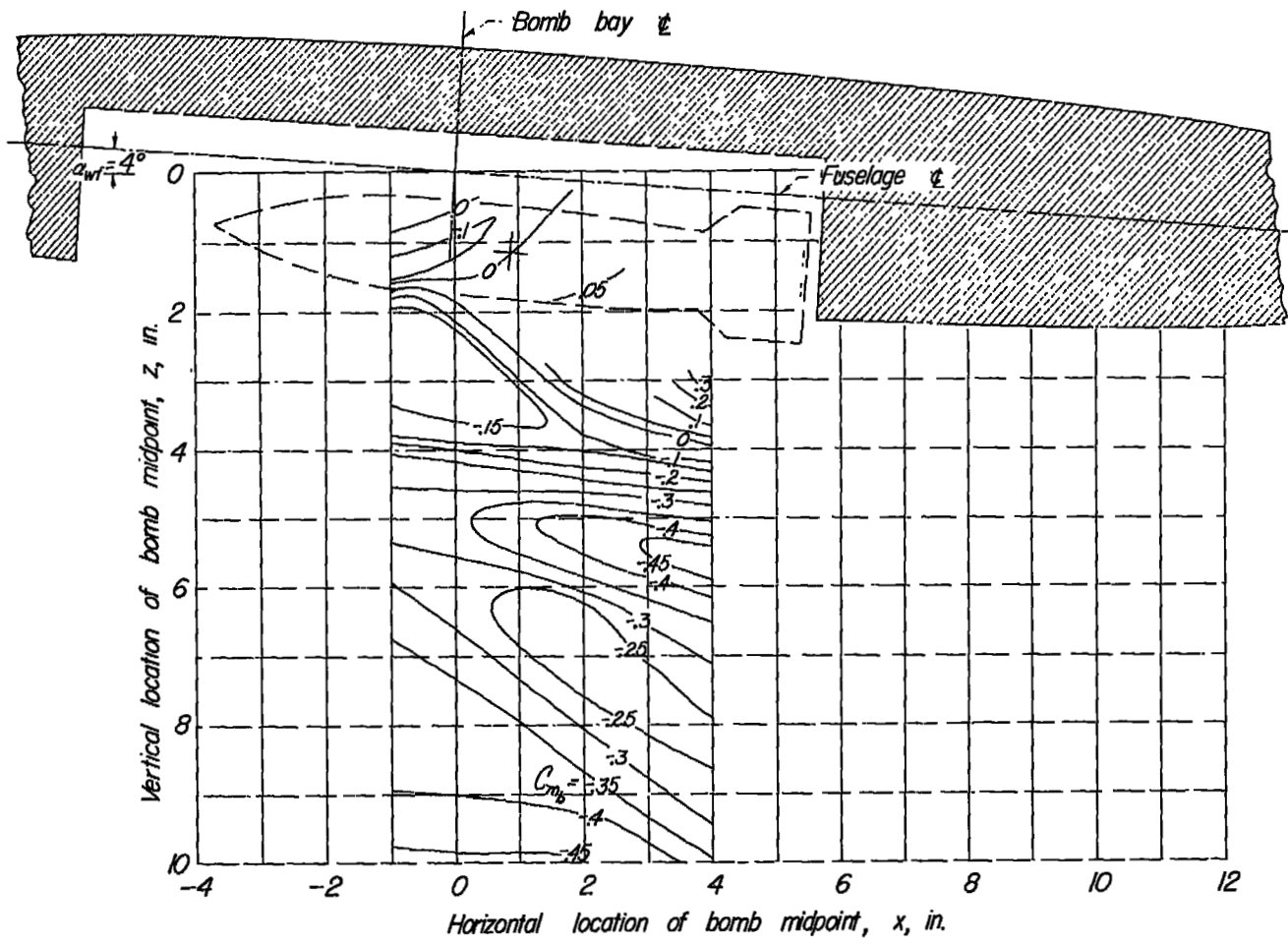
(a)  $\alpha_b = 15^\circ$ .

Figure 25.- Contour plot of the pitching moment of bomb 3 in presence of the wing-fuselage combination.  $\alpha_{wf} = 4^\circ$ .



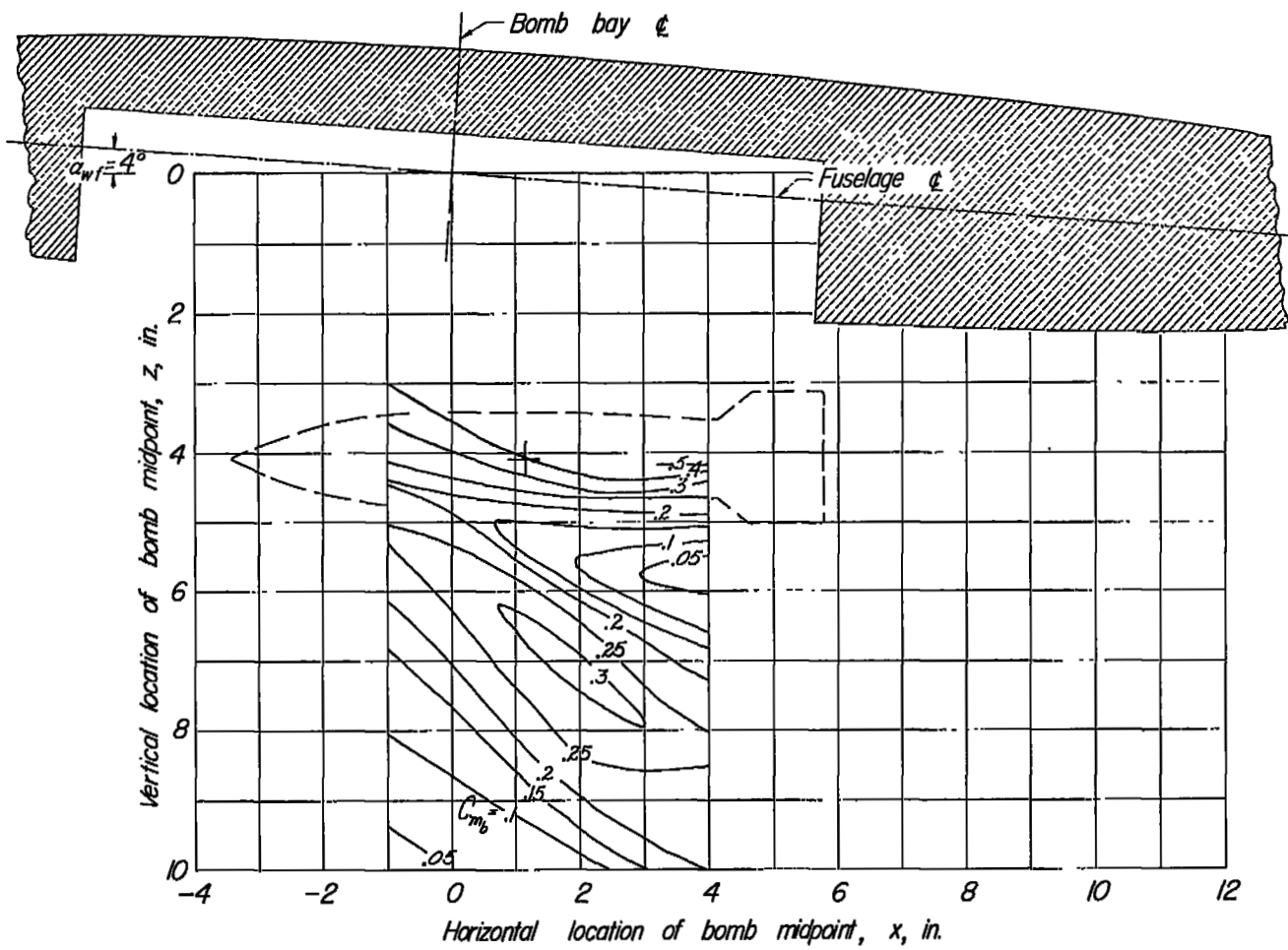
(b)  $\alpha_b = 10^\circ$ .

Figure 25.- Continued.



(c)  $\alpha_b = 5^\circ$ .

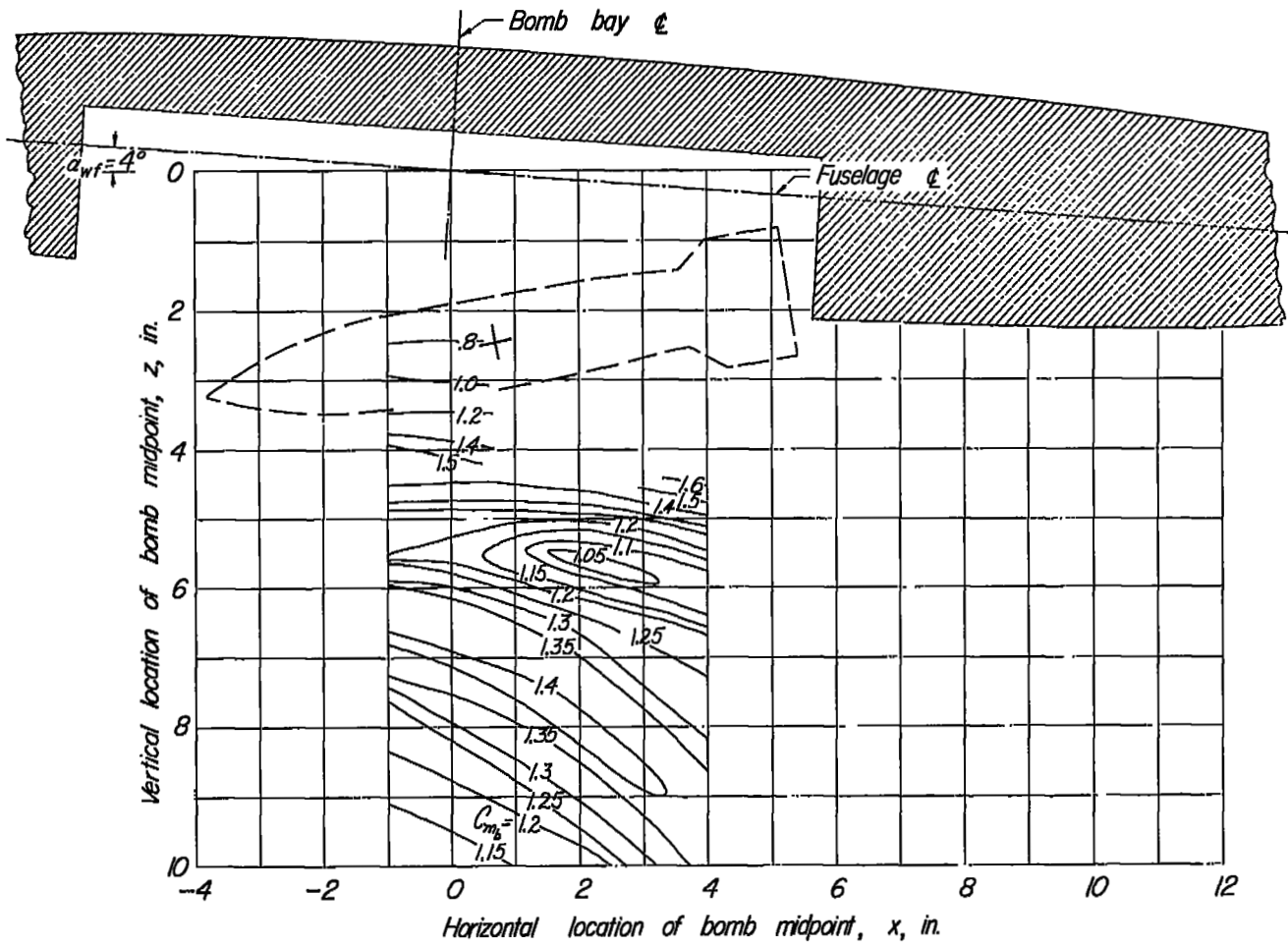
Figure 25.- Continued.



(d)  $\alpha_b = 0^\circ$ .

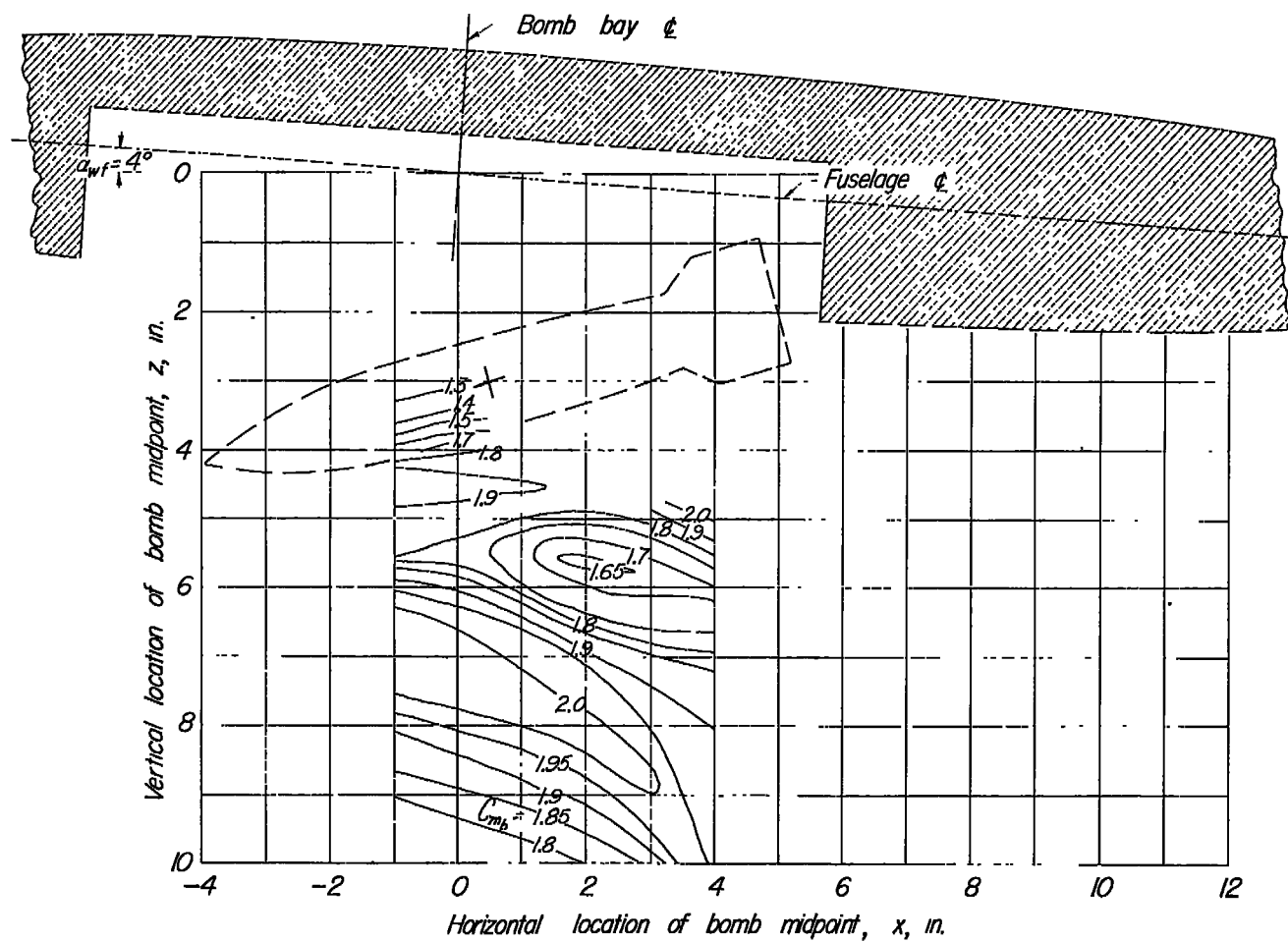
Figure 25.- Continued.





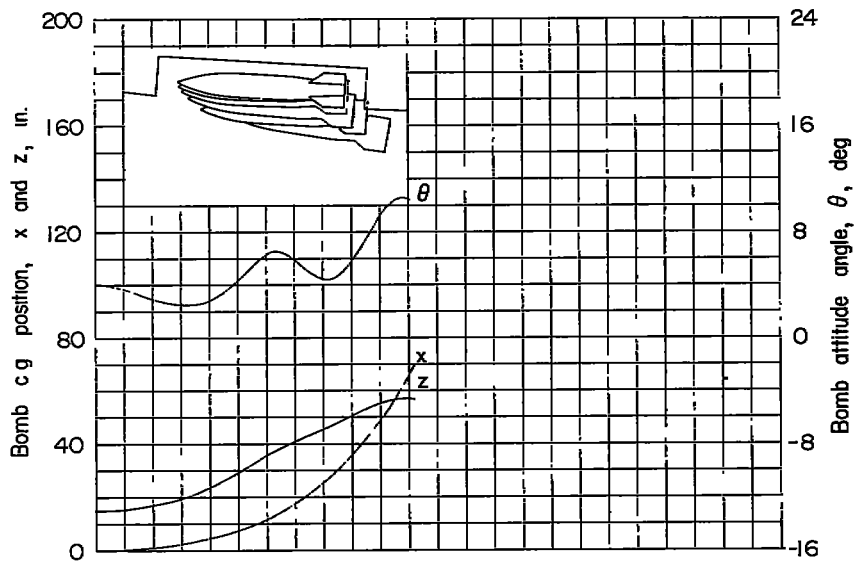
(f)  $\alpha_0 = -10^\circ$ .

Figure 25.- Continued.

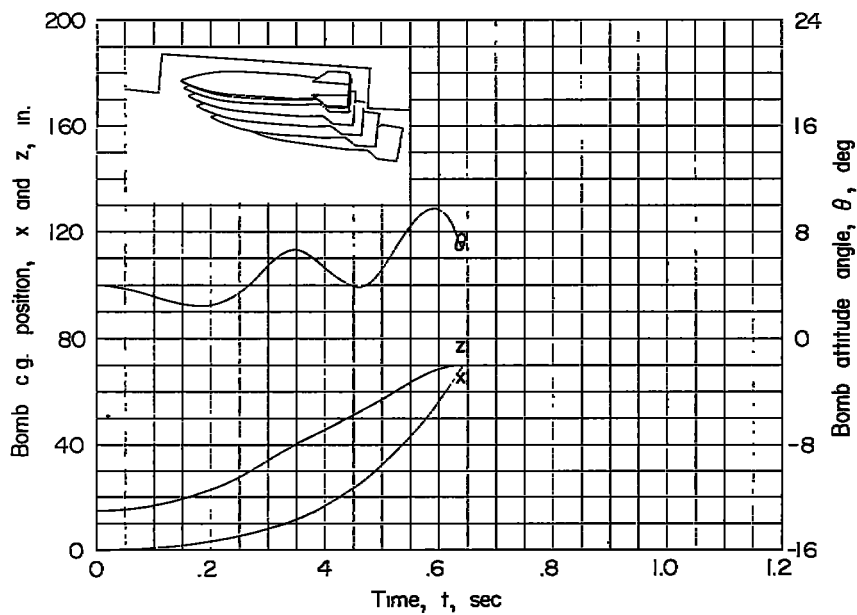


(g)  $\alpha_b = -15^\circ$ .

Figure 25.- Concluded.

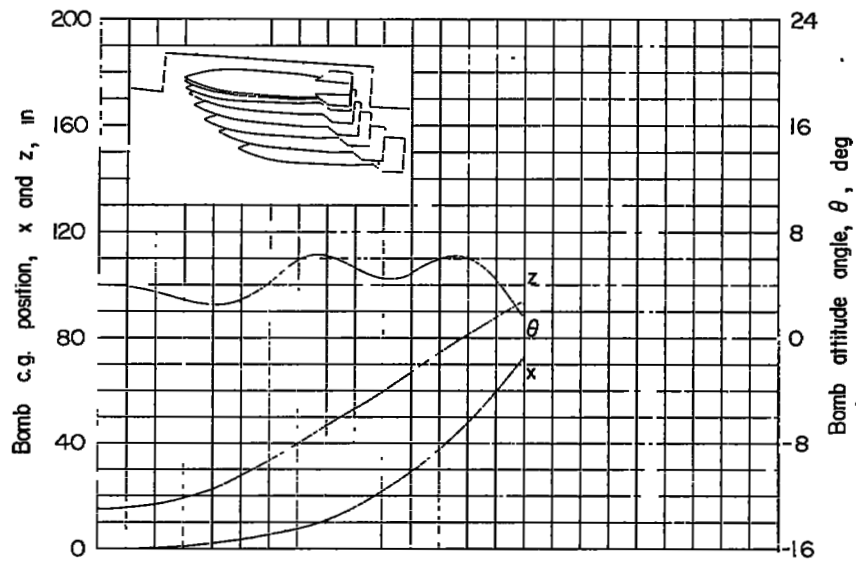


(a) 0 feet.

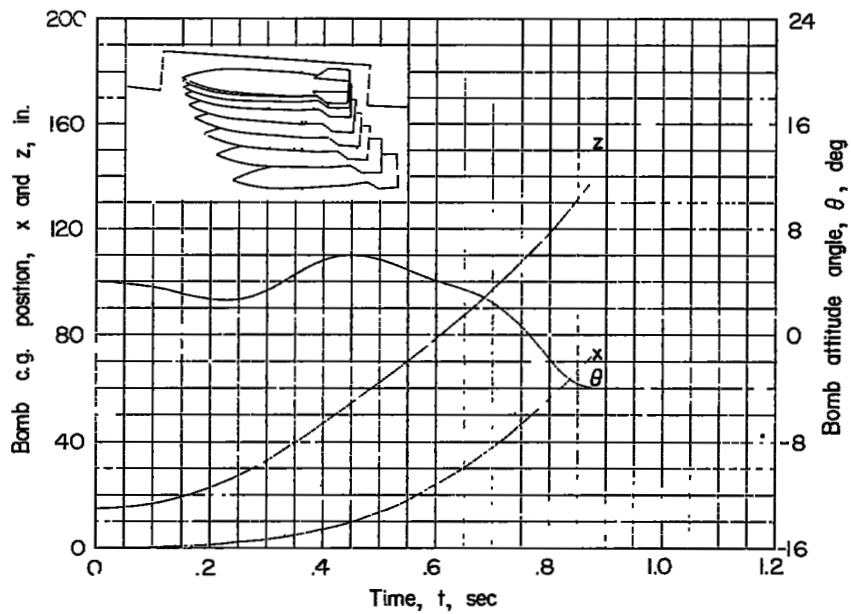


(b) 10,000 feet.

Figure 26.- Calculated time histories of motions of bomb 3 at various altitudes;  $\alpha_{wf} = 4^\circ$ ;  $\theta_0 = 4^\circ$ .

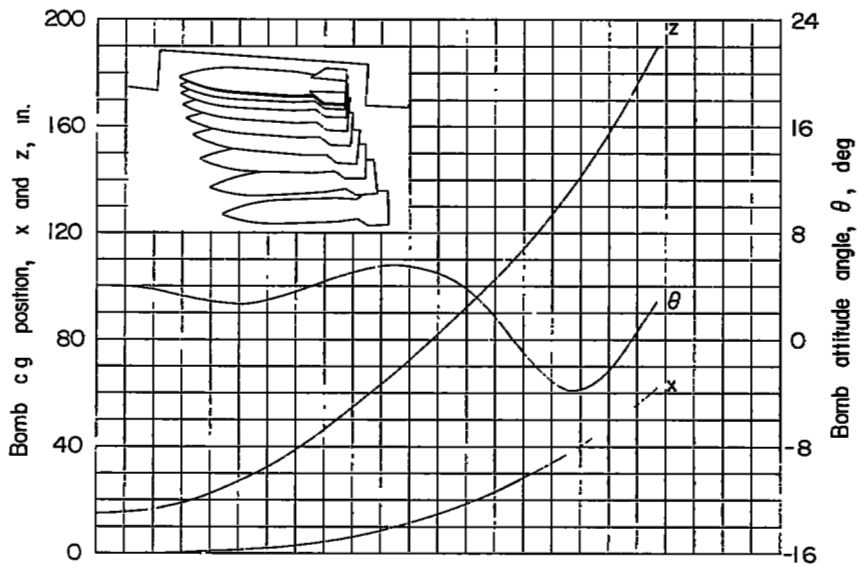


(c) 20,000 feet.

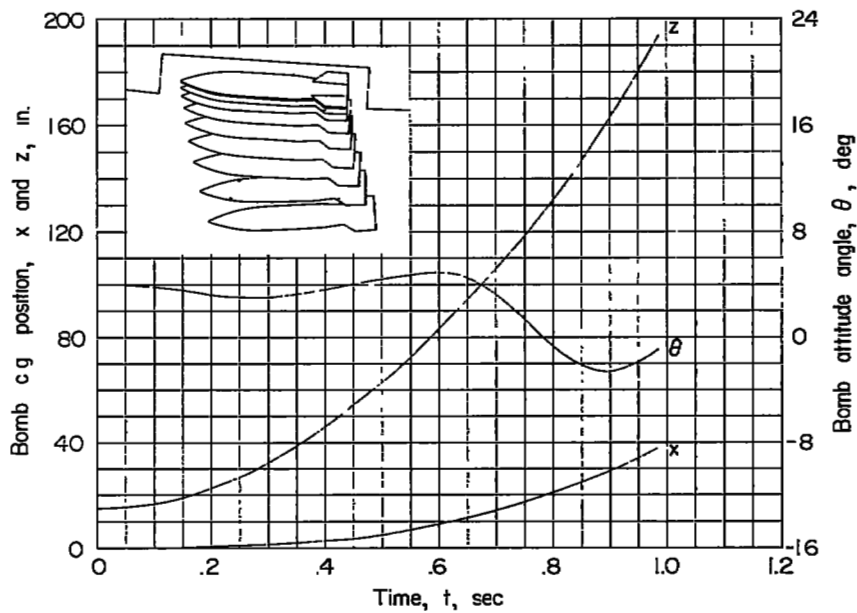


(d) 30,000 feet.

Figure 26.- Continued.



(e) 40,000 feet.



(f) 50,000 feet.

Figure 26.- Concluded.

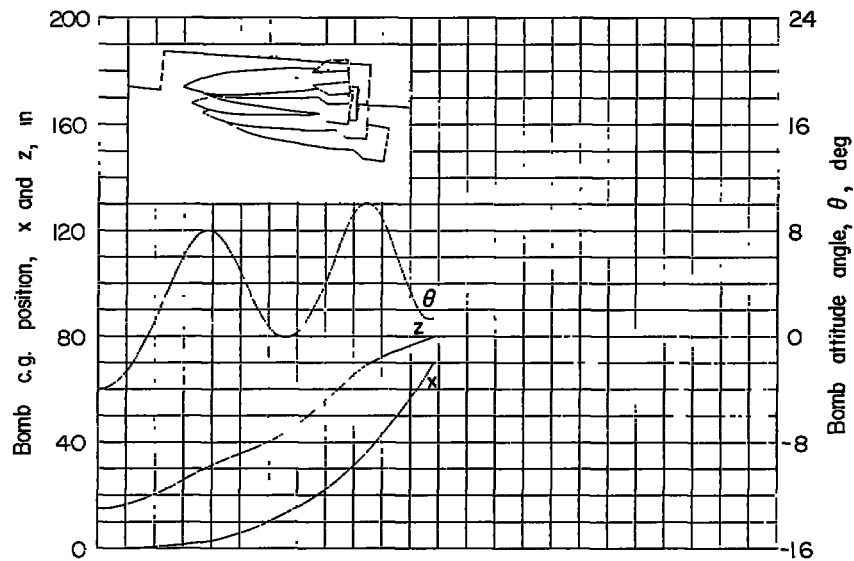
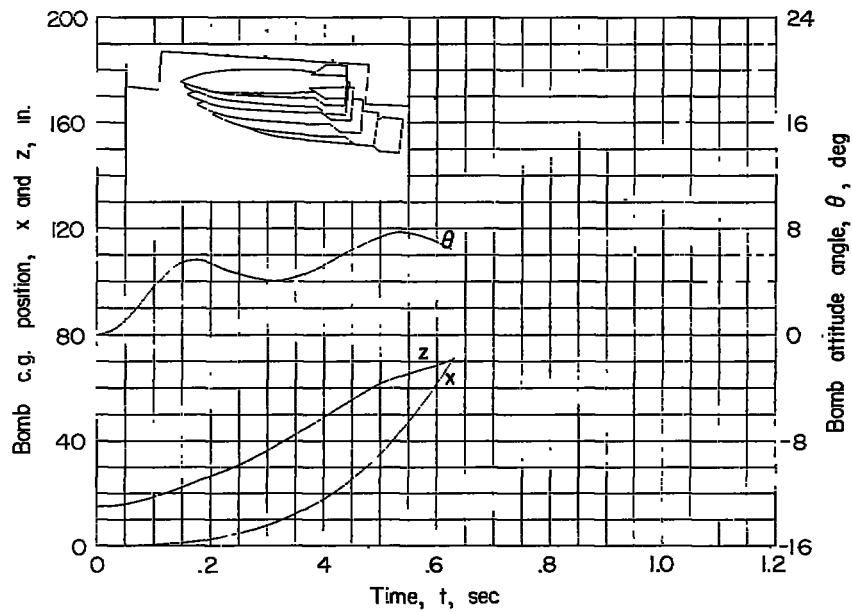
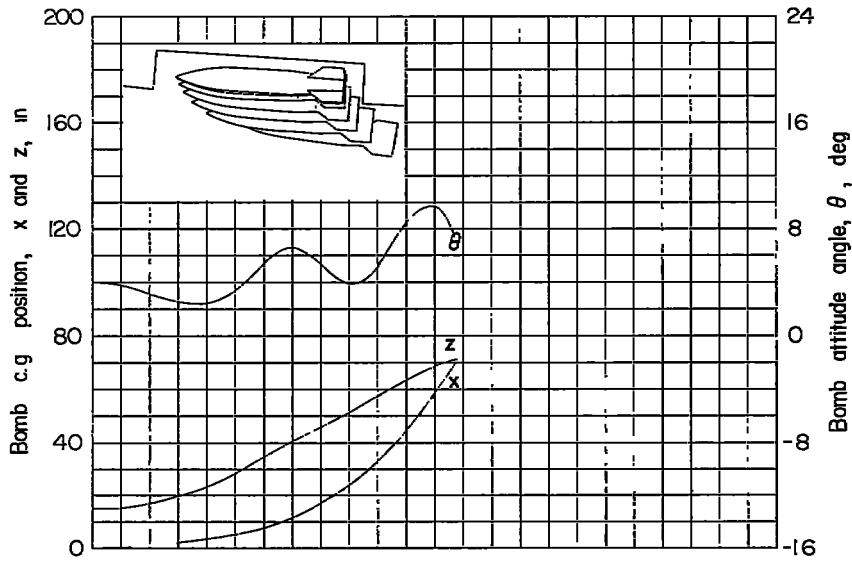
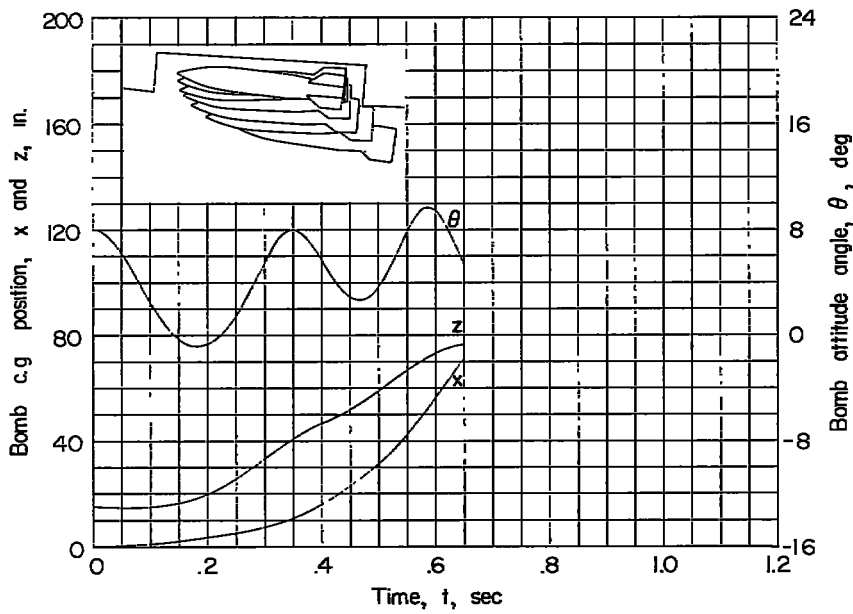
(a)  $\theta_0 = -4^\circ$ .(b)  $\theta_0 = 0^\circ$ .

Figure 27.- Calculated time histories of motions of bomb 3 with various bomb attitudes. Altitude = 10,000 feet;  $\alpha_{WF} = 4^\circ$ .

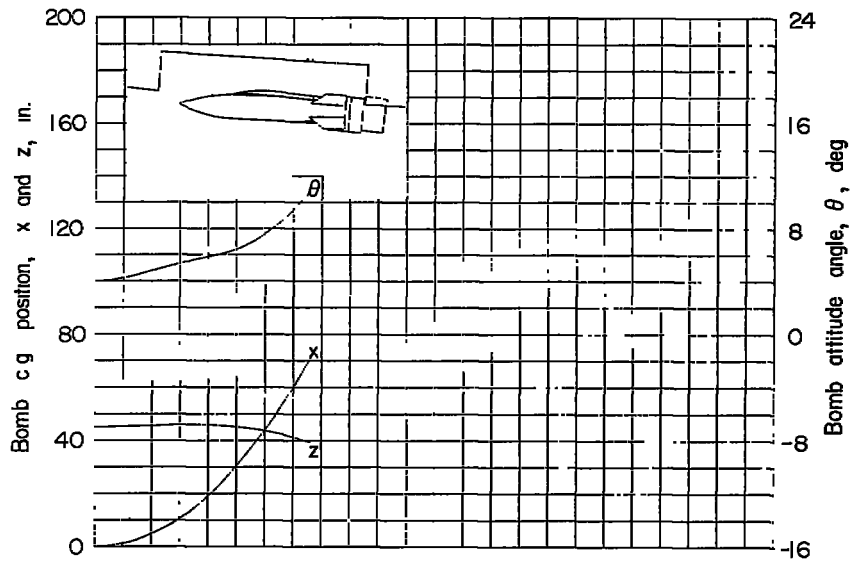


(c)  $\theta_0 = 4^\circ$ .

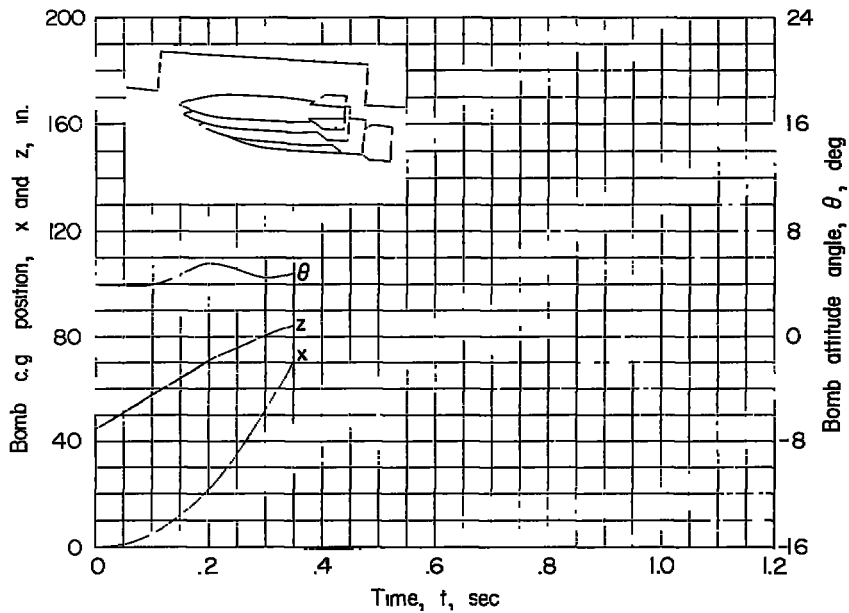


(d)  $\theta_0 = 8^\circ$ .

Figure 27.- Concluded.

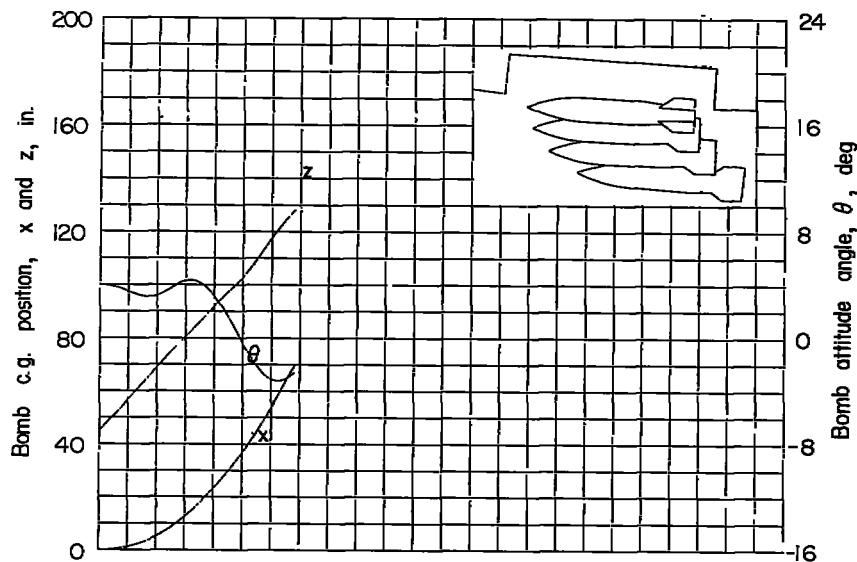


(a) 0 feet per second.

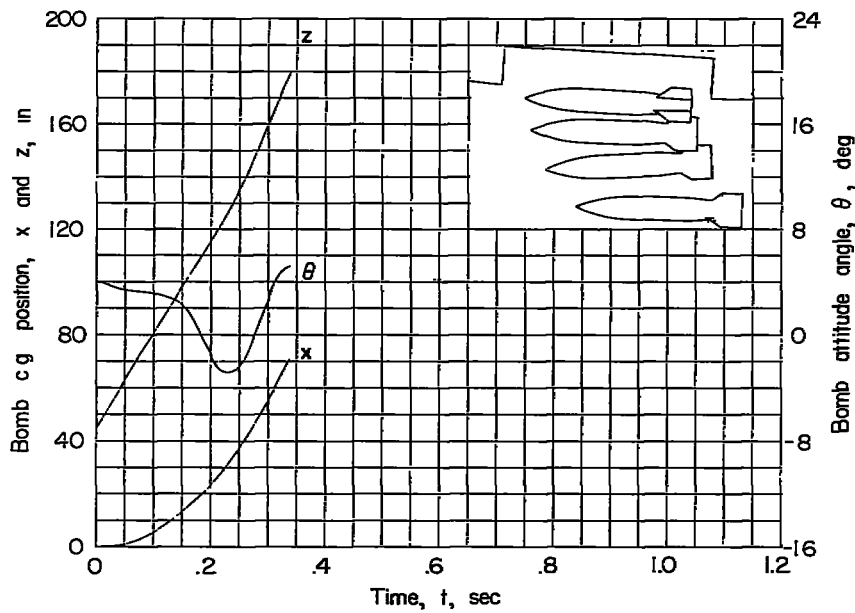


(b) 10 feet per second.

Figure 28.- Calculated time histories of motions of bomb 3 with various ejection velocities at sea level.  $\alpha_{wf} = 4^\circ$ ;  $\theta_0 = 4^\circ$ .

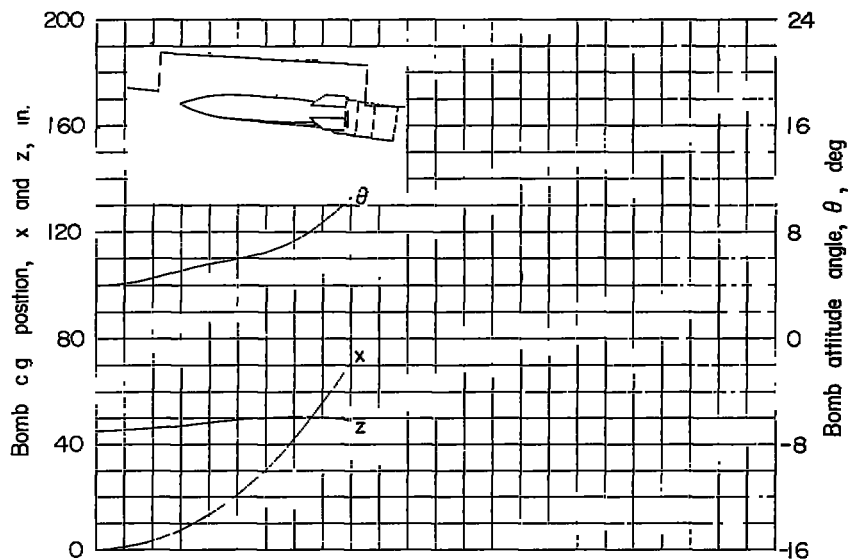


(c) 20 feet per second.

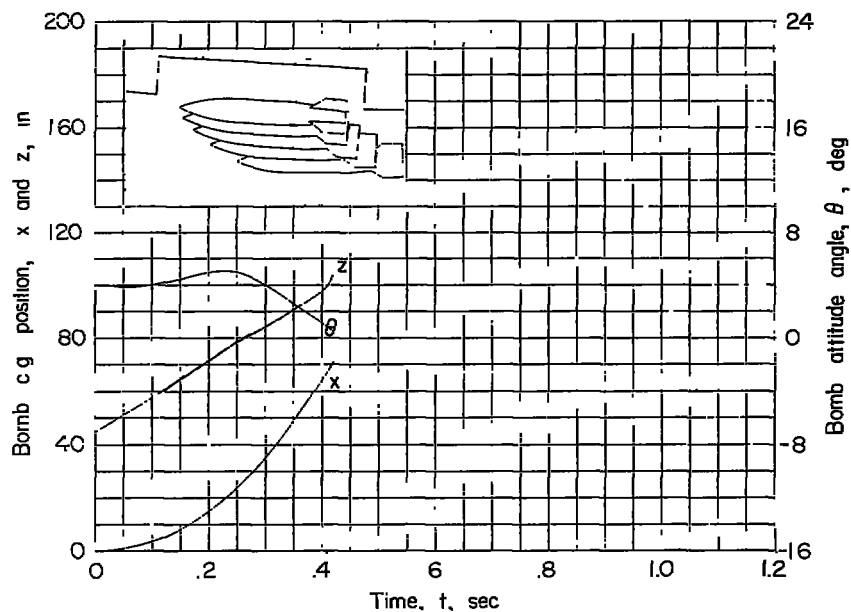


(d) 30 feet per second.

Figure 28.- Concluded.

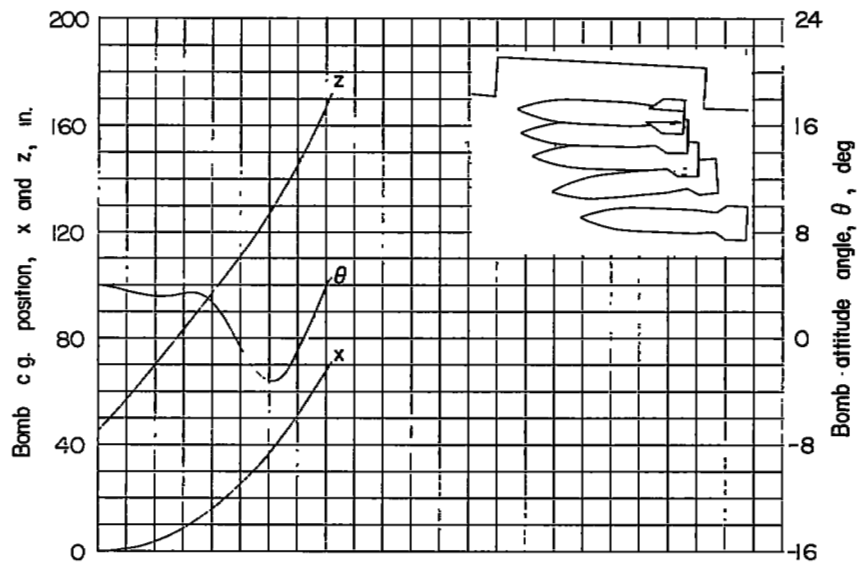


(a) 0 feet per second.

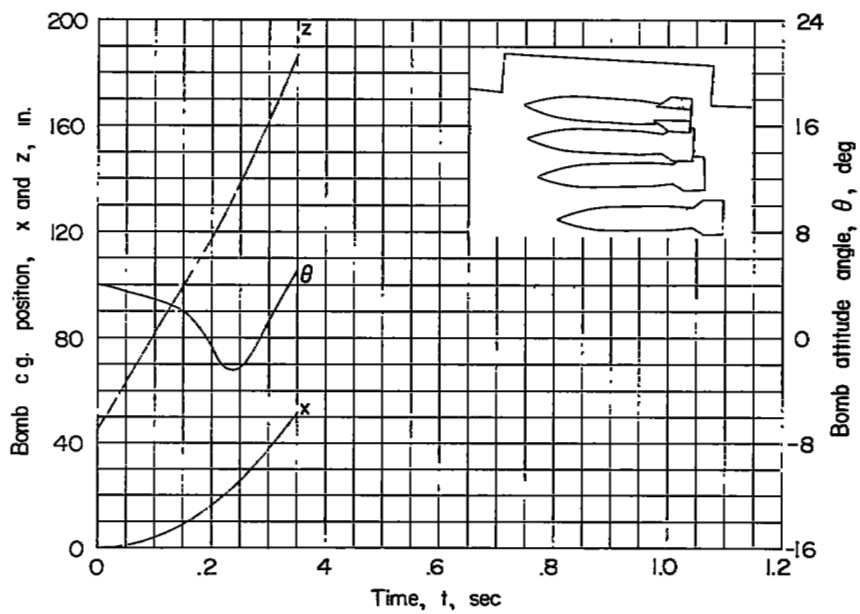


(b) 10 feet per second.

Figure 29.- Calculated time histories of motions of bomb 3 with various ejection velocities at an altitude of 10,000 feet.  $\alpha_{wf} = 4^\circ$ ;  $\theta_0 = 4^\circ$ .



(c) 20 feet per second.



(d) 30 feet per second.

Figure 29.- Concluded.

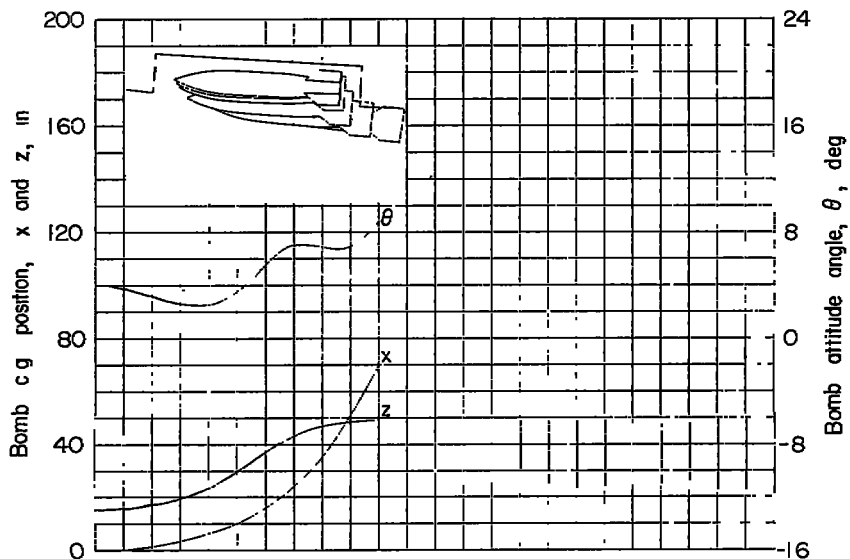
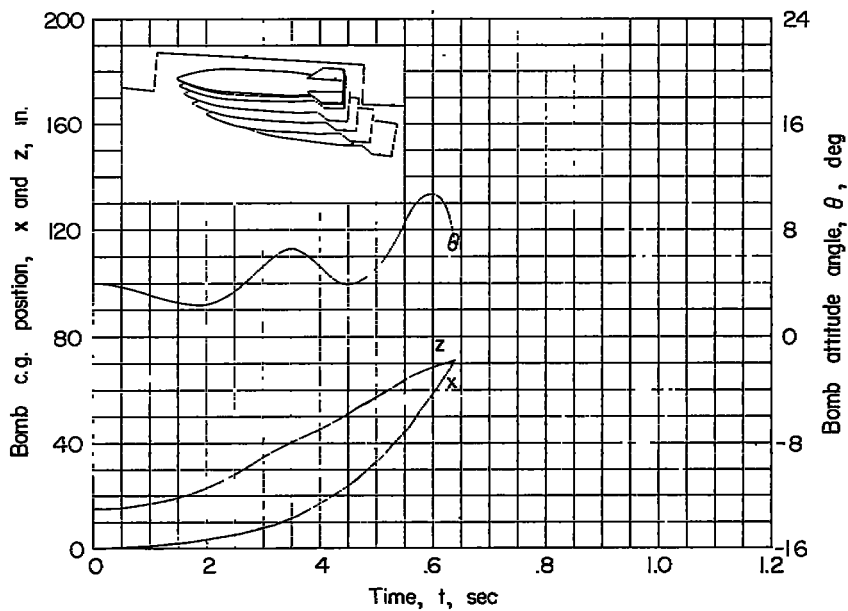
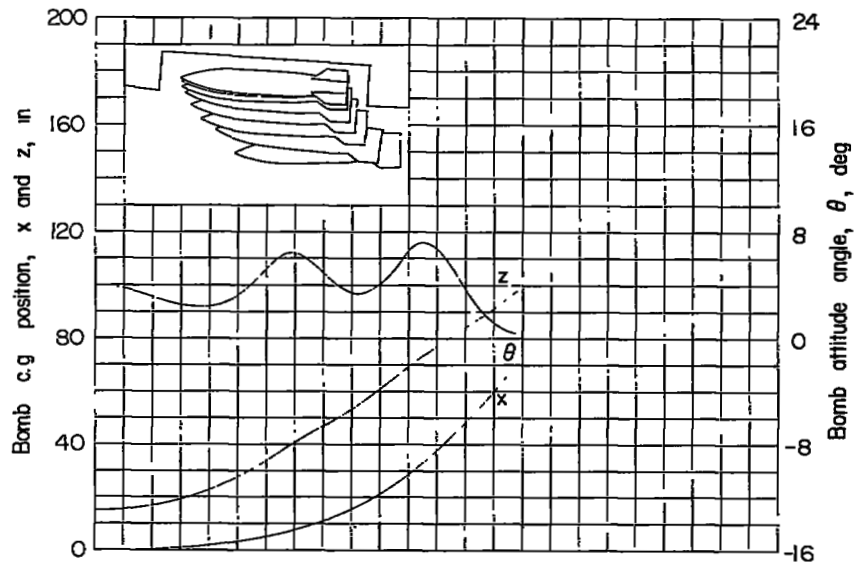
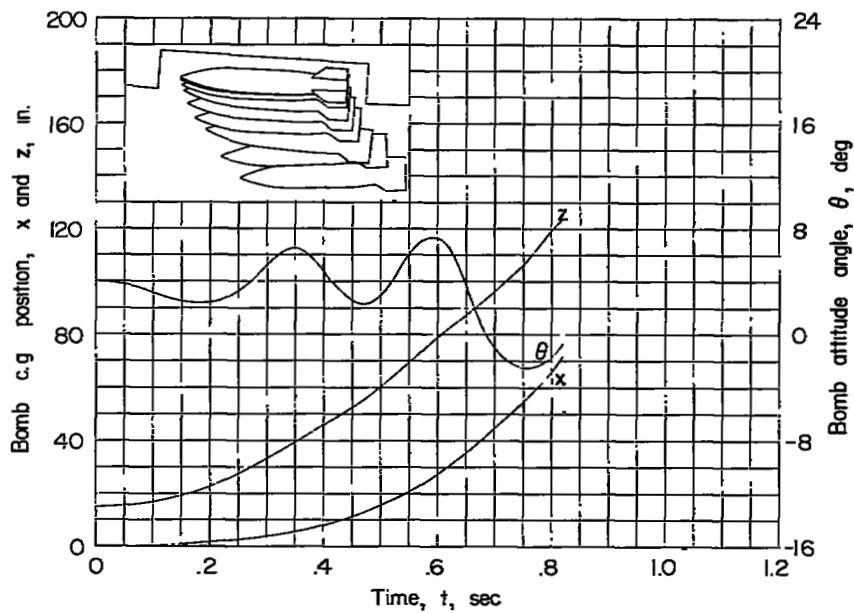
(a)  $W = 875$  pounds.(b)  $W = 1,750$  pounds.

Figure 30.- Calculated time histories of motions of bomb 3 with various bomb weights.  $\alpha_{wf} = 4^\circ$ ;  $\theta_0 = 4^\circ$ ; altitude, 10,000 feet.



(c)  $W = 2,625$  pounds.



(d)  $W = 3,500$  pounds.

Figure 30.- Concluded.

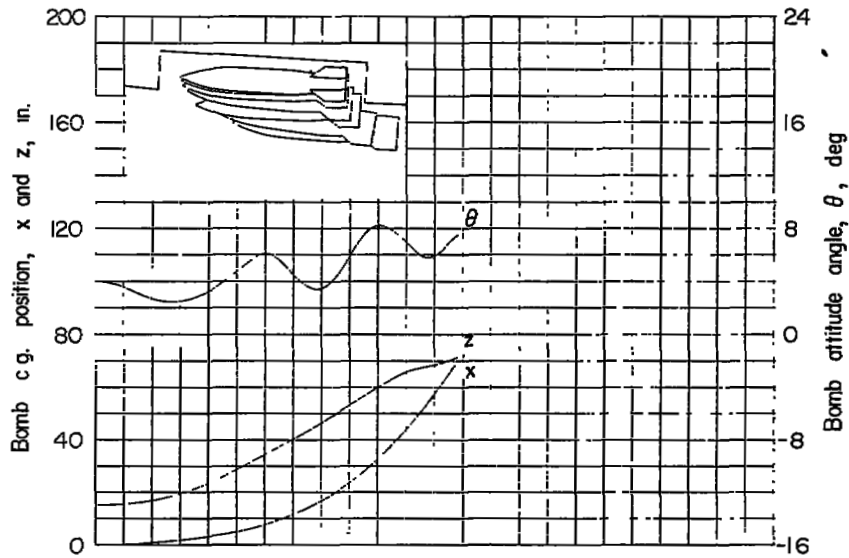
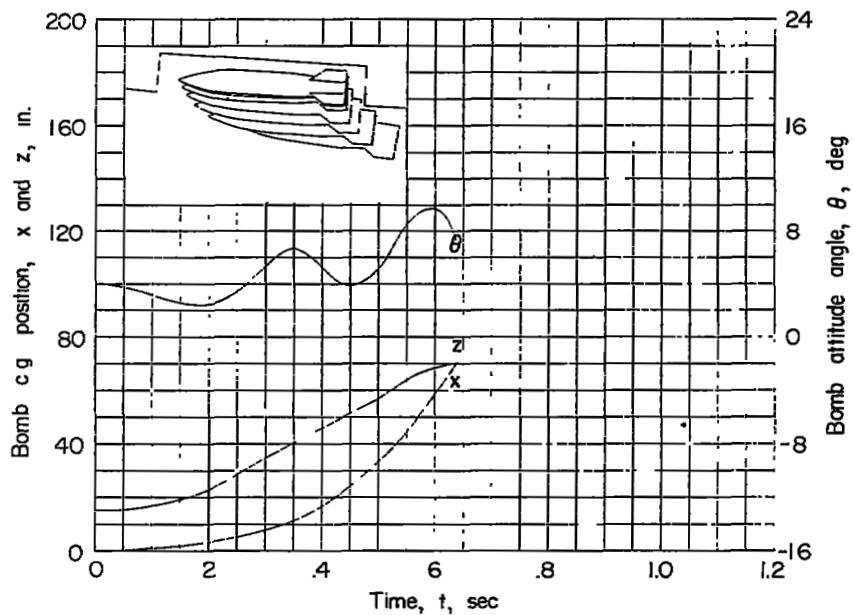
(a)  $I = 2,558 \text{ lb-sec}^2\text{-in.}$ (b)  $I = 5,178 \text{ lb-sec}^2\text{-in.}$ 

Figure 31.- Calculated time histories of motions of bomb 3 with various bomb moments of inertia.  $\alpha_{wP} = 4^\circ$ ;  $\theta_0 = 4^\circ$ ; bomb weight, 1,750 pounds; altitude 10,000 feet.

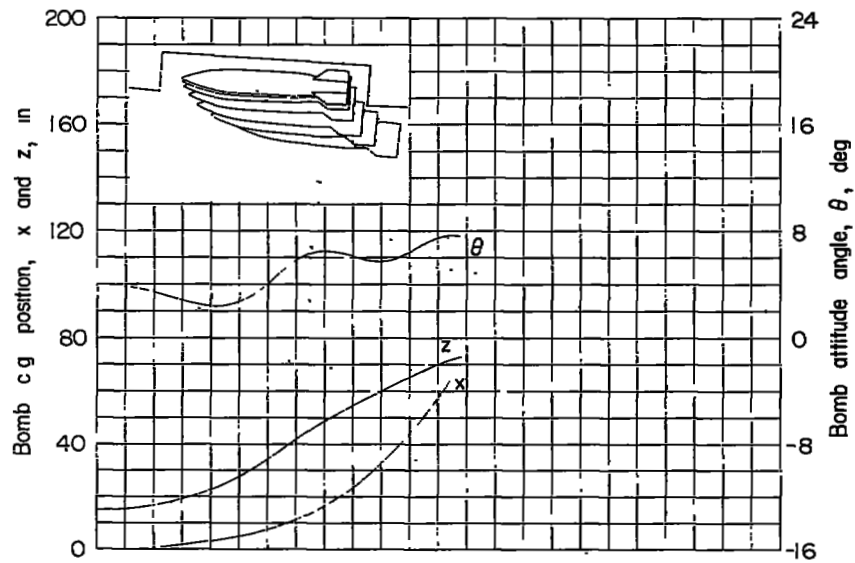
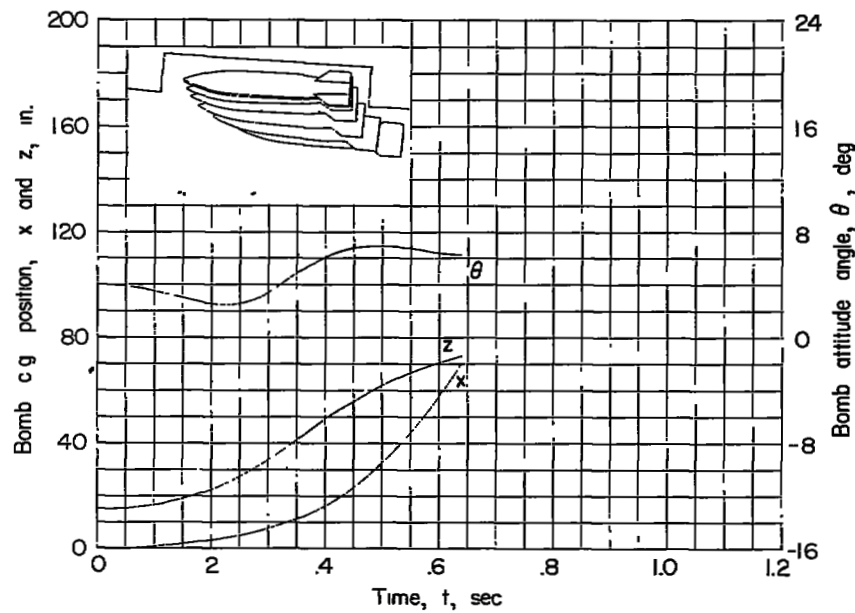
(c)  $I = 7,764 \text{ lb-sec}^2\text{-in.}$ (d)  $I = 10,352 \text{ lb-sec}^2\text{-in.}$ 

Figure 31.- Concluded.

~~CONFIDENTIAL~~

UNCLASSIFIED

LANGLEY RESEARCH CENTER  
3 1176 01345 8659

DO NOT REMOVE SLIP FROM MATERIAL	
Delete your name from this slip when returning material to the library.	
NAME	MS
Floyd Wilcox	413

NASA Langley (Rev. May 1988)

RIAD N-75

~~CONFIDENTIAL~~